NTNU
Norwegian University of
Science and Technology

Accidental Drop of Slender Cylindrical Bodies

A Numerical and Experimental Study of
Velocity and Trajectory of Cylinders Falling
Through Water

Helene Salte Håland

Marine Technology
Submission date: June 2018
Supervisor: Trygve Kristiansen, IMT
Co-supervisor: Hagbert Alsos, SINTEF

Norwegian University of Science and Technology
Department of Marine Technology

Preface

This thesis is the finalisation of my Master of Science degree in Marine Technology at the Norwegian University of Science and Technology (NTNU). The work has been carried out during the spring 2018 and is a continuation of my specialisation project, *A pre-study of accidental drop of a slender cylindrical body*. The main objective of this master thesis, is to analyse and investigate the trajectory and velocity of slender cylindrical objects falling in water, through numerical calculations and experiments. Performing the experiments was found very exciting, not least since it required creativity and innovation. The process of designing and performing the experiments and processing the experimental data, though time consuming, were found to be specially instructive.

I would like to thank my supervisor Professor Trygve Kristiansen and co-supervisor Hagbart Skage Alsos for good guidance and support during the work. I would also like to thank Torgeir Wahl for excellent help with the experimental set-up, and Trond Innset and Kristian Minde for great help building the drop-rig and the cylinder models. Finally, I would like to thank my fellow student Frid Grøtterud Birkeland for good collaboration during the design and execution of the experiments.

Helene Salte Håland

Helene Salte Håland
Trondheim, June 2018

Abstract

The oil and gas industry is continuously working to improve safety and minimise risk. Numerous offshore activities involve risks that may lead to accidents with serious consequences. The risk of accidental dropped objects, e.g. related to crane operations, is one of the most common threats during offshore operations. A falling object is of concern due to human safety, the environment and dangers related to damage to subsea structures and operational equipment.

The purpose of this thesis was to analyse and investigate slender cylindrical objects behaviour, for instance drill pipes, when falling through air, entry into the water phase and their travelling through the water column. Main focus however, were on the fully submerged condition. The velocity and trajectory of falling cylindrical objects into and through the water column have been investigated through numerical calculations and experiments. The control parameters were the cylinder's physical parameters (length to diameter ratio, centre of gravity location and open or closed ends) and the initial drop conditions (drop angle and drop position).

Experiments were carried out in a 5 meter deep tank, with breadth and length equal to 6 and 12 meter. Seven 1:20 cylindrical scale models, made of steel pipes, were used. The three dimensional motion of the falling cylinders in still water were measured by the use of an under water Oqus camera system. From the experiments, six different trajectory types were found, and it was demonstrated that the centre of gravity location and the initial drop angle were the most critical factors determining the trajectories. The influence from changing the length to diameter ratio or from dropping the cylinders with open or closed ends, were also found to have an impact. For instance, it was found that cylinder excursion decrease with increasing diameter and that open end cylinders had a smaller radial excursion than cylinders with closed ends. The largest radial excursion, of approximately six meter, was found for cylinders with a small displacement in centre of gravity. This excursion was one meter larger than the water depth. The cylinder velocities were found dependent on the cylinder orientation, that showed that the viscous forces were more dominant in the lateral, than in the axial direction. Comparing the experimental results to the recommended industry practice, DNVGL-RP-F107, the recommendations for calculating object excursions were in several cases found to be non conservative.

Results from the experiments were compared to the numerical simulations that were performed based on a two dimensional maneuvering theory corrected for viscous effects. Good agreements were observed, but the similarities were found extremely dependent on the chosen value for the effective trailing edge position and the drag coefficient in the transverse cylinder direction. Several possible error sources in the experiments and weaknesses in the theory were detected. But, even though some disagreements between the simulations and the experiments were found, the simple two dimensional method gave good indications of the trajectory and velocity of cylindrical

objects falling through the water column.

Samandrag

Olje og gass industrien arbeider kontinuerleg med å forbetre sikkerheita og minimere risikoen. Dei fleste offshoreaktivitetar inneber risiko for ulykker med alvorlege konsekvensar. Ein av dei vanlegaste uønska hendingane i samband med offshore operasjonar er fallande gjenstandar, til dømes i forbindelse med løfte operasjoner. Ein fallande gjenstand kan vere til fare for folks sikkerheit og miljøet, og kan føre til skade på undervansskonstruksjonar og driftsutstyr.

Formålet med denne oppgåva var å analyser og undersøke oppførselen til slanke sylinderforma objekt, til dømes borerøyr, når dei fell frå luft, gjennom vassoverflata og vidare gjennom vassøyla. Hovudfokuset vil vere retta mot den fullt neddykka tilstanden. Hastigheita og fallbanen til sylinderforma objekt som fell i vatn vart undersøkt med numeriske berekningar og forsøk. Kontrollparameterane var dei fysiske sylinderparameterane (lengde diameter forholdet, plasseringa av gravitasjonssenteret og opne eller lukka ender) og dei initielle dropp forholda (dropp vinkel og dropp posisjon).

Det vart utført forsøk i ein 5 meter djup tank, med bredde og lengde på 6 og 12 meter. Sju sylinder modeller laga av stålrøyr i skala 1:20 vart brukt. Den tredimensjonale bevegelsen til dei fallande sylindrane, i stille vatn, vart målt med eit Oqus undervansskamera system. Frå forsøka vart det funne seks forskjellige typar fallbaner. Dei faktorane som hadde størst innverknad påfallbanen viste seg å vere posisjonen til gravitasjonssenteret og dropp vinkelen til sylindrane. Det vart også funne ein påverknad på fallbanen avhengig av lengde diameter forholdet, og om sylinderen hadde opne eller lukka ender. Det vart til dømes funne at avstanden frå droppunktet til punktet der sylindrane landa på botnen minka med aukande sylinderdiameter, og at sylindrane med opne ender gjekk kortare enn dei med lukka ender. Dei sylindrane som landa på botnen med størst avstand frå droppunktet var dei med ein liten forskyving av gravitasjonssenteret, der den radielle avstanden var sirka seks meter, ein meter meir enn djupta i tanken. Sylinderhastigheita vart funne å vera avhengig av orienteringa til sylinderen, noko som viste at dei viskøse kreftene var meir dominerande i den perpendikulære sylinderretninga, enn i den langsgåande. Den radilelle ekskursjonen funne frå forsøka vart samanlikna med anbefalt industri praksis for objektekskursjon, DNVGL-RP-F107, og det vart funne at dei etablerte anbefalingane i fleire tilfelle ikkje var spesielt konservative.

Resultata frå forsøka vart samanlikna med dei numeriske simuleringane, som var basert på todimensjonale manøvrerings teori justert for viskøse effektar. Det vart funne gode overeinsstemmelsar, men likskapane avhenger av dei valde verdiane for posisjonen til den effektive avløysingskanten og dragkoeffisienten i tverrgåande sylinder retning. Fleire moglege feilkjelder i forsøka og svakheiter i teorien vart avdekka, men sjølv om det vart funne nokon avvik mellom simuleringa og forsøka så såg det ut til at den forenkla todimensjonale metoden som blei presentert, kan gje gode in-

dikasjonar på fallbanen og hastigheita for sylinderforma objekt som fell gjennom vassøyla.

Contents

1 Introduction

The oil and gas industry is continuously working to improve safety and minimise risks. Numerous offshore activities involve risks that may lead to accidents with serious consequences. One of the most common challenges are accidental drops. Dropped objects are among the top ten causes of fatalities and serious damages in the oil and gas industry (DROP , 2016). A falling object is of concern due to human safety, the environment and dangers related to damage to subsea structures and operational equipment. By definition, a dropped object is an item that falls from its previous position. Dropped objects can be categorised in two ways, static or dynamic. A static dropped object is «any object that falls from its previous position under its own weight (gravity) without any applied force» and a dynamic dropped object is «any object that falls from its previous position due to applied force, e.g. collisions involving travelling equipment or loads» (OES , n.d.).

1.1 Background and motivation

According to dropped objects statistics, a significant part of offshore accidents are caused by free falling objects (DROP , 2016). In other words, objects relatively frequently fall accidentally from platforms or vessels during lifting, hoisting or any other offshore operations. The Petroleum Safety Authority's report about risk trends in the Norwegian petroleum industry, gives clear indications that this still is a challenge (Carlsen , 2017). In the report, falling objects having a potential developing in to an accident, are categorised in objects falling either to deck or into the ocean. Based on reported events from year 2013 to 2016, The Petroleum Safety Authority has outlined the following diagram (see Figure 1). The diagram shows the number of free falling accidents split in fixed and mobile facilities. The total and the normalised number of events are shown. The normalisation is based on working hours related to drilling and well operations and number of hours worked within construction and maintenance.

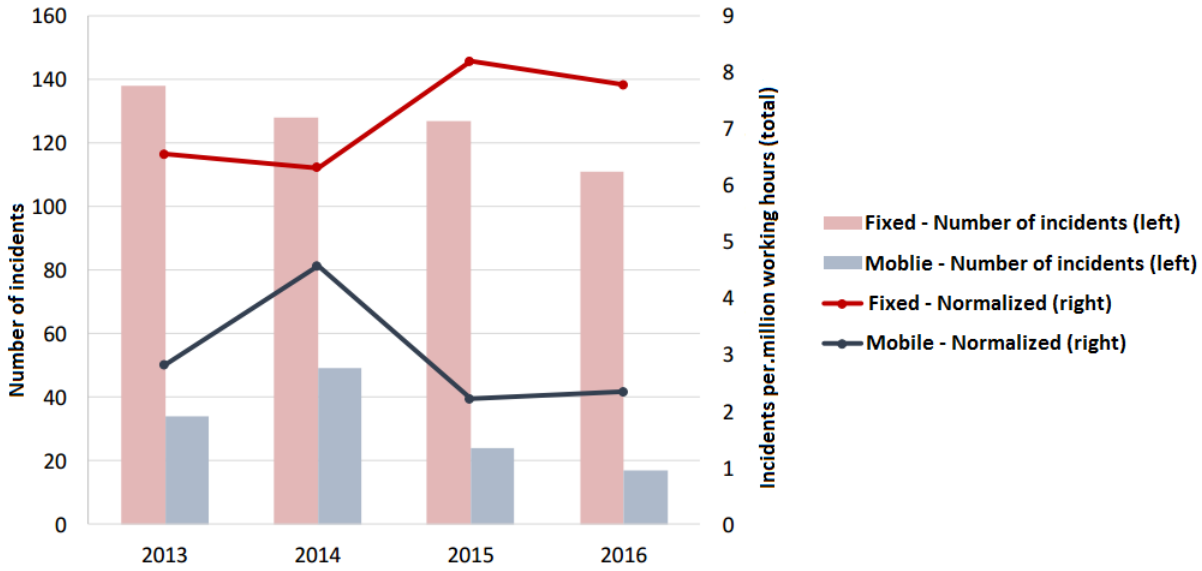

Figure 1: *Number of events and events per. million working hours classified as falling item, distributed between fixed and mobile facilities, in the period 2013-2016. (Carlsen , 2017)*

The causes of dropped objects are many, but the most frequently occurring ones are (DROP , 2016):

- Inadequate securing
- Failed fixtures and fittings
- Corrosion
- Poor housekeeping
- Procedures not followed

Small objects falling into the ocean during offshore operations, as for instance scaffolding bars and tools, often drops without major consequences. The critical situations are related to larger objects such as drill pipes, containers, templates, subsea modules and GRP covers, due to the high impact energy involved. When objects fall in to the ocean, they are a concern to safety of subsea installations, pipelines, mooring systems, platform jackets and for instance ROVs close to the platform.

In order to protect underwater structures and equipment and to avoid unnecessary safety measure, it is of vital importance to have good knowledge about dropped objects trajectory and impact energy. It is necessary to investigate possible hit points to ensure operating in an acceptable risk zone. DNV-GL has developed a recommended practice for risk assessment for pipeline protection. In the risk assessment, the object's excursions onto the seabed are assumed to follow a normal distribution as illustrated in Figure 2 (DNVGL , 2017).

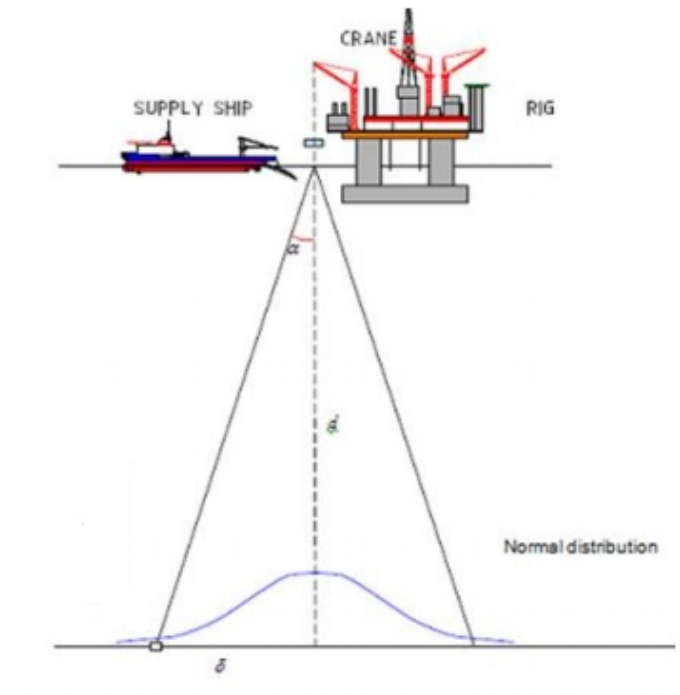

Figure 2: *Object excursion and hit probability (Awotahegn , 2015)*

The recommendations from DNV-GL claims that object excursion is extremely dependent on shape and weight of objects and that the fall pattern for pipes depend on the water entry angle. DNV-GL assume that the object excursions onto the seabed are normal distributed with a standard deviation depending on the water depth and the shape and weight of the falling object (DNVGL , 2017).

In order to meet challenges associated with falling objects and to assure operating within acceptable risk zones, it is important to understand motions and dynamics of free falling objects. The dropped object study involves a wide range of subjects, such as nonlinear dynamics, manoeuvring theory, fluid dynamics, probability and statistical methods and will therefore have a wide significance and application. In general, three phases will affect the projection of a falling object. These are are the object's drop through the air, through the free water surface and through the water column. It is necessary to gain knowledge about forces that affect the motion patterns in all these phases to investigate the projection of the object.

1.2 Objectives and scope

The purpose of this thesis was to analyse and investigate the trajectory and velocity of slender cylindrical objects falling in air, entry into the water surface and it's travel through the water column. The main focus has however been on cylindrical objects in fully submerged condition. Seven different cylinder types were investigated with respect to several control parameters. The control parameters were the cylinder's phys-

ical parameters (length to diameter ratio, centre of gravity location and open or closed ends) and the initial drop conditions (drop angle and drop position). The investigations are performed through numerical calculations and experiments.

Experiments were carried out in Dokka, a tank owned by SINTEF Ocean. The depth of the tank is 5 meter while breadth and length is 6 and 12 meter. The experiments were based on falling drill pipes. Seven 1:20 simplified scale models were used. The models used were different cylindrical steel pipes. The three dimensional motions of the cylinder's drop through the still water to the tank bottom, were measured by use of an under water Oqus camera system.

A general fundamental two dimensional theory for falling cylinders was studied. For the drop through the water column phase, a simple two dimensional theory based on manoeuvring equations corrected for viscous effects is presented. This two dimensional theory was implemented in MATLAB and the simulation program was used to calculate the trajectory and the velocity of the cylinders, numerically. To find the validity of the two dimensional theory and the sensitivity of the different parameters involved, the numerical calculations were compared to the experimental results.

The excursions of the falling cylindrical objects were also compared to DNVGL-RP-F107, that gives DNV's recommended practice for object excursion. The recommendations provides a simplified method to estimate the excursion of an accidentally dropped object.

1.3 Literature review

Some experiments with free falling cylindrical objects have been performed in the past, but few experiments have been performed with slender bodies. In this section, some relevant results and experimental procedures in the open literature are presented.

Awotahegn (2015) performed model tests with 8 and 12 inch (open ends) drill pipes, in model scale 1:16.67 and 1:33.3. The specifications in scale 1:16.67 are given in Table 1. The model tests were performed to investigate the trajectory and the seabed distribution. The experiment was performed in a 3 meter deep pool. The pipes were dropped with a clip from a position over the water surface, at 0, 30, 45, 60 and 90 degree initial drop angle. The motion was recorded in a visual manner with use of underwater cameras. The maximum pipe excursions were found for drop angels between 60 and 80 degree in both scales. After comparing the experimental data with DNV's recommendations for object excursion and hit probability (DNVGL , 2017), Awotahegn conclude that the methodology recommended is generally conservative (Awotahegn , 2015).

Table 1: *Scale 1:16.67 Awotahegn*

	Length	**Mass/Length**	**Outer diameter**
Pipe 8	0.5374 m	0.325 kg/m	0.0132 m
Pipe 12	0.5374 m	0.864 kg/m	0.0194 m

Aanesland (1986) performed two model tests. The first experiment with initial drop position over the water surface and the second experiment with initial drop position under the water surface. Aanesland used 1:9.54 and 1:20.32 scaled drill tubes and weight tubes with closed ends for the experiment. The specifications in scale 1:20.32 are given in Table 2. The cylinders were mounted in a clip, and dropped with initial drop angels at 0, 30, 45, 60 and 90 degrees into a 5 meter deep pool. The model tests were performed in order to investigate what happens when a drill tube is dropped from offshore platforms. The test was also used to verify a computer program simulating the motion of a freely dropped cylinder in water. The equations of motion were based on manoeuvring equations, corrected for viscous effects, using slender body theory.

Table 2: *Scale 1:20.32 Aanesland*

	Length	**Mass/Length**	**Outer diameter**
Drill tubes	0.45 m	0.079 kg/m	0.006 m
Weight tubes	0.45 m	0.548 kg/m	0.010 m

From the model test, Aanesland observed an interesting case related to directional stability of the motion. The cylinders were moving close to the vertical plane between the vertical global Z-axis and the cylinder axis, see Figure 8. Figure 4 clearly shows the phenomenon that the cylinder is pointing towards the centre of the target, indicating the actual plane of motion. This phenomenon strengthen the assumption that using two dimensional equations, a surge-heave-pitch equation system, to describe the cylinder trajectory, is reasonable (Aanesland , 1986).

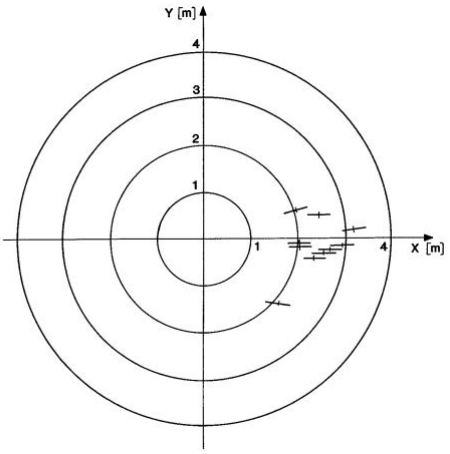

Figure 3: *Touchdowns on the bottom, $\alpha = 60°$, drop height=1.48 m and water depth= 2.46 m (Aanesland , 1987)*

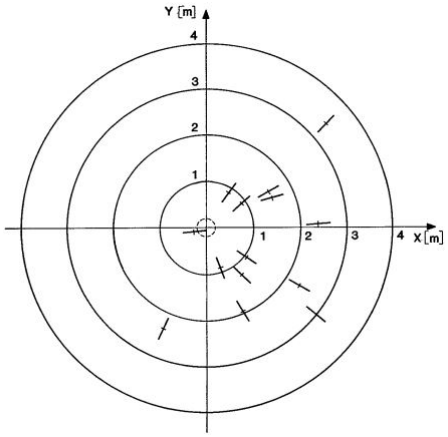

Figure 4: *Touchdowns on the bottom, $\alpha = 90°$, drop height=1.48 m and water depth= 4.92 m (Aanesland , 1987)*

Aanesland (1987) also observed how sensitive the cylinder touchdown point was to small changes in the conditions when it hit the water surface. This is illustrated in Figure 3 and Figure 4. The spreading of the touch down points illustrate the problem. It was observed that the cylinder was particularly sensitive to the angle between the cylinder axis and water surface, β (see Figure 8). In the model tests, Aanesland also observed a large time difference between a pure axial and a pure lateral motion. The time until the cylinder hit the bottom was significantly longer for the cylinders dropped with an initial angle $\beta = 0°$ compared to drops at higher initial angles. This showed that the viscous forces were more dominant in the lateral direction, than in the axial direction. From the experiments Aanesland (1986) also observed a number of different trajectories from the variety in initial drop angles, illustrated in Figure 5 (Aanesland , 1986).

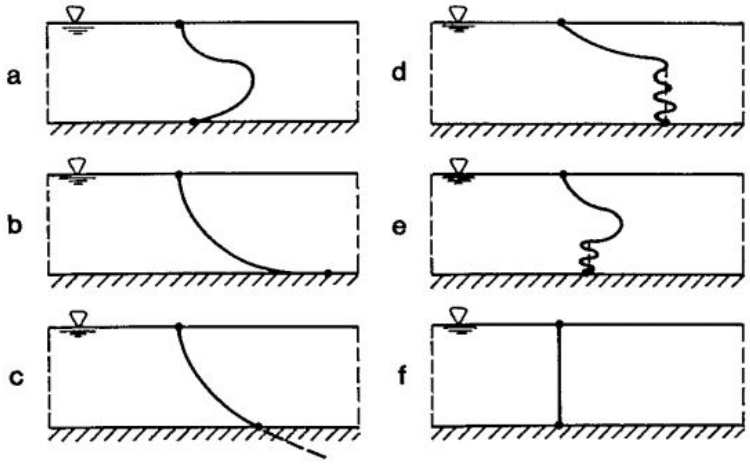

Figure 5: *Different paths followed by the cylinder (Aanesland , 1986)*

Aanesland (1986) compared the observed experimental touchdown points, the maximum excursions and the time until the cylinders hit the bottom, to the numerical calculations. A fairly good agreement between the experimental data and the equations of motion was found.

Yasseri (2014) and Chu et al. (2005) did experiments with cylinders (closed ends) dropped from an initial position over the water surface, by passing them through a tube. Three, non slender, cylindrical shapes which had a diameter of 4 cm, and lengths of about 9 cm, 12 cm and 15 cm, were used. The cylinders were dropped with three different centre of mass locations, and the initial drop angles were 15, 30, 45, 60 and 75 degrees. Six trajectory patterns were detected from the experiments. It was found that the transition between the patterns depended on the initial conditions, the initial angle, velocity and the physical parameters, such as length to diameter ratio and the centre of mass position. The centre of mass position had the largest influence of the trajectory of the cylinders. The experiments showed that the cylinders flipped only once for initial centre of mass positions located above the geometric centre. It was also found that the centre of mass position had the highest influence on the impact attitude on the bottom. This was due to the centre of mass affect if the cylinder hit the bottom in a parallel or vertical position (Chu et al. , 2005). Yasseri found that a lognormal distribution described the distance between the landing point and drop point fairly well. Summing up the data from several similar experiments, it was found that about 98% of the time objects land within 50% of the water depth (Yasseri , 2014).

1.4 Preparation of the experiments

In the experiment it was chosen to use cylinder dimensions that coincided with down scaled drill pipes. The model scale 1:20 was chosen because it was comparable with Aaneslands (1986) experiments and because it was the largest possible cylinders that could be tested according to the dimensions of the tank. It was preferable to keep the cylinders as large as possible considering the scaling effects. To ensure a controlled mechanism to drop the cylinders, it was decided to make a drop-rig with a magnet to release the cylinders. The magnet made the cylinders fall instantly without rotation, and it helped avoid possible undesirable influences, that e.g. passing the cylinder through a tube or dropping using a clip could have caused.

To track the position of the falling cylinders a three dimensional camera, based measurement system, was chosen. A Oqus camera system that made it possible to track the three dimensional cylinder trajectory and velocity at a quite high accuracy, was used. Compared to some of the earlier experiments, where more visual measurement systems were used, the Oqus camera system allowed for cylinder position tracking at a higher degree of accuracy and made it possible to find the cylinder velocity. The amount of experimental drops performed was also quit high, providing a wider understanding of the cylinder motion.

In the past, few experiments with slender cylindrical bodies with different centre of gravity locations have been performed. As studied by Yasseri (2014), for non slender cylindrical bodies, it was experienced that the centre of mass position had the highest influence on bottom impact attitude. The combination of a long slender body, that travels further than a not slender body, and a displaced centre of gravity were therefor found interesting to investigate in a worst case risk assessment study. Very few experiments comparing cylinders with closed and open ends have been performed in the past. Experiments on those two types of cylinders were found interesting since numerous offshore operations includes handling of drill pipes with and without end-caps.

2 Theory

This section gives an introduction and description of basic two dimensional theory of forces that affect a falling cylinder through the air phase, the water penetration and the water column phase. Main focus though, is on the fully submerged phase were a detailed theory is presented. For the air phase and the water penetrating phase, a simplified theory is outlined. The falling through the water column phase is described by using maneuvering equations corrected for viscous effects. This theory is presented for a cylinder with closed and open ends, and for cylinders with displaced centre of gravity. Finally, a method for scaling theory and similarity to experimental design is shared and DNV's simplified method for object excursion is presented.

2.1 Numerical investigation

2.1.1 Objects falling through air

Gravity forces make objects fall. Newton's 2nd law implies that the gravity force on a falling object is given by:

$$F_{grav} = mg \tag{1}$$

where m is the mass of the object and g the gravitational acceleration. The force due to air resistance works in the direction opposite to the motion and is proportional to the speed squared:

$$F_{air} = -kv^2 = -\frac{1}{2}\rho C_D A v^2 \tag{2}$$

where k is a constant that collects the effect of the density, drag and area. ρ is the air density, C_D is the drag coefficient, A is the area and v is the velocity of the falling object (Serway and Jewett , 2014). The total force acting on the falling object is given by:

$$F_{tot} = F_{grav} + F_{air} \tag{3}$$

However, for a relatively heavy object falling from lower heights, the air resistance is not of significance compared to the gravitational force. The velocity when the object hits the water surface, can therefore be expressed considering the conservation of kinetic- and potential energy. For an object falling from height h over the free water surface, the free water surface impact velocity is given by:

$$v = \sqrt{2gh} \tag{4}$$

2.1.2 The water entry face: 2D slamming theory

When a falling cylinder hits the free water surface, impulse loads will occur with high pressure peaks. These impulse loads, working during the cylinder impact with the water surface, are called slamming. It is assumed that the cylinder is in horizontal

position when going through an initially calm water surface with the constant velocity V (Faltinsen , 1990). An illustration of the model is shown in Figure 6.

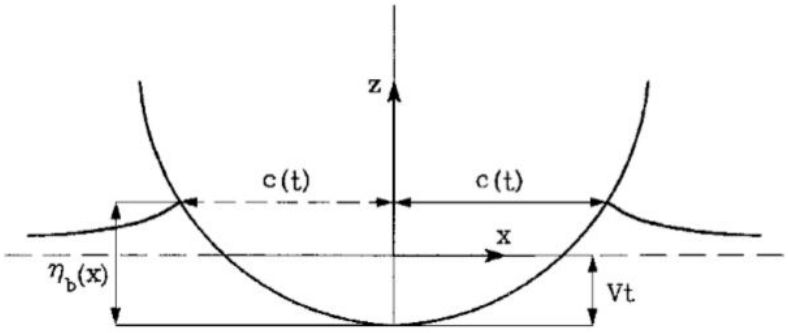

Figure 6: *Definition of parameters in the Wagner slamming model (Faltinsen , 1990)*

The submergence of the body is Vt, where t is the time variable. The wetted area of the cylinder is between the x-values $-c(t) \leq x \leq c(t)$. The wetted area due to spray is excluded because the pressure in the spray area is close to the atmospheric pressure. It is assumed that the fluid acceleration is much larger than the gravitational acceleration g, hence the problem is analysed using the free surface conditions $\phi = 0$ at $z = 0$. To solve the problem irrotational flow and incompressible fluid are assumed, and the cylinder is replaced by a flat plate with width $2c(t)$ in the mean free surface. Using the the body boundary condition for a flat plate and assuming that $Vt/c(t)$ is small, then the boundary value problem is as illustrated in Figure 7 (Faltinsen , 1990).

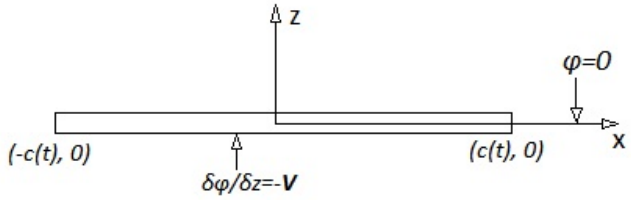

Figure 7: *Boundary value problem in simplified analysis of impact between a two dimensional body and water (Faltinsen , 1990)*

The velocity potential for the body can then be written as:

$$\phi = -V(c^2 - x^2)^{\frac{1}{2}}, \qquad |x| < c(t) \tag{5}$$

Then using the Bernoulli's equation, the pressure on the body can be found. Slamming occurs in a small time instant, meaning that the rate of change of ϕ with respect to x and z can be neglected because it is small compare to the rate of change of ϕ with time. The term $Vt/c(t)$ is also assumed to be small. Since the submergence of the body is

small, the hydrostatic pressure therm $-\rho gz$ is neglected. The hydrodynamic pressure can then be written as (Faltinsen , 1990):

$$p = -\rho \frac{\partial \phi}{\partial t} = \rho V \frac{c}{(c^2 - x^2)^{\frac{1}{2}}} \frac{dc}{dt} \tag{6}$$

The vertical force on the body is:

$$F_3 = \int_{-c}^{c} p dx = \rho V c \frac{dc}{dt} \int_{-c}^{c} \frac{dx}{(c^2 - x^2)^{\frac{1}{2}}} = V \frac{d}{dt} \left(\rho \frac{\pi}{2} c^2 \right) \tag{7}$$

To find the wetted body length ($\approx 2c(t)$) for a circular cylinder, the Wagner's approach is used. Defining that R is the cylinder radius, that gives the following expression for the wetted body length on a circular cylinder (Faltinsen , 1990):

$$c = 2\sqrt{VtR} \tag{8}$$

2.1.3 2D theory of cylinders falling trough water

There are several methods describing how to treat a falling cylinder in water theoretically, not only two dimensional methods, but also three dimensional methods. In this report a two dimensional method based on maneuvering equations, corrected for viscous effects will be considered. The theory will be based on how Aanesland (1987), Faltinsen (2005) and Hui and Faltinsen (2013) has presented it.

Figure 8 illustrates the coordinate systems used. The global coordinate system with $X - Y$ for the still water surface and Z vertically downwards, is used. The local coordinate system x, y, z, is fixed on the cylinder, with origin in in the centre of gravity. The x-axis is along the cylinder length. The two coordinate systems will coincide when the cylinder is horizontal at the water surface. β is the cylinder angle during the motion through the water, hence the angel between the local and the global x-axis. The cylinder geometry is defined by length L and diameter D. The X and Z-coordinates of the centre of gravity of the cylinder are denoted X_G and Z_G and x_T is the longitudinal position of the effective trailing edge (Faltinsen , 2005).

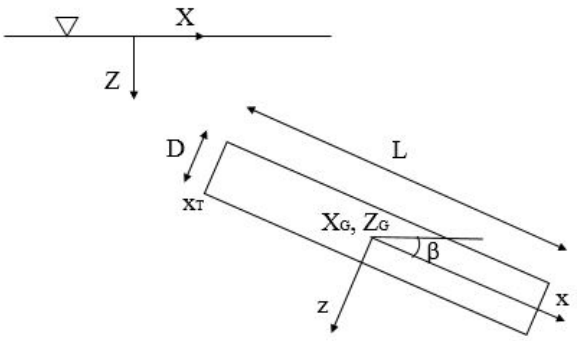

Figure 8: *Definition sketch of the local and global coordinate system.*

In the following equations, Equations 9, 10 and 11, it is assumed that the cylinder is moving as a rigid body, is slender, is symmetric about the centre of gravity and that the mass distribution is uniform (Aanesland , 1986). To describe the motions of the cylinder, two dimensional maneuvering equations based on slender body theory (Newman , 1977), corrected for viscous effects are used. Therefore only motions in the X-Z-plane will be considered. The velocity components are U_1 (surge), U_3 (heave) and Ω_2 (pitch) (Faltinsen , 2005), see Figure 9.

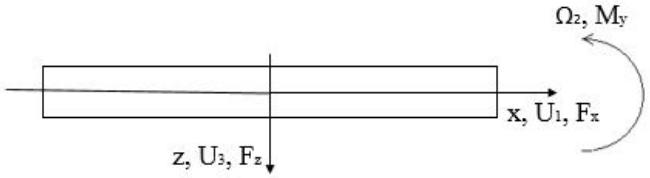

Figure 9: *Definition sketch for force and velocity direction.*

The equations of motion are given as (Hui and Faltinsen , 2013):

$$\underbrace{M\frac{dU_1}{dt}}_{\text{Inertial forces}} = \underbrace{F_{dx}}_{\text{Viscous force}} - \underbrace{(Mg-\rho g\nabla)\sin\beta}_{\text{Gravity and buoyancy force}} - \underbrace{MU_3\Omega_2}_{\text{Coriolis force}} \tag{9}$$

$$\begin{aligned}\underbrace{M(\frac{dU_3}{dt}-\Omega_2 U_1)}_{\text{Inertial forces}} = &-\underbrace{|U_1|U_3a_{33}+U_1\Omega_2x_Ta_{33}}_{\text{Lifting forces}} - \underbrace{A_{33}\frac{dU_3}{dt}}_{\text{Added mass force}} + \underbrace{F_{dz}}_{\text{Viscous force}} \\ &+ \underbrace{(Mg-\rho g\nabla)\cos\beta}_{\text{Gravity and buoyancy force}}\end{aligned} \tag{10}$$

$$\underbrace{I_{55}\frac{d\Omega_2}{dt}}_{\text{Inertial moment}} = \underbrace{U_1U_3x_Ta_{33}-|U_1|\Omega_2x_T^2a_{33}}_{\text{Lifting moment}} - \underbrace{A_{55}\frac{d\Omega_2}{dt}+A_{33}U_1U_3}_{\text{Added mass moment}} + \underbrace{M_{dy}}_{\text{Viscous moment}} \tag{11}$$

Where the variables are defines as follows:

β = instantaneous rotational angle between the cylinder axis and the free surface
M = cylinder mass
g = acceleration of gravity
ρ = density of water
∇ = volume of the cylinder
a_{33} = 2D added mass coefficient in heave direction at the trailing edge

x_T = longitudinal position of effective trailing edge
A_{33} = added mass in heave direction from strip theory
A_{55} = added mass in pitch direction from strip theory
I_{55} = moment of inertia in pitch direction

The motion equations above, referred to the body fixed coordinate system. The first equation, equation 9, is the force equilibrium in x-direction and the second equation, equation 10, is the force equilibrium in z-direction. Equation 11 is the moment equilibrium about the y-axis. x_T is introduced because the ends of the cylinder are not pointed. In slender body theory, smoothly varying geometries are assumed. The end of the cylinder dose not satisfy this assumption. An additional force component is therefore included to consider the trailing edge effect. The trailing edge effect is determined by the position of the effective trailing edge, x_T and the mass distribution coefficient at the trailing edge in 2D, a_{33} (Aanesland , 1986). The two dimensional added mass in heave and pitch direction from strip theory and the moment of inertia in pitch direction can be defined as follows (Pettersen , 2007):

$$a_{33} = \rho\pi\frac{D^2}{4} \tag{12}$$

$$A_{33} = \int_L a_{33}dx = a_{33T}L \tag{13}$$

$$A_{55} = \int_L x^2 a_{33}dx = a_{33T}\frac{L^2}{12} \tag{14}$$

$$I_{55} = M\frac{L^2}{12} \tag{15}$$

According to Faltinsen (2005), the longitudinal viscous force can be expressed as in Equation 16, where C_F is the friction coefficient assuming turbulent axis symmetric flow along a smooth surface. The expression of the friction coefficient is based on White (1972), assuming $10^6 < Rn < 10^9$ for a purely longitudinal motion.

$$F_{dx} = -0.5\rho C_F \pi DLU_1|U_1| - \frac{\rho}{8}\pi C_{dx}D^2U_1|U_1| \tag{16}$$

$$C_F = 0.0015 + (0.30 + 0.015(\frac{2L}{D})^{0.4})Rn^{-1/3} \tag{17}$$

The remaining viscous force and moment can be elevated from the following equations (Aanesland , 1987):

$$F_{dz} = 0.5 \int_L \rho C_{dz} D u_z(x) |u_z(x)| dx \tag{18}$$

$$M_{dy} = -0.5 \int_L \rho C_{dz} D x u_z(x) |u_z(x)| dx \tag{19}$$

where

D	=	diameter of the cylinder
ν	=	kinematic viscosity of water
L	=	length of the cylinder
C_{dx}	=	2D drag coefficient in x-direction
C_{dz}	=	2D drag coefficient in z-direction
Rn	=	Reynolds number : $U_1 L/\nu$

The viscous drag in z-direction, and the moment about the y-axis are estimated using Morisons formula (Aanesland , 1987). The relative velocity normal to the cylinder axis, $U_z(x)$, can be expressed as (Xiang , 2017):

$$U_z(x) = -(U_3 - \Omega_2 x), -0.5L < x < 0.5L \tag{20}$$

When inserting Equation 20 into Equation 18 and 19 the following equations are obtain:

$$F_{dz} = 0.5 \int_{-0.5L}^{0.5L} \rho C_{dz} D U_z(x) |U_z(x)| dx = -0.5 \rho C_{dz} D \int_{-0.5L}^{0.5L} (U_3 - \Omega_2 x) |U_3 - \Omega_2 x| dx \tag{21}$$

$$M_{dy} = -0.5 \int_{-0.5L}^{0.5L} \rho C_{dz} D x U_z(x) |U_z(x)| dx = 0.5 \rho C_{dz} D \int_{-0.5L}^{0.5L} x (U_3 - \Omega_2 x) |U_3 - \Omega_2 x| dx \tag{22}$$

Then the positions of the centre of gravity for the cylinder, according to the global coordinate system, can be expressed by the following relationships (Faltinsen , 2005):

$$\frac{dX_G}{dt} = U_1 \cos\beta + U_3 \sin\beta \tag{23}$$

$$\frac{dZ_G}{dt} = U_3 \cos\beta - U_1 \sin\beta \tag{24}$$

$$\frac{d\beta}{dt} = \Omega_2 \tag{25}$$

2D theory for cylinders falling through water with displaced centre of gravity

The two dimensional method based on maneuvering equations can also be extended to describe the behaviour of a falling cylinder with displaced centre of mass, as illustrated in Figure 10.

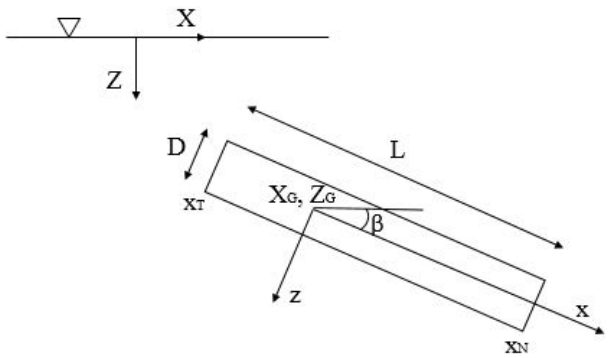

Figure 10: *Definition sketch of the local and global coordinate system for cylinder with displaced centre of gravity.*

Due to the displaced centre of mass the lifting force and lifting moment can be expressed as (Hui and Faltinsen , 2013):

$$F_3^l = U_1 U_3 [a_{33}(x)]_{x_T}^{x_N} - U_1 \Omega_2 [x a_{33}(x)]_{x_T}^{x_N} \tag{26}$$

$$F_5^l = -U_1 U_3 [x a_{33}(x)]_{x_T}^{x_N} - U_1 \Omega_2 [x^2 a_{33}(x)]_{x_T}^{x_N} \tag{27}$$

According to witch cylinder end that is the foremost the two dimensional added mass coefficient in heave direction can be expressed as:

$$U_1 > 0 : \begin{cases} a_{33}(x_N) = 0 \\ a_{33}(x_T) = \rho \pi \frac{D^2}{4} \end{cases} \tag{28}$$

$$U_1 < 0 : \begin{cases} a_{33}(x_N) = \rho \pi \frac{D^2}{4} \\ a_{33}(x_T) = 0 \end{cases} \tag{29}$$

where x_N and x_T are x-coordinates of the head and rear end of the cylinder respectively. Due to the displaced centre of gravity one also gets an additional moment due to buoyancy force. This additional moment is given as:

$$B_5 = \rho g \nabla \cos \beta \Delta_{CB} \tag{30}$$

where Δ_{CB} is the distance from the cylinder volume centre to the centre of gravity. The Added mass forces and moment becomes equal:

$$F_1 = -A_{33}U_3\Omega_2 - A_{35}\Omega^2 \tag{31}$$

$$F_3 = -A_{33}\frac{dU_3}{dt} - A_{35}\frac{d\Omega_2}{dt} \tag{32}$$

$$M_5 = -A_{53}\frac{dU_3}{dt} - A_{55}\frac{d\Omega_2}{dt} + A_{33}U_1U_3 + A_{35}U_1\Omega_2 \tag{33}$$

where the added mass in heave and pitch due to motion in pitch is given as follows:

$$A_{35} = -\int_L xa_{33}dx = -a_{33}\Delta_{CB} \tag{34}$$

$$A_{55} = a_{33T}\frac{L^2}{12} + L\Delta_{CB}^2 a_{33} \tag{35}$$

Then the equations of motion for a cylinder with displaced centre of gravity is given as:

$$\underbrace{M\frac{dU_1}{dt}}_{\text{Inertial forces}} = \underbrace{-A_{33}U_3\Omega_2 - A_{35}\Omega_2^2}_{\text{Added mass forces}} + \underbrace{F_{Dx}}_{\text{Viscous force}} \underbrace{-(Mg - \rho g\nabla)\sin\beta}_{\text{Gravity and buoyancy force}} - \underbrace{MU_3\Omega_2}_{\text{Coriolis force}} \tag{36}$$

$$\underbrace{M(\frac{dU_3}{dt} - \Omega_2U_1)}_{\text{Inertial forces}} = \underbrace{U_1U_3[a_{33}(x)]_{x_T}^{x_N} - U_1\Omega_2[xa_{33}(x)]_{x_T}^{x_N}}_{\text{Lifting forces}} \underbrace{-A_{33}\frac{dU_3}{dt} - A_{35}\frac{d\Omega_2}{dt}}_{\text{Added mass force}} \underbrace{+F_{Dz}}_{\text{Viscous force}} \underbrace{+(Mg - \rho g\nabla)\cos\beta}_{\text{Gravity and buoyancy force}} \tag{37}$$

$$\underbrace{I_{55}\frac{d\Omega_2}{dt}}_{\text{Inertial moment}} = \underbrace{-U_1U_3[xa_{33}(x)]_{x_T}^{x_N} - U_1\Omega_2[x^2a_{33}(x)]_{x_T}^{x_N}}_{\text{Lifting moment}} \underbrace{-A_{53}\frac{dU_3}{dt} - A_{55}\frac{d\Omega_2}{dt} + A_{33}U_1U_3 + A_{35}U_1\Omega_2}_{\text{Added mass moment}} \underbrace{+M_{Dy}}_{\text{Viscous moment}} \underbrace{+\rho g\nabla\cos\beta\Delta_{CB}}_{\text{Buoyancy moment}} \tag{38}$$

2D theory of cylinder with open ends falling in water

The two dimensional method based on maneuvering equations has also been suggested in order to describe the behaviour of a cylinder with open ends falling in water. Two changes to the theory for a closed cylinder described above are suggested. First, there will be an increase in the added mass and lift forces and moment, due to the water flowing through. This is suggested to be modelled by increasing the two dimensional added mass coefficient, described as follows:

$$a_{33} = \rho\pi\frac{(D_{out} + D_{in})^2}{4} \tag{39}$$

where D_{out} and D_{in} is the outer and inner cylinder diameter. Secondly C_F, the friction coefficient, is increased due to a larger wet surface.

2.2 Similarity to experimental design

When performing model tests, the physical models are intended to represent the full scale system as close as possible, but in a much smaller scale. To achieve similarity in forces between model and full scale, there must be geometric similarity, kinematic similarity and dynamic similarity (Steen , 2014).

2.2.1 Geometric similarity

Geometrical similarity means that the structure in model and full scale has the same shape. Then a constant length scale exists:

$$\lambda = \frac{L_F}{L_M} \tag{40}$$

Where L_F and L_M is any dimension of the structure in full and model scale respectively. It is not just for the structure, equal length ratio is required, but also for the surrounding environment (Steen , 2014).

2.2.2 Kinematic similarity

Kinematic similarity requires that the length-scale and the time-scale ratios are equal for model and full scale. The result is that the ratio between the velocity in model scale has to be equal the corresponding velocity ratio in full scale. If dynamic and geometric similarity is achieved, kinematic similarity is also achieved (Steen , 2014).

2.2.3 Dynamic similarity

Dynamic similarity is achieved if the length-scale, time-scale and force-scale ratios are the same for model and full scale (Steen , 2014). For a falling cylinder in water the viscous forces will be most important. Equality in Reynolds number between full scale and model scale will ensure that the viscous forces are correctly scaled. The scaling factors for Reynolds similarity are given in Table 3.

Viscous forces and moments depend on the drag coefficient (see equations 16, 18 and 19). C_{dx}, the drag coefficient in the along-cylinder direction depends less on the axial Reynolds number. For a cylinder falling trough the water column the drag coefficient in the along-cylinder direction depends more on the length to diameter ratio, $\delta = L/D$. The drag coefficient across the cylinder, C_{dz}, depends on the Reynolds number (Equation 41). V is the velocity, D is the cylinder diameter and ν is the water viscosity (Chu et al. , 2005).

$$R_e = \frac{VD}{\nu} \tag{41}$$

Table 3: *Scaling factors for Reynolds similarity (Kirkegaard et al. , 2011)*

Parameter	**Reynolds**
Length, Diameter- $\frac{L_M}{L_F}$	$\frac{1}{\lambda}$
Time- $\frac{t_M}{t_F}$	$\frac{1}{\lambda^2}$
Velocity- $\frac{U_M}{U_F}$	λ
Mass- $\frac{m_M}{m_F}$	$\frac{1}{\lambda^3}$
Force- $\frac{F_M}{F_F}$	1

According to Aanesland (1986), the drag coefficient in z-direction is supposed to be in the Subcritical area of Reynolds numbers in model scale, from about 1000 to 10000, see Figure 11. This results in a drag coefficient between 0.8 and 1.4. In full scale conditions the Reynolds number will, for most cases, be in the Post-super critical flow range. This implies that the viscous drag forces are in many cases significantly over-predicted in model tests. The Reynolds dependency will in general be different for different cases, meaning that the scaling method can only give a rough estimate of the scale effects. In general conditions no accurate procedure for scaling of drag forces exists (Steen , 2014).

	A Subcritical	B Critical	C Supercritical	D Post-supercritical
Boundary layer	laminar	transition	turbulent	turbulent
Separation	about 82 deg.	transition	120 - 130 deg.	about 120 deg.
Shear layer near separation	laminar		laminar separation, bubble turbulent reattachment	turbulent
Strouhal number	$S = 0.212 - \frac{2.7}{Re}$	transition	0.35 - 0.45	about 0.29
Make	Re<60 laminar; 60<Re<5000 vortex street Re > 5000 turbulent	not periodic		
Approximate Re range	$< 2x10^5$	$2x10^5$ to $5x10^5$	$5x10^5$ - $3x10^6$	$> 3x10^6$

Incompressible flow regimes and their consequences.

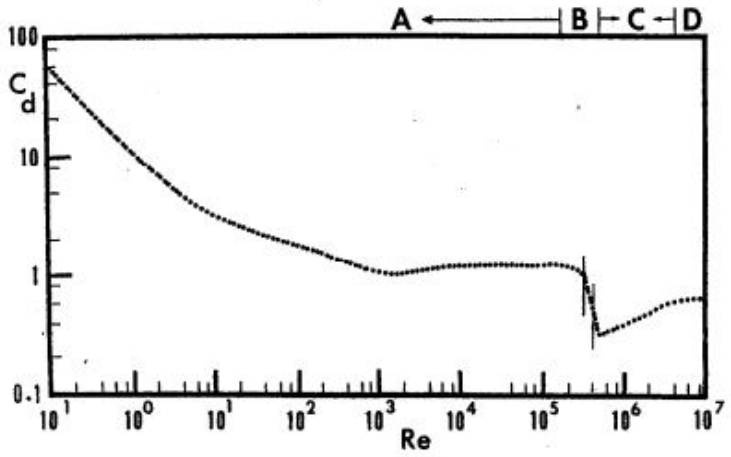

Figure 11: *Drag coefficient for circular cylinder in steady incident flow (Steen , 2014)*

2.3 DNV's simplified method

The DNV's recommended practice for dropped object risk assessments is given in DNVGL-RP-F107 (DNVGL , 2017). The recommended practice present a simplified and analytic approach to define the dropped object's lateral deviation, impact damage and hit probability. Simplified shapes are used in the method, as specified in Table 4. A normal distribution given in Equation 42 is used to describe the object excursion onto the sea bed for each of the object categories. It is stated that for shallower water depths, current has a limited effect on the object excursion and therefore does not has to be taken into account. At deeper water depths, it says that the effect of currents becomes more pronounced.

$$p(x) = \frac{1}{\sqrt{2\pi}\delta} e^{\frac{1}{2}(\frac{x}{\delta})^2} \tag{42}$$

An angular deviation, α, is assigned based on object shape and weight. Based on this

values the lateral deviation, δ, can be found for the given water depth d (see Figure 12).

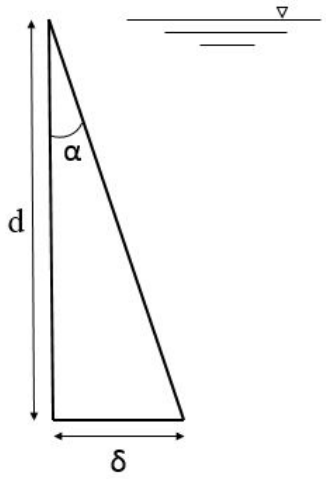

Figure 12: *DNV's simplified method for calculation of lateral deviation of dropped objects (DNVGL , 2017).*

Table 4 gives the angular deviations related to weight and shape for objects that are recommended for use in calculations of object excursion onto the seabed. A spread on the surface before the objects sinks is included.

Table 4: *DNV's recommended angular deviation for the different object categories (DNVGL , 2017).*

No	Description	Weight [tonnes]	Angular deviation α [deg]
1	Flat/Longed shaped	<2	15
2		2 - 8	9
3		>8	5
4	Box/round shaped	<2	10
5		2 - 8	5
6		>8	3
7	Box/round shaped	>>8	2

Considering object excursions in deep water, DNV refers to the Katteland and Øygarden (1995) report that states that from 180 meter depth and further down, the spreading will not increase significantly and may conservatively be set constant. It is also remarked that at deep water depths, the spreading of objects on the seabed will not necessarily follow the normal distribution.

3 Method and test set-up

3.1 Experiments

This section describes the experimental set-up, how the experiment was performed and the different cylindrical models used in the experiment.

3.1.1 Experimental set-up

The experiments were carried out in Dokka, a tank owned by SINTEF Ocean. The dimensions of the tank are 6 meter width, 12 meter length and 5 meter water dept. This is illustrated in Figure 13 and 14 representing the experimental set-up for cylinders with closed and open ends, respectively (see also Figure 15 and 16). The cylinders were dropped from the drop-rig at two different initial positions, one over and one under the free water surface. The cylinders were dropped from 65 centimetre height in horizontal position over the water surface. Under the water surface, the cylinders were dropped from a fully submerged position. The cylinders were dropped from the drop-rig with initial drop angles of 15, 30, 45, 60 and 75 degrees so that the cylinders in Figure 13 travelled away from the cameras and the cylinders in Figure 14 travelled in the direction normal to cameras. Zero degrees is when the cylinder is parallel to the water surface.

As illustrated in Figure 13 and 14, the cylinder trajectory and velocity were tracked by four Oqus cameras placed at the right hand side of the tank on two bars. The camera positions were 1.25 and 3.75 meter respectively over the tank floor at both bars, and the distance between the bars were 2.13 meter in Figure 13 and 2.40 meter in Figure 14. Oqus are high-speed motion capture cameras that track a marker position through a three dimensional motion. The Oqus cameras emit light at a frequency of 179 hertz, and pick up reflections from the marker. If two cameras can see the marker, the cylinder position can bee tracked. In this experiment the markers were placed at the rear cylinder end, witch was the cylinder end pointing towards the cameras for the experimental set-up in Figure 13.

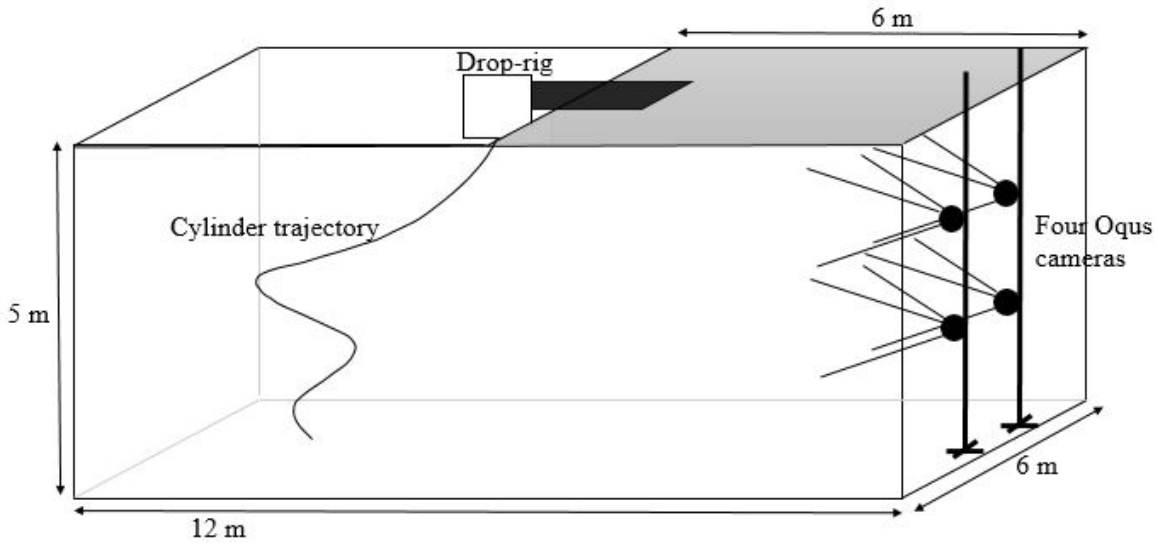

Figure 13: *Description of the experimental set-up for the cylinders with closed ends.*

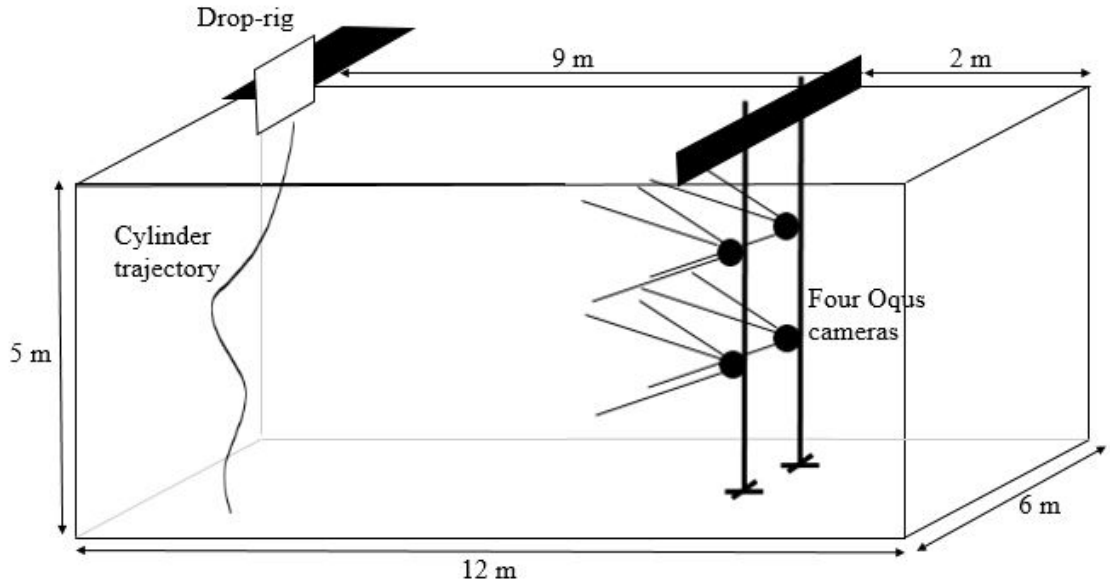

Figure 14: *Description of the experimental set-up for the cylinders with open ends.*

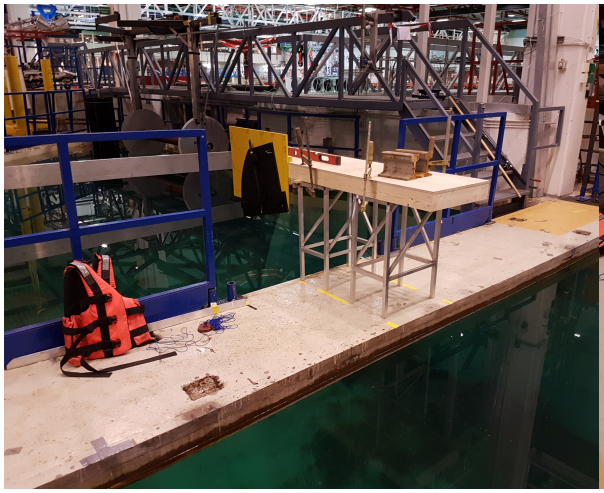

Figure 15: *Picture of the experimental set-up for cylinders with closed ends. The drop-rig is mounted for initial drop positions over the water surface.*

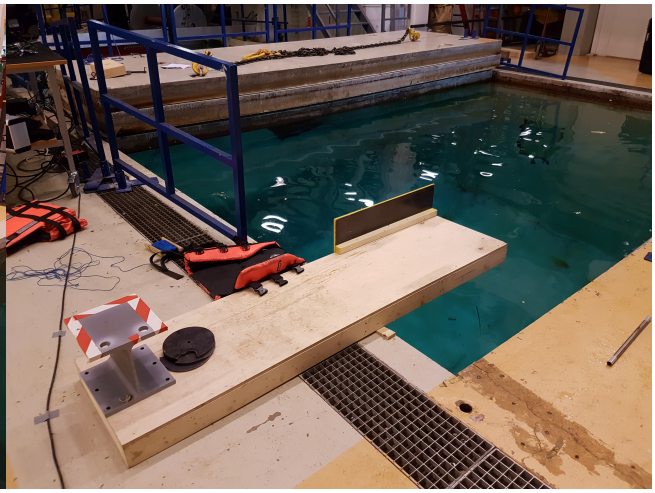

Figure 16: *Picture of the experimental set-up for cylinders with open ends. The drop-rig is mounted for initial drop positions under the water surface.*

The drop-rig mounted for drops over and under the water surface is illustrated in Figure 17 and 18. To release the cylinder a magnet was used, the mechanism is illustrated in Figure 19. The magnet consists of a bar, with a magnet attached to the end of the bar. As illustrated in the figure, the magnet was placed through a pipe. Pulling the magnet in the direction indicated in the figure, made the cylinder drop without any rotation. The pin to adjust the drop angle is also indicated in the figure.

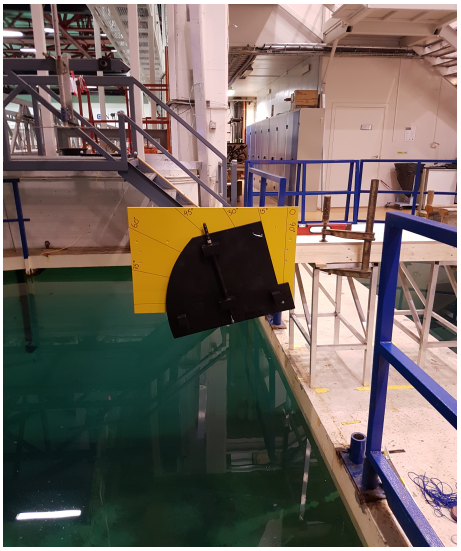

Figure 17: *Drop-rig mounted for initial drop position over the water surface*

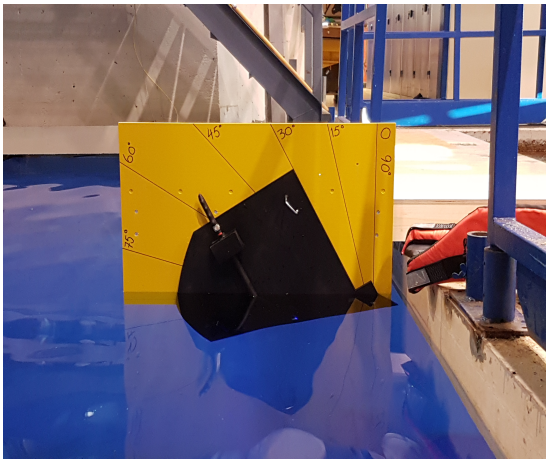

Figure 18: *Drop-rig mounted for initial drop position under the water surface*

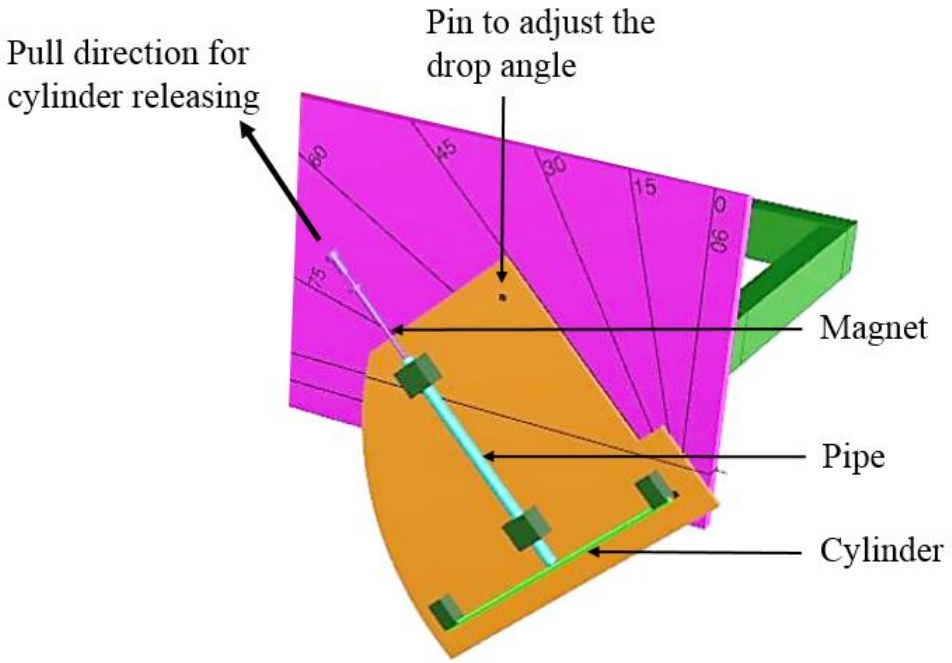

Figure 19: *Description of the drop-rig*

Seven different cylinder types were used through the experiments. All cylinders used were at the same length, 0.45 meter. Different cylinder diameters and centre of gravity locations were tested. 10, 16 and 19 millimetre cylinder diameters were used in the experiments. For the 10 millimetre diameter cylinders, tests were the centre of gravity was displaced by 1.4 and 3.0 centimetre from the volume centre were also performed. The cylinders used were steel pipes. Both pipes with open ends and hence water flow through and pipes with sealed ends with air inside, were used. An overview of the cylinder types is showed in Table 5 and a detailed description specifying weight and dimensions is given in Table 6.

Table 5: *Description of the seven different cylinder types tested during the experiment.*

	Description of the cylinder type
Cylinder 1	A 10 millimetre diameter cylinder with closed ends
Cylinder 2	A 16 millimetre diameter cylinder with closed ends
Cylinder 3	A 19 millimetre diameter cylinder with closed ends
Cylinder 4	A 10 mm diameter cylinder with closed ends and the centre of gravity displaced 1.4 cm from the cylinder volume centre
Cylinder 5	A 10 mm diameter cylinder with closed ends and the centre of gravity displaced 3 cm from the cylinder volume centre
Cylinder 6	A 10 mm diameter cylinder with open ends. Wall thickness 1 mm
Cylinder 7	A 19 mm diameter cylinder with open ends. Wall thickness 1.25 mm

Table 6: *Specifications of the cylinders. The COG column describes the position of the centre of gravity indicating the distance from the cylinder volume centre.*

	Model scale 1:20				Full scale			
	Mass	**Length**	**Diameter**	**COG**	**Mass**	**Length**	**Diameter**	**COG**
Cylinder 1	97 g	45 cm	10 mm	0 cm	776 kg	9 m	0.20 m	0 m
Cylinder 2	203 g	45 cm	16 mm	0 cm	1624 kg	9 m	0.32 m	0 m
Cylinder 3	240 g	45 cm	19 mm	0 cm	1920 kg	9 m	0.38 m	0 m
Cylinder 4	105 g	45 cm	10 mm	1.4 cm	840 kg	9 m	0.32 m	0.28 m
Cylinder 5	114 g	45 cm	10 mm	3 cm	912 kg	9 m	0.32 m	0.6 m
Cylinder 6	94 g	45 cm	10 mm	0 cm	750 kg	9 m	0.20 m	0 m
Cylinder 7	231 g	45 cm	19 mm	0 cm	1848 kg	9 m	0.38 m	0 m

Figure 20 shows the cylinders used in the experiments, one 10, one 16 and one 19 millimetre diameter cylinder is pictured. The cylinder marker tape can be seen on the right hand side of the cylinder. There were also a circular marker attached to the right cylinder ends.

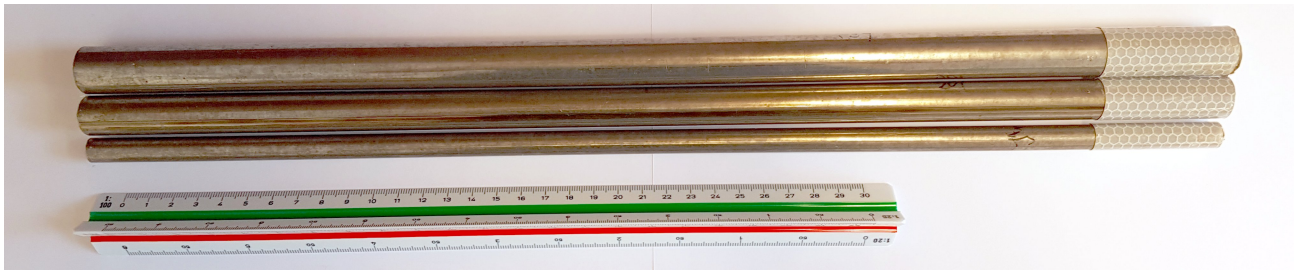

Figure 20: *The cylinders used in the experiment.*

In full size dimensions the experiments will approximately coincide with 8, $12\frac{2}{3}$ and $13\frac{1}{3}$ inches drill pipes dropped drop from 13 meter above the sea surface, or at a position under the surface. In full scale the water depth will correspond to a sea depth equal 100 meter.

3.1.2 Test matrix

The experiments were performed with seven different cylinder types, as specified in Table 6 and Table 5. For the closed end cylinders with different diameters, Cylinder 1, 2 and 3, drops over and under the water surface were performed, at 15, 30, 45, 60 and 75 degree initial drop angle. For cylinders with displaced centre of gravity, Cylinder 4 and 5, the initial drop positions were under the water surface, and they were dropped at 15, 30, 45, 60 and 75 degree angle. The cylinders with open ends were also dropped from an initial position under the water surface, at 15, 30, 45, 60 and 75 degrees drop angle.

The number of drops that were executed for each drop angle is given in the Table 7, which shows the test matrix. In general, at least eight drops at each drop condition were performed, but as can bee seen from the table, some conditions have fewer drops. This is because of some poor measurements. For some initial conditions where large variations were observed, some additional drops were performed. For each of the two centre of gravity displaced cylinders, Cylinder 4 and 5, two set of tests were performed. First a set with the initial centre of gravity positioned above the volume centre and then a set with the initial centre of gravity positioned under the cylinder volume centre. For each cylinder type, at least four cylinders were used. This was done to detect if some of the cylinders behaved different to the others.

Table 7: *The test matrix. The table shows the number of measurements for each initial drop condition. Cylinder 4 and Cylinder 5 is dropped in two series, with the initial position of the centre of gravity placed over and under the cylinder volume centre.*

	Drop under the water surface					**Drop over the water surface**				
	15°	30°	45°	60°	75°	15°	30°	45°	60°	75°
Cylinder 1	8	7	8	8	8	8	8	8	8	8
Cylinder 2	8	8	7	14	8	8	8	8	8	16
Cylinder 3	8	8	8	15	15	6	8	8	16	16
Cylinder 4	8	8	7	8	8					
Cylinder 4	8	8	8	8	8					
Cylinder 5	8	8	8	8	8					
Cylinder 5	8	8	8	8	8					
Cylinder 6	8	8	8	8	8					
Cylinder 7	0	7	8	8	8					

3.1.3 Post-processing

The Oqus camera system saved the measured data in structured arrays in MATLAB format. The raw data were X-, Y- and Z-cylinder marker position data, sampled with a sample frequency of 179 hertz. These data were plotted by use of MATLAB. The position plots are presented in Appendix A. By studying the graphs, it can be observed that some of the graph lines are quite smooth, while others are more jagged. This is because the *smooth*-function in MATLAB was used for some of the plots. For some plots though, the notches in the measurements were so large that using the *smooth*-function would have changed the trajectories. The *smooth*-function was hence not used for these plots. For the X-Z-plots in Appendix A, the X-coordinates are transformed from the X-Y-plane, so that that the X-position in these plots represents the actual cylinder travelling distance in the X-Y-plane (This is referred to as radial excursion).

The velocity plots in Appendix B were calculated by dividing the distance between two measurements by the time between each measurement. This is expressed by the blue colour in Figure 21. In the velocity calculations, some illogical peaks were de-

tected. The largest peaks were identified and removed. They were identified by comparing each point with values two steps to the left and two steps to the right. If the difference was larger than 0.2, the point was replaced by the mean of the two values the point was compared to. This is illustrated by the red colour in Figure 21. The MATLAB *smooth*-function was used to draw a line through the data, shown as a green line in Figure 21.

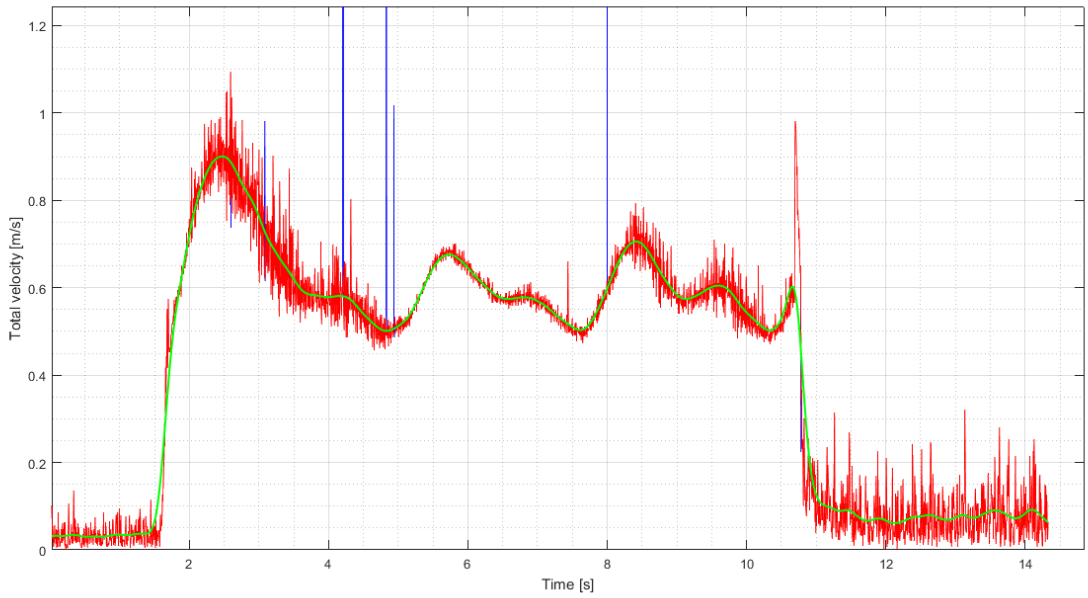

Figure 21: *Example illustrating the Post-processing of the velocity plots. Blue colour illustrates the calculated velocity from the position data, red colour is the calculated velocity with the largest peaks removed and green colour is a line fitted to this data in order to draw a line for the velocity development.*

3.2 Numerical calculations

The numerical calculations were performed for some of the cylinder types as described in Table 6, using the model scale 1:20 with the drop angels, β, set to 15, 30, 45, 60 and 75 degrees. This corresponded to the experiments performed as described in Section 3.1. The numerical calculations were done implementing and solving the equations present in Section 2.1.3, in this report, in MATLAB. Thereby the calculated trajectories and velocities are for cylinders dropped from a fully submerged condition, staring at rest without velocity and acceleration. The time step used were 0.01 seconds. To integrate over the differential equations Runge Kutta's 4th order method was used. This is a method that uses numerical integration to solve ordinary differential equations (Kreyszig , 2006). The acceleration of gravity was set to 9.8085 m/s^2, the water viscosity to $1.14 \cdot 10^{-6} m^2/s$ and the density equal to 1000 kg/m^3. The longitudinal drag coefficient, C_{dx}, was set to 0.65 according to Hoerner (1958).

The drag coefficient in z-direction, C_{dz}, will for a dropped cylinder vary with time. According to experiments performed by Sarpkaya (1966) the drag coefficient will first increase rapidly to about 1.5 and then decrease slowly to about 1.2. Figure 22 shows experimental data for the lateral drag coefficient for a circular cylinder with nearly impulsively started laminar boundary layer flow as a function of non-dimensional time. The effect from using values from 0.6 to 1.4 will be shown.

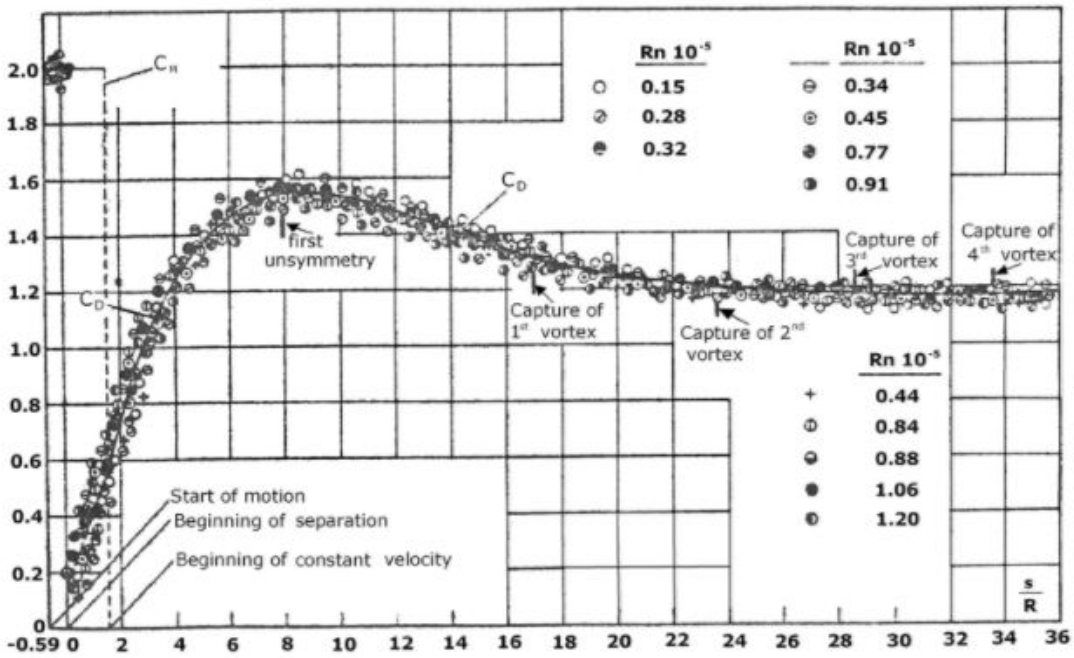

Figure 22: *Lateral drag coefficient, C_{dz}, for a circular cylinder in nearly impulsively started laminar flow. The particle motion s of the ambient low is defined by $\frac{s}{R} = \int_{t_0}^{t} U_3 dt/R$. R is the radius and U_3 is the velocity of cross flow. (Sarpkaya , 1966).*

Further, the influence of the tail effects will be investigated using different positions ,x_T, of the effective trailing edge. The upper limit investigated is $x_T = 0.5L$ which is the geometric trailing edge and the lower limit investigated is $x_T = 0.3L$, which is a value often used in maneuvering of ships with a blunt aftbody (Aanesland , 1986).

4 Results and discussion

This section presents the results found from the experiments and from the numerical calculations. First the experiment findings will be discussed and compared to DNV's recommended practice for calculation of object excursion. Further the numerical calculations will be compared to the experimental results and then the validity of the numerical calculations will been discussed.

4.1 Experimental results

The Appendix gives a complete overview of the experimental results. Here the trajectories found form the experimental data is represented from a X-Y-view, a X-Z-view and a three dimensional view. Equal colour in the X-Y-view, the X-Z-view and the three dimensional view indicates the same drop, but showed from different directions. The X-axis in the X-Z-view plots show radial coordinates (travel length) from the X-Y-plane. First drops of 10, 16 and 19 millimetre cylinders with closed ends, dropped from under and over the water surface, are represented in Appendix A.1-A.3 and Appendix A.4-A.6. Then drops of 10 and 19 millimetre cylinders with open ends, dropped from under the water surface, are given in Appendix A.6 and A.7. Further, drops of 10 millimetre cylinders with the centre of gravity displaced with 1.4 and 3 centimetre, dropped with the initial centre of gravity positions over and under the cylinder volume centre are presented in Appendix A.9-A.12. In each of the figures in Appendix A, eight drops are represented, with some deviations. The current initial condition is specified in the figure caption. The trajectories given in Appendix, shows in general the position of the rear cylinder end, with some exceptions. The exceptions are for the cylinder with the centre of gravity displaced 1.4 cm, dropped with the gravity centre upward at 15, 30 and 45 degrees drop angle. Here the leading cylinder end position were measured.

Appendix B gives the total velocity of the rear cylinder end as a function of time and depth. Each plot line in the figures represents an example of the total velocity development for the relevant cylinder and drop angle. The velocity plots for 10, 16 and 19 millimetre diameter cylinders with closed ends, dropped from under and over the water surface, are given in Appendix B.1-B.3 and Appendix B.4-B.6. The velocity plots for the 10 and 19 millimetre diameter cylinders, with open ends, are given in Appendix B.7 and B.8. Finally the velocity of 10 millimetre cylinders with the centre of gravity displaced with 1.4 and 3 centimetre, with initial centre of gravity positions over and under the cylinder volume centre, are presented in Appendix B.9-B.12.

In Appendix C, tabled position data is given for the different cylinders dropped. The mean value and the associated standard deviations are given for the radial excursion (x-position), the depth (z-position) and the y-position at different positions. Position data are given for the first and second turn in the trajectory, and at three and four meter depth. Appendix D gives tabled data for the average maximum velocity with associated standard deviation for the different drop angles.

By studying the graphs, it is observed that some are not totally smooth, but are a bit jagged. There is also some graphs that are broken and have some illogical peaks. This is due to some poor measurements. It could be expected that the actual motion pattern for these graphs followed the same trends as indicated by the smooth graph lines. In addition quite many measurements did not reach the tank floor, this is mainly due to the orientation of the marker relative to the Oqus cameras. It could also be useful to note that several of the cylinders that turned much in the X-Y-plane has shorter measurements because of the marker orientation and the fact that some of the cylinders hit the tank walls.

4.1.1 The trajectories observed from the experiment

Cylinders with no displacement of the centre of gravity

Typical trajectories observed from the experiment for closed and open end cylinders with centre of gravity placed in the cylinder volume centre are shown in Figure 23. These are trajectories that were observed at 15, 30, 45, 60 and 75 degree drop angles in a five meter deep tank. If the cylinders were dropped at 0 or 90 degrees, an additional trajectory would have been observed. The cylinders would have fallen straight to the bottom, either with the longitudinal axis parallel with the vertical axis in water or with the longitude axis oriented horizontally.

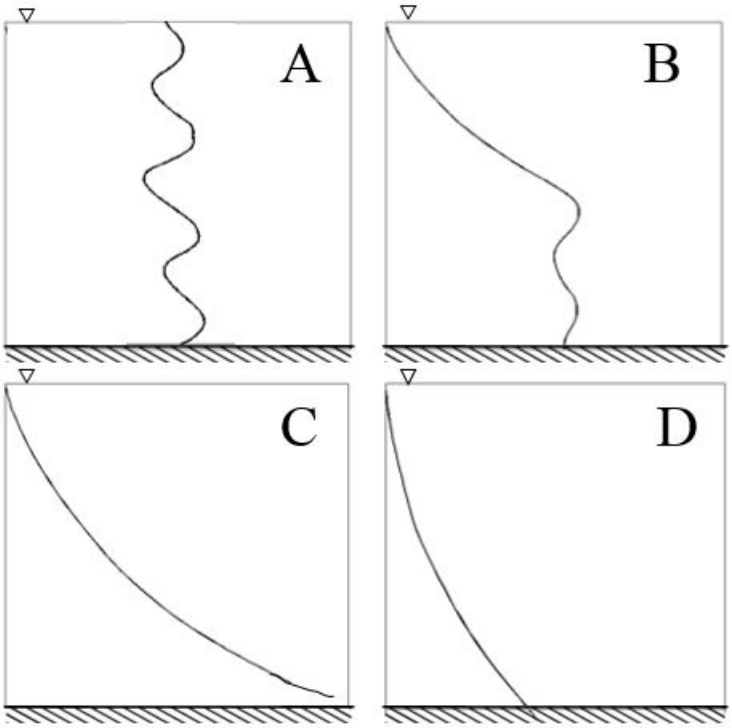

Figure 23: *Two dimensional X-Z-view: Trajectories of cylinders with centre of gravity placed in the cylinder volume centre found from the experiments.*

Trajectory A, in Figure 23, were observed for drops from an initial position under the water surface at 15 degree initial angle for a 19 millimetre diameter closed end cylinder. It was also found for drops from an initial position over the water surface at 15 degree initial angle, and for 19 and 16 millimetre cylinders with 30 degree drop angle (see Appendix A.3.5, A.4.1, A.5.1, A.6.1, A.5.2 and A.6.2). The cylinder angle and velocity will decrease almost immediately and the cylinder angel will go to zero and rotate further to an increasingly negative angle. When the longitudinal velocity is zero the cylinder will change the direction of motion and start to fall towards the bottom with an oscillatory horizontal motion, like a "falling leaf in air". This oscillating motion between the positive and negative x-direction (see Figure 8 for the axis system) will continue until the cylinder hits the bottom at an orientation close to horizontal. An illustration of the cylinder orientation during the oscillating motion can be seen in Figure 24 after a drop through approximately 2.5 meter water column. During the oscillatory motion the cylinders will go back to x-positions approximately equal to or smaller than the initial x-value, hence the cylinder excursion will be small. The velocity will also be quite low, due to the orientation of the cylinder in water. The orientation is close to horizontal during the entire motion, giving a high viscous resistance. Graphs illustrating the velocity as function of time and depth are given in Appendix B.3, B.4, B.5 and B.6.

The cylinder trajectory B, in Figure 23, was observed for initial drop potions under the water surface at 15, 30, 45 and 60 degree initial angles for closed cylinders. For open cylinders the same trajectory was also found for 75 degree initial drop angles. For initial drop positions over the water surface, the same trajectory was observed at initial drop angles equal to 15, 30, 45, 60 and 75 degrees (see Appendix A.1-A.8). During the experiment, several different variations of this trajectory were observed. It were found variations in the radial excursion to the position where the oscillating motion developed and therefore also in the total travelling distance. Trajectory B is characterised by that the cylinder moves a distance before it starts to oscillate between motion in the positive and negative x-direction. An illustration of the cylinder orientation for this trajectory type is given in Figure 24. The distance the cylinders travels before it starts to oscillate depends on the initial drop angle. A higher drop angle makes the cylinder move further away from the drop position and closer to the bottom before it starts oscillating. A higher drop angle also results in less oscillations since the oscillating motions starts at a position closer to the tank floor. Because of the oscillating motion, the cylinder hits the bottom close to horizontally. The peak velocity for this type of trajectory, is reached somewhere between the release position and the first turn into the oscillating motion. During the oscillating motion, the cylinder velocity settles around a lower velocity (see Appendix B.1-B.8).

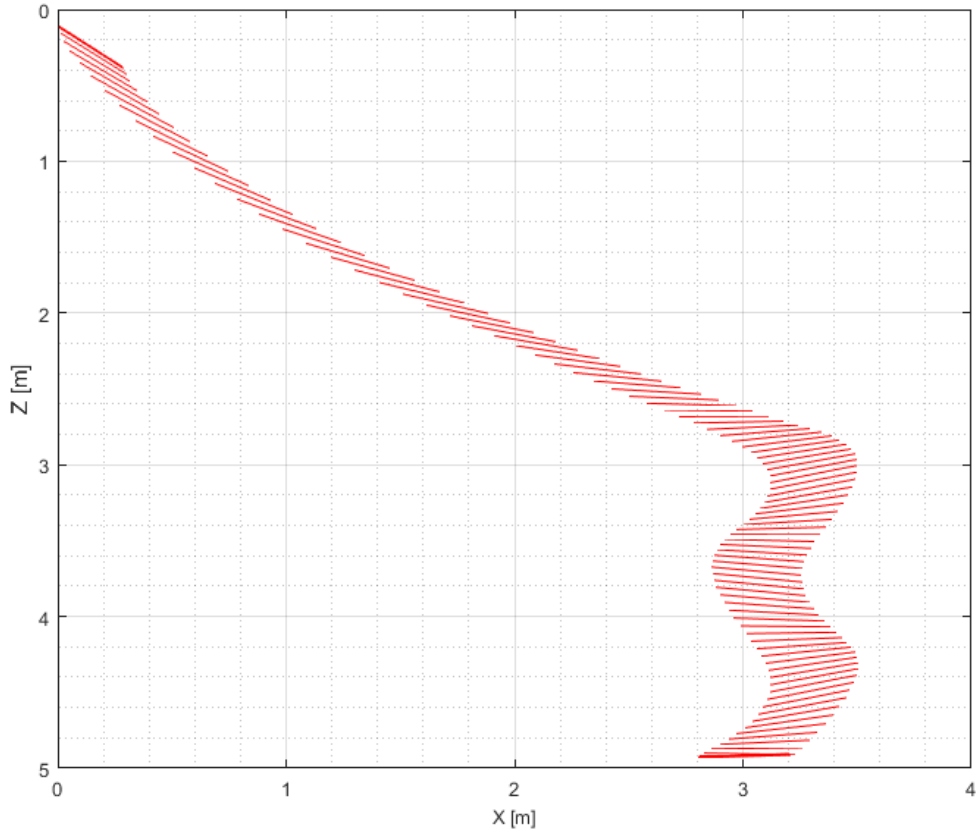

Figure 24: *An illustration of the orientation of cylinders with the centre of gravity placed in the cylinder volume centre found from the experiment. The figure illustrates the orientation of a 19 millimetre cylinder with closed ends dropped with 45 degree angle. The vertical axis shows the depth, and the horizontal axis shows the radial excursion.*

Trajectory C, in Figure 23, were observed for closed end cylinders with initial drop positions under the water surface for drop angles of 60 and 75 degrees, and for drops from over the water surface at 75 degrees drop angle for the 10 millimetre diameter cylinder (see Appendix A.1.4, A.1.5, A.2.4, A.2.5,A.3.4, A.3.5 and A.4.5). For this trajectory the cylinders had only motions in the positive x-direction. The peak velocity developed quite fast (see Appendix B.1-B.4), and the cylinder velocity decreased, as the cylinder angle decreased during the motion. The cylinder hit the tank bottom with the nose first, but at a small angle compared to the bottom. The impact angle observed were so small that the cylinder slid a short distance on the tank bottom before it stopped. Figure 25 illustrates the cylinder orientation during the motion.

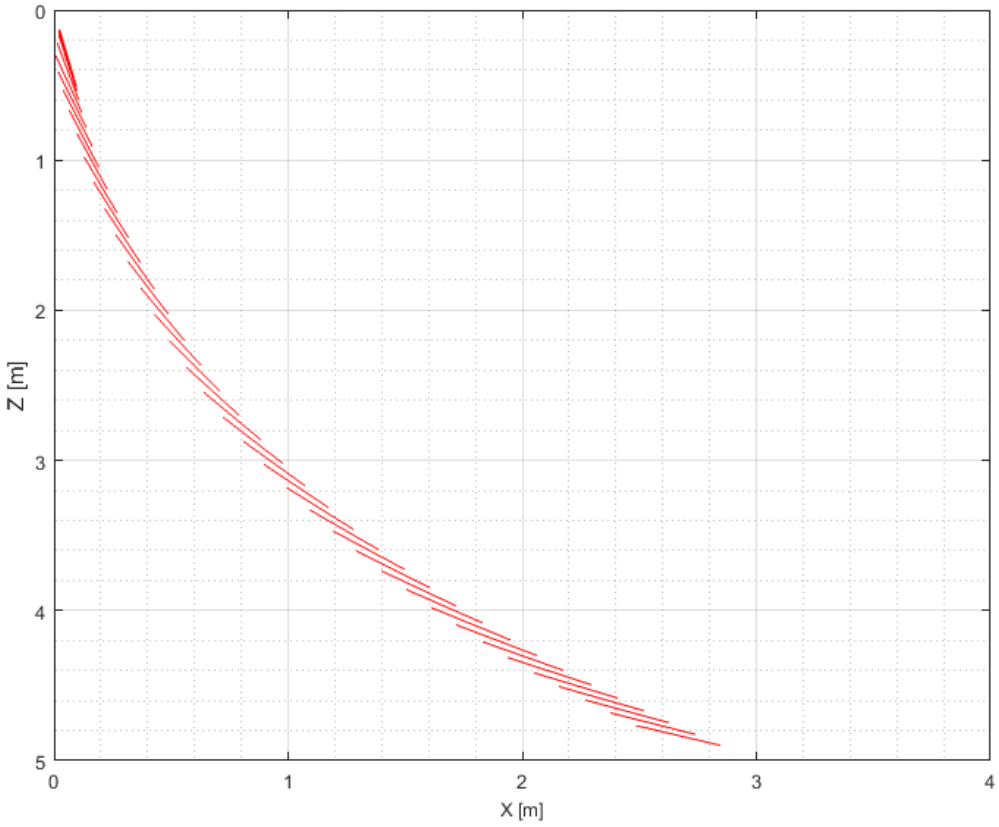

Figure 25: *Cylinder orientation for a 19 millimetre diameter cylinder with closed ends dropped with 75 degree angle, illustrating the cylinder orientation during trajectory C. The vertical axis shows the depth, and the horizontal axis shows the radial excursion.*

The cylinder trajectory D were observed for 10 millimetre diameter cylinders dropped with a 75 degree initial angle from a position under the water surface (see Appendix A.1.1). The cylinders had only positive motions in x-direction. In this case the cylinder angle decrease less during the motion, than for trajectory C, and the cylinder hit the tank bottom with a relatively large angle compare to the bottom. The cylinder leading edge motion stopped almost immediately after the it hit the bottom. Due to the relative large cylinder angle, the velocity was quite high during the entire motion (see Appendix B.1).

Cylinders with displaced centre of gravity

Typical trajectories observed from the experiment for cylinders with displaced centre of gravity are shown in Figure 26.

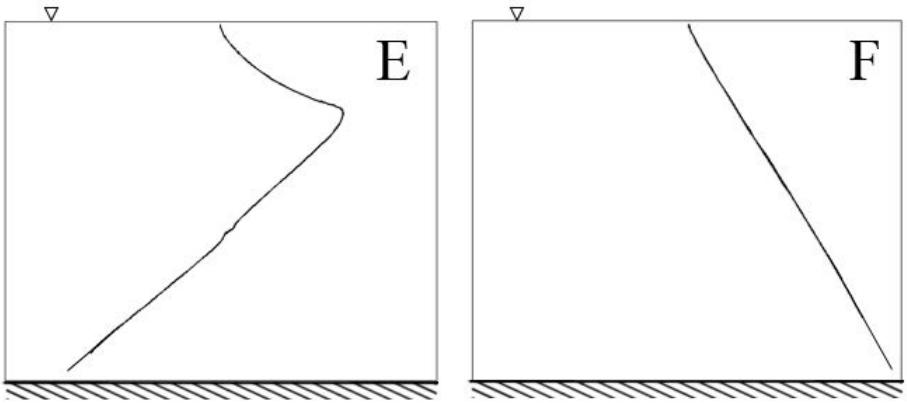

Figure 26: *Two dimensional X-Z-view: Trajectories of cylinders with displaced centre of gravity found from the experiments.*

The cylinder trajectory E, in Figure 26, was found for cylinders dropped from an initial position with the centre of gravity located above the cylinder volume centre (see Appendix A.9 and A.11). The cylinders first travelled a distance in the positive x-direction. During this motion the cylinder angle decreased. At the point were the trajectory started to make a turn the centre of mass location changed from a position over the volume centre to a position under. That caused the cylinder to change the direction of motion and it started to move in the negative x-direction, following a more or less straight trajectory to the bottom. How fast the cylinder trajectory makes a curve, depends on the cylinder initial drop angle. For the smallest initial drop angle, of 15 degrees, the cylinder trajectory made a curve almost immediately. With increasing drop angle the cylinder moved further before the trajectory curved at a position closer to the bottom. For this type of trajectory the velocities were in general quite high during the entire motion, except for the point were the trajectory made a turn. Velocities as function of time and depth are given in Appendix B.9 and B.11.

Trajectory F, in Figure 26, were observed for cylinders with displaced centre of gravity, with a initial position of the centre of gravity under the cylinder volume centre (see Appendix A.10 and A.12). The cylinders followed a relatively directional stable motion with a quite stable orientation to the bottom and the radial excursion decreased with increasing drop angles. The peak velocity developed after a relatively short time, and the velocity stabilised at this value. That resulted in the cylinders hitting the bottom with the nose first at a high velocity. Velocities as function of time and depth are given in Appendix B.10 and B.12.

4.1.2 Tendencies in the results according to the cylinders physical parameters

In this section the governing trends in the results will be discussed according to the cylinders physical parameters. First the closed end cylinders with 10, 16 and 19 millimetre diameter will be investigated. Then the behaviour of cylinders with two dif-

ferent displacements of the centre of gravity will be studied. Finally cylinders with open ends will be studied. The numerical values given in this section are found from the experiments, and complete tables with average values and related standard deviations are given in Appendix C and D.

Closed end cylinders with different length to diameter ratio

When comparing the trajectories for closed end cylinders dropped from under the water surface with equal lengths, and diameters equal to 10, 16 and 19 millimetre, some governing trends were observed. This is illustrated in Figure 27, showing one drop for each cylinder diameter at 45 degree initial drop angle.

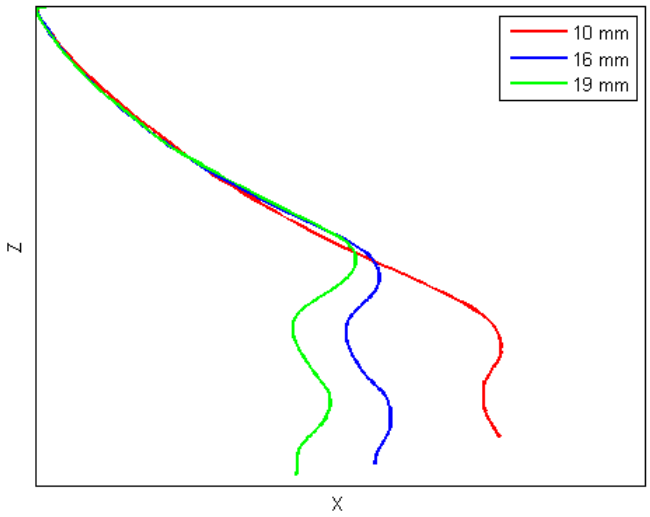

Figure 27: *Comparison of closed ends cylinders drop at 45 degree initial drop angle from under the water surface, with different diameters. The cylinder diameters dropped were 10 mm, 16 mm and 19 mm. The figure shows experimental results.*

As can be seen from Figure 27, increasing the cylinder diameter made the cylinders turn after a shorter time, and at a smaller radial excursion and depth. Increasing the diameter results in increased cylinder weight, see Table 6 for details, leading to higher velocities and longer cylinder travel before it starts oscillating. But, it seems like the increased diameter and frontal area of the cylinder has a larger influence on the cylinder trajectory and excursion than the weight increase. The effect of increasing the frontal area and diameter is among other factors a reduction of the longitudinal velocity. When the longitudinal velocity is equal to zero the cylinder trajectory will start to make a turn, and develop the oscillating motion. Hence, increased cylinder diameter will reduce the radial excursion. The general trends can be seen in Table 8.

Table 8: *The average radial excursion at four meter depth, and average radial excursion and dept at the first turn for 10 mm, 16 mm and 19 mm diameter cylinders dropped at 15, 30, 45, 60 and 75 degree initial drop angle from under the water surface. The table shows experimental results.*

	Average radial excursion at four meter depth			**Average radial excursion to the first turn**			**Average depth to the first turn**		
	10 mm	**16 mm**	**19 mm**	**10 mm**	**16 mm**	**19 mm**	**10 mm**	**16 mm**	**19 mm**
15°	0.89 m	0.79 m	0.35 m	0.73 m	0.49 m	0.40 m	1.13 m	0.98 m	0.88 m
30°	2.32 m	1.51 m	1.35 m	2.37 m	1.61 m	1.47 m	2.20 m	1.72 m	1.60 m
45°	3.67 m	2.79 m	2.58 m	3.79 m	2.89 m	2.76 m	3.63 m	2.93 m	2.84 m
60°	2.79 m	2.94 m	2.48 m						
75°	1.49 m	1.68 m	1.81 m						

The table shows the radial excursion at four meter depth and the distance to the first turn for 10 mm, 16 mm and 19 mm diameter cylinders dropped at 15, 30, 45, 60 and 75 degree initial angle. At 15, 30 and 45 degree drop angle the cylinders developed an oscillating motion before they reached the tank bottom. Investigating the excursion at four meter depth for this drop angles in the table, it can bee seen that the radial excursion decreased significantly with increasing diameter. For 60 and 75 degree drop angle, were the oscillating behaviour did not have enough time to develop, the radial excursion is larger for increased diameters. This is because of the curvature of the trajectories. If the tank had been deep enough, the same trend as for the smaller drop angles would have been observed.

When investigating the velocities for the three cylinder types, it was observed that the cylinders with the smallest diameter had the largest velocities. So, when studying the experiment experienced velocities, the increase in diameter dominated over the weight increase. An increased diameter gave lower maximum velocities, as can be seen in Table 9 showing the average maximum velocity for 10 mm, 16 mm and 19 mm cylinders dropped with 15, 30, 45, 60 and 75 degree drop angles. The peak velocities occurs at a position before the oscillating motions starts, this is showed in the velocity plots in Appendix B.1, B.2 and B.3.

Table 9: *The average maximum velocity for 10 mm, 16mm and 19 mm diameter cylinders dropped at 15, 30, 45, 60 and 75 degree initial drop angle from under the water surface. The table shows experimental results.*

	Average maximal velocity				
	15°	30°	45°	60°	75°
10 mm	0.85 m/s	1.53 m/s	2.17 m/s	2.68 m/s	2.96 m/s
16 mm	0.85 m/s	1.33 m/s	1.92 m/s	2.43 m/s	2.60 m/s
19 mm	0.79 m/s	1.17 m/s	1.70 m/s	2.43 m/s	2.33 m/s

When the oscillating motion has developed, the total cylinder velocities will vary around a lower velocity, approximately equal for the three cylinder types and independent on the drop angle. For the three cylinder types, these values were approximately equal to 0.6 m/s. During the oscillating motion, the cylinders will keep a quite horizontal orientation and the low velocity shows that the viscous forces are more dominate in the lateral, than in the axial cylinder direction.

Closed end cylinders with displaced centre of gravity

Experiments with 10 millimetre diameter and 0.45 meter length cylinders with displaced centre of gravity were performed. Two different positions for the centre of gravity were investigated. Studying the results form the experiments, some governing trends were found. This is illustrated in Figure 28 and Figure 29, which shows drops from 60 degree initial angle with centre of gravity placed over and under the cylinder volume centre. The centre of gravity is displaced with 1.4 and 3 cementer, showed by the green and blue lines.

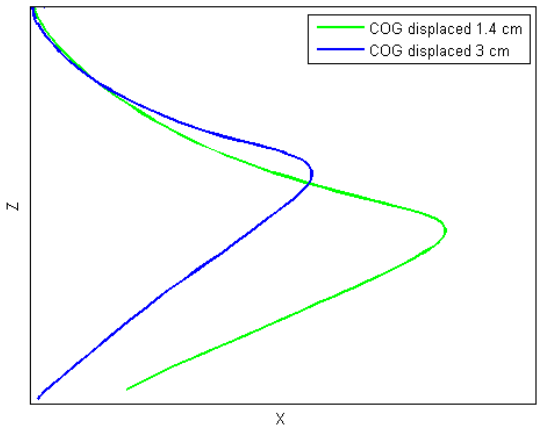

Figure 28: *Comparison of the trajectories of cylinders with 1.4 and 3 centimetre displaced centre of gravity, dropped from under the water surface at 60 degree initial angle with centre of gravity over the cylinder volume centre. The figure shows experimental results.*

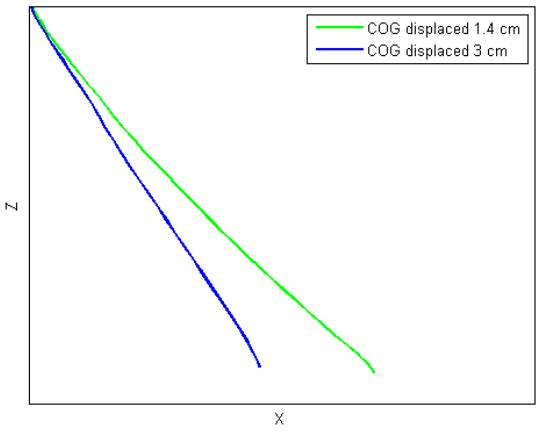

Figure 29: *Comparison of the trajectories of cylinders with 1.4 and 3 centimetre displaced centre of gravity, dropped from under the water surface at 60 degree initial angle with centre of gravity under the cylinder volume centre. The figure shows experimental results.*

As can be seen from the figures, the degree of displacement of the centre of gravity has a significant impact on the radial excursion. If the cylinders were dropped with initial position of the centre of gravity over the cylinder volume centre, as in Figure 28, increasing the displacement of the centre of gravity makes the cylinder turn after a shorter distance and the trajectory towards the bottom follows a steeper slope. This trend can be seen in Table 10 that gives the average values of the turning position, and the excursion at four meter dept.

Table 10: *The average radial excursion at four meter depth, and average radial excursion and dept for the direction change for 10 millimetre diameter cylinders with the centre of gravity displaced 1.4 and 3 centimetre. The initial position of the cylinder centre of gravity is over the volume centre. The cylinders are dropped at 15, 30, 45, 60 and 75 degree initial drop angle from under the water surface. The table shows experimental results.*

	Drop of cylinders with the initial position of centre of gravity over the cylinder volume centre					
	Average radial excursion at four meter depth		**Average radial excursion to the direction change**		**Average depth to the direction change**	
	COG dispalced 1.4 cm	**COG dispalced 3 cm**	**COG dispalced 1.4 cm**	**COG dispalced 3 cm**	**COG dispalced 1.4 cm**	**COG dispalced 3 cm**
15°	-4.35 m	-2.49 m	0.21 m	0.07 m	0.36 m	0.45 m
30°	-3.43 m	-1.66 m	0.65 m	0.41 m	0.57 m	0.84 m
45°	-1.04 m	-0.71 m	1.74 m	1.04 m	1.29 m	1.35 m
60°	1.72 m	0.65 m	2.62 m	1.66 m	2.97 m	2.15 m
75°	2.73 m	1.80 m	3.04 m	2.14 m	4.31 m	3.17 m

For the cylinders dropped with the centre of gravity placed under the cylinder volume centre, as showed in Figure 29, an increase in the displacement of the centre of gravity will cause a smaller radial excursion. Table 11 shows the average radial excursions at three an four meter depth. For both degree of displacement of the cylinder mass centre it can bee seen that the relatively slight change in the rate of displacement of the cylinder centre of gravity had a large impact on the cylinder excursion.

Table 11: *The average radial excursion at four and three meter depth for 10 millimetre diameter cylinders with the centre of gravity displaced (COG) 1.4 and 3 centimetre. The initial position of the cylinder centre of gravity is under the volume centre. The cylinders are dropped at 15, 30, 45, 60 and 75 degree initial drop angle from under the water surface. The table shows experimental results.*

	Drop of cylinders with the initial position of centre of gravity under the cylinder volume centre			
	Average radial excursion at three meter depth		**Average radial excursion at four meter depth**	
	COG dispalced 1.4 cm	**COG dispalced 3 cm**	**COG dispalced 1.4 cm**	**COG dispalced 3 cm**
15°	3.55 m	2.26 m	4.65 m	2.81 m
30°	2.77 m	1.85 m	3.79 m	2.34 m
45°	1.89 m	1.33 m	2.59 m	1.73 m
60°	1.19 m	0.84 m	1.70 m	1.14 m
75°	0.60 m	0.37 m	0.98 m	0.52 m

The cylinders with displaced centre of gravity do not experience any oscillations. During most of the motion the longitudinal velocity will probably be higher than the lateral velocity, due to the cylinder orientation. When the centre of gravity was under the cylinder volume centre the cylinder angle kept quite constant at a relatively high angle, that made the maximum total cylinder velocities quite high. For the cylinder with the initial position of the centre of gravity over the cylinder volume centre, the position of the maximum velocity was either before or after the directional change. This depended on the depth were the directional change occurred. The maximum total velocities are given in Table 12.

Table 12: *The average maximum velocity for 10 millimetre diameter cylinders with the centre of gravity (COG) displaced 1.4 and 3 centimetre. The cylinders are dropped at 15, 30, 45, 60 and 75 degree initial drop angle from under the water surface, with the initial position of the centre of gravity upwards or downwards. The table shows experimental results.*

	Average maximal velocity				
	15°	30°	45°	60°	75°
COG upwards displaced 1.4 cm	1.88 m/s	1.94 m/s	2.11 m/s	2.39 m/s	2.88 m/s
COG downwards displaced 1.4 cm	2.03 m/s	2.33 m/s	2.75 m/s	2.98 m/s	3.08 m/s
COG upwards displaced 3 cm	2.94 m/s	3.04 m/2	3.03 m/s	3.07 m/s	2.82 m/s
COG downwards displaced 3 cm	3.20 m/s	3.23 m/s	3.27 m/s	3.33 m/s	3.47 m/s

When the cylinders kept the same orientation for a while, it reached a terminal velocity. Then the drag and buoyancy force balanced the gravity force, and the acceleration is zero. The terminal velocity increased with increasing cylinder angle. The velocity plots as function of time and depth are given in Appendix B.9-B.12.

Open end cylinders

Experiments with 10 and 19 millimetre diameter open ends cylinders with length 0.45 meter, was also performed. Compering the trajectories for the two different types of open cylinders a clear difference was found. Figure 30 shows the difference between a 10 and 19 millimetre cylinder dropped from under the water surface at 45 degree drop angle. Increasing the cylinder diameter made the oscillating motion start after a shorter distance. As a consequence of the earlier oscillation the radial excursion also became smaller. Table 13 shows this trend, giving the average values for the radial excursion at four meter depth and the position of the first turn for the two cylinder types.

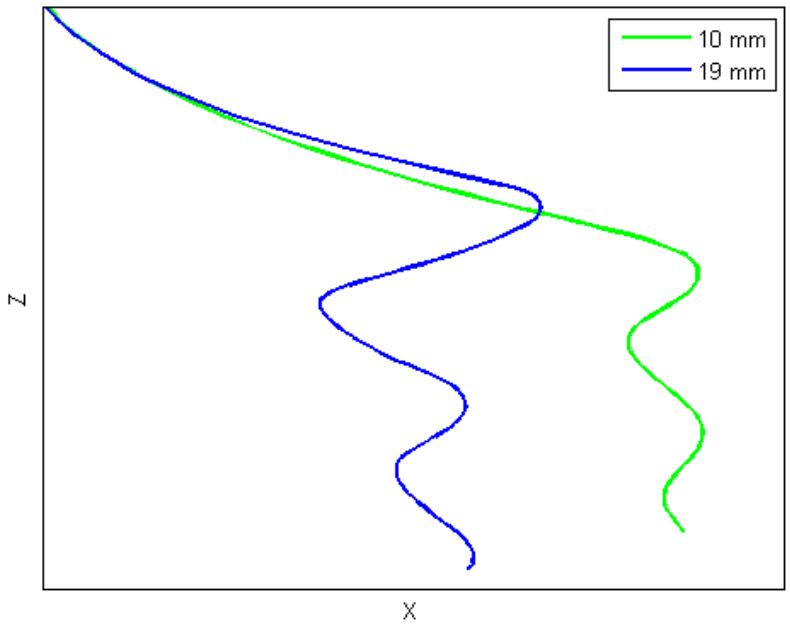

Figure 30: *Comparison of trajectories of 10 and 19 millimetre diameter open end cylinders dropped from under the water surface at 45 degree initial drop angle. The figure shows experimental results.*

Table 13: *The average radial excursion at four meter depth and average radial excursion and dept at the first turn for 10 mm and 19 mm diameter cylinders with open ends dropped at 15, 30, 45, 60 and 75 degree initial angle from under the water surface. The table shows experimental results.*

	Average radial excursion at four meter depth		**Average radial excursion to the first turn**		**Average depth to the first turn**	
	10 mm	**19 mm**	**10 mm**	**19 mm**	**10 mm**	**19 mm**
15°	0.85 m		0.71 m		1.01 m	
30°	1.91 m	1.20 m	1.85 m	1.29 m	1.63 m	1.23 m
45°	2.57 m	1.38 m	2.63 m	1.98 m	2.31 m	1.70 m
60°	3.12 m	2.09 m	3.41 m	2.55 m	3.41 m	2.43 m
75°	2.62 m	1.79 m	3.70 m	2.67 m	4.57 m	3.23

The weight of the 19 millimetre diameter cylinder used, was higher than for the 10 millimetre diameter cylinder. Higher weight gave in general a larger radial excursion and would alone lead to that the first turn occurred at a deeper depth. But, the 19 millimetre diameter cylinder also had a larger surface leading to larger frictional resistance and hence smaller radial excursion. The frontal area was quite small for both of the cylinders, that had wall thicknesses of 1.0 and 1.25 millimetre, and would thereby probably not reduce the longitudinal velocity significantly. The fact that the 19 millimetre diameter cylinder developed the oscillating motion earlier, may be explained by an additional moment; the lift force that attacked the cylinder nose. This can be related to the effect, stated by Newman (1977), who studied rectangular lifting surfaces

with small aspect ratios and found that the lift forces were concentrated around the leading edge, particularly when leading edge separations does not occur. The leading edge separation will probably be small for cylinders with open ends due to the small frontal area. The effect of the additional moment seems to increase with increasing diameter, this can be seen studying Figures 31 and 32, that gives the orientation of one 10 and one 19 millimetre cylinder with open ends dropped at 45 degrees. From the figures it can be seen that the 19 millimetre cylinder had large differences in cylinder angle during the oscillating motion. This difference in cylinder orientation between a 10 and 19 millimetre diameter cylinder was not observed for the cylinders with closed ends.

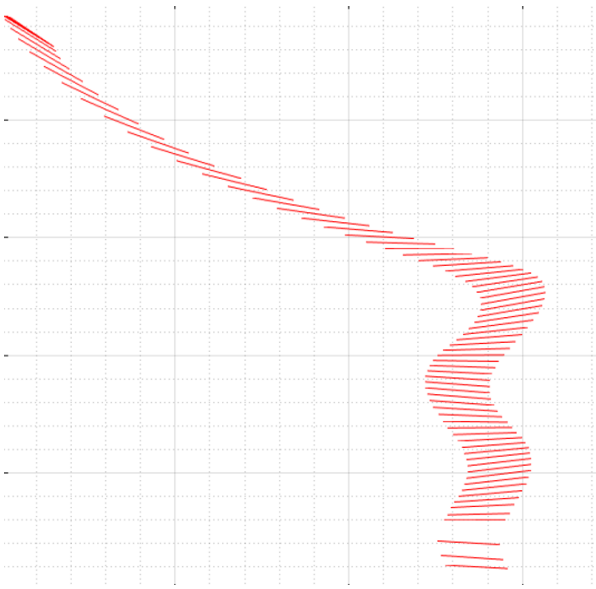

Figure 31: *The orientation of a 10 millimetre cylinder with open ends dropped with 45 degree initial drop angle. The figure shows experimental results.*

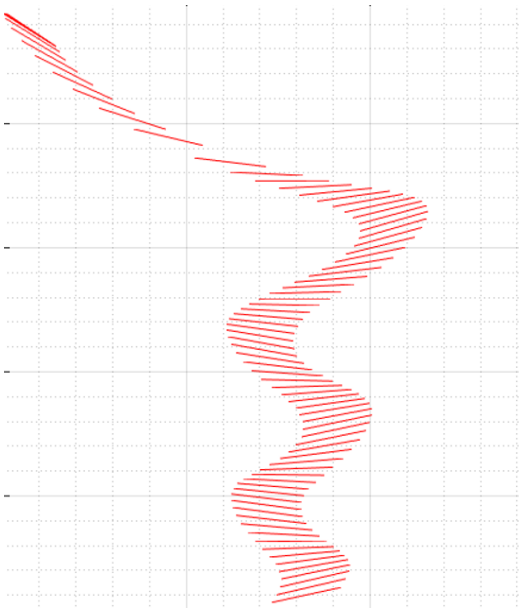

Figure 32: *The orientation of a 19 millimetre cylinder with open ends dropped with 45 degree initial drop angle. The figure shows experimental results.*

A comparison of the trajectories of the 19 millimetre open and closed end diameter cylinders dropped at 45 and 75 degree are given in Figure 33 and Figure 34. The figures are examples illustrating the general behaviour of the closed versus the open ends cylinders tested in the experiment. Before starting the comparison, it is important to keep in mind that the closed end cylinder is filled with air, meaning that submerged in water it had an additional buoyancy force compared to the cylinder with open ends. So, in submerged condition the cylinder with open ends was the heaviest.

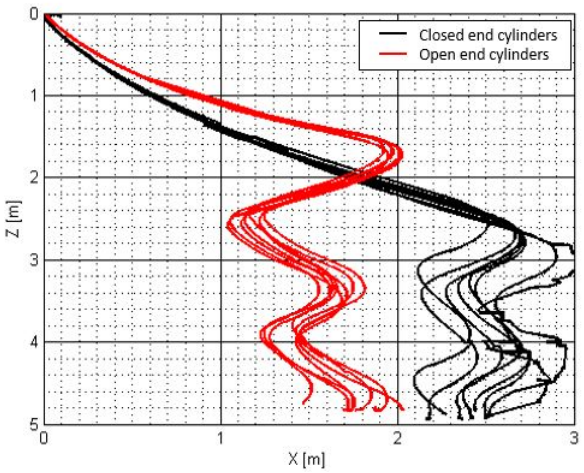

Figure 33: *X-Z-view: Comparison of the trajectories for open and closed end cylinders with 19 mm diameter, dropped from 75 degree initial angle under the water surface. The figure shows experimental results. The X-axis shows radial excursion.*

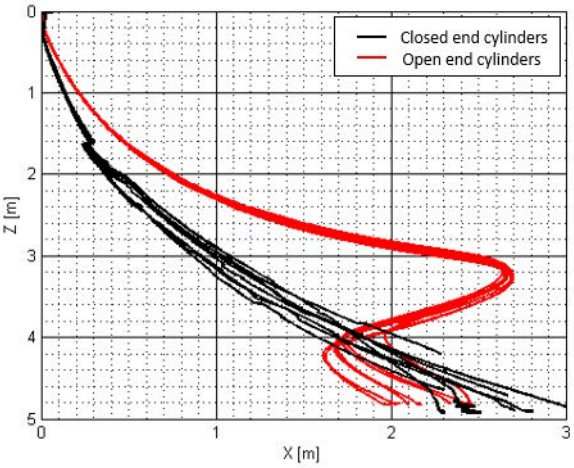

Figure 34: *X-Z-view: Comparison of the trajectories of open and closed end cylinders with 19 mm diameter, dropped from 45 degree initial angle under the water surface. The figure shows experimental results. The X-axis shows radial excursion.*

When comparing the two dimensional trajectories for the open and closed ends cylinders, shown as black and red lines in the figures, differences were found. Cylinders with open ends started the oscillating motion at an earlier position and therefore also reached a smaller radial excursion. The observation that the cylinder started the oscillating motion earlier may be a result of an additional moment in pitch due to a lift force in the cylinder nose. This is resulted in a difference in the orientation of the cylinders that can be seen comparing Figure 24 to Figure 32. The figures shows the orientation of a 19 millimetre cylinder with closed and open ends, respectively. From the figures it can be seen that the open cylinders had larger variations in cylinder angles through the oscillating motion.

4.1.3 Drop over versus under the water surface

So far, only the behaviour of cylinders dropped from under the water surface has been discussed. For a cylinder dropped from air the water impact conditions will be essential to initial conditions at the submerged part of the motion. When a cylinder penetrates the surface, water-impact loads will occur. The impact loads will initiate a cylinder rotation and decrease the cylinder angle. In addition buoyancy and drag forces will act on the submerged cylinder part. The cylinder trajectories will therefore be sensitive to small changes in the water impact conditions, because the angle of the submerged body determines the cylinder trajectory. The trajectories for cylinders dropped from over the water surface are showed in Appendix A.4-A.6. Comparing these trajectories to the cylinders dropped from under the water surface, it can bee seen that the trajectories for cylinders dropped at the same angles does not coincide

well, but drops at a smaller angles results in more similar paths.

Another difference between cylinders dropped from over and under the water surface is air cavities. For the cylinders dropped from air, formation of air cavities were observed both at the front and aft end of the cylinder, as showed in Figure 35. The air cavity formation was observed for all drop angles larger than 15 degrees. The amount of captured air at the front and aft cylinder end seemed to increase with increased drop angle. The air cavities followed the cylinder quite deep into the water, deeper for larger angles, and may have an influence on the motion and stability. For instance for lifeboats, it is found that air cavity contributes to retardation in the motion and that the pressure in a closed cavity oscillates leads to an oscillatory pressure, that results in an unsteady boat retardation (DNVGL , 2016). As a result of this, the air cavity impact on cylinder trajectory and velocity should be investigated closer, but this is beyond the scope of this thesis.

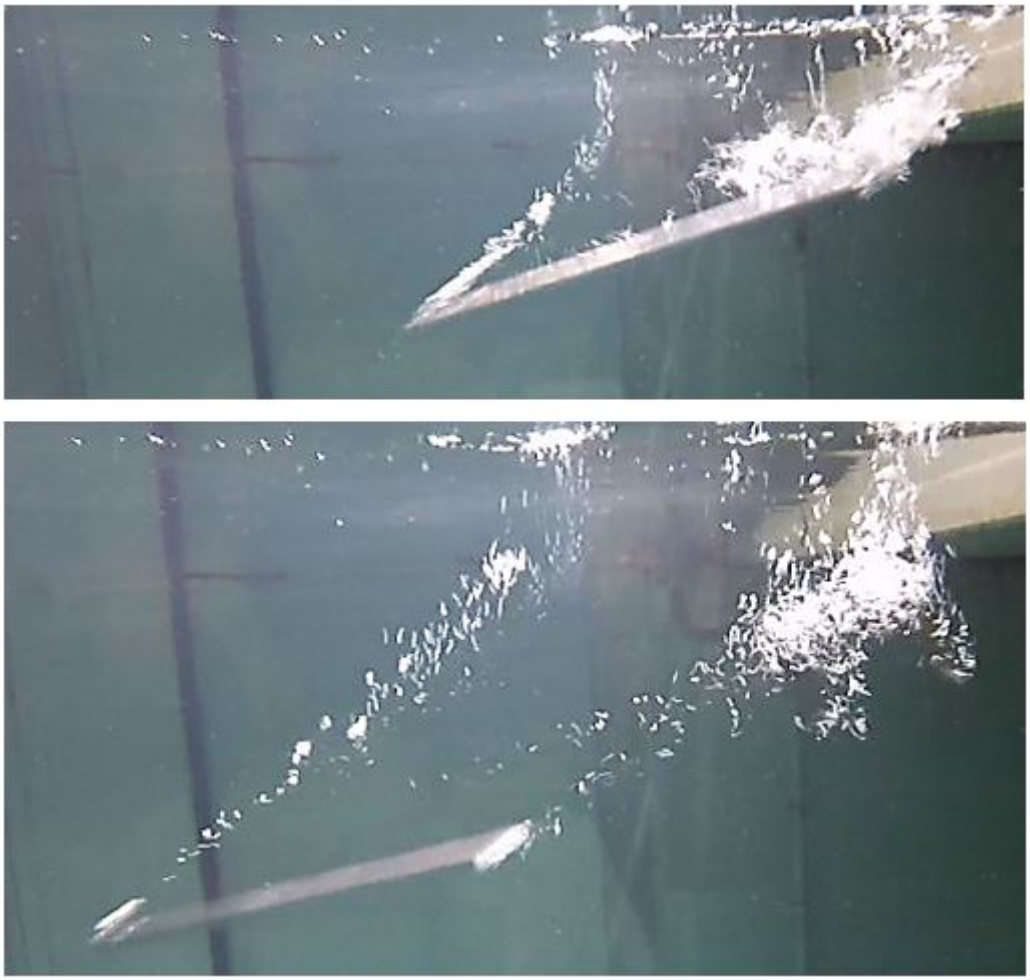

Figure 35: *Air cavity formation on the front and back end of a closed end cylinder dropped from over the water surface observed from the experiment. The cylinder is 19 millimetre dropped with 45 degree initial angle from over the water surface.*

To illustrate how this air cavities were formed the experiment performed by Ueda et al. (2010) was studied. Figure 36 shows the water entry of a 12 millimetre diameter and 300 millimetre length cylinder dropped at 200 millimetre height from the bottom edge of the cylinder to the water surface. The initial inclination compared to the water surface is 36 degrees. As can be observed from the figure, the air cavity formed from the bottom end of the cylinder at the beginning of the water entry, and the cavity is shed from the cylinder end (Figure 36 b-d). Then the resulting air cavity formed at the bottom end of the cylinder, breaks of (36 e-f), and the upper end of the cylinder also formed air cavity when it entered the water (36 g-i) (Ueda et al. , 2010).

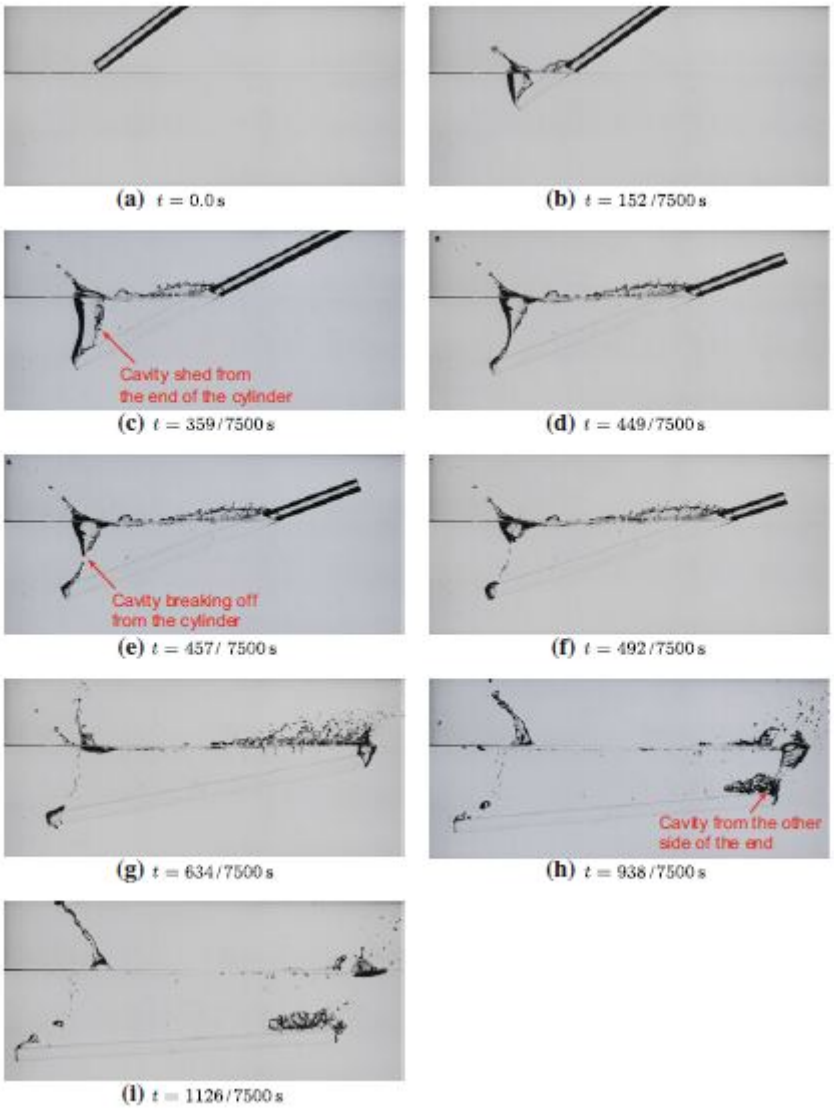

Figure 36: *Air cavity formation on the front and back end of a cylinder dropped with a 36 degree inclination entry the water. The cylinder had a 12 millimetre diameter and was 300 millimetre long. (Ueda et al. , 2010)*

The cylinder drop experiments conducted, during the work with this thesis, were performed in a tank were the water surface only experienced small ripples. However, in the ocean surface it will be significantly more undulations affecting the angle of the object, as illustrated in Figure 37. According to Katteland and Øygarden (1995) for crane accidents, the majority of the falling pipes will fall with an angle between 45 and 90 degrees, as a result of how the pipes are bundled together when lifted. But, the fully submerged angle may become completely different. If the cylindrical object hit a wave, the angle may increase or decrease depending on the wave slope and condition.

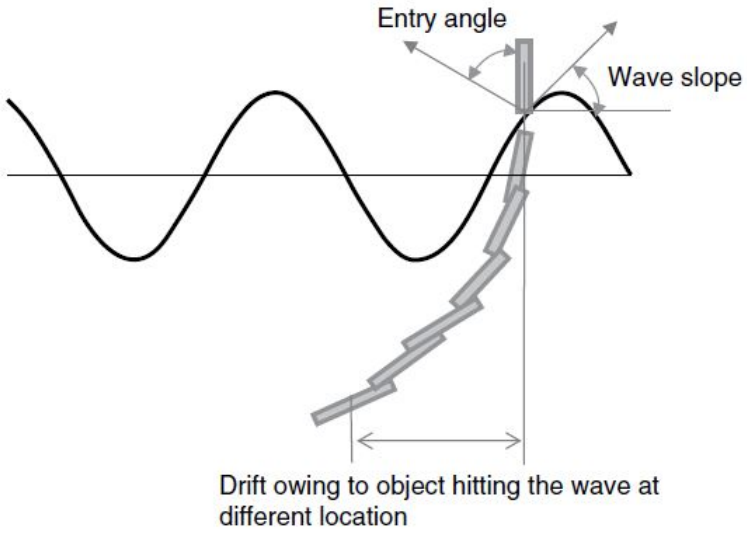

Figure 37: *The effect of an undulating sea surface (Yasseri , 2014).*

4.1.4 Worst case scenarios

In order to identify witch cylinder types that can lead to the "worst case scenarios" in a risk assessment study on accidental drops, investigation the highest values from the experiments can provide some answers.

The largest radial excursion observed and the object that hit the tank bottom furthest from the drop position was observed for the cylinder with centre of gravity displaced 1.4 centimetre form the cylinder volume centre dropped at 15 degree angle. The radial excursion for this objects are given in Figure 38 and Figure 39, which shows the cylinders dropped with the centre of gravity over and under the cylinder volume centre. The radial excursion on the tank floor for these cases, were found to be approximately six meter. This means that the radial excursions were found larger than the water depth. If the tank had been deeper the cylinder would have followed on in the same direction and the excursion would have increased with depth. This is different to what happens to a cylinder with no displacements of the centre of gravity, were the radial excursion reaches a maximum value. This maximum will be around the point were

the oscillating motion develops, after this the excursion will not change significantly with increasing water depth. The largest radial excursions for these cylinder types, was found to occur for initial drop angles around 60 degrees (see Appendix C).

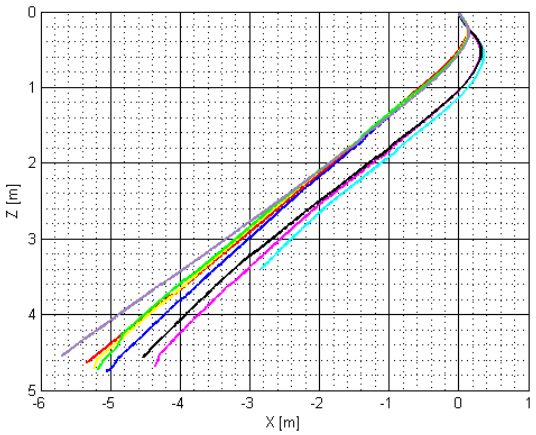

Figure 38: *X-Z-view: Drop of 10 millimetre diameter cylinders with the centre of gravity displaced 1.4 centimetre from the cylinder volume centre. Dropped at 15 degree angle with centre of gravity placed over the cylinder volume centre. The figure shows experimental results. The X-axis shows radial excursion.*

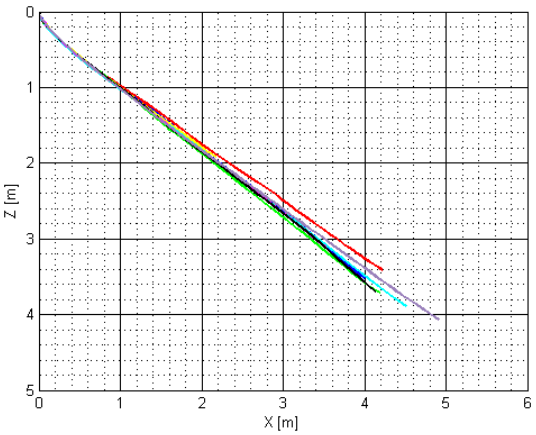

Figure 39: *X-Z-view: Drop of 10 millimetre diameter cylinders with the centre of gravity displaced 1.4 centimetre from the cylinder volume centre. Dropped at 15 degree angle with centre of gravity placed under the cylinder volume centre. The figure shows experimental results. The X-axis shows radial excursion.*

As a general trend, the maximum total velocity was observed to increased with increasing drop angles. The largest velocity was observed for the cylinder with the centre of gravity displaced by 3 centimetre, dropped with the centre of gravity under the cylinder volume centre (see Figure 40). For the cylinders with the centre of gravity in the cylinder volume centre, the largest velocity was measured for the 19 millimetre diameter cylinder with open ends (see Figure 41).

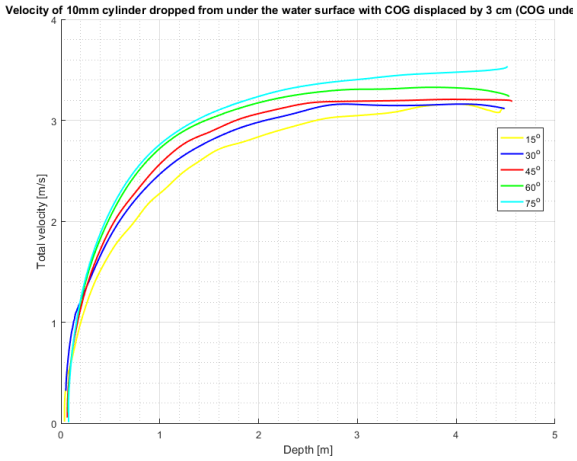

Figure 40: *Velocity development with depth for 10 millimetre diameter cylinders dropped with the centre of gravity displaced 3 centimetre from the cylinder volume centre. Dropped with centre of gravity placed under the cylinder volume centre from under the water surface. The figure shows experimental results.*

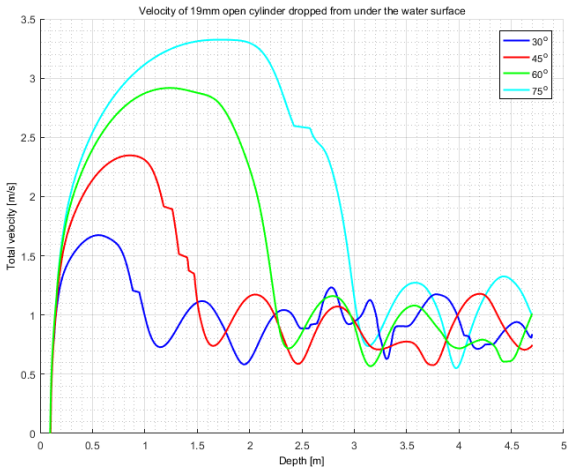

Figure 41: *Velocity development with depth for 19 millimetre diameter cylinders with open ends dropped from under the water surface. The figure shows experimental results.*

By investigating the velocity plots, it can be observed that cylinders with displaced centre of gravity will reach a relatively high velocity for all drop angles after approximately 2.5 meter depth and keep this velocity to the bottom. The period where the cylinder with no displacements of the centre of gravity has the highest velocity is quite small, and the velocity decreased significantly for smaller drop angels. The cylinder impact force depends on the velocity and mass. In this experiment the highest impact force was observed for the 19 millimetre diameter cylinder with open ends, dropped at 75 degree angle at around 1.5-2 meter depth. This special drop case had a high maximum velocity and the cylinder was the heaviest cylinder in submerged condition used in the experiment. But, to impact forces on seabed subsea structures at larger depths, cylinders with displaced centre of gravity will be of larger concern.

4.1.5 Comparison of DNV's recommended practice with the results obtained from the experiments

According to the DNV's recommended practice, DNVGL-RP-F107 (DNVGL , 2017), object excursion for dropped objects can be found from the simplified approximation $\delta = d \tan \alpha$ (see Section 2.3). For these experiments the full scale object can for instance be drill pipes, which will be under the category longed shaped in Table 4. The weight of drill pipes in full scale, as specified in Table 6, will be smaller than two tonnes and the angular deviation, α, will therefore be equal 15. The experiments were performed at five meter water depth, but since few measurements reached this depth, a water depth of four meter has been considered. The full scale water depth investigated, was

therefore 80 meter. Table 14 shows a comparison of DNV's methodology with the results obtained for the 10 millimetre diameter cylinder with closed ends (see Cylinder 1 in Table 6) dropped from under the water surface, which was the cylinder (disregarding the cylinders with displaced centre of gravity) that had the largest excursion. The table shows the mean radial excursion, standard deviation and a value for the radial excursion given as the sum of the mean and standard deviation value, from the experimental data. The values are given in full scale using the scaling method described in Section 2.2, meaning a drill pipe with end caps are considered. It is important to also keep in mined that this is measurements of the rear cylinder end, so the leading pipe end will probably go further, depending on the orientation of the pipe.

Table 14: *Comparison of the excursion found for experiments on a 10 millimetre diameter cylinder with closed ends dropped from under the water surface with the the DNV's simplified method. The values are in full scale.*

Fullscale values: 0.2 meter diameter cylinder						
	Data from the experiments			**DNV's simplified method**		
Depth	**80 [m]**				**180 [m]**	**300 [m]**
	mean rad. x-pos. [m]	st. dev. [m]	rad. x-pos. [m]	δ [m]	δ [m]	δ [m]
15°	17.8	3.8	21.6	21.4	48.2	80.4
30°	46.4	11.2	57.6	21.4	48.2	80.4
45°	73.4	10.2	83.6	21.4	48.2	80.4
60°	55.8	7.8	63.6	21.4	48.2	80.4
75°	29.8	3.6	33.4	21.4	48.2	80.4

Comparing the radial excursion, from the experiments, with DNV's estimation of the excursion at 80 meter water depth, it can bee seen that there is a great mismatch. DNV's recommendations assumes a considerable smaller excursion for all drop angles except for 15 degrees. The DNV's recommendation is based on a report by Katteland and Øygarden (1995) that provides dropped object distributions for larger water depths of 300 meters. It is stated that the maximum excursion is observed before the object reaches 180 meter and that the distribution will not increase significantly beyond this depth. According to the results found at 80 meter water depth the cylinders dropped from 15, 30 and 45 degrees has started to oscillate, see Appendix A.1. When the oscillating motion has developed the change in excursion will not be significant, but oscillate around approximately the same value. The cylinders dropped with 60 and 75 degree angle has at 80 meters depth not achieved the oscillating motion, but it is likely that the oscillating motion will develop in good time before 180 meters water depth is reached. Therefore, the assumption that the maximum excursion occurs before 180 meter depth appears to be reasonable, but the calculated value for object excursion, according to DNV's simplified method, at this depth is to low.

According to Katteland and Øygarden (1995), large water depth is set to 300 meter and deeper. A clear definition of water depths was not found in DNV's recommended

practice. The smallest water depth discussed is an example in appendix A.5 in DNVGL (2017) that concerns calculations of the excursion of an object in category one, flat or longed shaped, at 100 meter water depth. As showed in Table 14, the model that DNV suggest for calculation of excursion, will be fairly reasonable at 300 meter water depth for 15, 30 and 45 degree drop angle. For 60 and 75 degrees it is likely to believe that the maximal radial excursion, when the oscillation has developed, will be larger than for the smaller drop angles. It means that even deeper water depth than 300 meter is needed for DNV's simplified method to be valid.

For a pipe with a small displacement of the centre of gravity, equal to Cylinder 6 in Table 6, dropped with the centre of gravity under the cylinder volume centre, the full size radial excursion compared to the DNV's recommendations is given in Table 15. In DNVGL-RP-F107 (DNVGL , 2017) there are no object specifications beyont that the object is longed shaped. As can be seen from the table, only drop angles of 75 degrees will be within the recommendations at 80 meter depth.

Table 15: *Comparison of the experimental values for the cylinder with centre of gravity displaced 3 centimetre dropped with the centre of gravity under the volume centre with the the DNV's simplified method. The values are in full scale.*

Fullscale values: 0.2 m diameter cylinder, COG displaced 0.28 m						
	Data from the experiments			**DNV's simplified method**		
Depth	**80 [m]**				**180 [m]**	**300 [m]**
	mean rad. x-pos. [m]	st. dev. [m]	rad. x-pos. [m]	δ [m]	δ [m]	δ [m]
15°	93.0	4.4	97.4	21.4	48.2	80.4
30°	75.8	5.4	81.2	21.4	48.2	80.4
45°	51.8	3.4	55.2	21.4	48.2	80.4
60°	34.0	3.2	37.2	21.4	48.2	80.4
75°	19.6	0.8	20.4	21.4	48.2	80.4

Drops at 15 degrees gives the larges deviations from the recommendations for the cylinder with displaced centre of gravity. By investigating the trajectory in a X-Z-view given in Appendix A.10.1, it can be seen that the pipe will follow a more or less straight line. If there are no disturbances, the pipe will continue in the same direction until it reach the sea bottom. Figure 42 gives the full scale radial excursion from the experiments at 80 meter depth for the cylinder, and the appurtenant angular deviation α. The angular deviation becomes 50.6 degrees, which is 3.4 times higher than the value given in DNV's recommended practice for a longed shaped object.

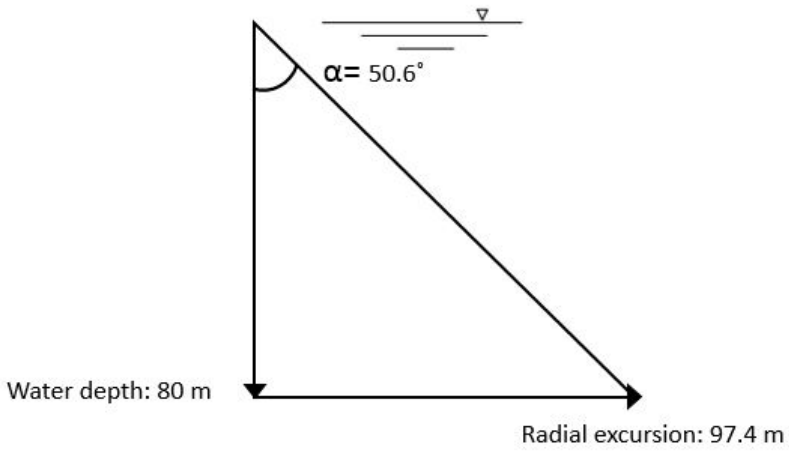

Figure 42: *Angular deviation found from the experiments for a 0.2 meter diameter and 9 meter length, pipe with the centre of gravity displaced 0.28 meter. The pipe is dropped with the centre of gravity under the cylinder volume centre from a position under the water surface at 15 degree initial drop angle.*

DNV's recommended practice assumes a normal distribution for the object excursion on the seabed for all object shapes, as illustrated in Figure 2. Investigating the excursion at four meter dept for the seven different cylinder types used in the experiment, the distribution given in Figure 43 was found. The distribution shows the absolute values for the radial excursion at four meter depth for all the cylinder drop measurements that reach this depth. The amount of data is not sufficient to give a complete statistic distribution for the radial distribution of dropped cylindrical objects. For instance it should be noted that no drops at 0 and 90 degrees are performed. According to Katteland and Øygarden (1995), for crane accidents, possible hit angles with the water surface will be between 0 and 90 degrees. A pipe dropped at 0 and 90 degrees without any disturbance will fall straight down to the sea floor, with close to zero excursion. Even though the statistical distribution is far from prefect, it can give an indication. The distribution of the drops that reach four meter depth indicates that a Rayleigh distribution can be used to describe the excursion on the sea bed. Lie et al. (2009) has also studied some experiments with two different types of falling anchors. They conclude that, for both anchor types, the horizontal excursion can approximately be statistically modelled by use of the Rayleigh distribution. Hence, the Rayleigh distribution might, for some type of objects, give a better distribution of the excursion on the sea bed than the normal distribution assumed in the DNV's recommended practise.

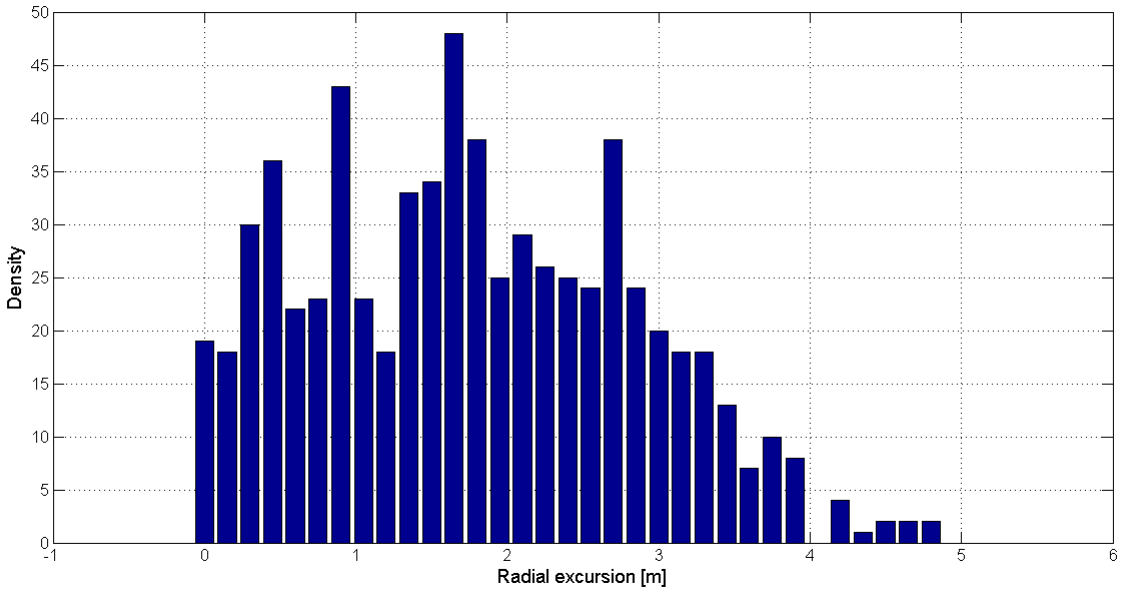

Figure 43: *Distribution of the absolute value of radial excursion at four meter depth for all drops performed during the experiment that reached four meter depth.*

4.1.6 Directional stability of the cylinder motion

Later in this thesis, two dimensional calculations of the cylinder trajectory and velocity will be performed. A fundamental assumption for this theory is that the cylinder moves close to the vertical plane between vertical global Z-axis and the cylinder axis, as showed in Figure 4 were the cylinders is pointing towards the centre of the target. From the experiments it seems like this assumption can be reasonable for many cases investigating the plot of the X-Y-views in Appendix A, but there are some exceptions. For instance large deviations were observed for the closed end cylinders dropped from under the water surface at 60 degree drop angle. The deviation observed seams to increases with the cylinder diameter. For the 19 millimetre diameter cylinders dropped, the X-Y-view are given in Figure 44.

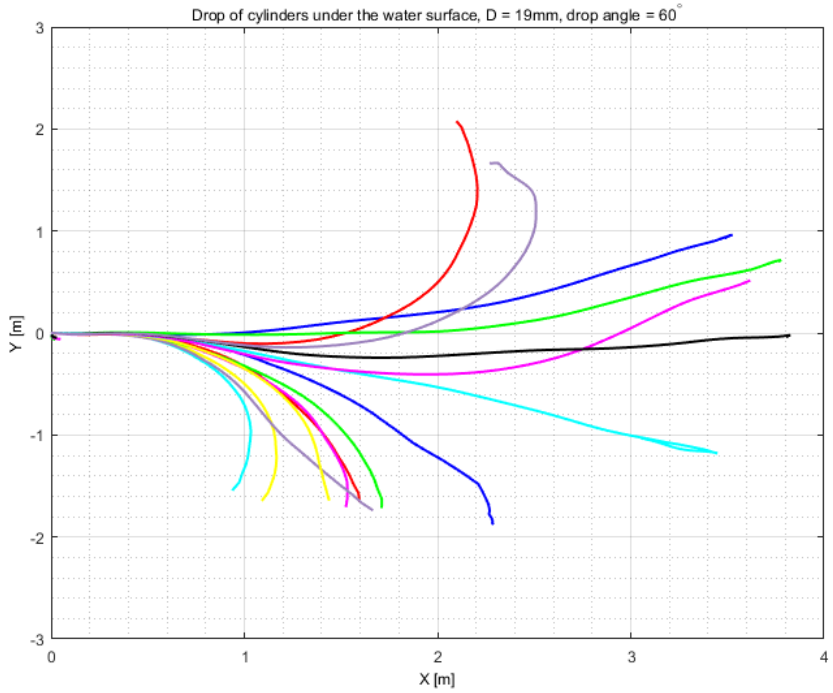

Figure 44: *X-Y-view of a closed end 19 millimetre diameter cylinder dropped at 60 degrees from under the water surface. The figure shows experimental results.*

In order to explain why this unstable motion occurs, it could be relevant to consider the flow separation on the body. As studied by Werle (1979) an asymmetric cross-flow separation will occur at a distance from the pointed cylinder nose, depending on the cylinder diameter and inclination. According to Sarpkaya (1978) the vortices separate from the cylinder must acquire a certain strength and position relative to the cylinder in order to reach a state at which they are most susceptible to disturbances. Additionally, as a consequence of the asymmetric cross-flow separation, the falling cylinder will be affected by a side force (Alsos and Faltinsen , n.d.). In experiments performed by Lamont and Hunt (1976), an increase in this force, at moderately high angles of inclination, was observed. So, the direction instability observed in the X-Y-plane may be a consequence of asymmetric cross-flow separation. The direction stability may then depend on the inclination and diameter. At a certain combination of inclination and cylinder diameter the vortices probably reach a strength and position relative to the cylinder were the motion is more sensitive to disturbances. This may be the case for instance for a 19 millimetre cylinder dropped with 60 degree initial angle.

As indicated above the instability in the motion has a connection to the drop angle, but a quite large variation depending on the cylindrical object type was also observed. For instance, for cylinders with open ends, a larger direction stability compared to closed end cylinders was observed. This can bee seen by comparing Figure 44 and 45 which shows the X-Y-view of a closed and open end 19 millimetre diameter cylinder dropped at 60 degree angle. Investigating the motion before the oscillation has

developed, until approximately 2.5 meter excursion, the cylinder with open ends will have a quite directional stable motion. Compared to the closed end cylinder there is a radical difference. For the closed end cylinder trajectory in the X-Y-plane, several of the cylinders changed direction of motion significantly after less than one meter excursion. The more directional stable motion may be explained by the fact that the frontal area is smaller, giving less pressure and velocity reduction in the front part of the cylinder. How far from the pointed nose the asymmetric cross-flow occurs will also depend on the frontal area (Werle , 1979). A smaller frontal area may defer the trigging of the instability and lead to less instabilities in the wake.

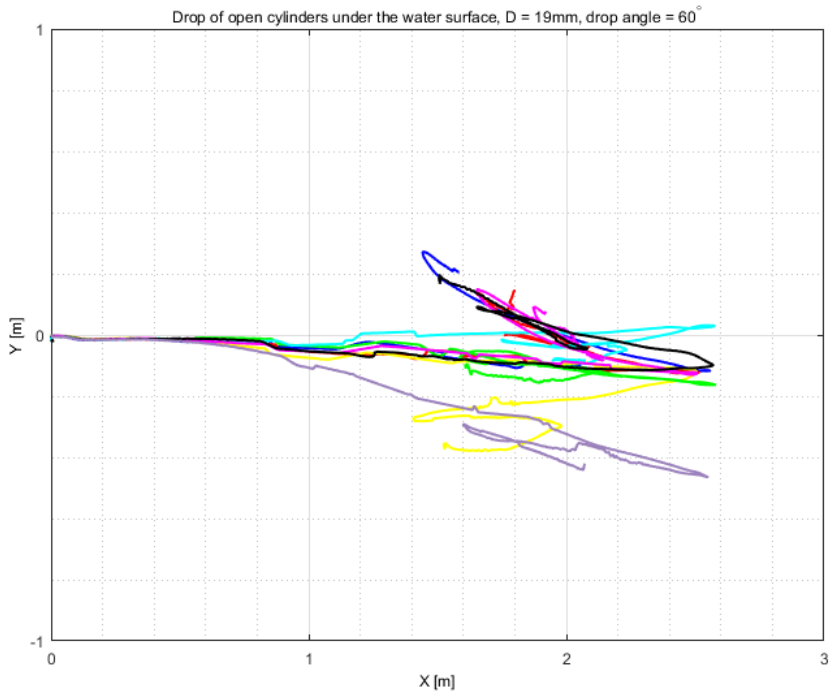

Figure 45: *X-Y-view of a open end 19 millimetre diameter cylinder dropped at 60 degrees from under the water surface. The figure shows experimental results.*

It was also observed that the cylinders with displaced centre of gravity were quite directional stable. This is related to the fact that the gravity force will work in the cylinder centre of mass. Therefore, when the centre of mass is located below the buoyancy centre, the motion of the cylinders will be stable and follow a relatively straight path to the bottom. This can be seen at the X-Y-plots in Appendix A.9-A.12 considering the fact that none of the dropped cylinders turned much in this plane compared to the radial excursion.

4.2 Comparison of experimental and numerical results

In this section the sensitivity of the parameters X_T/L, C_{dz} and C_{dx} will be studied, for cylinders with closed and open ends, and for cylinders with displaced centre of

gravity, dropped from under the water surface. The investigation will be performed comparing the numerical simulations to the experimental results. The numerical calculations are performed as described in Section 2.1.3 using the values given in Section 3.2. The theory described is a calculation of the centre of gravity motion. However, the following plot shows the simulated position of the same cylinder end as the marker were located during the experiment.

4.2.1 Cylinder with closed ends

Figure 46 to 55 shows a comparison of trajectories found from experiments and simulations. The 10 millimetre diameter closed end cylinder, specified as Cylinder 1 in Table 6, is selected as the dropped cylindrical object. Several trajectories are shown for drop angle of 15, 30, 45, 60 and 75 degrees which is presented by black lines for the experiments and coloured lines for the numerical calculations performed as described in Section 2.1.3.

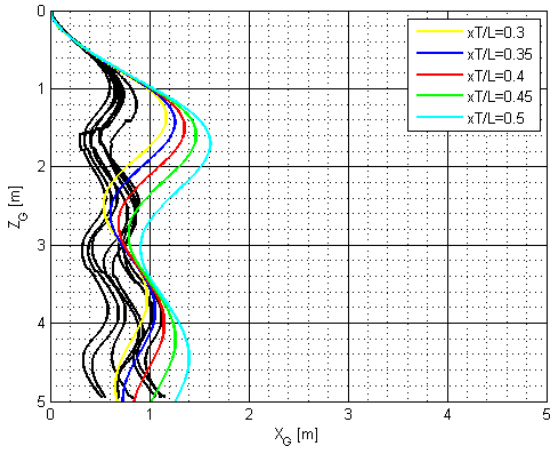

Figure 46: *X-Z-view: Comparison of the numerical and experimental results for Cylinder 1 in Table 6 dropped at 15 degree. The numerical calculations are represented with coloured lines, each colour represents a ten present change in the trailing edge position.* $C_{dz} = 1$ *and* $C_{dx} = 0.65$.

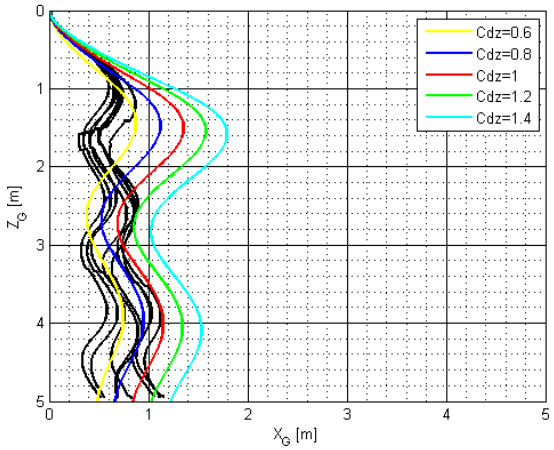

Figure 47: *X-Z-view: Comparison of the numerical and experimental results for Cylinder 1 in Table 6 dropped at 15 degree. The numerical calculations are represented with coloured lines, each colour represents a twenty present change in the* C_{dz}*-value.* $x_T/L = 0.4$ *and* $C_{dx} = 0.65$.

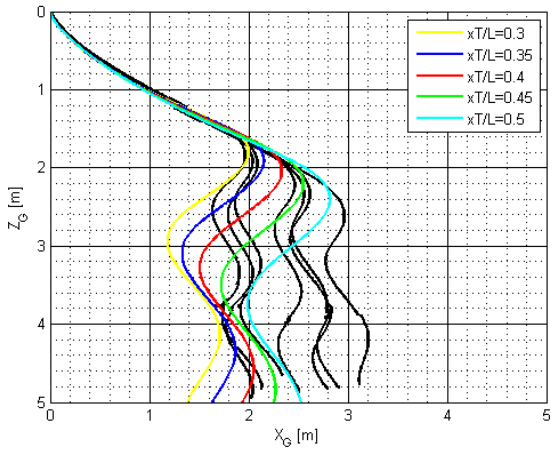

Figure 48: *X-Z-view: Comparison of the numerical and experimental results for Cylinder 1 in Table 6 dropped at 30 degree. The numerical calculations are represented with coloured lines, each colour represents a ten present change in the trailing edge position.* $C_{dz} = 1.0$ *and* $C_{dx} = 0.65$.

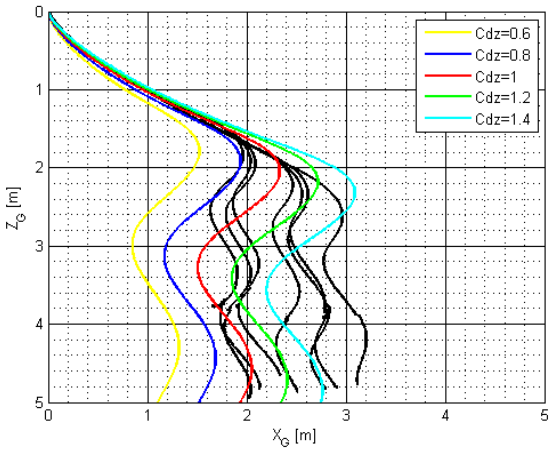

Figure 49: *X-Z-view: Comparison of the numerical and experimental results for Cylinder 1 in Table 6 dropped at 30 degree. The numerical calculations are represented with coloured lines, each colour represents a twenty present change in the* C_{dz}*-value.* $x_T/L = 0.4$ *and* $C_{dx} = 0.65$.

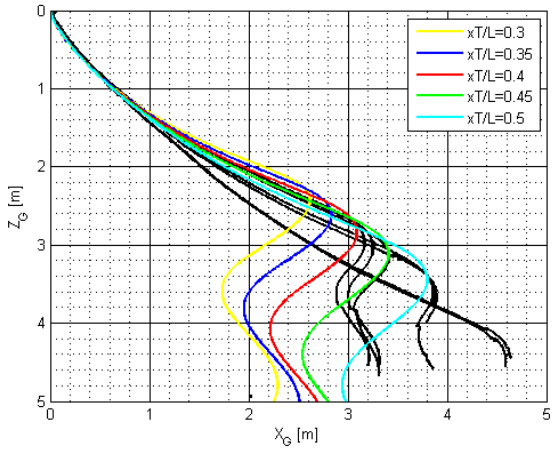

Figure 50: *X-Z-view: Comparison of the numerical and experimental results for Cylinder 1 in Table 6 dropped at 45 degree. The numerical calculations are represented with coloured lines, each colour represents a ten present change in the trailing edge position.* $C_{dz} = 1.0$ *and* $C_{dx} = 0.65$.

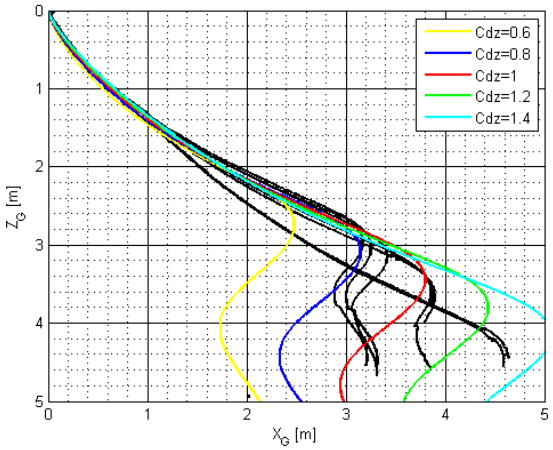

Figure 51: *X-Z-view: Comparison of the numerical and experimental results for Cylinder 1 in Table 6 dropped at 45 degree. The numerical calculations are represented with coloured lines, each colour represents a twenty present change in the* C_{dz}*-value.* $x_T/L = 0.5$ *and* $C_{dx} = 0.65$.

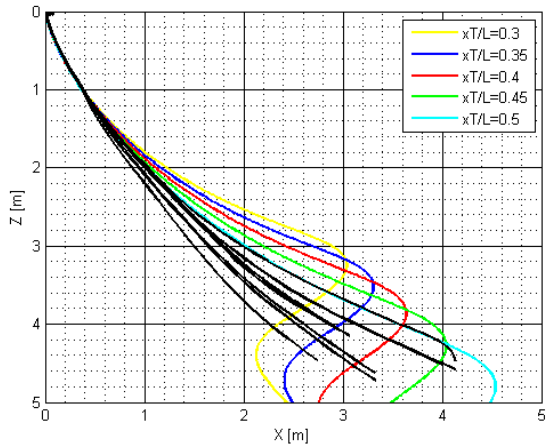

Figure 52: *X-Z-view: Comparison of the numerical and experimental results for Cylinder 1 in Table 6 dropped at 60 degree. The numerical calculations are represented with coloured lines, each colour represents a ten present change in the trailing edge position.* $C_{dz} = 1.0$ *and* $C_{dx} = 0.65$.

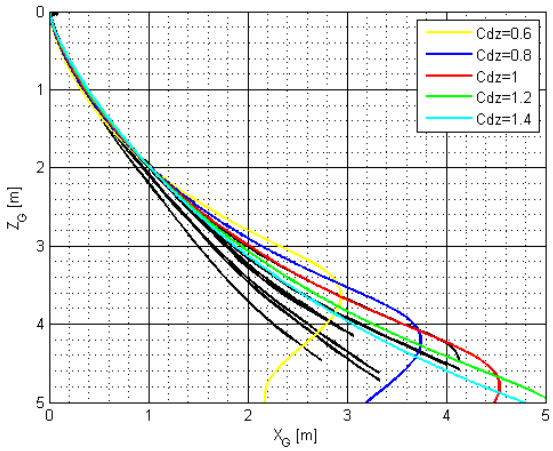

Figure 53: *X-Z-view: Comparison of the numerical and experimental results for Cylinder 1 in Table 6 dropped at 60 degree. The numerical calculations are represented with coloured lines, each colour represents a twenty present change in the* C_{dz}*-value.* $x_T/L = 0.5$ *and* $C_{dx} = 0.65$.

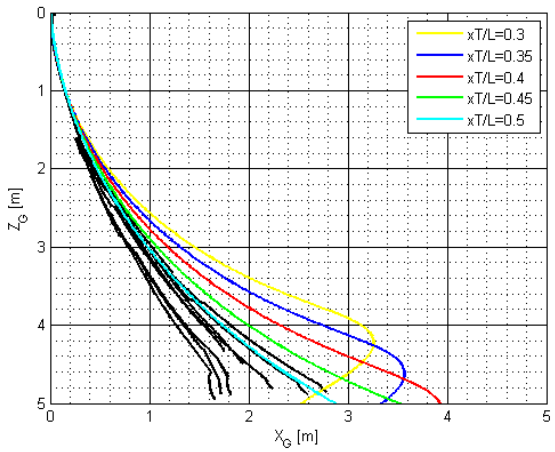

Figure 54: *X-Z-view: Comparison of the numerical and experimental results for Cylinder 1 in Table 6 dropped at 75 degree. The numerical calculations are represented with coloured lines, each colour represents a ten present change in the trailing edge position.* $C_{dz} = 1.0$ *and* $C_{dx} = 0.65$.

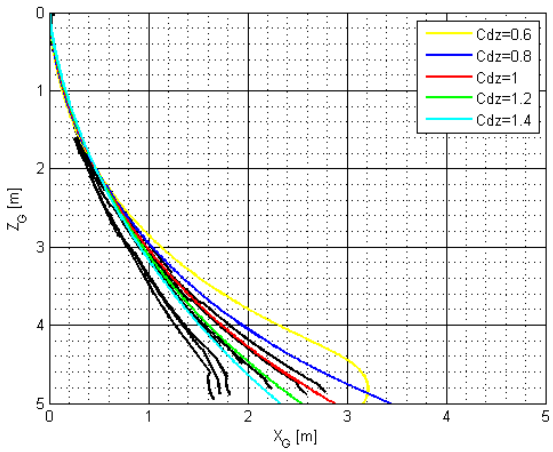

Figure 55: *X-Z-view: Comparison of the numerical and experimental results for Cylinder 1 in Table 6 dropped at 75 degree. The numerical calculations are represented with coloured lines, each colour represents a twenty present change in the* C_{dz}*-value.* $x_T/L = 0.5$ *and* $C_{dx} = 0.65$.

A comparison between X-Z-plane trajectories keeping the C_{dz}-value constant equal to 1.0 and the C_{dx}-value equal to 0.65, and variate the position of the effective trailing edge between $x_T = 0.3L$ and $x_T = 0.5L$, are shown in Figure 46, 48, 50, 52 and 54. As can be seen from the figures, a ten percent changing in the trailing edge position has a great influence on the calculated cylinder trajectory. It is interesting to observe that the

cylinder moves a greater distance in the horizontal direction when the position of the trailing edge is moved towards the geometrical trailing edge. This is a result of that an increased x_T-value will result in a smaller total moment on the cylinder, and that again will reduce the rotation accordingly (Aanesland , 1986). Studying the figures it also seems to be a general trend that larger x_T-values should be used for greater drop angles. For instance, at 75 degree drop angle $x_T = 0.5L$ seems to give the most similar trajectory, while at 15 degree drop angle this trailing edge position had the poorest fit. At smaller drop angles, using $0.5L$ as the effective trailing edge, the stabilisation effect seems to be overestimated. Therefore, for further simulations, $x_T = 0.5L$ will be used for cases with drop angles larger than 30 degrees and for drop angles equal 15 and 30 degrees $x_T = 0.4L$.

Trajectories were also simulated with different z directional drag coefficients, C_{dz}, given in Figure 47, 49, 51, 53 and 55. The trailing edge position was constant as indicated above and $C_{dx} = 0.65$. As can bee seen from the figures, an increased drag coefficient, C_{dz}, results in an increase in the spread in the X-direction. That indicates that a larger lateral resistance force slows down the falling motion and allows the cylinder to travel further in X-direction. The effect of changing the C_{dz}-value was found to be significant. As showed in the figures a twenty percent change has a significant impact on the position where the oscillating motion develops and the effect seems to increase with increasing drop angles. This may be a consequence of that higher drop angles cause larger velocities before the oscillating motion develops (see Figure 57).

The effect of changing the drag coefficient in the x-direction has also been investigated. Figure 56 shows the effect of changing the C_{dx}-value with twenty percent keeping C_{dz} and x_T/L constant equal to 1.0 and 0.5 for drops with initial angle equal to 45 degree. As can be seen from the figure, increasing this drag coefficient decreases the amplitude of the oscillating motion and has a slight impact on the vertical position of the first turn. But, in general the effect of changing this drag coefficient with twenty percent was found to be relatively small.

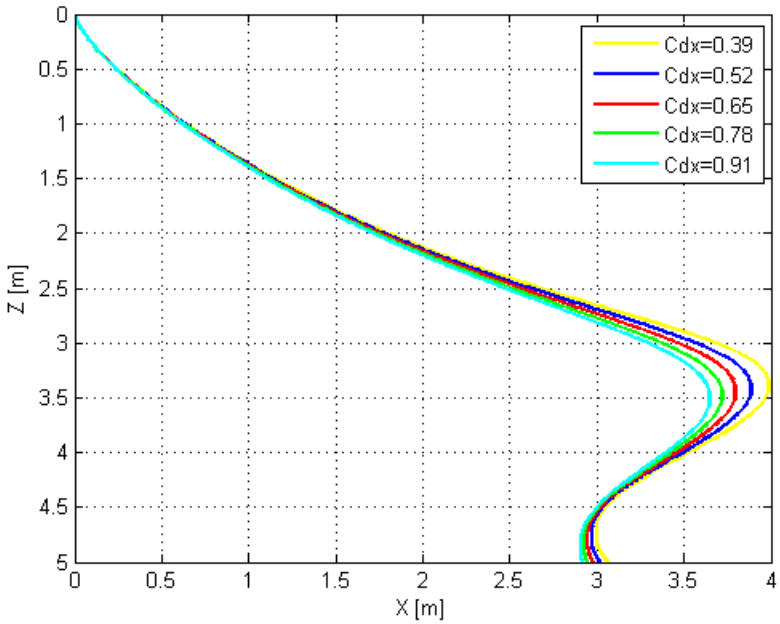

Figure 56: *The numerical calculations for Cylinder 1 in Table 6, dropped at 45 degree. Each coloured line represents a twenty present change in the C_{dx}-value. $x_T/L = 0.5$ and $C_{dz} = 1$.*

As showed in Figure 47 to 55 a relatively good agreement was found between the numerical and experimental trajectory for the 10 millimetre diameter cylinder with closed ends. But, the degree of similarity were found to be clearly sensitive to the chosen value of the effective trailing edge and the drag coefficient in z-direction, changing the values with a magnitude of twenty percent. The impact changing the drag coefficient in x-direction with this magnitude was found to be significantly smaller. So, by keeping the drag coefficient in x-direction constant at 0.65, which is a value suggested by Hoerner (1958), and the drag coefficient in z-direction at 1.0, the numerical calculation seems to fit quite well before the oscillating motion has developed (see Figure 47, 49, 51, 53 and 55). The position of the first turn from the simulations seams to have a good fit compared to the trajectories found from the experiment, except for at 15 degrees. But, as the oscillations develop the simulated oscillation period and amplification has a larger value than found from the experiment. For instance increasing C_{dx} to a high value will give a more equal amplification of the oscillation and decreasing the effective trailing edge value will reduce the oscillation period, but that will also have a large influence on for instance the position of the first turn. So, the simulated trajectories fit quite well to the first turn, but the calculated touch down point may deviate from the experiments due to the properties of the simulated oscillations.

The velocities of the 10 millimetre diameter cylinder are shown in Figure 57. The solid lines indicate the velocities found from the experiments and the dashed lines represent the numerical calculated total velocity. Equal colours means that the cylinders are dropped from equal initial drop angles. The drag coefficients used were $C_{dx} = 0.65$ and $C_{dz} = 1.0$. The trailing edge positions used were, as state earlier, in this thesis.

As can be seen from the figure, significant similarities between the experiment and the numerical calculations were found. The maximum total velocities seam to be around the same values and arise at similar depths. When the the oscillating motion has developed, the velocities decrease and start to vary around similar values. There are also some deviations, but it should be kept in mind that the plotted velocities from the experiments only represent one of the drops performed at this particular angle. Depending one the chosen drop from the experiments, the plotted velocity value will vary. The similarities observed between the simulations and the experiments emphasise that the three parameters chosen for velocity calculations, are fairly reasonable.

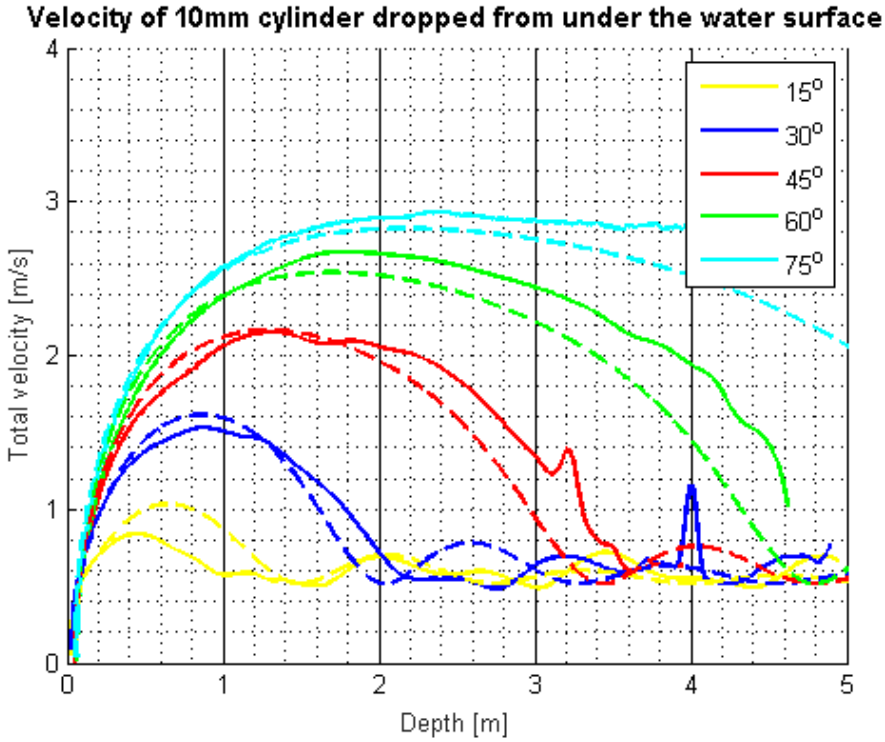

Figure 57: *Comparison between the total velocity found from the experiment and the numerical calculations. The solid lines represent the experiment, and the dashed lines the numerical calculations. Equal colour means equal drop angles. The cylinder is 10 millimetre diameter, equal to Cylinder 1 in Table 6.* $C_{dz} = 1$, $C_{dx} = 0.65$, $x_T/L = 0.4$ *for angles* $\leq 30^\circ$ *and* $x_T/L = 0.5$ *for angles* $> 30^\circ$.

The same three parameters for the drag coefficients and the trailing edge were also used to find the simulated cylinder orientation. Comparing the orientations of the cylinders found from the numerical calculations to the experiments, relatively great similarities were found. Figure 58 and 59 shows the orientation, calculated numerically and found from the experiments, of the 19 millimetre cylinder with closed ends dropped with 45 degree initial angle. Comparing the cylinder orientations in the X-Z-plane during the falling motion, it can be seen that for both cases the largest angle is the drop angle. After the drop the cylinder angle decreases and for both cases reach a horizontal position at approximately 0.5 meter above the maximal amplification of the first turn. Then the cylinder, for both cases, oscillate to the bottom with a small angle of orientation.

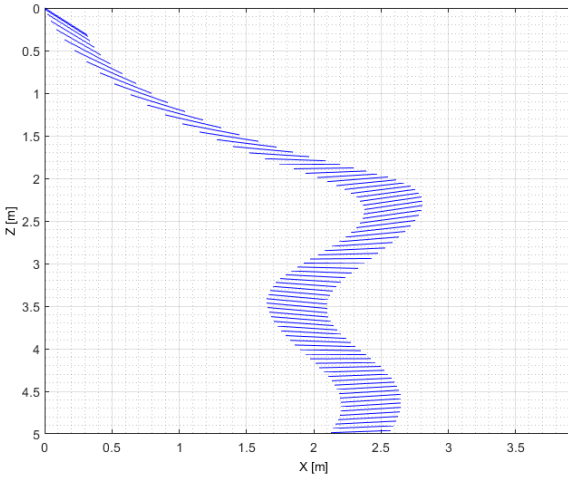

Figure 58: *The orientation, according to the numerical calculations, of a 19 millimetre diameter cylinder dropped with initial angle of 45 degree.*

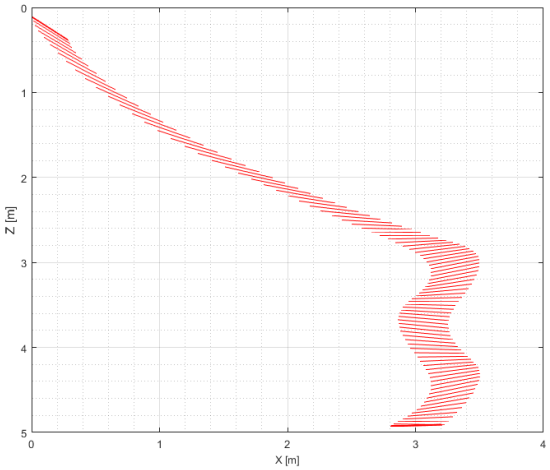

Figure 59: *The orientation, according to the experiment, of a 19 millimetre diameter cylinder dropped with initial angle of 45 degree.*

4.2.2 Cylinder with displaced centre of gravity

Figure 60 to 69 shows a comparison between numerical and experimental results for a cylinder with displaced centre of gravity, Cylinder 4 in Table 6. The numerical simulations are based on the theory presented in Section 2.1.3, presented by coloured lines. The figures presents the numerical simulation with constant drag coefficients. The drag coefficient in x-direction is 0.65 and the drag coefficient in z-direction is 1.0. Figure 60, 62, 64, 66 and 68 shows the cylinder dropped with the initial centre of gravity position over the cylinder volume centre and Figure 61, 63, 65, 67 and 69 gives the trajectories for the cylinder dropped with the initial centre of gravity position under the cylinder volume centre.

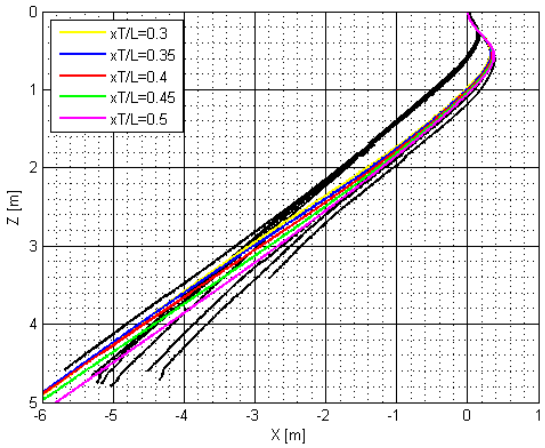

Figure 60: *X-Z-view: Comparison of the numerical and experimental results for cylinders with displaced centre of gravity, equal to Cylinder 4 in Table 6, dropped at 15 degree with the gravity centre upwards. The numerical calculations are represented with coloured lines. Each colour represents a ten present change in the trailing edge position.* $C_{dz} = 1.0$ *and* $C_{dx} = 0.65$.

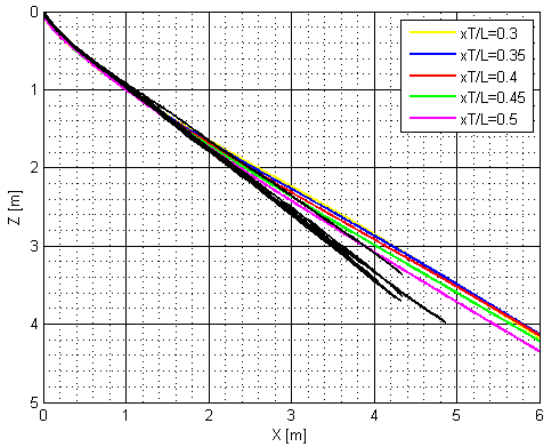

Figure 61: *X-Z-view: Comparison of the numerical and experimental results for cylinders with displaced centre of gravity, equal to Cylinder 4 in Table 6, dropped at 15 degree with the gravity centre downwards. The numerical calculations are represented with coloured lines. Each colour represent a ten present change in the trailing edge position.* $C_{dz} = 1.0$ *and* $C_{dx} = 0.65$.

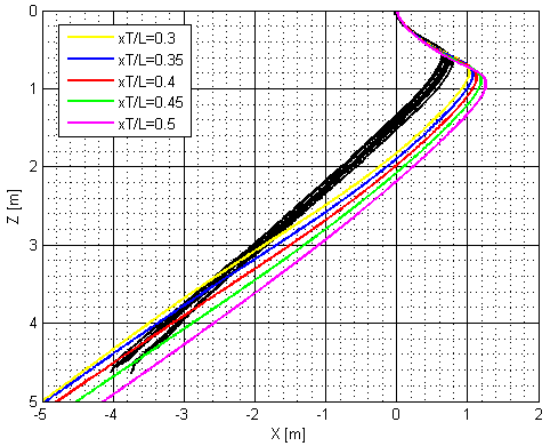

Figure 62: *X-Z-view: Comparison of the numerical and experimental results for cylinders with displaced centre of gravity, equal to Cylinder 4 in Table 6, dropped at 30 degree with the gravity centre upwards. The numerical calculations are represented with coloured lines. Each colour represents a ten present change in the trailing edge position.* $C_{dz} = 1.0$ *and* $C_{dx} = 0.65$.

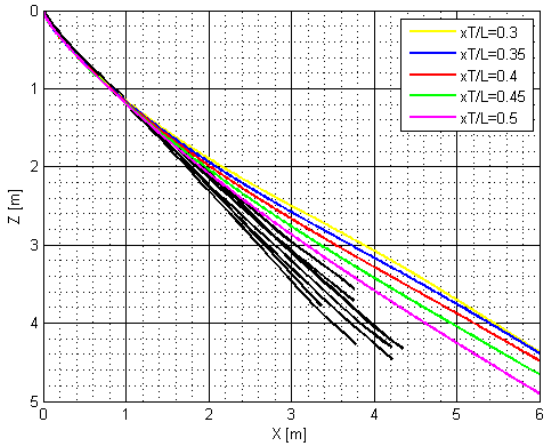

Figure 63: *X-Z-view: Comparison of the numerical and experimental results for cylinders with displaced centre of gravity, equal to Cylinder 4 in Table 6, dropped at 30 degree with the gravity centre downwards. The numerical calculations are represented with coloured lines. Each colour represents a ten present change in the trailing edge position.* $C_{dz} = 1.0$ *and* $C_{dx} = 0.65$.

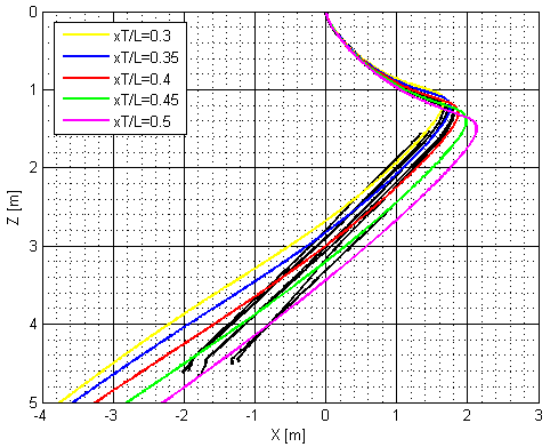

Figure 64: *X-Z-view: Comparison of the numerical and experimental results for cylinders with displaced centre of gravity, equal to Cylinder 4 in Table 6, dropped at 45 degree with the gravity centre upwards. The numerical calculations are represented with coloured lines. Each colour represents a ten present change in the trailing edge position.* $C_{dz} = 1.0$ *and* $C_{dx} = 0.65$.

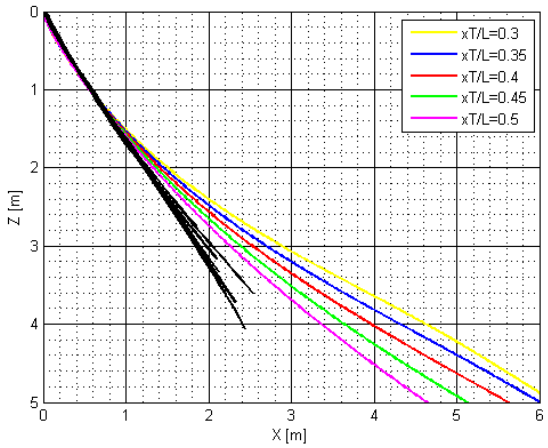

Figure 65: *X-Z-view: Comparison of the numerical and experimental results for cylinders with displaced centre of gravity, equal to Cylinder 4 in Table 6, dropped at 45 degree with the gravity centre downwards. The numerical calculations are represented with coloured lines. Each colour represents a ten present change in the trailing edge position.* $C_{dz} = 1.0$ *and* $C_{dx} = 0.65$.

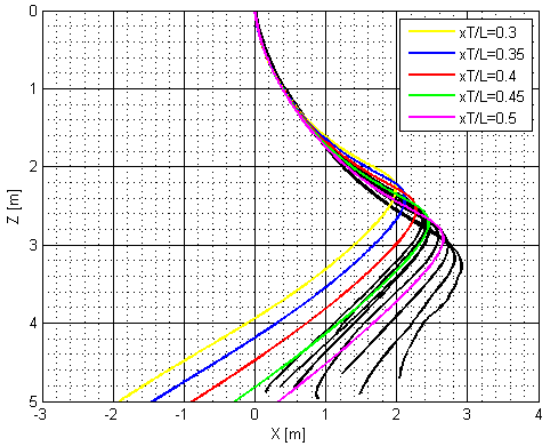

Figure 66: *X-Z-view: Comparison of the numerical and experimental results for cylinders with displaced centre of gravity, equal to Cylinder 4 in Table 6, dropped at 60 degree with the gravity centre upwards. The numerical calculation are represented with coloured lines. Each colour represents a ten present change in the trailing edge position.* $C_{dz} = 1.0$ *and* $C_{dx} = 0.65$.

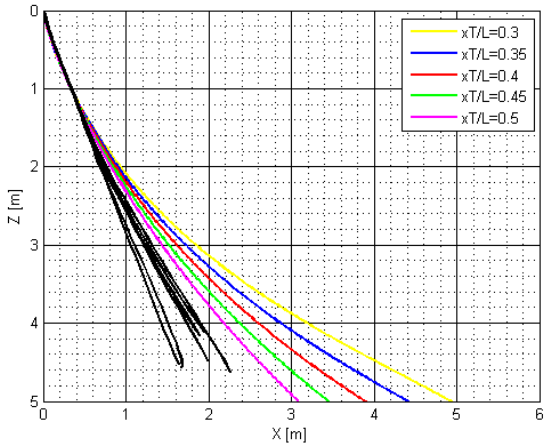

Figure 67: *X-Z-view: Comparison of the numerical and experimental results for cylinders with displaced centre of gravity, equal to Cylinder 4 in Table 6, dropped at 60 degree with the gravity centre downwards. The numerical calculations are represented with coloured lines. Each colour represents a ten present change in the trailing edge position.* $C_{dz} = 1.0$ *and* $C_{dx} = 0.65$.

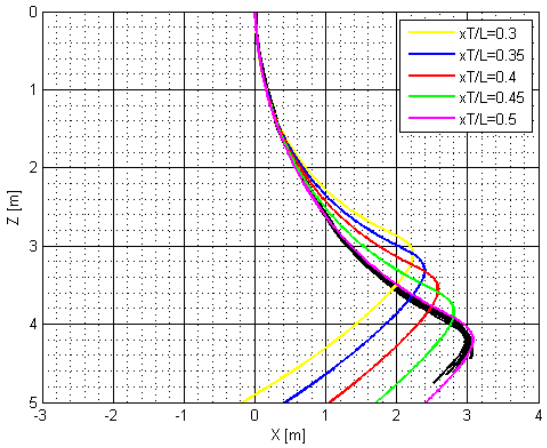

Figure 68: *X-Z-view: Comparison of the numerical and experimental results for cylinders with displaced centre of gravity, equal to Cylinder 4 in Table 6, dropped at 75 degree with the gravity centre upwards. The numerical calculations are represented with coloured lines. Each colour represents a ten present change in the trailing edge position.* $C_{dz} = 1.0$ *and* $C_{dx} = 0.65$.

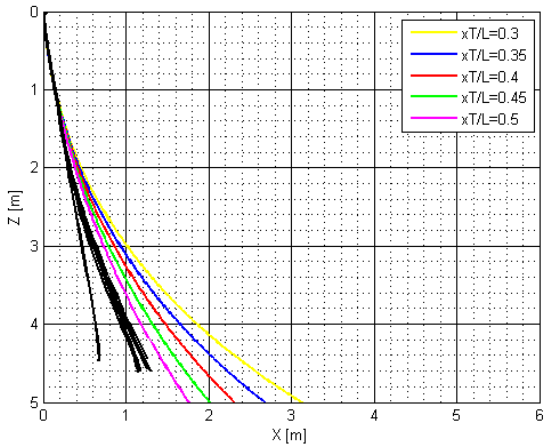

Figure 69: *X-Z-view: Comparison of the numerical and experimental results for cylinders with displaced centre of gravity, equal to Cylinder 4 in Table 6, dropped at 75 degree with the gravity centre downwards. The numerical calculations are represented with coloured lines. Each colour represents a ten present change in the trailing edge position.* $C_{dz} = 1.0$ *and* $C_{dx} = 0.65$.

By studying Figure 60 to 69, the effect of changing the trailing edge position is illustrated. It was found that the chosen value of the trailing edge position has considerable influence on the simulated trajectory, especially when the drop angle increases. In general it seams that the geometrical trailing edge has the nearest similarities to the experimental results, except for the smallest drop angles, were the centre of gravity initially were placed over the cylinder volume centre. For these, it looks like a smaller value of the trailing edge will give a better fit. When travelling to the bottom with the centre of gravity under the cylinder volume centre, it also looks like the cylinders dropped during the experiments followed a straighter trajectory than the numerical calculated trajectory. The calculated trajectory follows a slightly concave path. The numerical simulations will therefore in general give a more conservative value for the touch down point.

The effect of changing the drag coefficient in z-direction is shown in Figure 70 and 71, that shows cylinders dropped at 45 degree with the centre of gravity upwards and downwards. Similar effects as described in Section 4.2.1 were found. A twenty percent change in the the C_{dz}-value had an effect on the excursion in the X-direction and the positions were the cylinder trajectories made a turn. The effect of changing the drag coefficient in x-direction was also for this cylinder type found to be relatively small compared to the effect of changing trailing edge position and the drag coefficient in z-direction.

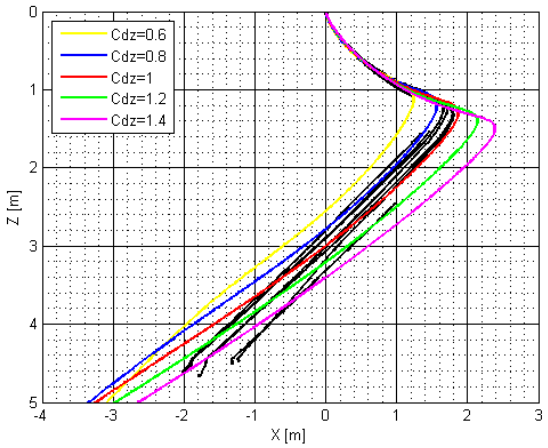

Figure 70: *X-Z-view: Comparison of the numerical and experimental results for a cylinder with displaced centre of gravity, equal to Cylinder 4 in Table 6, dropped at 45 degree with the gravity centre upwards. The numerical calculations are represented with coloured lines. Each colour represents a twenty present change in the C_{dz}-value. $x_T/L = 0.4$ and $C_{dx} = 0.65$.*

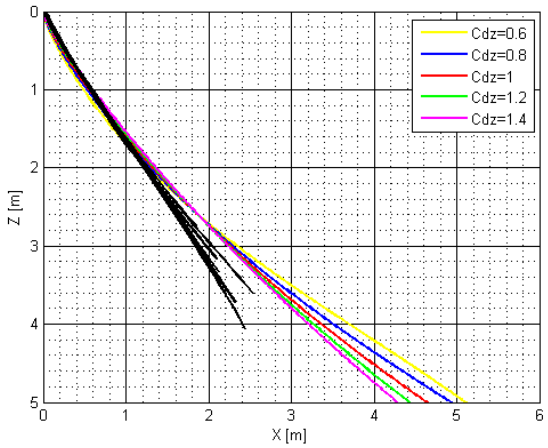

Figure 71: *X-Z-view: Comparison of the numerical and experimental results for a cylinder with displaced centre of gravity, equal to Cylinder 4 in Table 6, dropped at 45 degree with the gravity centre downwards. The numerical calculations are represented with coloured lines. Each colour represents a twenty present change in the C_{dz}-value. $x_T/L = 0.5$ and $C_{dx} = 0.65$.*

Figure 72 and 73 shows the numerical calculated total velocity versus the total velocity found from the experiments. The dotted lines represents the simulated values and the solid line represents an example of the total velocity development found from the experiments. Figure 72 shows the total velocity for the cylinder dropped with the centre of gravity upwards, a trailing edge value equal to $0.4L$ is used for the three smallest drop angles and a trailing edge value equal to $0.5L$ is used for the highest drop angles. Figure 73 shows the total velocity development for cylinders dropped with the centre of gravity downwards. For this case, a trailing edge position equal to $0.5L$, is used for all drop angles. The drag coefficients for both cases, C_{dz} and C_{dx}, are set equal to 1.0 and 0.65. Studying the figures, great similarities between the total velocity from the simulation and from the experiments were found. A general difference in velocity at the tank bottom, was however found. According to the velocity found from the experiments, it looks like the cylinders will reach a constant terminal velocity prior to reaching five meter depth, but the simulations does not coincide. The simulated velocity seams to reach the same value as the terminal velocity from the experiments, but the velocity does not stabilise at this value. It was found that the simulated velocity decreases to lower velocity before it reached a constant value. This is illustrated in Figure 74, that shows the velocity development at larger depths for the cylinder dropped with the centre of gravity downwards. This observation may be as a consequence of a miss match between the simulated cylinder orientation and the cylinder orientation in the experiments. It seams like the cylinder orientation takes longer time to stabilise in the simulations than in the experiments. This will also lead to a smaller bottom impact angle for the simulations compared to the experiments.

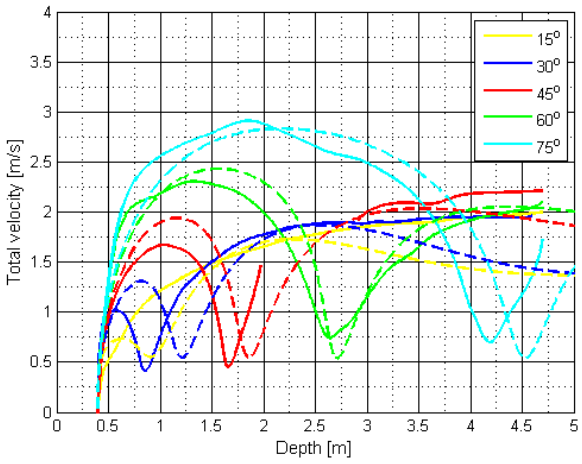

Figure 72: *Comparison between the total velocity found from the experiments and the numerical calculations dropped with the centre of gravity upwards. The solid lines represent the experiment, and the dashed lines is the numerical calculations. Equal colour means equal drop angles. The cylinder is a 10 millimetre diameter equal to Cylinder 1 in Table 6.* $C_{dz} = 1.0$, $C_{dx} = 0.65$, $x_T/L = 0.4$ *for angles* $\leq 45°$ *and* $x_T/L = 0.5$ *for angles* $> 45°$.

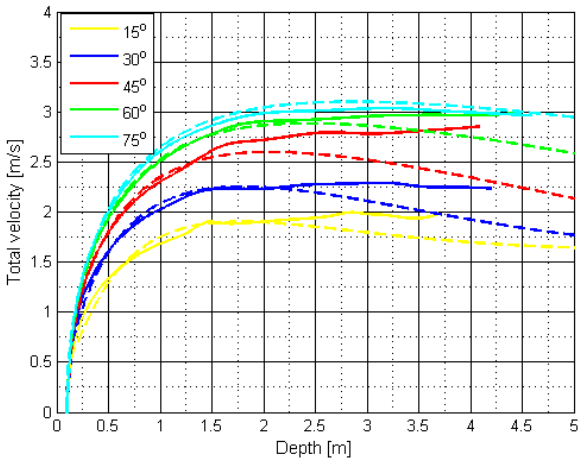

Figure 73: *Comparison between the total velocity found from the experiments and the numerical calculations dropped with the centre of gravity downwards. The solid lines represent the experiment, and the dashed lines is the numerical calculations. Equal colour means equal drop angles. The cylinder is a 10 millimetre diameter equal to Cylinder 1 in Table 6.* $C_{dz} = 1.0$, $C_{dx} = 0.65$, $x_T/L = 0.4$ *and* $x_T/L = 0.5$.

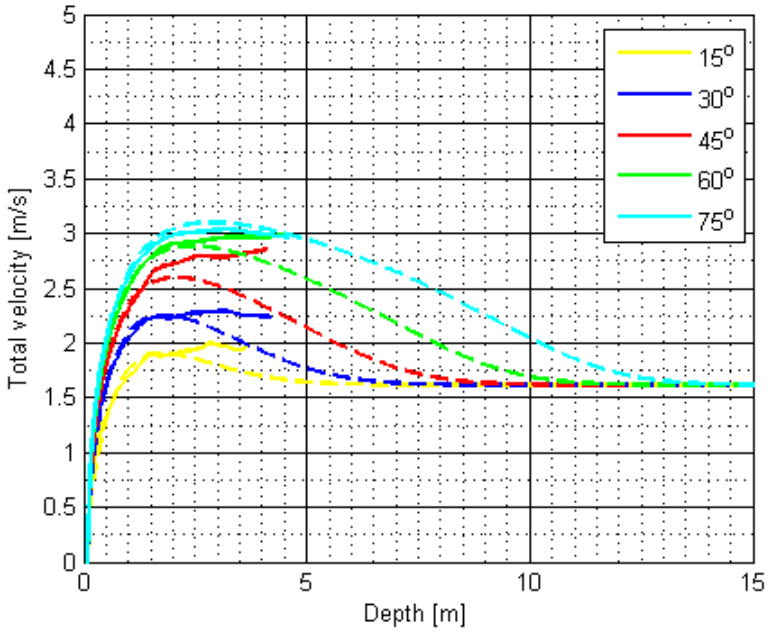

Figure 74: *Stabilisation of the total velocity, comparing the total velocity found from the experiments and the numerical calculations dropped with the centre of gravity downwards. The solid lines represent the experiment, and the dashed lines is the numerical calculations. Equal colour means equal drop angles.*

4.2.3 Cylinder with open ends

Experiments with open ends cylinders have also been performed. Figure 75 and 76 shows the trajectories for a 10 millimetre diameter cylinder dropped with 45 degree initial angle, were the black lines represents the experiments. The coloured lines shows the numerical simulations based on the theory for open cylinders presented in Section 2.1.3. The different colours shows the variation in the effective trailing edge position and drag coefficient. The effect from changing the trailing edge position and the drag coefficient in z-direction were found similar, as described for the cylinders with closed ends. The figures illustrate the general trend comparing the simulations and the experiments. As showed in Figure 76, keeping the trailing edge position equal to $0.5L$, does not match very well to the experiments, as the oscillating motion develops at deeper water depths. If the effective trailing edge position was set equal to $0.4L$, it would have followed the experimental trajectories until the oscillation motion developed. But, in this case, the oscillations would have developed too early and would have given a smaller excursion than found from the experiments. So, in general the suggested theory gives a too small radial excursion or a oscillating motion that develops on too deep water depths.

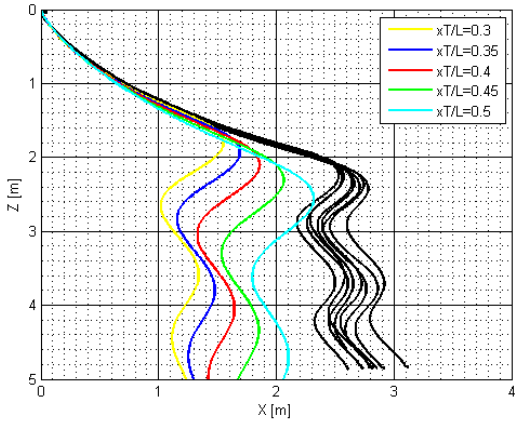

Figure 75: *X-Z-view: Comparison of the numerical and experimental results for a cylinder with open ends equal to Cylinder 6 in Table 6, dropped at 45 degree. The numerical calculations are represented with coloured lines. Each colour represents a ten present change in the trailing edge position.* $C_{dz} =$ 1.0 *and* $C_{dx} = 0.65$.

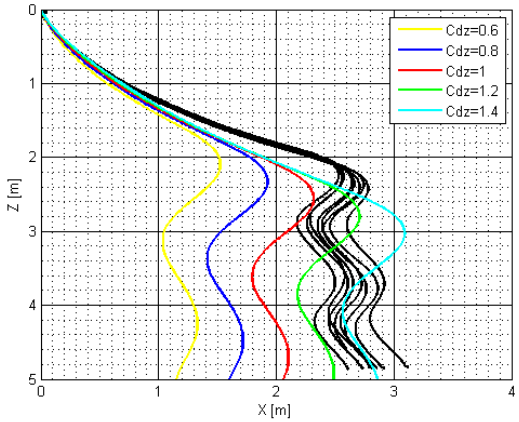

Figure 76: *X-Z-view: Comparison of the numerical and experimental results for a cylinder with open ends equal to Cylinder 6 in Table 6, dropped at 45 degree. The numerical calculations are represented with coloured lines. Each colour represents a twenty present change in the* C_{dz}*-value.* $x_T/L = 0.5$ *and* $C_{dx} = 0.65$.

A possible explanation for the larger differences between the simulations and experiments for open cylinders, could be that the viscous forces in x-direction are to high. The friction coefficient used assumes a turbulent axisymmetric flow, both inside and outside the cylinder. This was found to be reasonable since the flow mainly will be inside the turbulent range of Reynolds numbers. For an open cylinder, the front area is smaller than for a closed end cylinder, reducing the triggering of instabilities. It is

therefore likely that the flow will be less turbulent, specially on the outer side of the cylinder. Therefore the fiction coefficient suggested by Aanesland (1987) was also investigated. He assumed a laminar boundary layer flow, using Blasius formula for the friction coefficient. The viscous forces in the x-direction are expressed as in Equation 43. Assuming these viscous forces, both inside and outside the cylinder, the simulated trajectories for a 45 degree drop angle becomes as showed in Figure 77, were the trajectories for laminar and turbulent boundary layer flow are compared. As can be seen from the figure, assuming a laminar boundary layer seems to give a more similar trajectory. The amplitude and the period of the oscillating motions are still to large, but the excursion to the first turn seams to be more similar.

$$F_{dx} = -0.664\pi D\sqrt{\nu\rho^2 L}U_1\sqrt{|U_1|} - \frac{1}{8}\rho\pi C_{dx}D^2U_1|U_1| \tag{43}$$

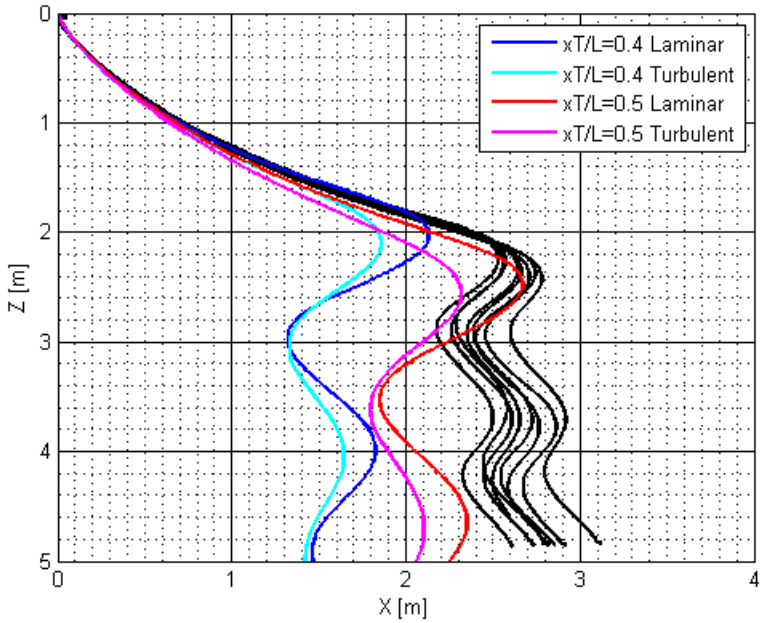

Figure 77: *X-Z-view: Comparison of the numerical and experimental results for cylinders with open ends equal to Cylinder 6 in Table 6, dropped at 45 degrees. The numerical calculations are represented with coloured lines. The colours indicate if it is assumed laminar or turbulent flow in the simulations, and the position of the trailing edge.* $C_{dz} = 1.0$ *and* $C_{dx} = 0.65$.

4.3 Error souses and possible improvements to the theory

The numerical theory presented is a two dimensional theory obviously causing that there will be some three dimensional effects lost compare to the experiments. For instance, as studied by Werle (1979), an asymmetric cross-flow on the cylinder in the experiment will occur. In the paper, written by Alsos and Faltinsen (n.d.), it is proposed that the motions in the X-Y-plane is a consequence of non-symmetric vortex

shedding along the length of the cylinder. The effect of the asymmetric cross-flow, variate the drop angle between 0 and 90 degrees, were found largest between 60 and 70 degree drop angle. The largest excursion in Y-direction was found to be approximately 0.5 meter. In Aanesland (1987) it is also stated that the axial rotation of the cylinder will create a small lift force normal to the X-Z-plane, this is called the Magnus effect. This effect is studied by Xiang (2017) and is claimed to have a significant effect on the motion in X-Y-plane, with greatest impact between 0 and 45 degree drop angel.

Some adjustments to the two dimensional theory implemented, could also be performed. For instance, as performed by Alsos and Faltinsen (n.d.), a varying drag coefficient in z-direction is used. This is based on the effect found by Sarpkaya (1966), that an impulsive started flow will not have a constant drag coefficient in z-direction, but the drag coefficient will variate with time (see Figure 22). Another effect neglected in the simulations is the influence from the tank bottom. When the cylinder moves close to the bottom, there will be an increase in the added mass that will cause a reduction in the vertical velocity (Aanesland , 1987).

Some of the differences between the numerical simulations and experimental results can also be explained by possible error sources in the experiments. For instance, a Oqus camera system is sensitive to vibrations and a smaller movement or vibration can possibly affect the calibration of the cameras. The cylinders were also equipped with a approximately 0.25 millimetre thick reflective marker tape (see Figure 20). The markers were placed around the cylinder end and on the rear cylinder side. The marker could possibly lead to an increase in the drag coefficient and may have an influence on the vortex shedding. To control this influence, some drop experiments with an additional symmetric and asymmetric drag at the rear cylinder end was performed. From the experiments with an additional asymmetric drag, large variations for drops with the same initial drop conditions were found, and an essential increase in the X-Y-plane spreading compared to the initial experiments were also observed. This indicates that the marker influence on the spreading is likely to be small. Fore the experiments with an additional symmetric drag, a 16 millimetre diameter circular plastic disk was placed at the aft cylinder end of a 10 millimetre diameter cylinder. Slightly smaller excursions, compared to the initial experiments, were found. But, the fact that the differences in excursions were relatively small, even though the diameter of the disk were considerable larger than the cylinder diameter, indicates that the marker influence to the drag may be relatively small. During the experiment it was also a problem that some of the cylinders with closed ends started to leak water. Therefore the cylinder weights were measured before every drop. However, the measured weight had a deviation of ± 1 gram. A weight variation could therefore have an effect on the cylinder trajectory.

5 Conclusions

Slender cylinders falling in still water has been studied both with a numerical two dimensional theory based on manuvering equations, and by 1:20 model scale experiments in a water tank. The trajectories and velocities were investigated with respect to the cylinder's physical parameters (length to diameter ratio, centre of gravity location and open or closed ends) and the initial drop conditions (drop angle and drop position).

Six different types of trajectories were found through the experiments. The results showed that the centre of gravity location and the initial drop angle were the most critical factors determining the trajectories. These parameters also had a significant influence on cylinder velocity, due to their considerable impact on cylinder orientation. It was found that the maximum cylinder velocity increased with increasing drop angle. The total cylinder velocity was found lowest when the cylinder had developed the oscillating motion with a close to horizontal orientation. This showed that the viscous forces were more dominant in the lateral, than in the axial direction.

The effect of the cylinder physical parameters were studied. It was found that an increase in cylinder diameter made the oscillating motion develop earlier. Hence, increased cylinder diameter result in reduced radial excursion. The maximum total velocities were also found to decrease with increasing diameter and occurred at a position prior to development of the oscillating motion. When the oscillations had developed, the velocities were found varying around a smaller value at approximately 0.6 m/s. Studying cylinders with displaced centre of gravity, it was experienced that the degree of displacement had a significant impact on the excursion. Increasing the displacement of the centre of gravity, made the cylinders that dropped with the centre of gravity upwards turn after a shorter distance and the cylinders with the initial position of the centre of gravity downwards got a smaller radial excursion. The largest radial excursions were found for cylinders with the smallest centre of gravity displacement, displaced by 1.4 centimetre and dropped at 15 degree angle. The largest excursion was found to be around six meter, one meter longer than the water depth. For the cylinders with displaced centre of gravity, it was also found that they will reach a terminal velocity and have relatively large bottom impact velocities. For cylinders with open ends, it was found that an increase in diameter resulted in an earlier development of the oscillating motion. When comparing open ended cylinders with closed ended ones, it was found that the oscillations developed earlier for cylinders with open ends. This again resulted in shorter radial excursions for open ended cylinders.

Comparing the experimental results to DNV's recommended practice, DNVGL-RP-F107, longer excursions were experienced in the experiments than when using DNV's simplified method for calculations of object excursion. So, for excursions at sea depths lower than approximately 400 meter, DNV's method will in several cases not be conservative at all. It was found that an angular deviation for longed shaped objects,

3.4 times higher than DNV's recommended value, would have provided a better approach for the cylinders with the largest excursion.

Studying the directional stability of the cylinders, how much the trajectories turn in the X-Y-plane, the instability was found to increase with diameter for closed ends cylinders. The directional stability was largest for open cylinders and cylinders with displaced centre of gravity.

Results from the experiments were compared to the numerical simulations. Good agreements were observed, but the similarities were significantly dependent on the chosen value for the effective trailing edge position, x_T, and the drag coefficient in z-direction, C_{dz}. Large x_T-values was seemingly better for simulations with large initial angles. The largest deviations between the simulations and the experiments were found for cylinders with open ends. To explain the differences between the experiments and the simulations, several causes were detected. First of all, the presented theory is a two dimensional theory and will obviously cause loss of some three dimensional effects compared to the experiments. Further, weaknesses in the numerical theory and possible error sources during the experiments could also be an explanation. Even though some disagreements between the simulations and the experiments were found, the simple two dimensional method presented provides good indications for the trajectory and velocity of cylindrical objects falling through the water column.

6 Further work

For further work there are several effects that could be interesting investigating, both through experiments and as further development of the numerical calculations.

- The effect of using a non constant transverse drag coefficient as presented by Alsos and Faltinsen (n.d.) in the two dimensional numerical calculation should be considered
- Different shapes and more complex shaped objects, which may accidentally fall into the ocean during offshore operations should be investigated
- The effect of water impact loads, and air cavities during water penetrating should be studied closer
- The influence changing the drop height would be of interest to study
- The effect of surface waves and current should be studied
- In order to make a proper statistical distribution for expected excursions, it would be of interest to perform a higher number of cylinder drops during the experiment. Both a higher number and a larger variation in the physical parameters would be beneficial in this respect.

References

Aanesland, V. , 1986, Experimental and numerical investigations of accidental drops of drilling tubes, Technical report, Marintek.

Aanesland, V. , 1987, Numerical and experimental investigation of accidentally falling drilling pipes, 19th Annual OTC.

Alsos, H. S. and Faltinsen, O. M. , n.d., 3d motion dynamics of axisymmetric bodies falling through water. Revised revision submitted to Ocean Engineering.

Awotahegn, M. B. , 2015, Experimental investigation of accidental drops of drill pipes and containers during offshore operations., Master's thesis, UIS.

Carlsen, F. , 2017, Sammendragsrapport utviklingstrekk 2016 norsk sokkel, risikonivå i norsk petroleumsvirksomhet, Technical report, Ptil.

Chu, P. C., Gilles, A. and Fan, C. , 2005, Experiment of falling cylinder through the water column, Technical report, Experimental Thermal and Fluid Science.

DNVGL , 2016, Standard, DNVGL-ST-E406, Design of free-fall lifeboats, Technical report, DNVGL.

DNVGL , 2017, Recommended practice, DNV-RP-F107, Risk assessment of pipeline protection, Technical report, DNVGL.

DROP , 2016, 'Dropped objects register of incidents & statistics'.
URL: *http://www.doris.dropsonline.org/*

Faltinsen, O. M. , 1990, *Sea loads on ships and offshore structures*, Cambridge University Press.

Faltinsen, O. M. , 2005, *Hydrodynamics of High-Speed Marine Vehicles*, Cambridge University Press.

Hoerner, S. F. , 1958, *Fluid Dynamic Drag*.

Hui, S. and Faltinsen, O. M. , 2013, 'Accidentally dropped pipe. Exercise 10.10.5 in Faltinsen, O. M., 2005, Hydrodynamics of high-speed marine vehicles, Cambridge university press.', Exercise solution.

Katteland, L. H. and Øygarden, B. , 1995, Risk analysis of dropped objects for deep water development, Technical report, Proc. of the 14th OMAE.

Kirkegaard, J., Wolters, G., Sutherland, J., Soulsby, R. and Frostick, L. , 2011, *User Guide to Physical Modelling and Experimentation*, CRC Press.

Kreyszig, E. , 2006, *Advanced Engineering Mathematics*, 9th ed. edn, John Wiley & Sons.

Lamont, P. and Hunt, B. , 1976, Pressure and force distributions on a sharp-nosed circular cylinder at large angles of inclination to a uniform subsonic stream, Technical report, J. Fluid Mech., 76, 519-59.

Lie, H., Fylling, I. and Lehn, E. , 2009, Hydrodynamic and safety aspects of mooring line anchors in accidental free fall, *in* 'OMAE2009-80168'.

Newman, J. N. , 1977, *Marine Hydrodyamics*, The MIT Press, Cambridge, Massachusetts, and London, England.

OES , n.d., 'Dropped objects – what are they and what is the impact to your business?'. **URL:** *https://www.oesgroup.com/dropped-objects-article/*

Pettersen, B. , 2007, *Kompendium: TMR4247 Marin teknikk 3 Hydrodynamikk*, INSTITUTT FOR MARIN TEKNIKK.

Sarpkaya, T. , 1966, Separated flow about lifting bodies and impulsive flow about cylinders, Technical report, University of Nebraska.

Sarpkaya, T. , 1978, Impulsive flow about a circular cylinder, Technical report, Monterey, California. Naval Postgraduate School.

Serway, R. A. and Jewett, J. W. , 2014, *Physics for scientists and engineers*, Brooks/Cole, Cengage learning.

Steen, S. , 2014, *Lecture notes: TMR7 Experimental Methods in Marine Hydrodynamics*, INSTITUTT FOR MARIN TEKNIKK.

Ueda, Y., Uemura, T. and Iguchi, M. , 2010, Entry of inclined hydrophobic and hydrophilic circular cylinders into water, Technical report, J Vis 14:7–9.

Werle, H. , 1979, Vortices on slender bodies at high angles of attack, Technical report, L'Aeronautique et l'Astronautique, 79, 3-22.

White, F. M. , 1972, 'An analysis of axisymmetric turbulent flow past a long cylinder', *Journal of Basic Engineering* .

Xiang, G. , 2017, Motion Dynamics of Dropped Cylindrical Objects, PhD thesis, University of New Orlean.

Yasseri, S. , 2014, 'Experiment of free-falling cylinders in water', *Underwater Technology 32* .

Appendix

A complete overview of the experimental results

June 2018

Contents

A Position plots

A.1 Drop of 10 mm diameter cylinders under the water surface

A.1.1 15° initial drop angle

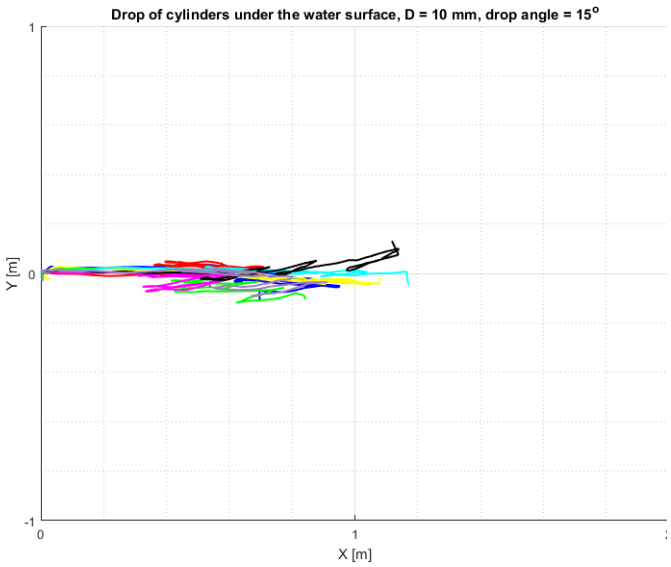

Figure 1: X-Y view: Drop of 10 mm diameter cylinders under the water surface at 15° initial drop angle. Each coloured line represents a drop.

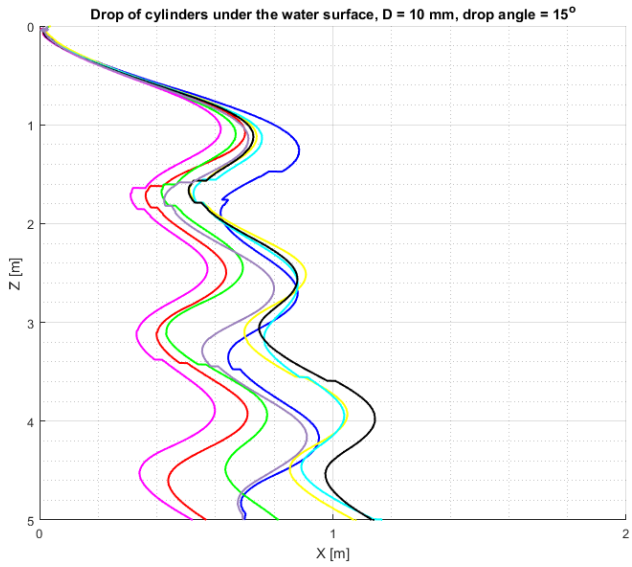

Figure 2: X-Z view: Drop of 10 mm diameter cylinders under the water surface at 15° initial drop angle. The X-coordinates are radial coordinates from the X-Y plane and each coloured line represents a drop.

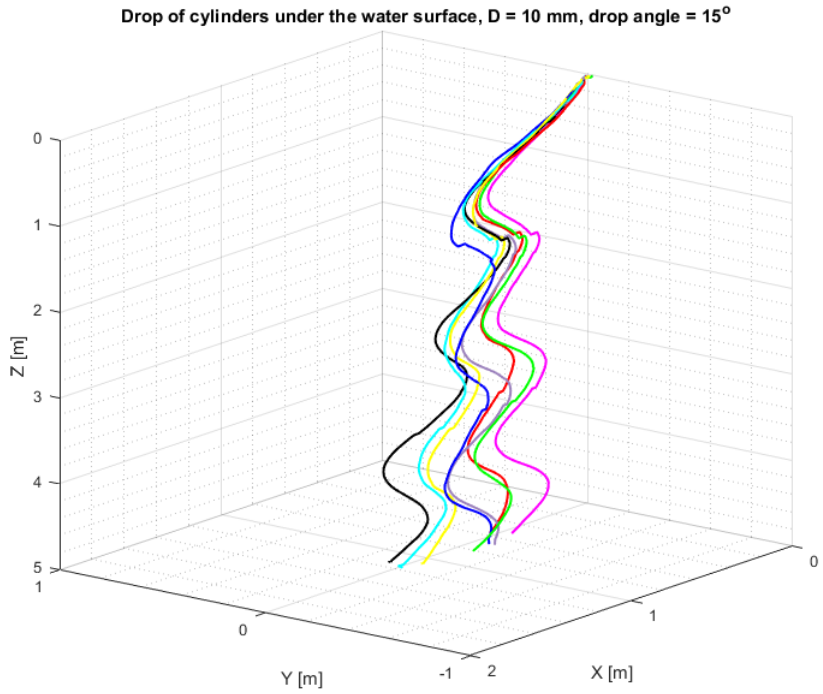

Figure 3: X-Y-Z view: Drop of 10 mm diameter cylinders under the water surface at 15° initial drop angle. Each coloured line represents a drop.

A.1.2 30° initial drop angle

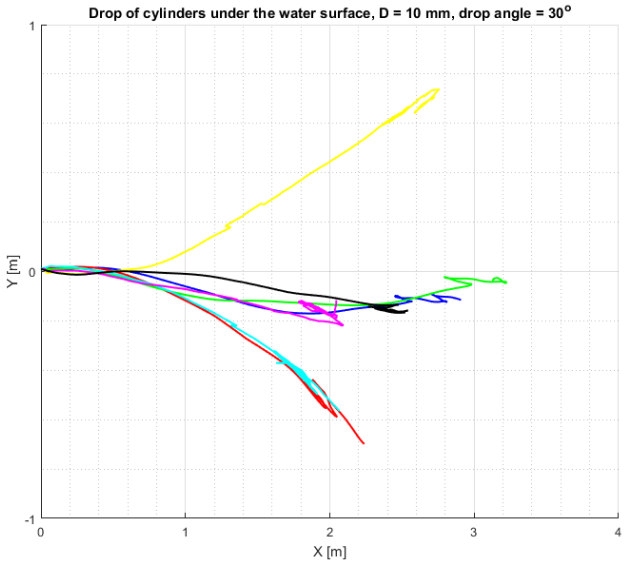

Figure 4: X-Y view: Drop of 10 mm diameter cylinders under the water surface at 30° initial drop angle. Each coloured line represent a drop in order.

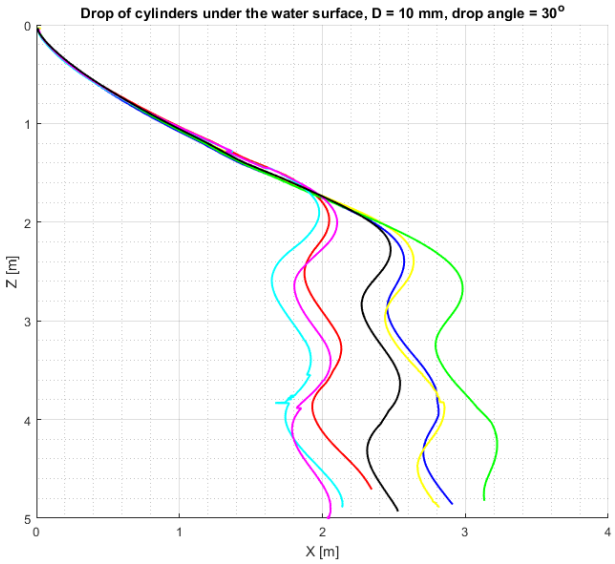

Figure 5: X-Z view: Drop of 10 mm diameter cylinders under the water surface at 30° initial drop angle. The X-coordinates are radial coordinates from the XY plane and each coloured line represents a drop.

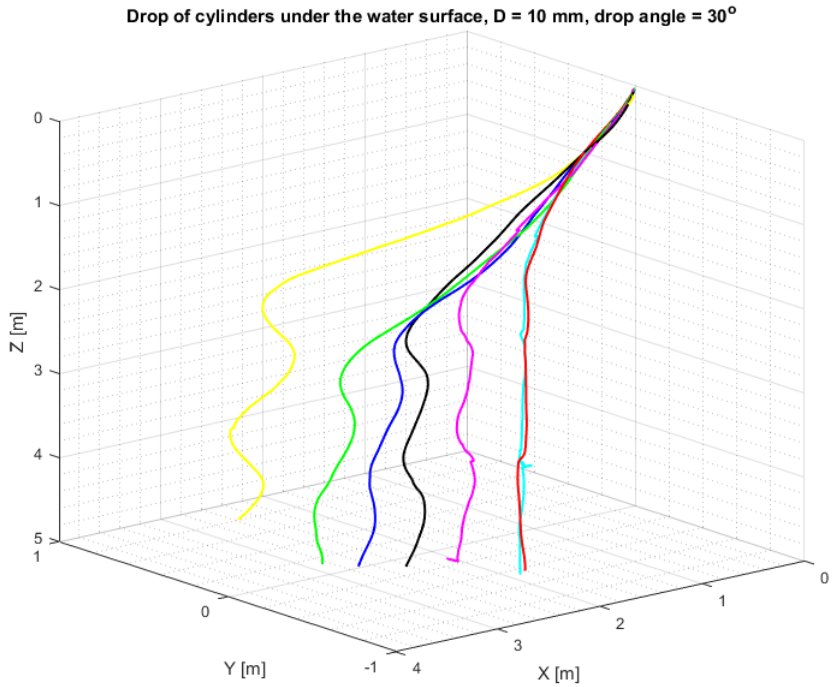

Figure 6: X-Y-Z view: Drop of 10 mm diameter cylinders under the water surface at 30° initial drop angle. Each coloured line represents a drop.

A.1.3 45° initial drop angle

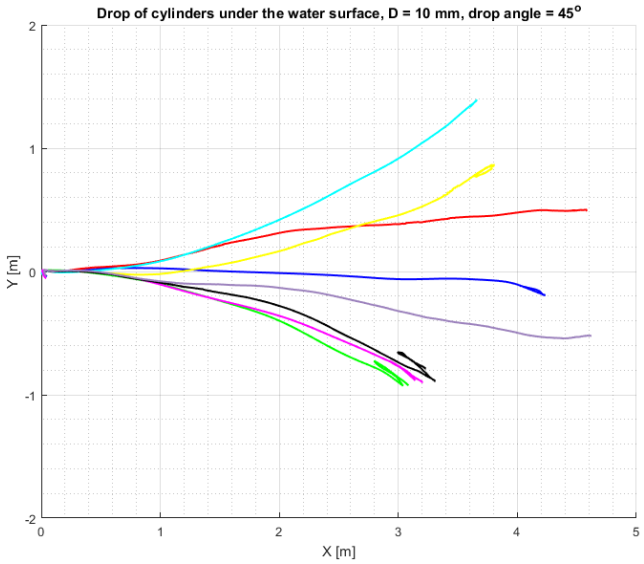

Figure 7: X-Y view: Drop of 10 mm diameter cylinders under the water surface at 45° initial drop angle. Each coloured line represent a drop in order.

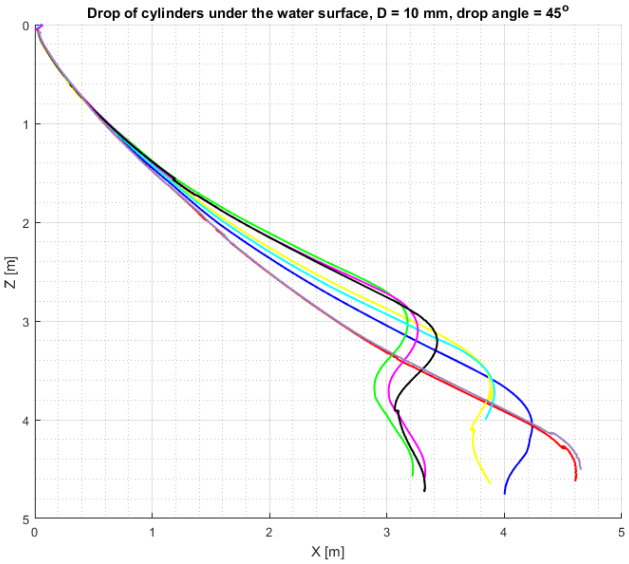

Figure 8: X-Z view: Drop of 10 mm diameter cylinders under the water surface at 45° initial drop angle. The X-coordinates are radial coordinates from the XY plane and each coloured line represents a drop.

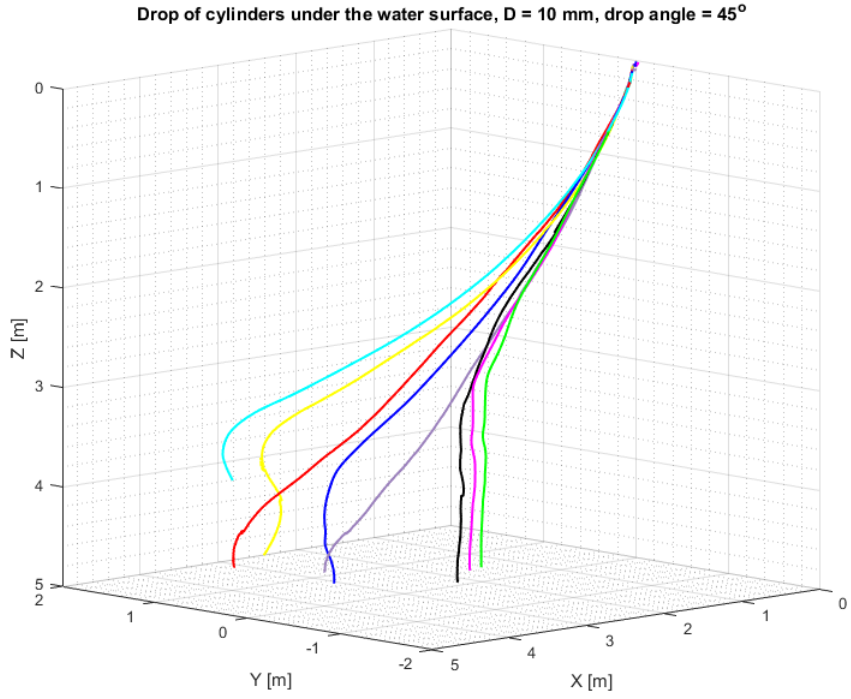

Figure 9: X-Y-Z view: Drop of 10 mm diameter cylinders under the water surface at 45° initial drop angle. Each coloured line represents a drop.

A.1.4 60° initial drop angle

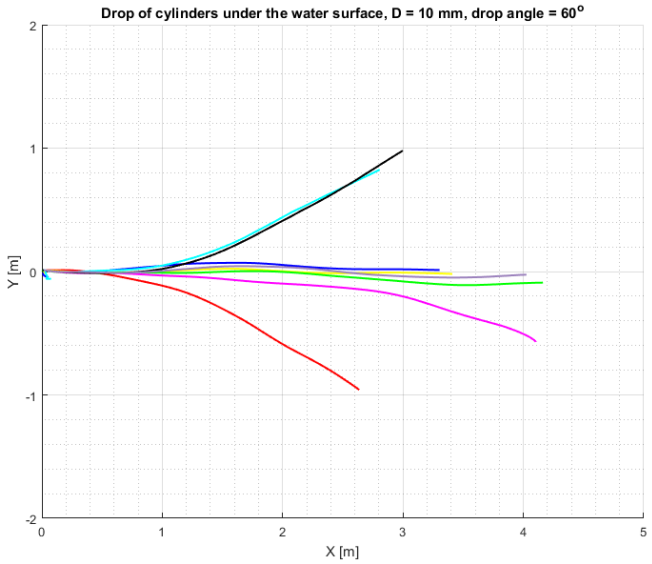

Figure 10: X-Y view: Drop of 10 mm diameter cylinders under the water surface at 60° initial drop angle. Each coloured line represent a drop in order.

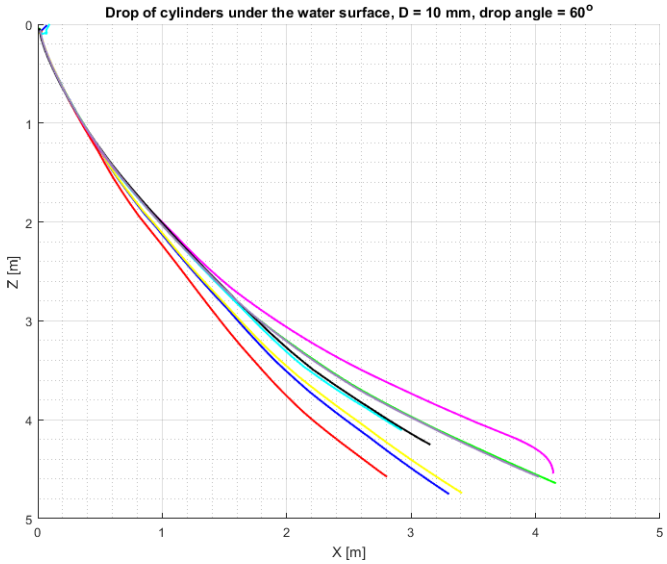

Figure 11: X-Z view: Drop of 10 mm diameter cylinders under the water surface at 60° initial drop angle. The X-coordinates are radial coordinates from the XY plane and each coloured line represents a drop.

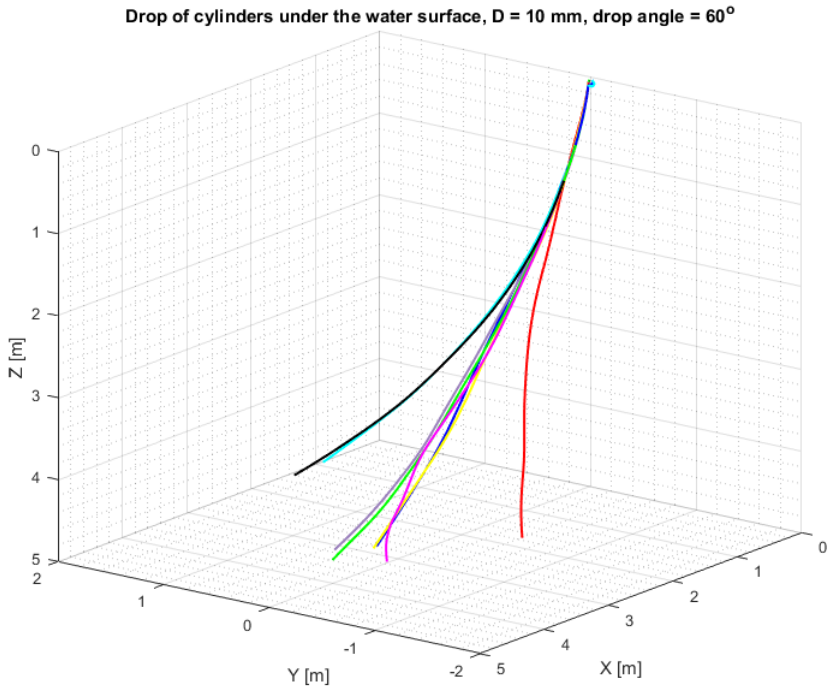

Figure 12: X-Y-Z view: Drop of 10 mm diameter cylinders under the water surface at 60° initial drop angle. Each coloured line represents a drop.

A.1.5 75° initial drop angle

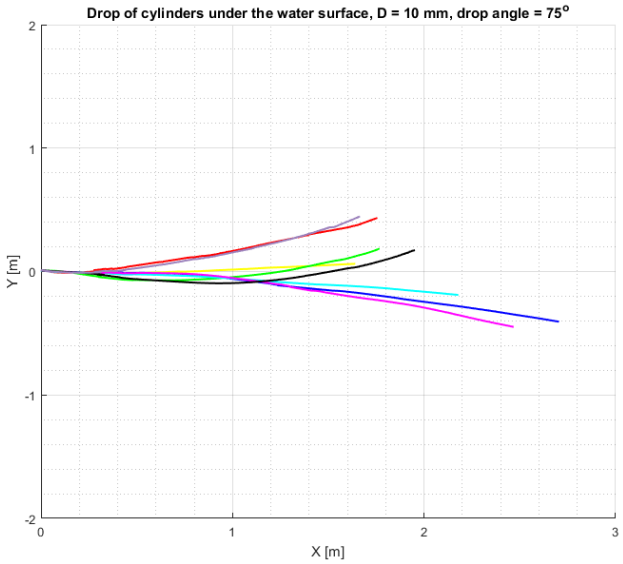

Figure 13: X-Y view: Drop of 10 mm diameter cylinders under the water surface at 75° initial drop angle. Each coloured line represent a drop in order.

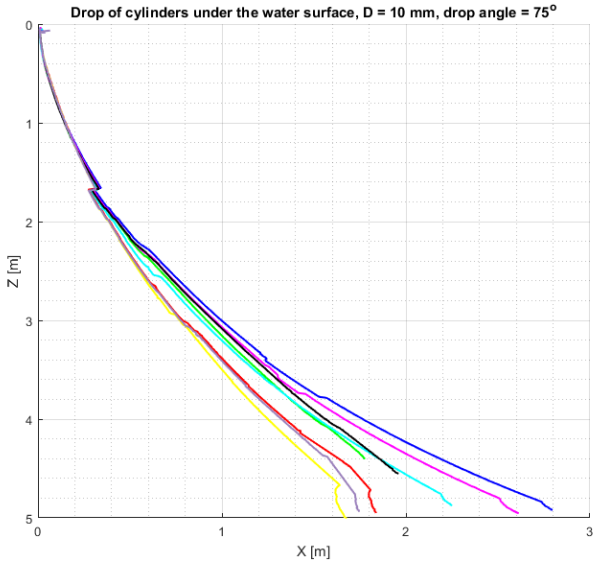

Figure 14: X-Z view: Drop of 10 mm diameter cylinders under the water surface at 75° initial drop angle. The X-coordinates are radial coordinates from the XY plane and each coloured line represents a drop.

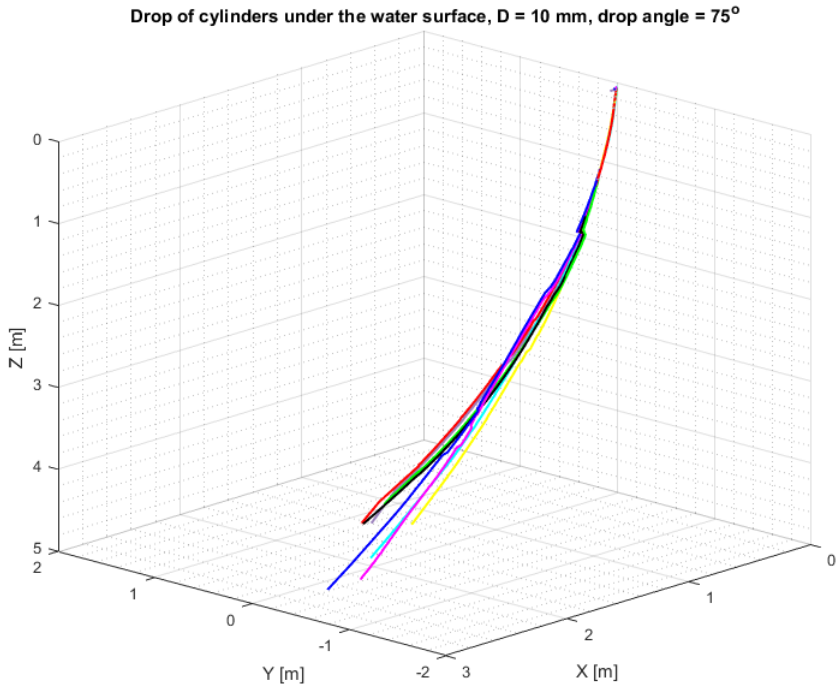

Figure 15: X-Y-Z view: Drop of 10 mm diameter cylinders under the water surface at 75° initial drop angle. Each coloured line represents a drop.

A.2 Drop of 16 mm diameter cylinders under the water surface

A.2.1 15° initial drop angle

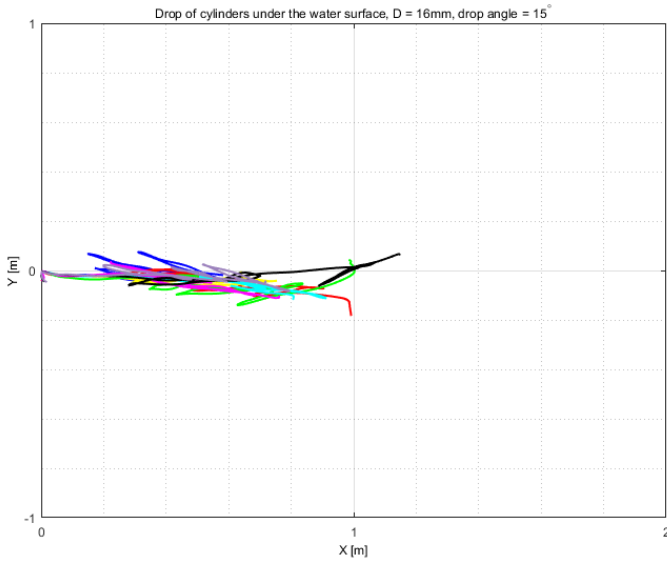

Figure 16: X-Y view: Drop of 16 mm diameter cylinders under the water surface at 15° initial drop angle. Each coloured line represent a drop in order.

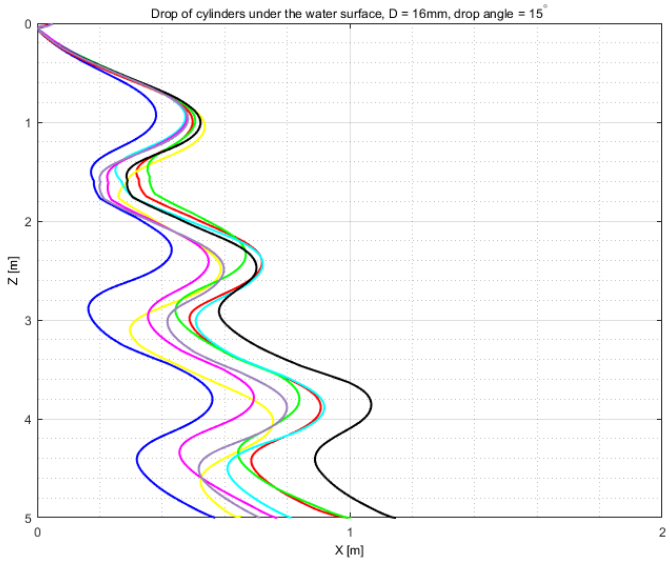

Figure 17: X-Z view: Drop of 16 mm diameter cylinders under the water surface at 15° initial drop angle. The X-coordinates are radial coordinates from the XY plane and each coloured line represents a drop.

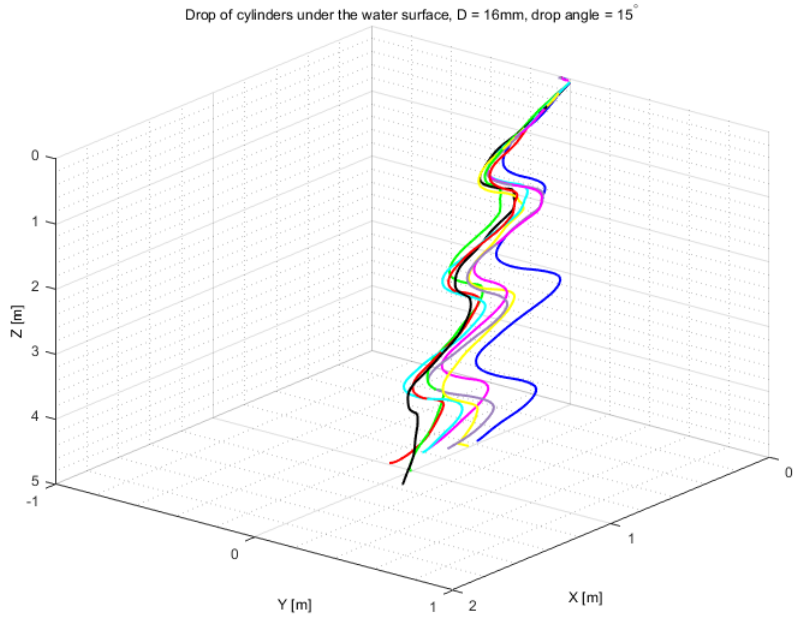

Figure 18: X-Y-Z view: Drop of 16 mm diameter cylinders under the water surface at 15° initial drop angle. Each coloured line represents a drop.

A.2.2 30° initial drop angle

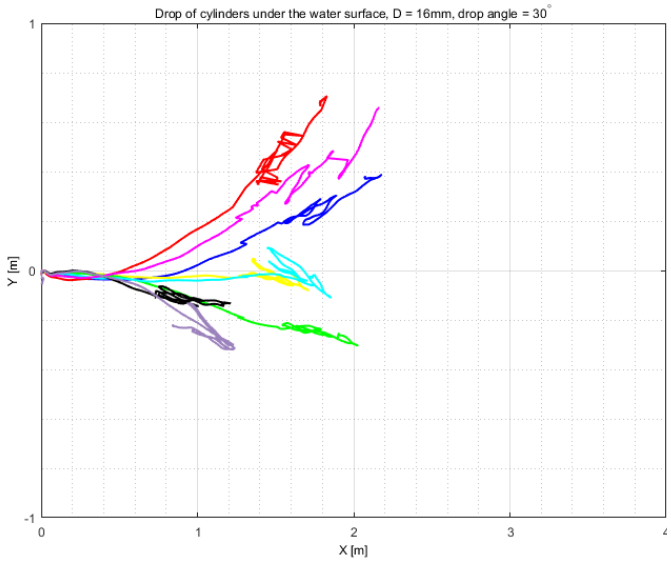

Figure 19: X-Y view: Drop of 16 mm diameter cylinders under the water surface at 30° initial drop angle. Each coloured line represent a drop in order.

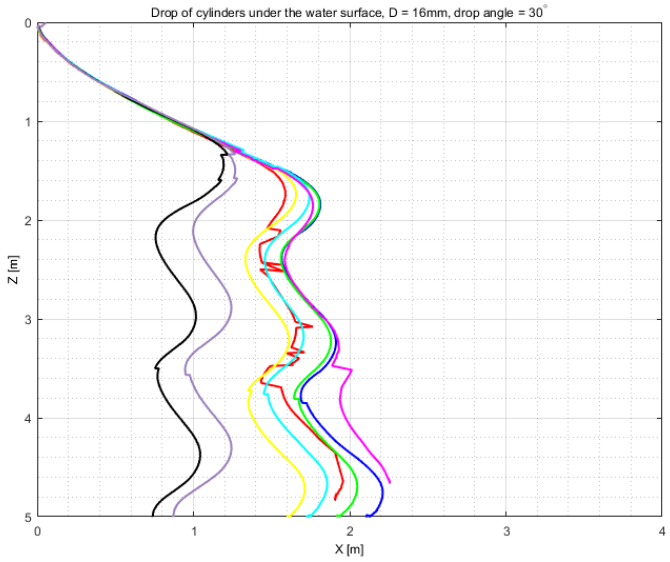

Figure 20: X-Z view: Drop of 16 mm diameter cylinders under the water surface at 30° initial drop angle. The X-coordinates are radial coordinates from the XY plane and each coloured line represents a drop.

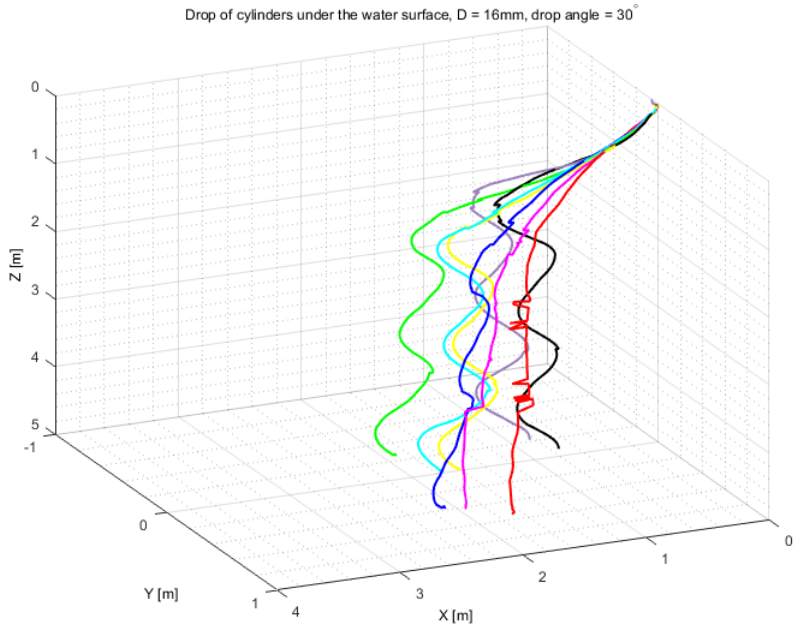

Figure 21: X-Y-Z view: Drop of 16 mm diameter cylinders under the water surface at 30° initial drop angle. Each coloured line represents a drop.

A.2.3 45° initial drop angle

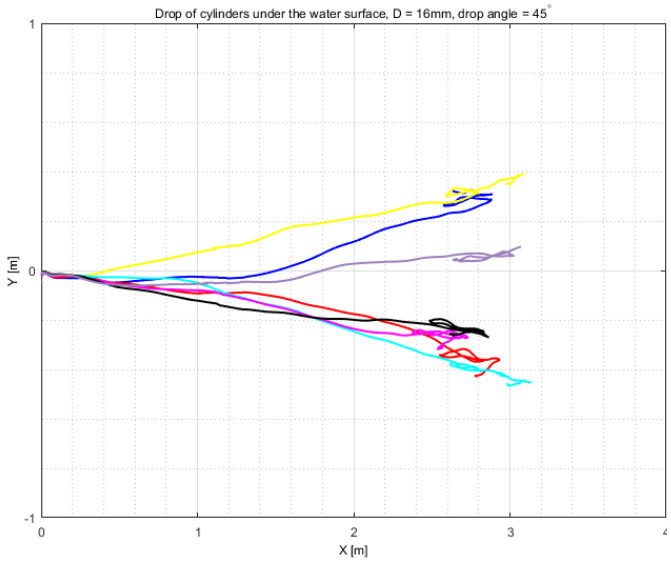

Figure 22: X-Y view: Drop of 16 mm diameter cylinders under the water surface at 45° initial drop angle. Each coloured line represent a drop in order.

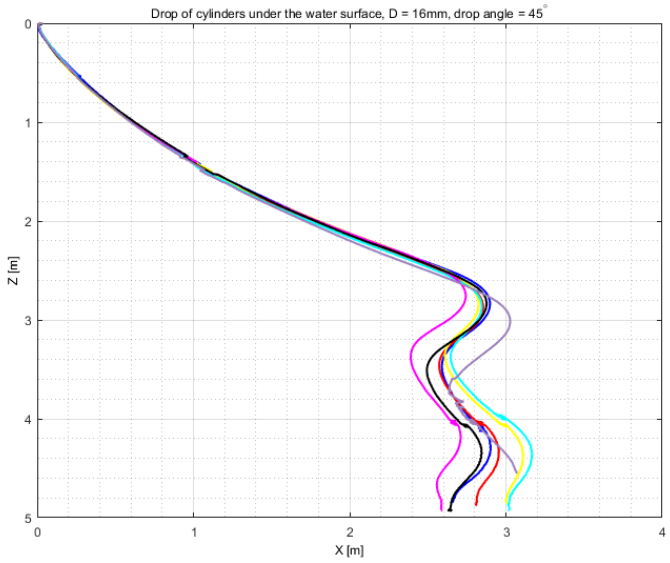

Figure 23: X-Z view: Drop of 16 mm diameter cylinders under the water surface at 45° initial drop angle. The X-coordinates are radial coordinates from the XY plane and each coloured line represents a drop.

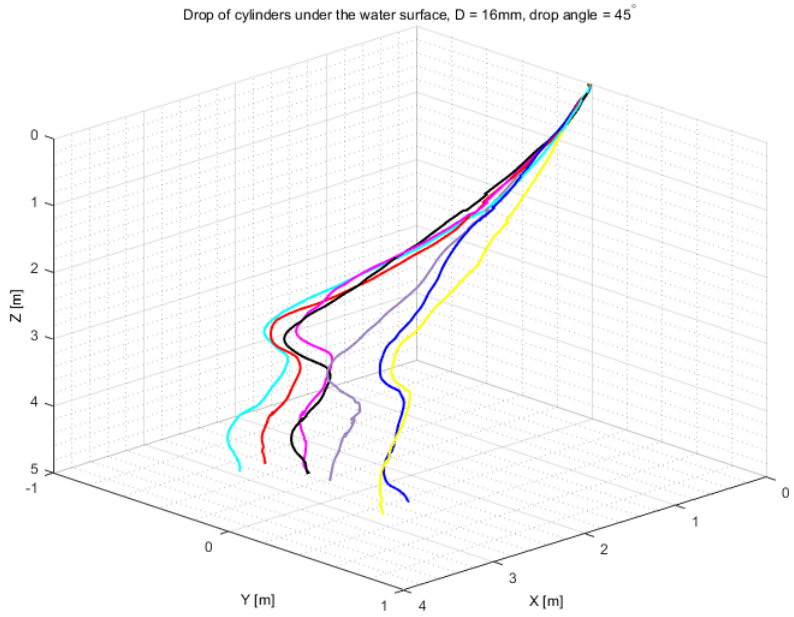

Figure 24: X-Y-Z view: Drop of 16 mm diameter cylinders under the water surface at 45° initial drop angle. Each coloured line represents a drop.

A.2.4 60° initial drop angle

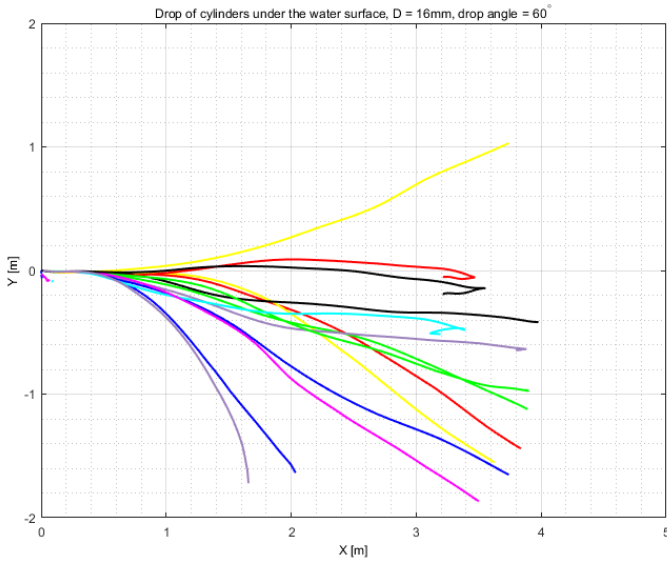

Figure 25: X-Y view: Drop of 16 mm diameter cylinders under the water surface at 60° initial drop angle. Each coloured line represent a drop in order.

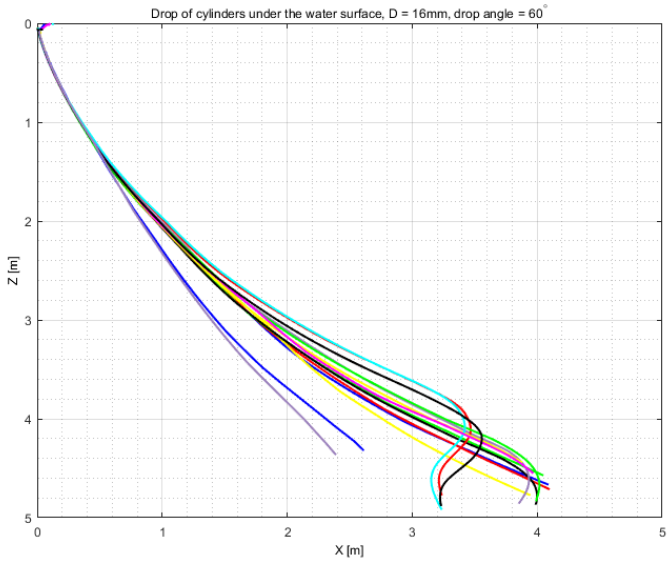

Figure 26: X-Z view: Drop of 16 mm diameter cylinders under the water surface at 60° initial drop angle. The X-coordinates are radial coordinates from the XY plane and each coloured line represents a drop.

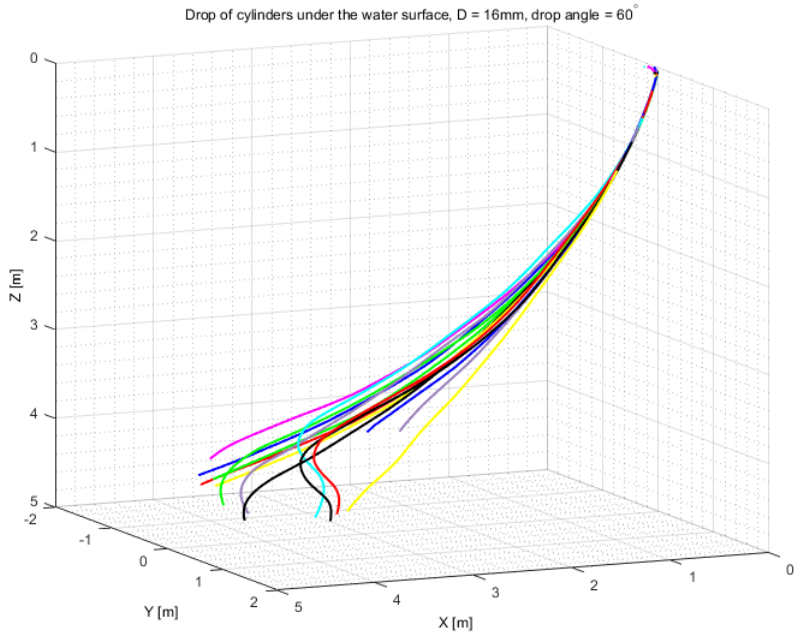

Figure 27: X-Y-Z view: Drop of 16 mm diameter cylinders under the water surface at 60° initial drop angle. Each coloured line represents a drop.

A.2.5 75° initial drop angle

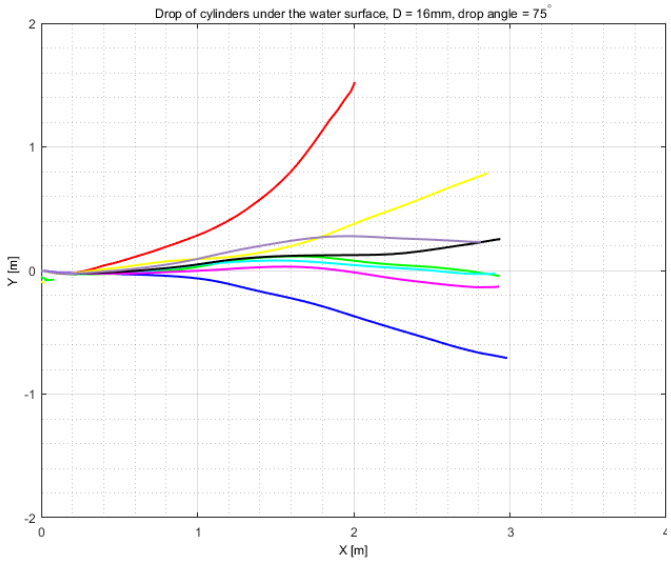

Figure 28: X-Y view: Drop of 16 mm diameter cylinders under the water surface at 75° initial drop angle. Each coloured line represent a drop in order.

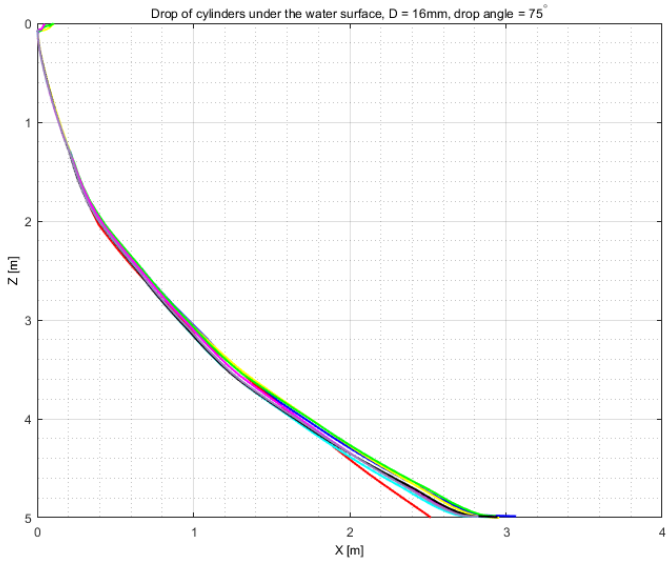

Figure 29: X-Z view: Drop of 16 mm diameter cylinders under the water surface at 75° initial drop angle. The X-coordinates are radial coordinates from the XY plane and each coloured line represents a drop.

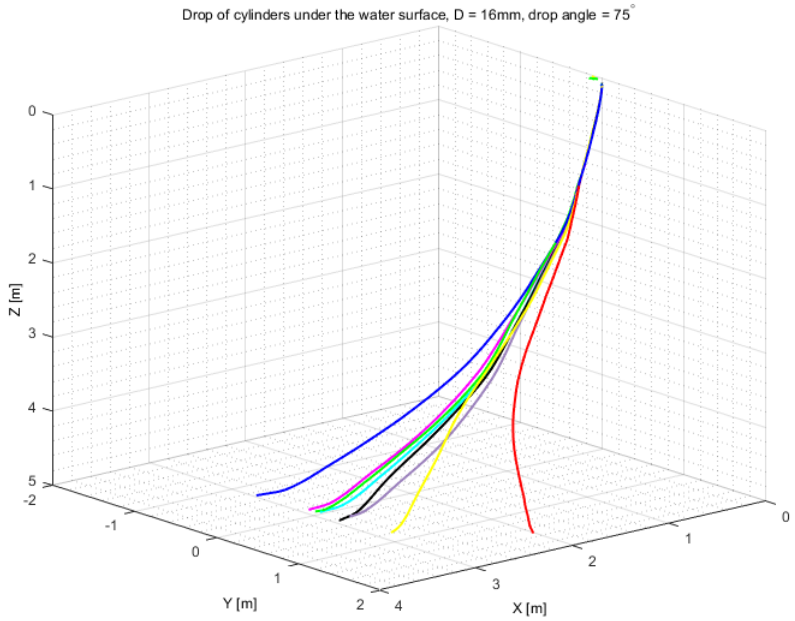

Figure 30: X-Y-Z view: Drop of 16 mm diameter cylinders under the water surface at 75° initial drop angle. Each coloured line represents a drop.

A.3 Drop of 19mm diameter cylinders under the water surface

A.3.1 15° initial drop angle

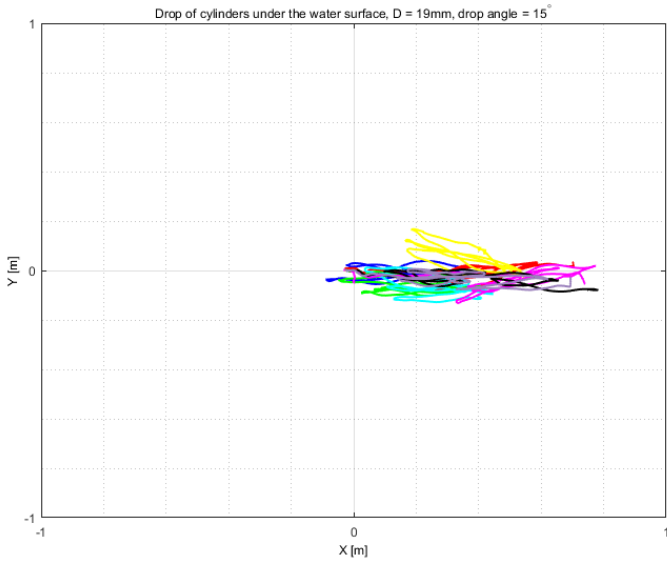

Figure 31: X-Y view: Drop of 19 mm diameter cylinders under the water surface at 15° initial drop angle. Each coloured line represent a drop in order.

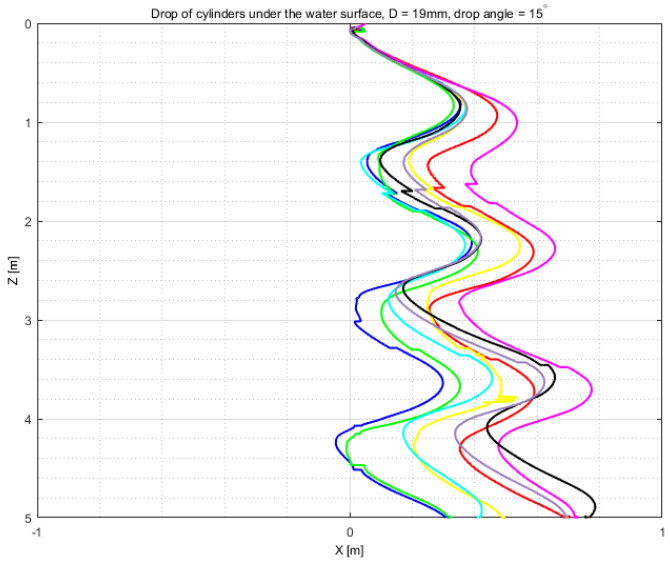

Figure 32: X-Z view: Drop of 19 mm diameter cylinders under the water surface at 15° initial drop angle. The X-coordinates are radial coordinates from the XY plane and each coloured line represents a drop.

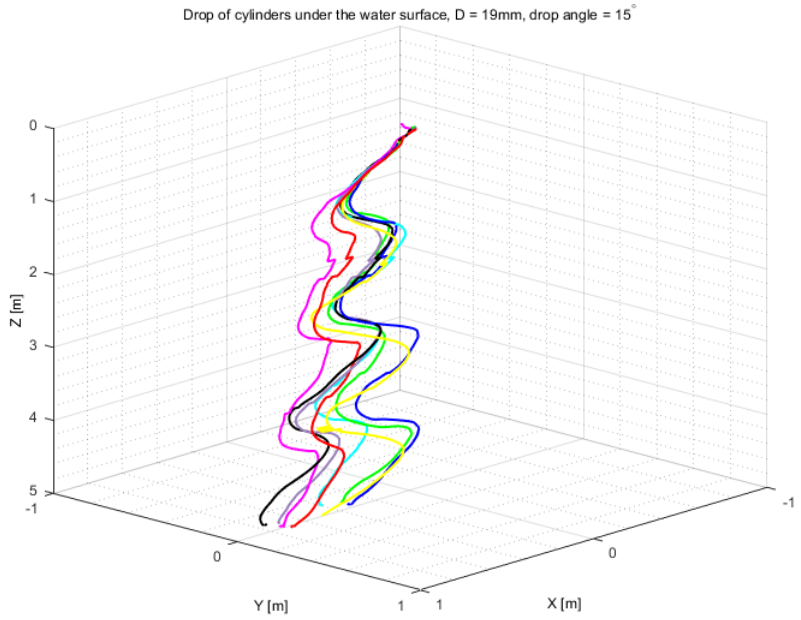

Figure 33: X-Y-Z view: Drop of 19 mm diameter cylinders under the water surface at 15° initial drop angle. Each coloured line represents a drop.

A.3.2 30° initial drop angle

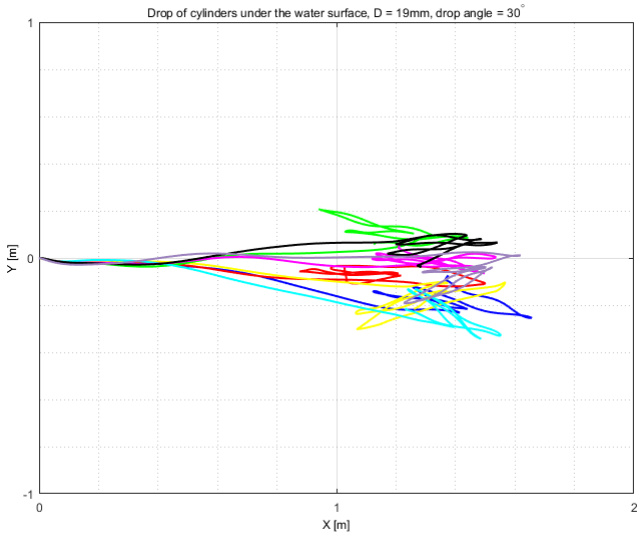

Figure 34: X-Y view: Drop of 19 mm diameter cylinders under the water surface at 30° initial drop angle. Each coloured line represent a drop in order.

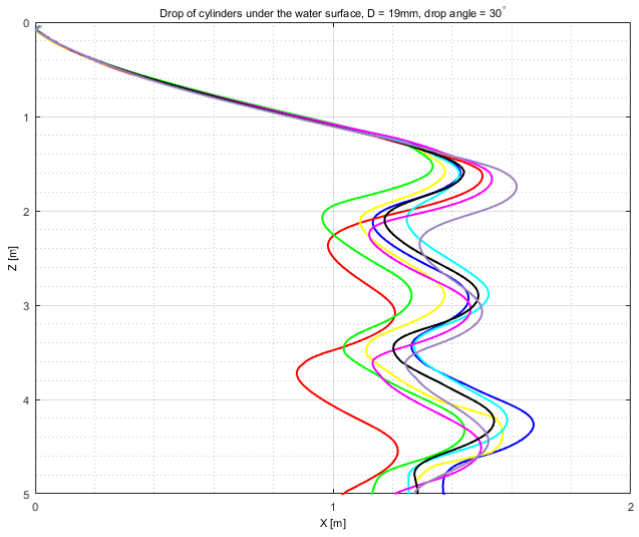

Figure 35: X-Z view: Drop of 19 mm diameter cylinders under the water surface at 30° initial drop angle. The X-coordinates are radial coordinates from the XY plane and each coloured line represents a drop.

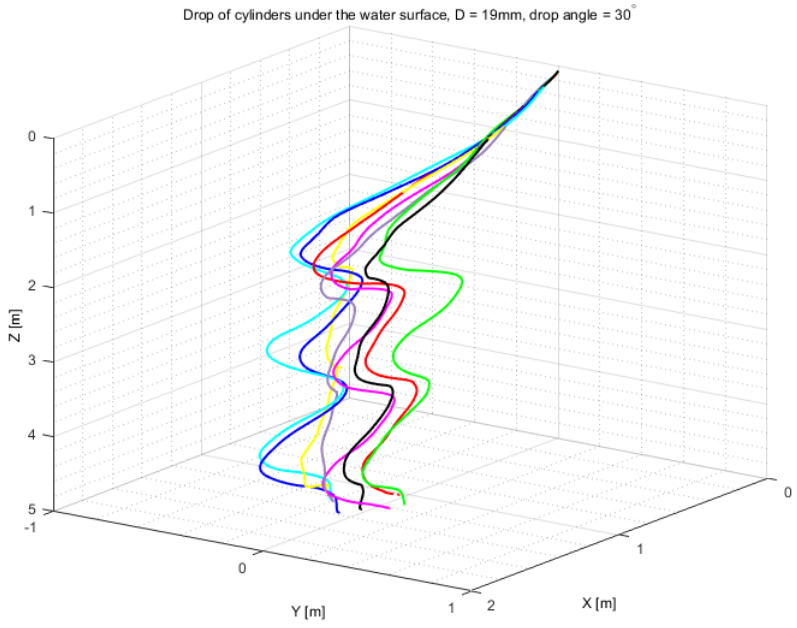

Figure 36: X-Y-Z view: Drop of 19 mm diameter cylinders under the water surface at 30° initial drop angle. Each coloured line represents a drop.

A.3.3 45° initial drop angle

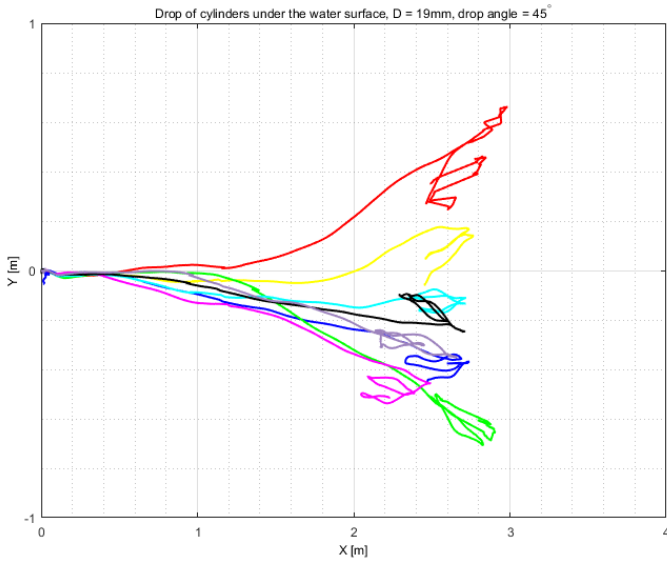

Figure 37: X-Y view: Drop of 19 mm diameter cylinders under the water surface at 45° initial drop angle. Each coloured line represent a drop in order.

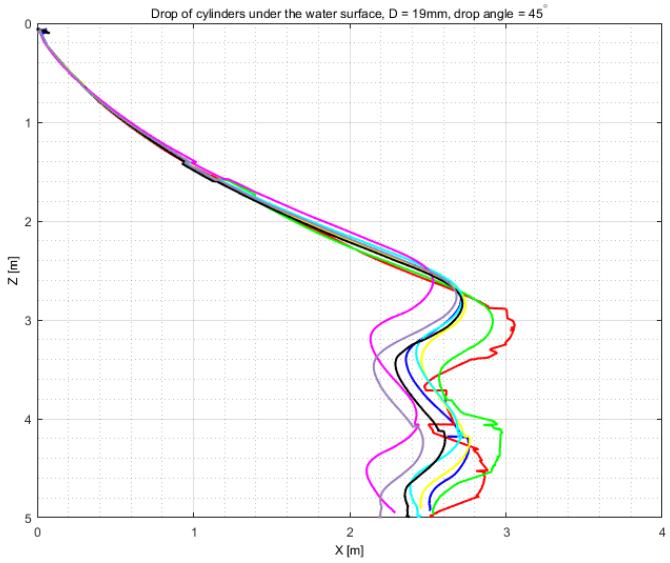

Figure 38: X-Z view: Drop of 19 mm diameter cylinders under the water surface at 45° initial drop angle. The X-coordinates are radial coordinates from the XY plane and each coloured line represents a drop.

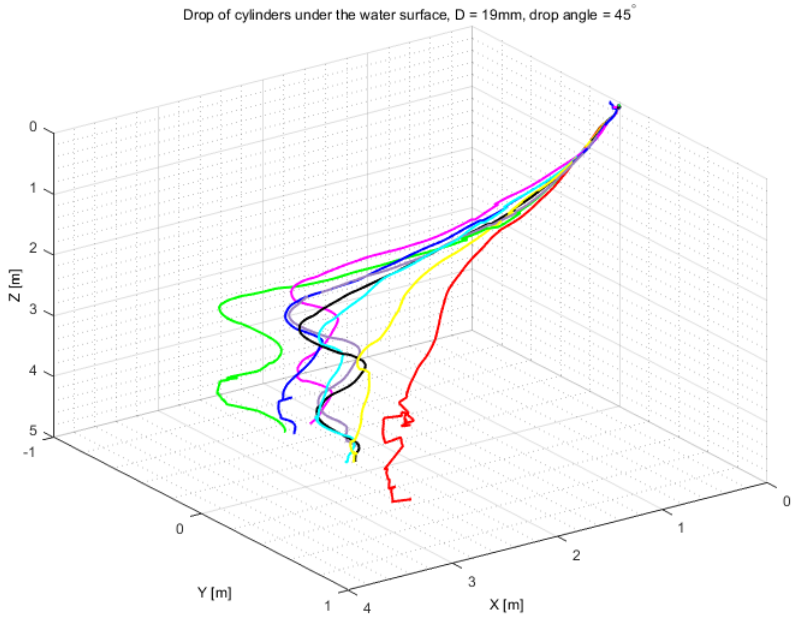

Figure 39: X-Y-Z view: Drop of 19 mm diameter cylinders under the water surface at 45° initial drop angle. Each coloured line represents a drop.

A.3.4 60° initial drop angle

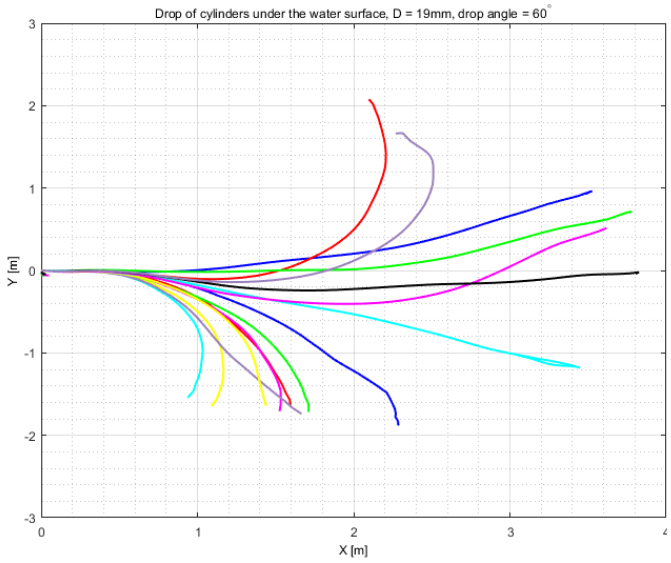

Figure 40: X-Y view: Drop of 19 mm diameter cylinders under the water surface at 60° initial drop angle. Each coloured line represent a drop in order.

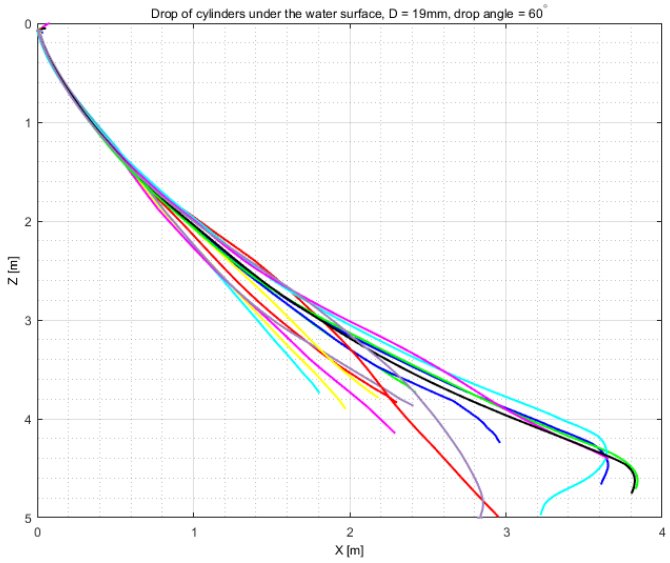

Figure 41: X-Z view: Drop of 19 mm diameter cylinders under the water surface at 60° initial drop angle. The X-coordinates are radial coordinates from the XY plane and each coloured line represents a drop.

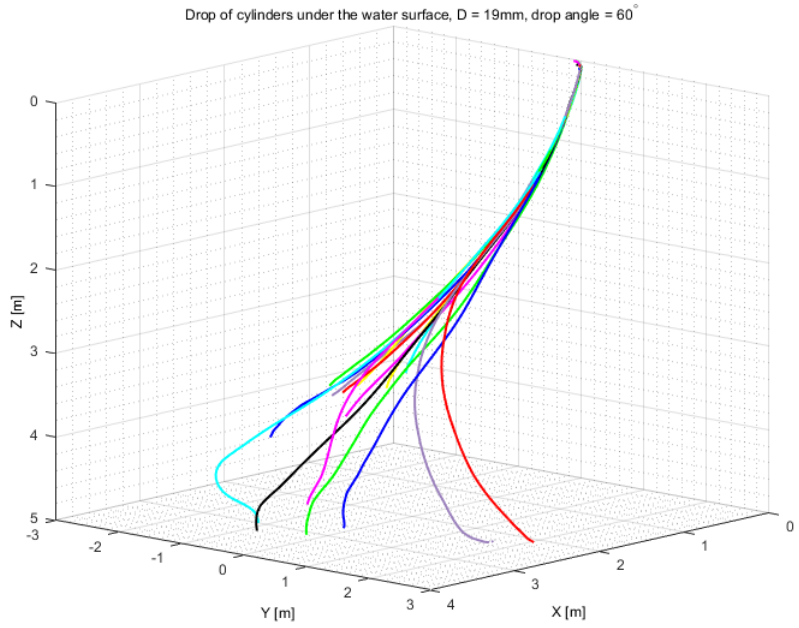

Figure 42: X-Y-Z view: Drop of 10mm diameter cylinders under the water surface at 60° initial drop angle. Each coloured line represents a drop.

A.3.5 75° initial drop angle

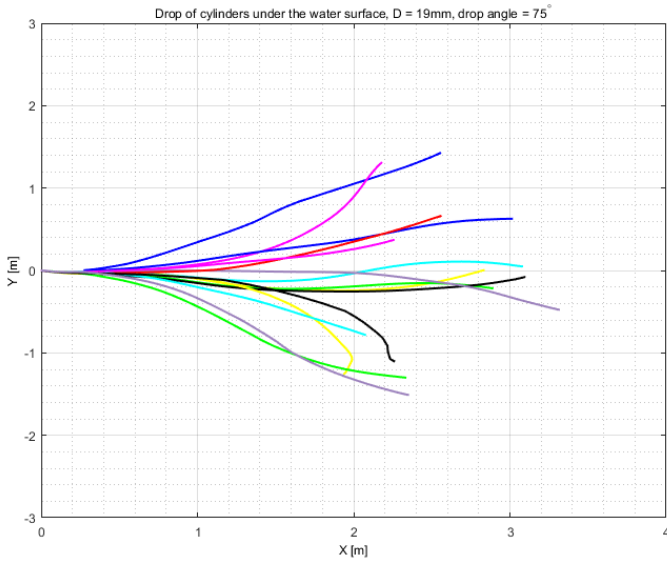

Figure 43: X-Y view: Drop of 19 mm diameter cylinders under the water surface at 75° initial drop angle. Each coloured line represent a drop in order.

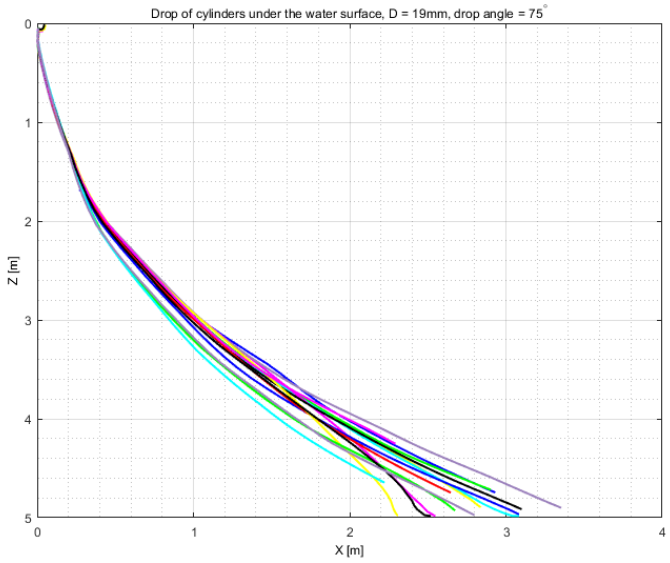

Figure 44: X-Z view: Drop of 19 mm diameter cylinders under the water surface at 75° initial drop angle. The X-coordinates are radial coordinates from the XY plane and each coloured line represents a drop.

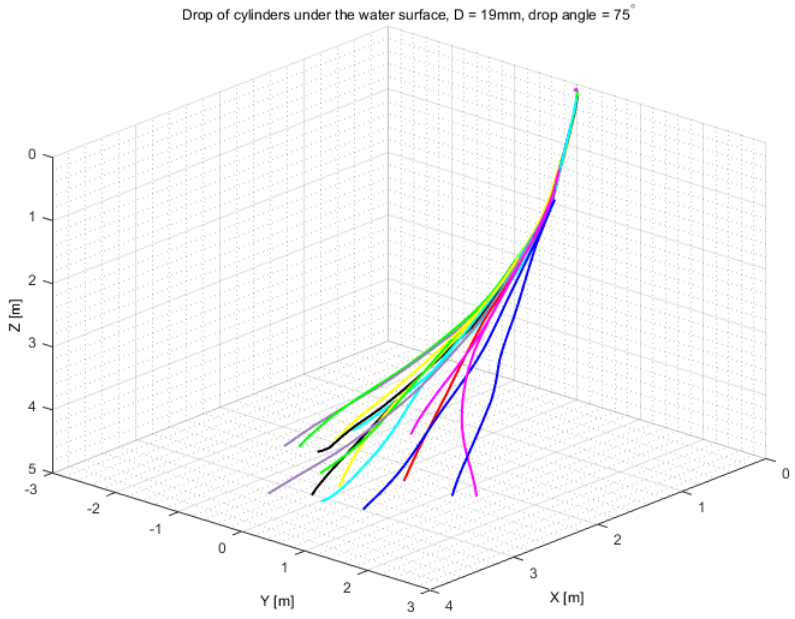

Figure 45: X-Y-Z view: Drop of 19 mm diameter cylinders under the water surface at 75° initial drop angle. Each coloured line represents a drop.

A.4 Drop of 10mm diameter cylinders over the water surface

A.4.1 15° initial drop angle

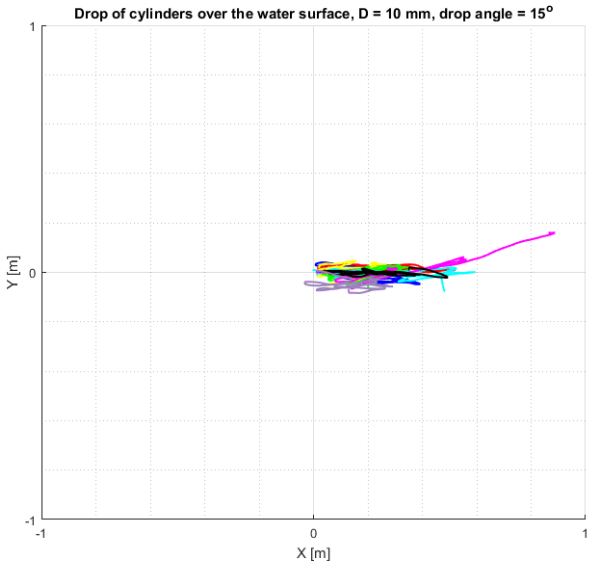

Figure 46: X-Y view: Drop of 10mm diameter cylinders over the water surface at 15° initial angle. Each coloured line represents a drop.

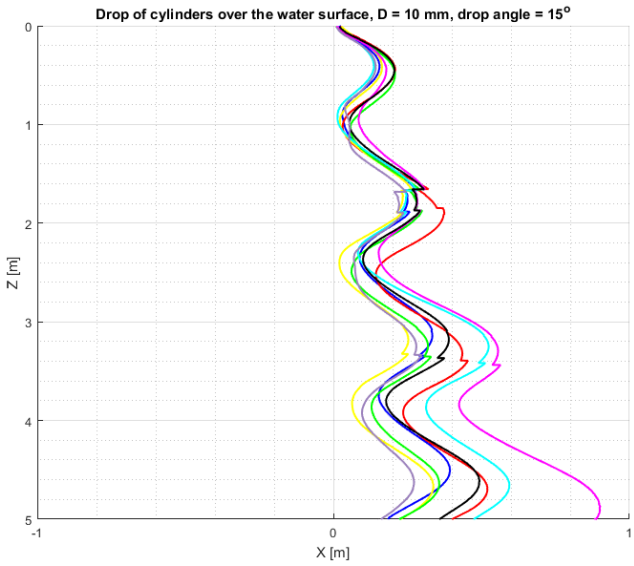

Figure 47: X-Z view: Drop of 10mm diameter cylinders over the water surface at 15° initial angle. The X-coordinates are radial coordinates from the XY plane and each coloured line represents a drop.

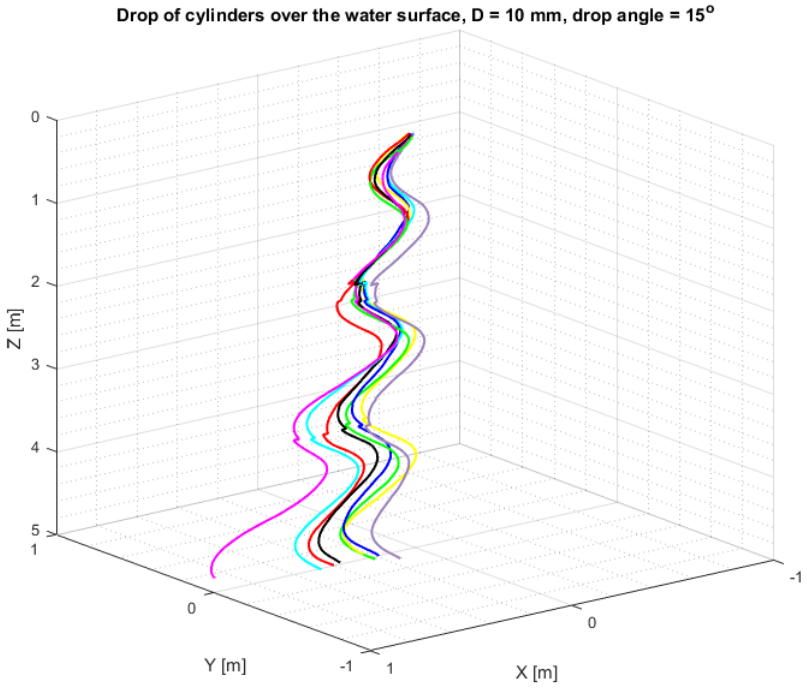

Figure 48: X-Y-Z view: Drop of 10mm diameter cylinders over the water surface at 15° initial angle. Each coloured line represents a drop.

A.4.2 30° initial drop angle

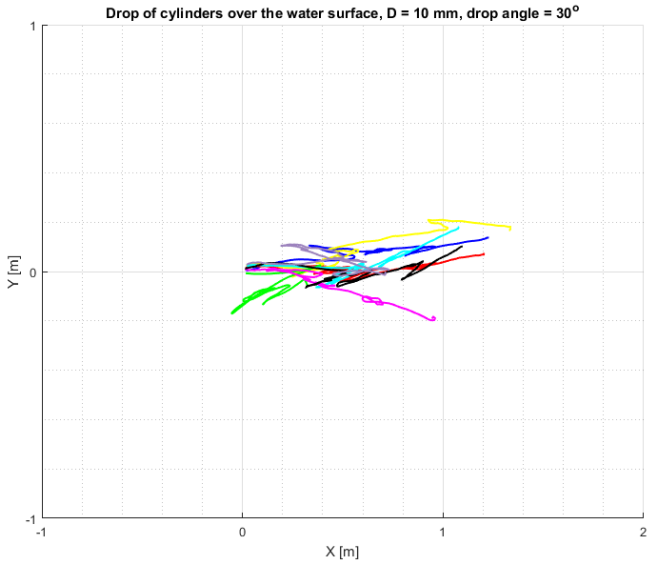

Figure 49: X-Y view: Drop of 10mm diameter cylinders over the water surface at 30° initial angle. Each coloured line represents a drop.

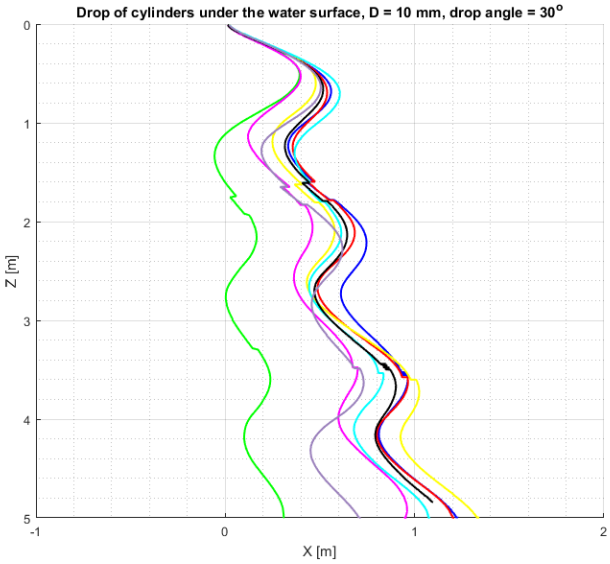

Figure 50: X-Z view: Drop of 10mm diameter cylinders over the water surface at 30° initial angle. The X-coordinates are radial coordinates from the XY plane and each coloured line represents a drop.

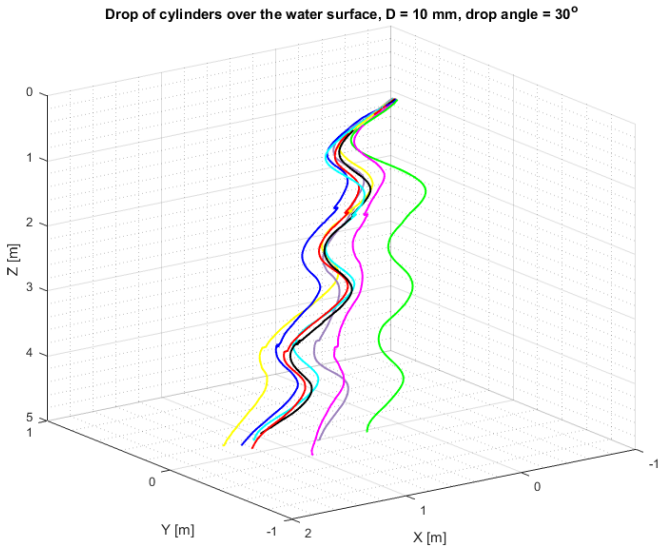

Figure 51: X-Y-Z view: Drop of 10mm diameter cylinders over the water surface at 30° initial angle. Each coloured line represents a drop.

A.4.3 45° initial drop angle

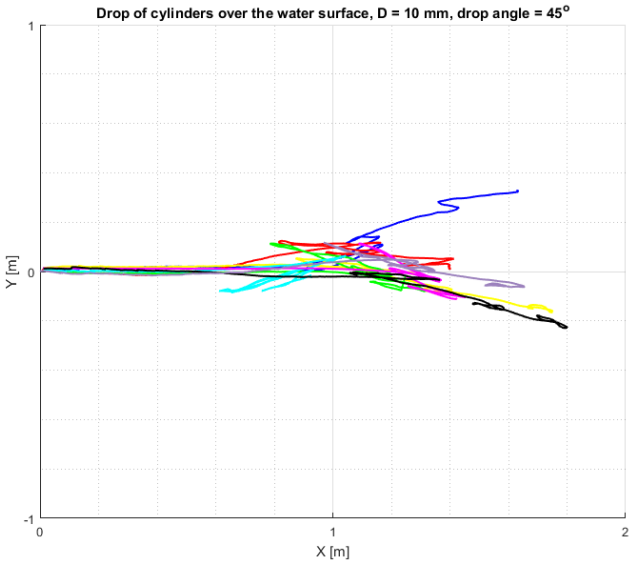

Figure 52: X-Y view: Drop of 10mm diameter cylinders over the water surface at 45° initial angle. Each coloured line represents a drop.

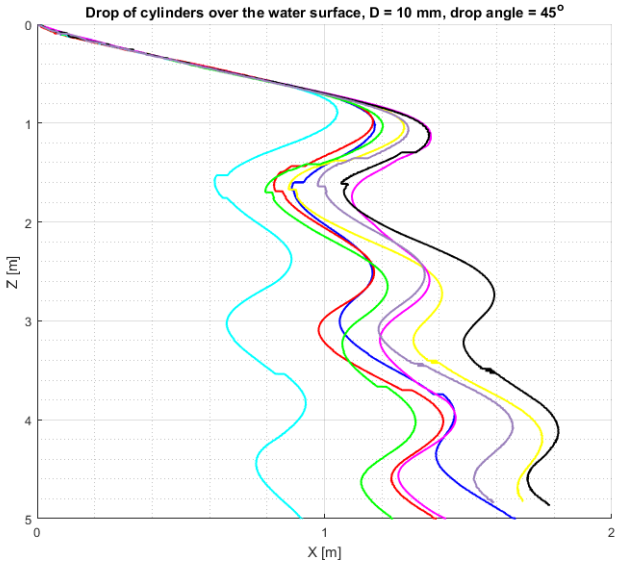

Figure 53: X-Z view: Drop of 10mm diameter cylinders over the water surface at 45° initial angle. The X-coordinates are radial coordinates from the XY plane and each coloured line represents a drop.

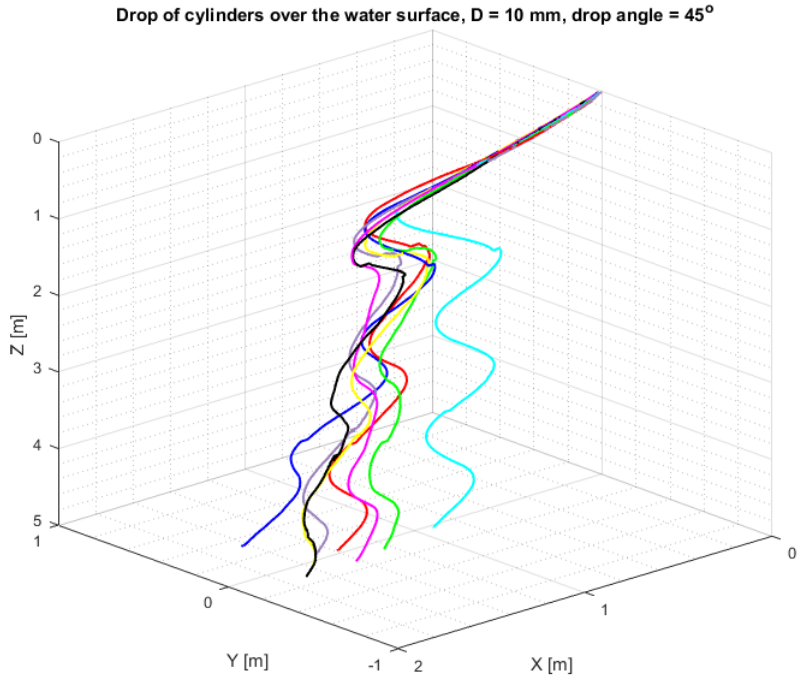

Figure 54: X-Y-Z view: Drop of 10mm diameter cylinders over the water surface at 45° initial angle. Each coloured line represents a drop.

A.4.4 60° initial drop angle

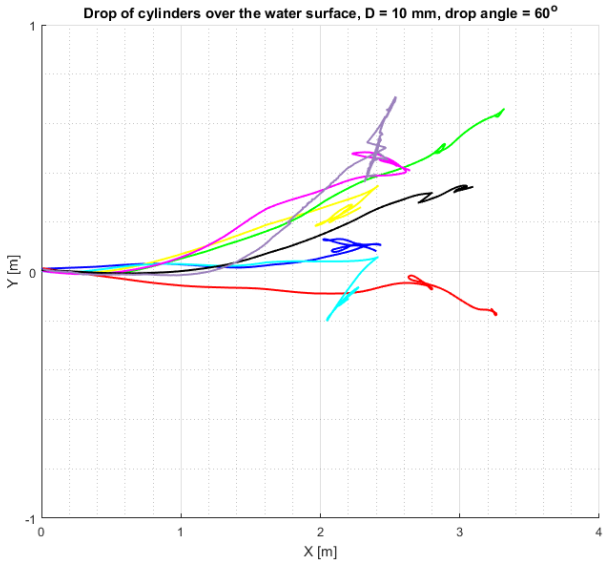

Figure 55: X-Y view: Drop of 10mm diameter cylinders over the water surface at 60° initial angle. Each coloured line represents a drop.

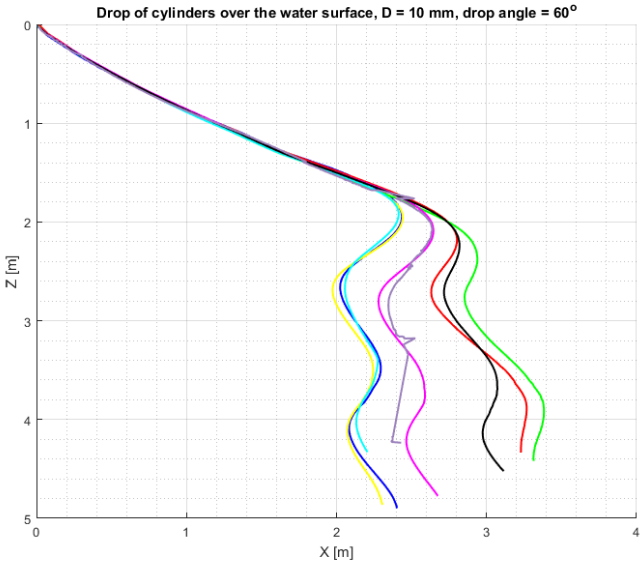

Figure 56: X-Z view: Drop of 10mm diameter cylinders over the water surface at 60° initial angle. The X-coordinates are radial coordinates from the XY plane and each coloured line represents a drop.

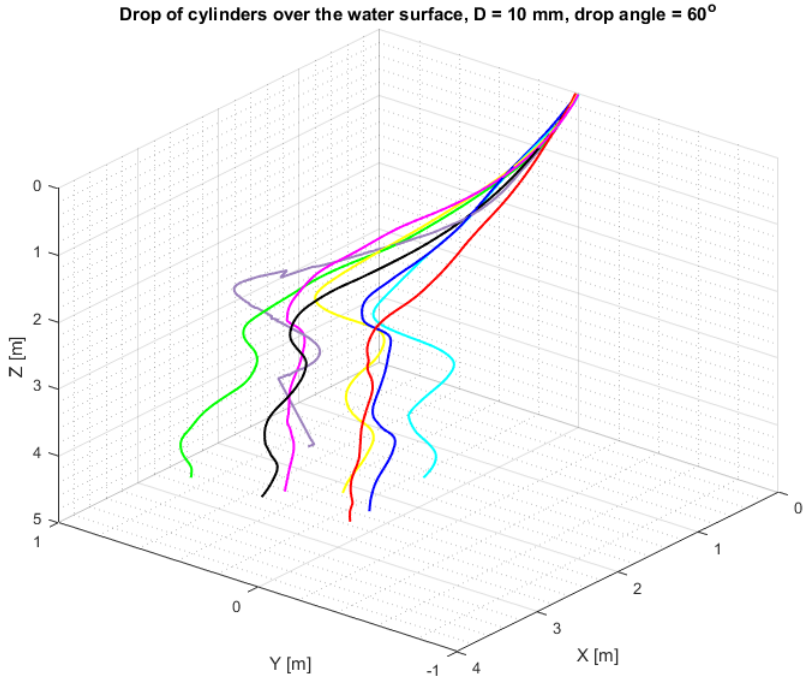

Figure 57: X-Y-Z view: Drop of 10mm diameter cylinders over the water surface at 60° initial angle. Each coloured line represents a drop.

A.4.5 75° initial drop angle

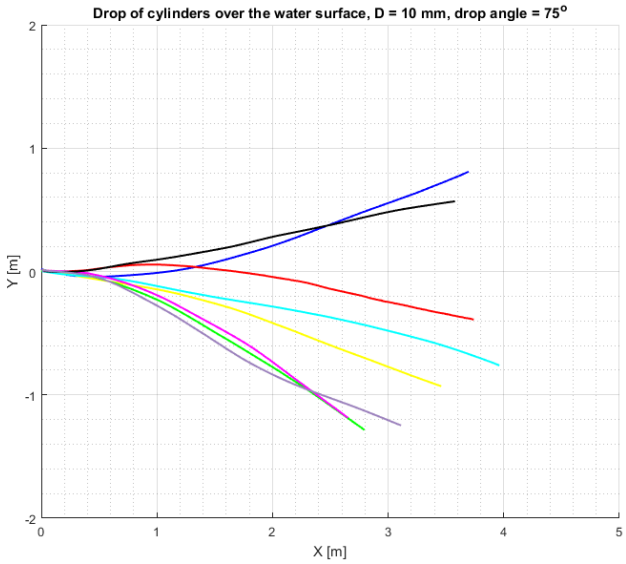

Figure 58: X-Y view: Drop of 10mm diameter cylinders over the water surface at 75° initial angle. Each coloured line represents a drop.

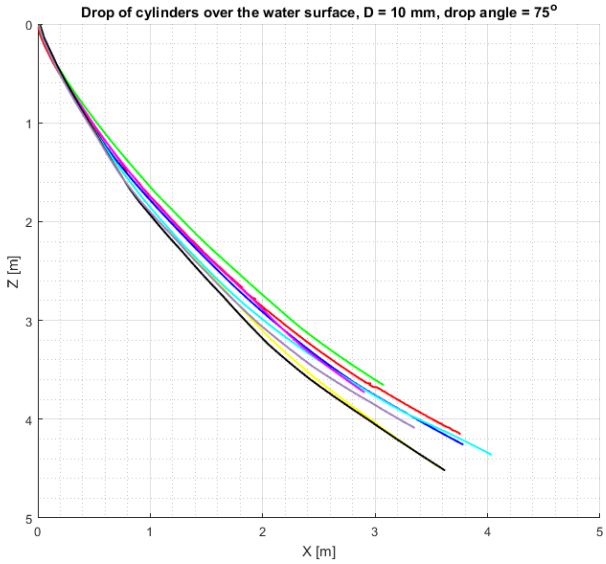

Figure 59: X-Z view: Drop of 10mm diameter cylinders over the water surface at 75° initial angle. The X-coordinates are radial coordinates from the XY plane and each coloured line represents a drop.

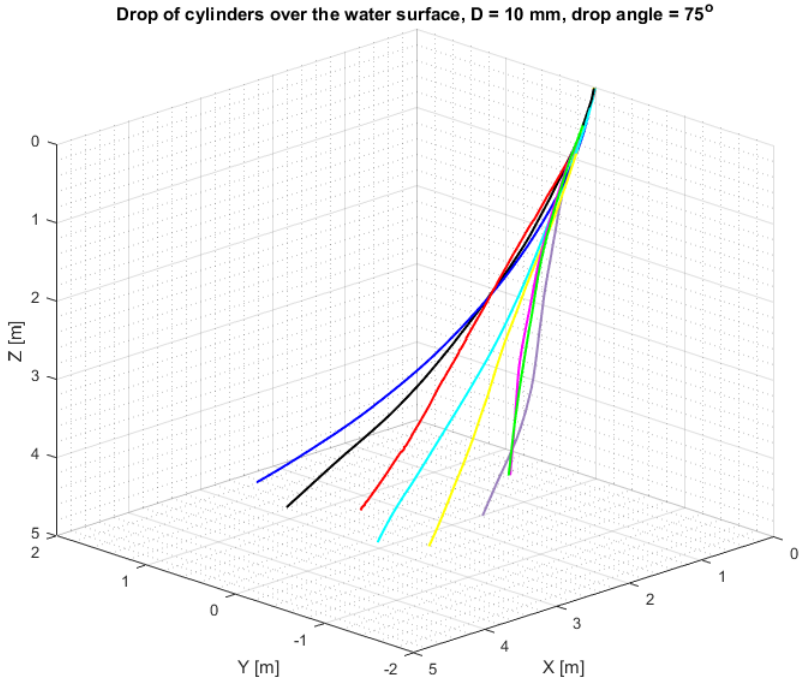

Figure 60: X-Y-Z view: Drop of 10mm diameter cylinders over the water surface at 75° initial angle. Each coloured line represents a drop.

A.5 Drop of 16 mm diameter cylinders over the water surface

A.5.1 15° initial drop angle

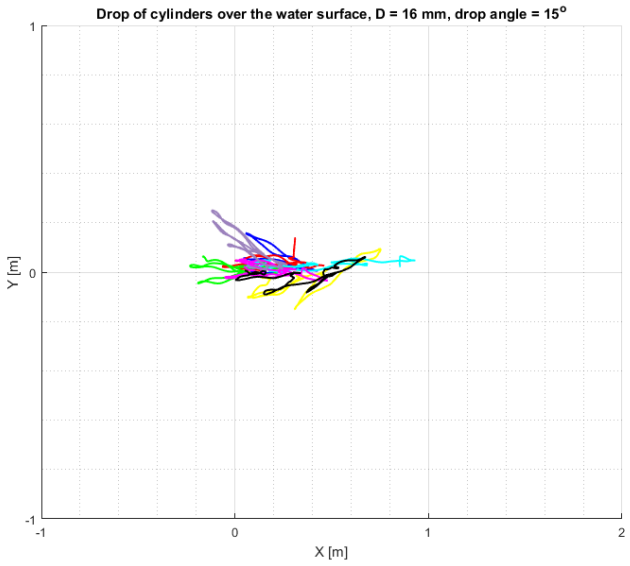

Figure 61: X-Y view: Drop of 16 mm diameter cylinders over the water surface at 15° initial angle. Each coloured line represents a drop.

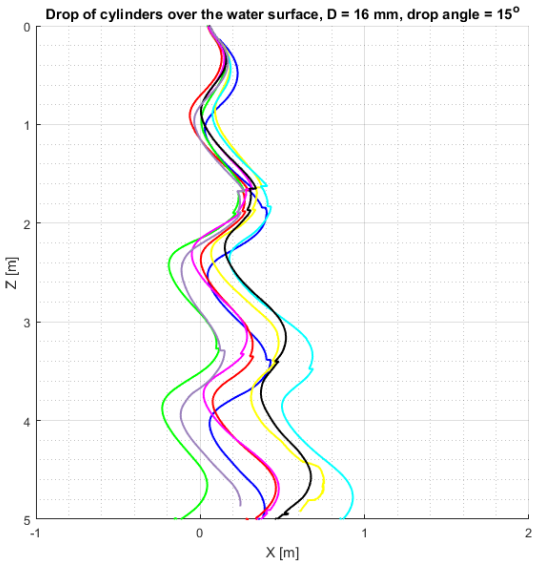

Figure 62: X-Z view: Drop of 16 mm diameter cylinders over the water surface at 15° initial angle. The X-coordinates are radial coordinates from the XY plane and each coloured line represents a drop.

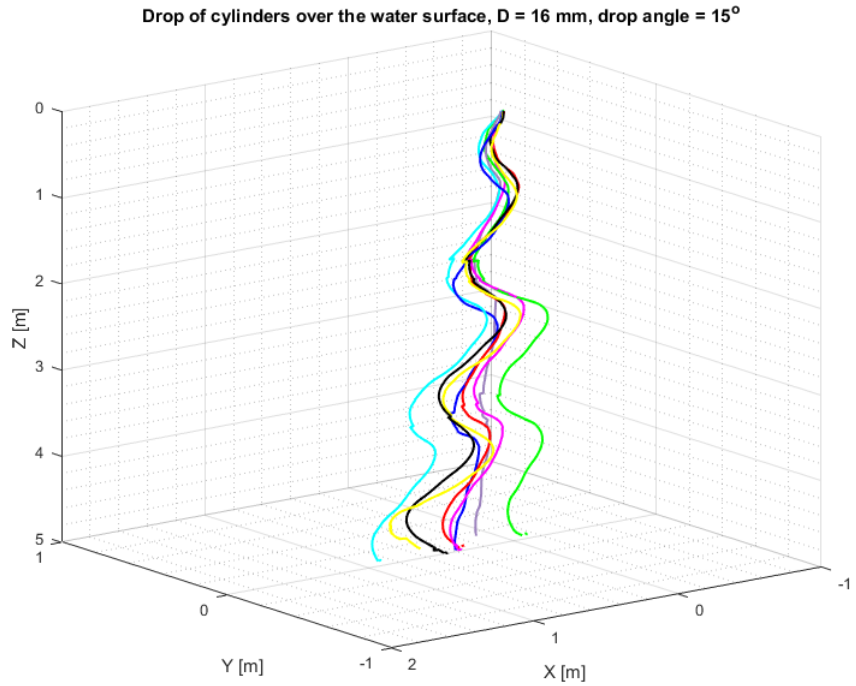

Figure 63: X-Y-Z view: Drop of 16 mm diameter cylinders over the water surface at 15° initial angle. Each coloured line represents a drop.

A.5.2 30° initial drop angle

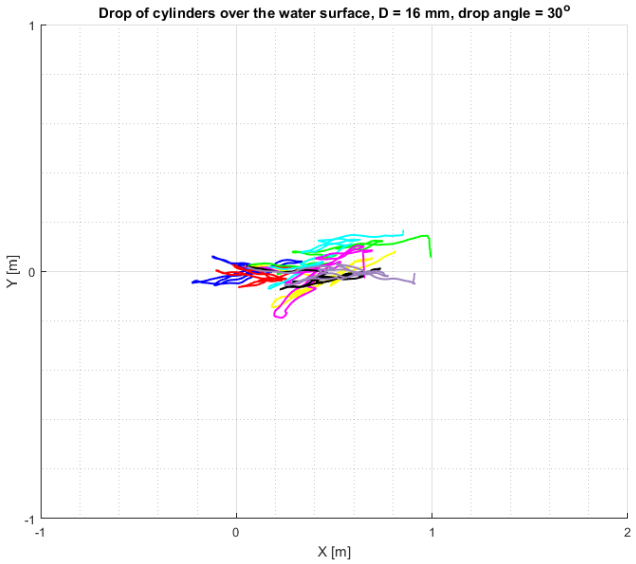

Figure 64: X-Y view: Drop of 16 mm diameter cylinders over the water surface at 30° initial angle. Each coloured line represents a drop.

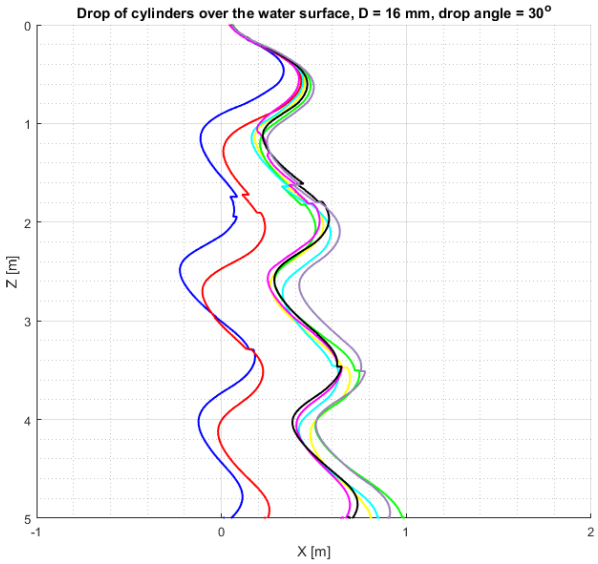

Figure 65: X-Z view: Drop of 16 mm diameter cylinders over the water surface at 30° initial angle. The X-coordinates are radial coordinates from the XY plane and each coloured line represents a drop.

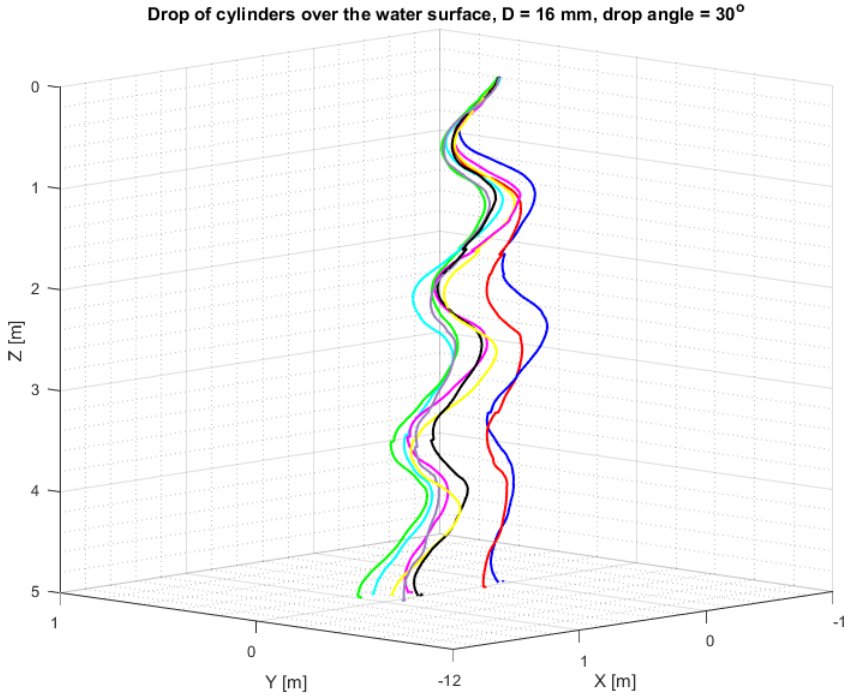

Figure 66: X-Y-Z view: Drop of 16 mm diameter cylinders over the water surface at 30° initial angle. Each coloured line represents a drop.

A.5.3 45° initial drop angle

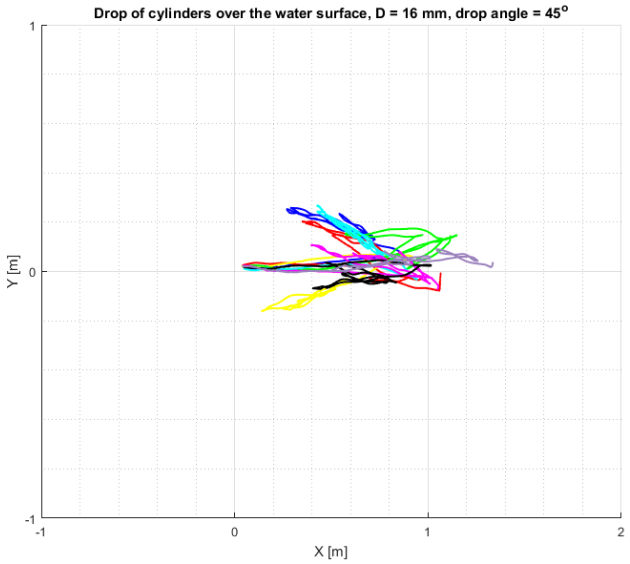

Figure 67: X-Y view: Drop of 16 mm diameter cylinders over the water surface at 45° initial angle. Each coloured line represents a drop.

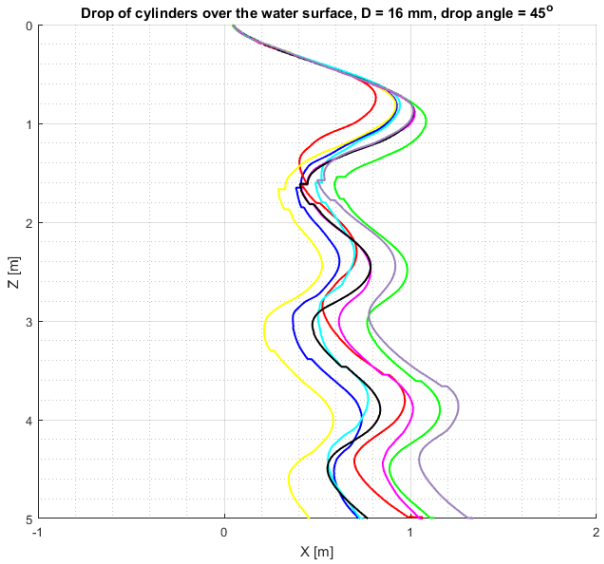

Figure 68: X-Z view: Drop of 16 mm diameter cylinders over the water surface at 45° initial angle. The X-coordinates are radial coordinates from the XY plane and each coloured line represents a drop.

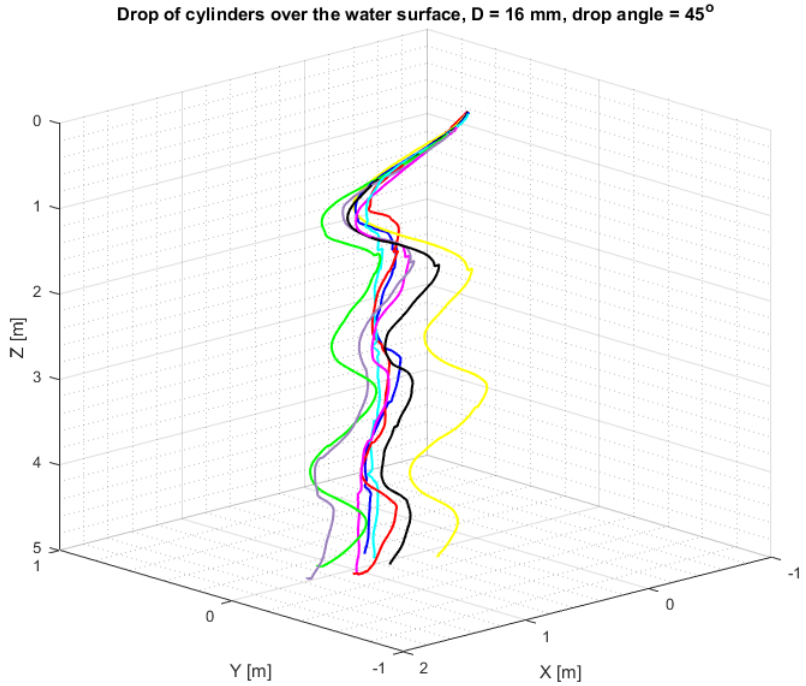

Figure 69: X-Y-Z view: Drop of 16 mm diameter cylinders over the water surface at 45° initial angle. Each coloured line represents a drop.

A.5.4 60° initial drop angle

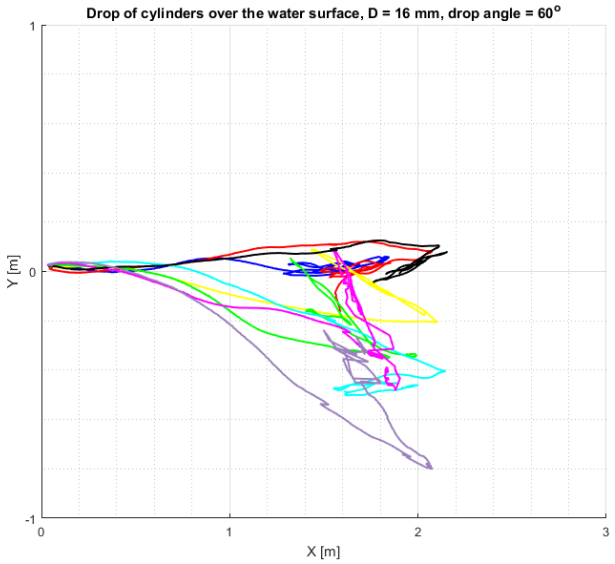

Figure 70: X-Y view: Drop of 16 mm diameter cylinders over the water surface at 60° initial angle. Each coloured line represents a drop.

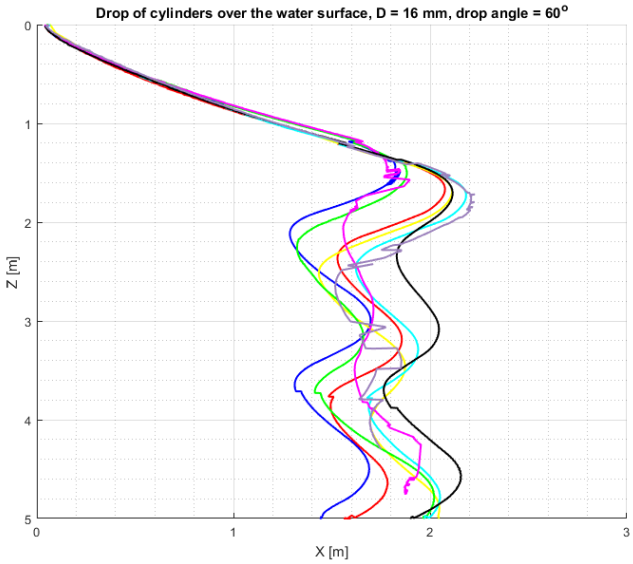

Figure 71: X-Z view: Drop of 16 mm diameter cylinders over the water surface at 60° initial angle. The X-coordinates are radial coordinates from the XY plane and each coloured line represents a drop.

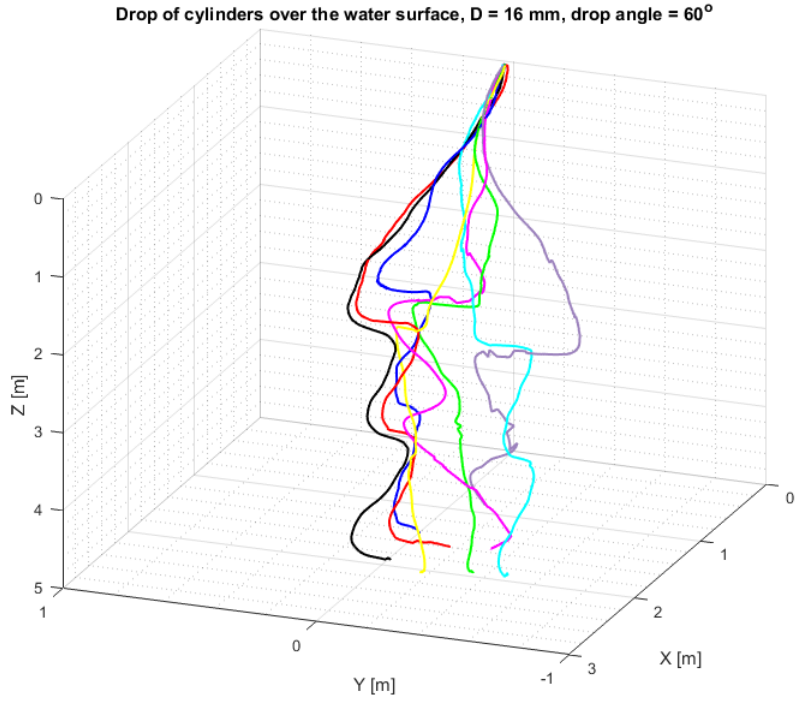

Figure 72: X-Y-Z view: Drop of 16 mm diameter cylinders over the water surface at 60° initial angle. Each coloured line represents a drop.

A.5.5 75° initial drop angle

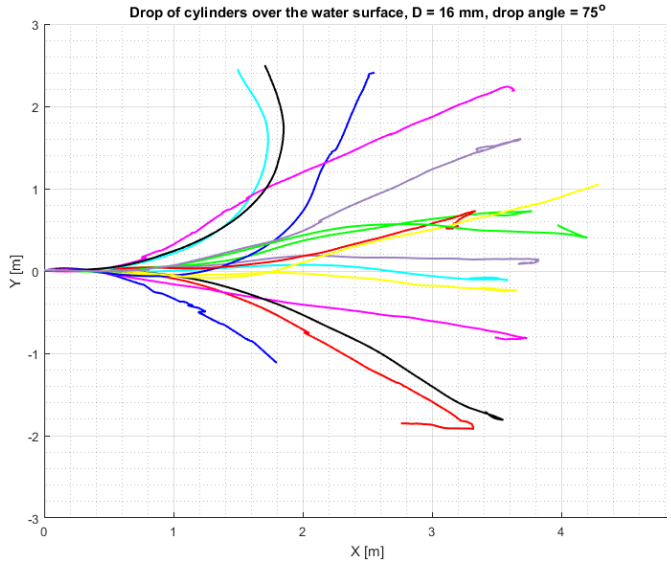

Figure 73: X-Y view: Drop of 16 mm diameter cylinders over the water surface at 75° initial angle. Each coloured line represents a drop.

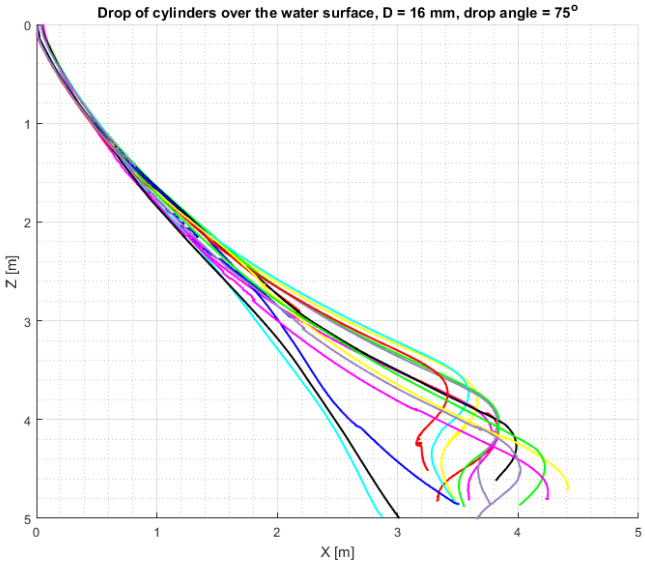

Figure 74: X-Z view: Drop of 16 mm diameter cylinders over the water surface at 75° initial angle. The X-coordinates are radial coordinates from the XY plane and each coloured line represents a drop.

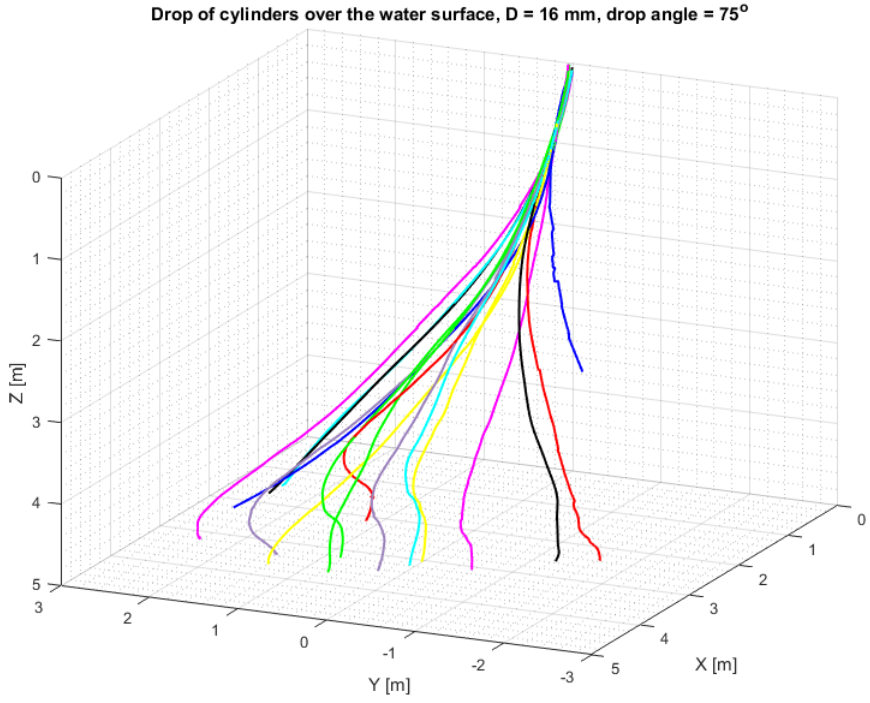

Figure 75: X-Y-Z view: Drop of 16 mm diameter cylinders over the water surface at 75° initial angle. Each coloured line represents a drop.

A.6 Drop of 19mm diameter cylinders over the water surface

A.6.1 15° initial drop angle

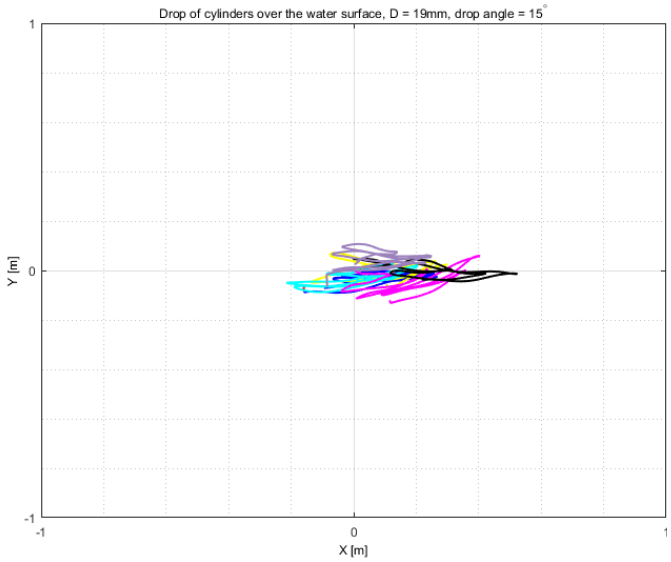

Figure 76: X-Y view: Drop of 19mm diameter cylinders over the water surface at 15° initial angle. Each coloured line represents a drop.

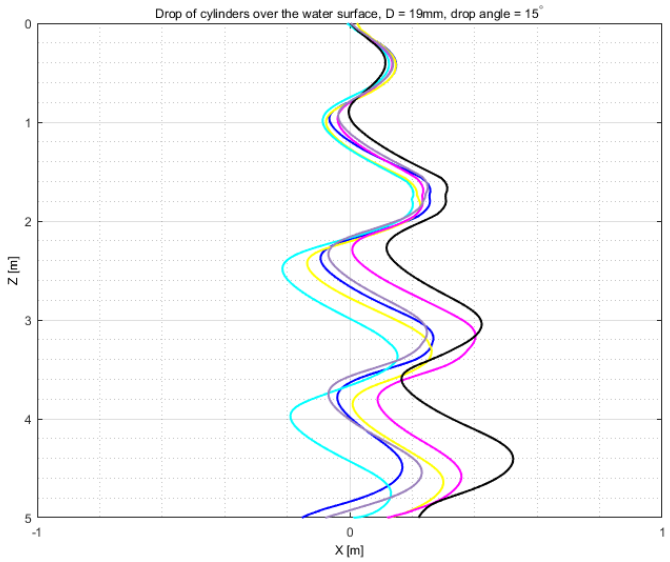

Figure 77: X-Z view: Drop of 19mm diameter cylinders over the water surface at 15° initial angle. The X-coordinates are radial coordinates from the XY plane and each coloured line represents a drop.

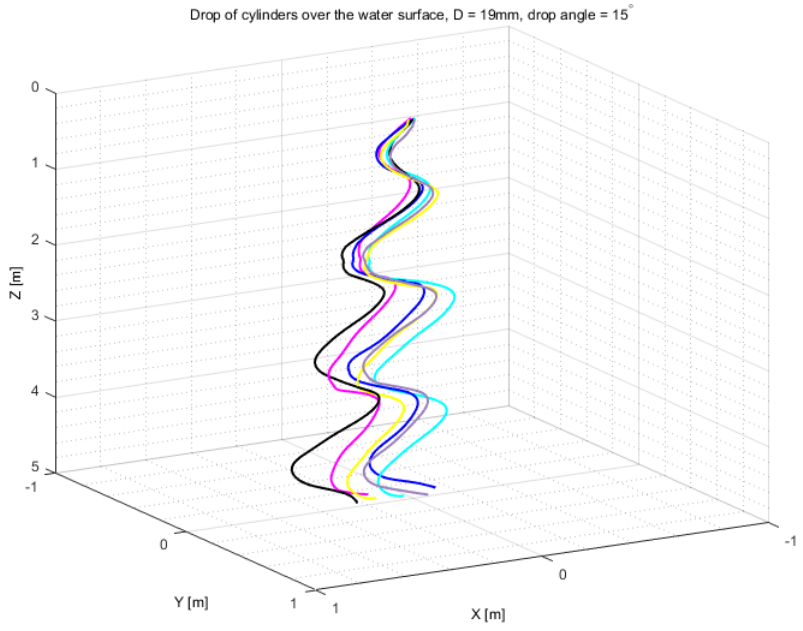

Figure 78: X-Y-Z view: Drop of 19mm diameter cylinders over the water surface at 15° initial angle. Each coloured line represents a drop.

A.6.2 30° initial drop angle

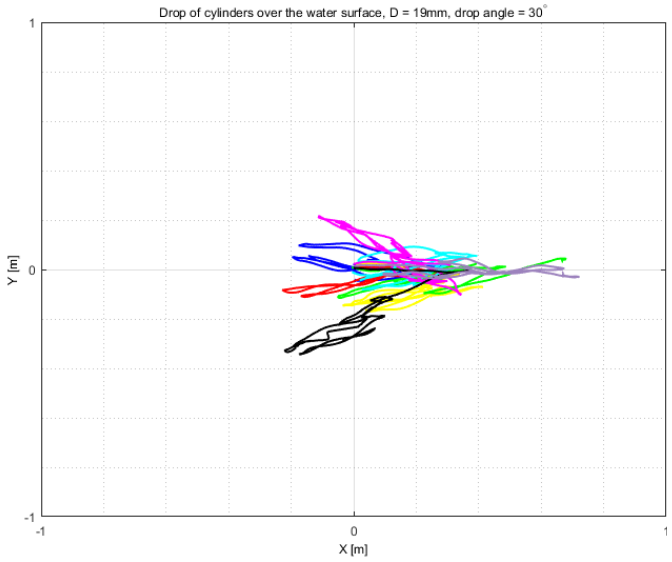

Figure 79: X-Y view: Drop of 19mm diameter cylinders over the water surface at 30° initial angle. Each coloured line represents a drop.

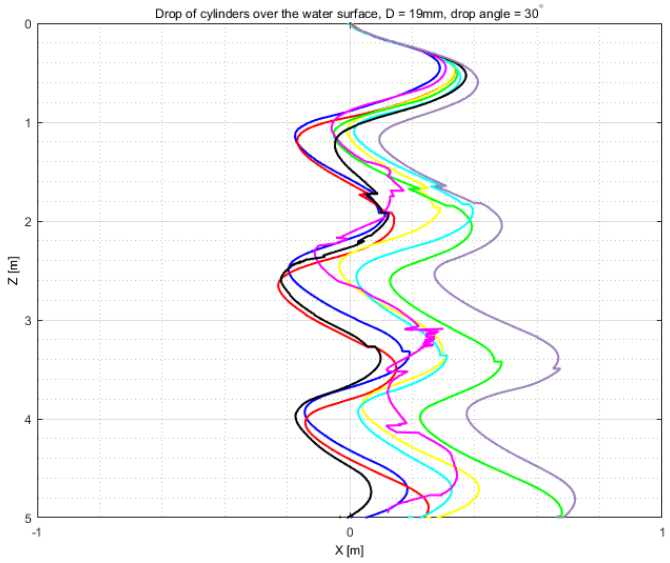

Figure 80: X-Z view: Drop of 19mm diameter cylinders over the water surface at 30° initial angle. The X-coordinates are radial coordinates from the XY plane and each coloured line represents a drop.

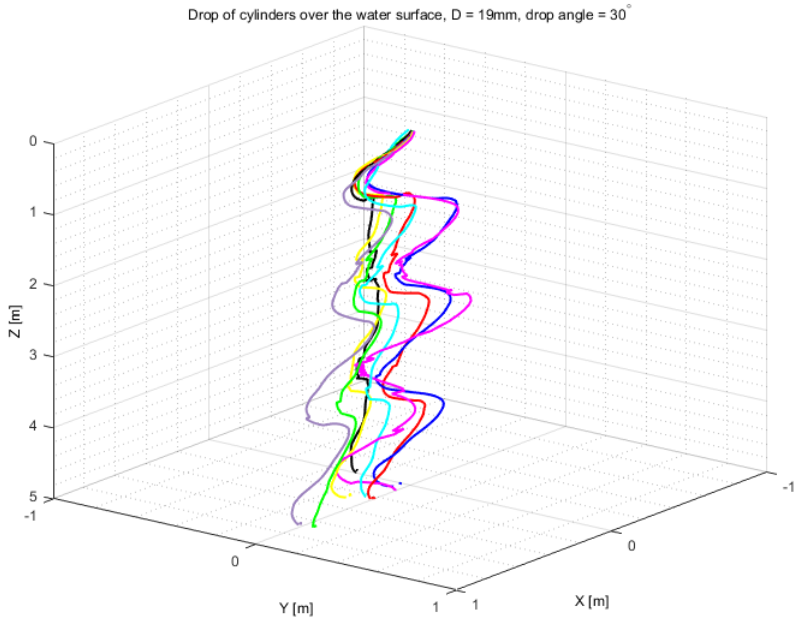

Figure 81: X-Y-Z view: Drop of 19mm diameter cylinders over the water surface at 30° initial angle. Each coloured line represents a drop.

A.6.3 45° initial drop angle

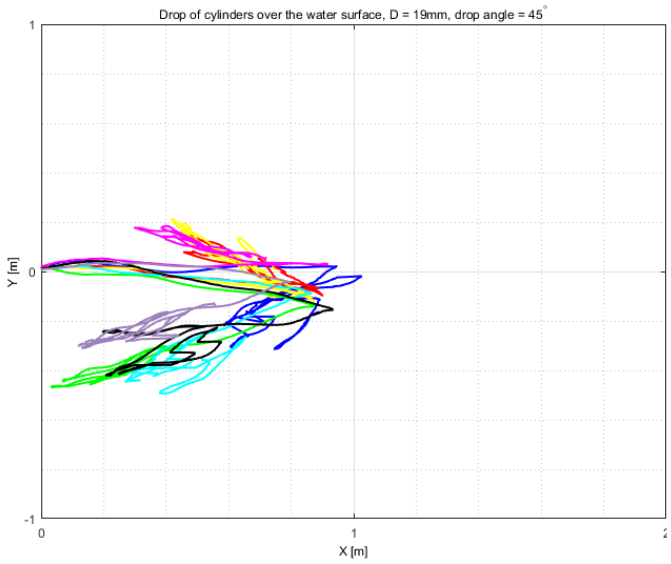

Figure 82: X-Y view: Drop of 19mm diameter cylinders over the water surface at 45° initial angle. Each coloured line represents a drop.

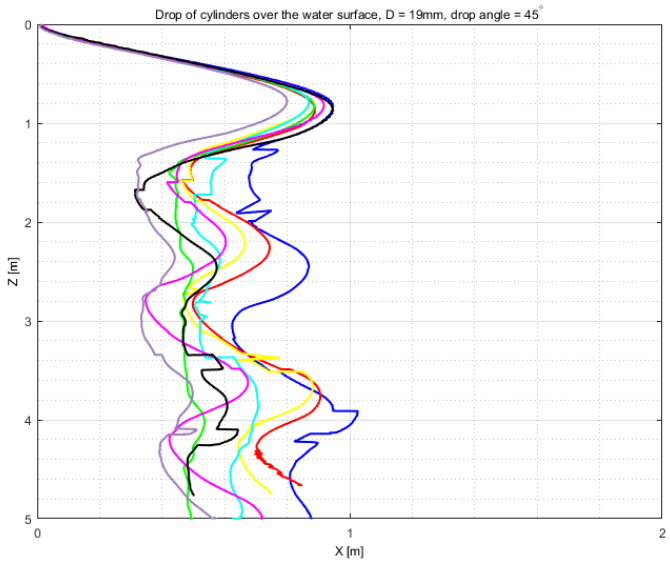

Figure 83: X-Z view: Drop of 19mm diameter cylinders over the water surface at 45° initial angle. The X-coordinates are radial coordinates from the XY plane and each coloured line represents a drop.

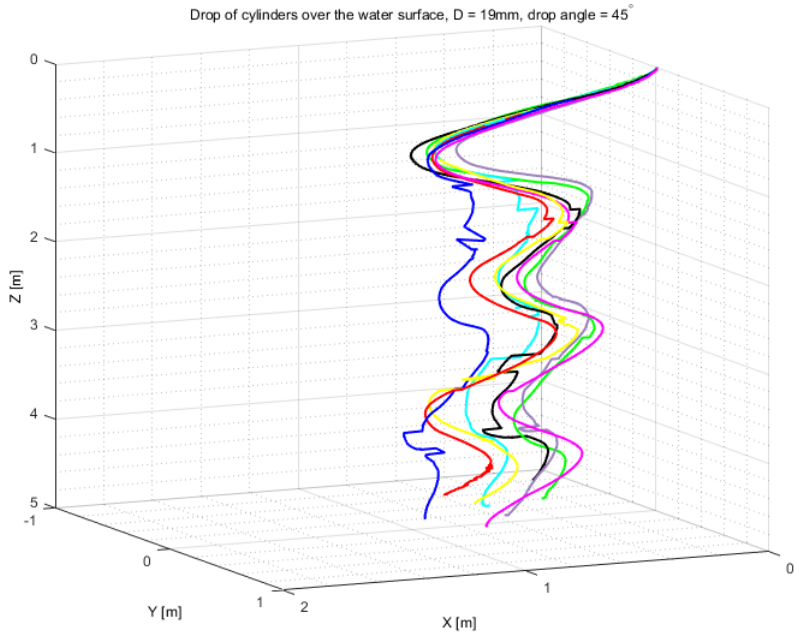

Figure 84: X-Y-Z view: Drop of 19mm diameter cylinders over the water surface at 45° initial angle. Each coloured line represents a drop.

A.6.4 60° initial drop angle

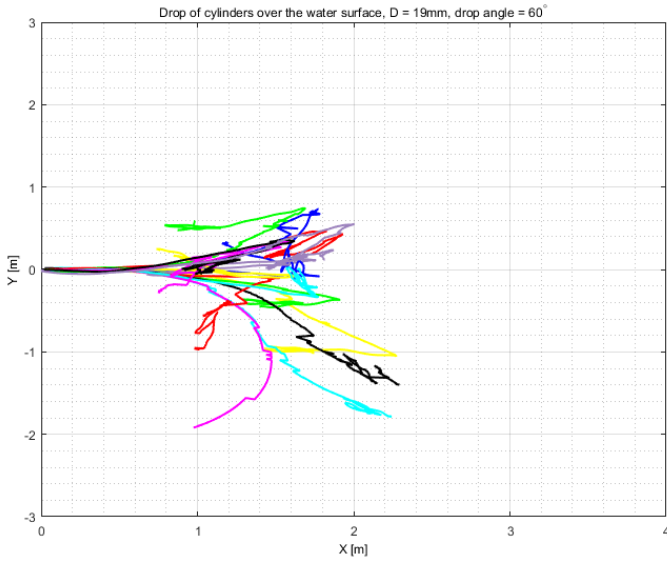

Figure 85: X-Y view: Drop of 19mm diameter cylinders over the water surface at 60° initial angle. Each coloured line represents a drop.

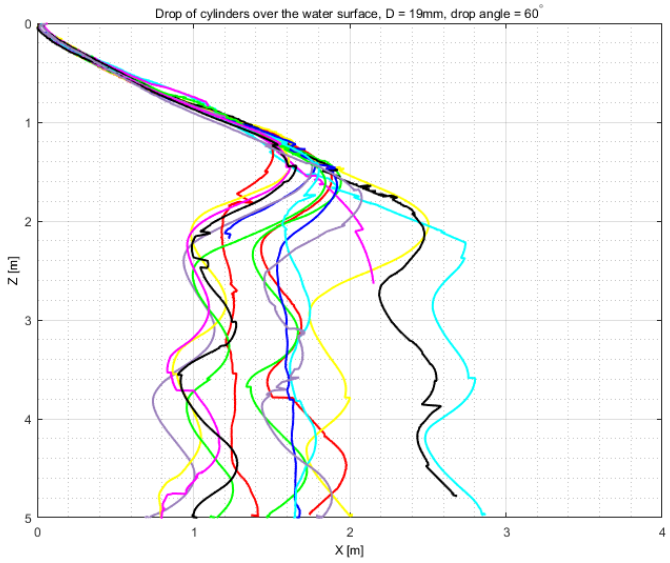

Figure 86: X-Z view: Drop of 19mm diameter cylinders over the water surface at 60° initial angle. The X-coordinates are radial coordinates from the XY plane and each coloured line represents a drop.

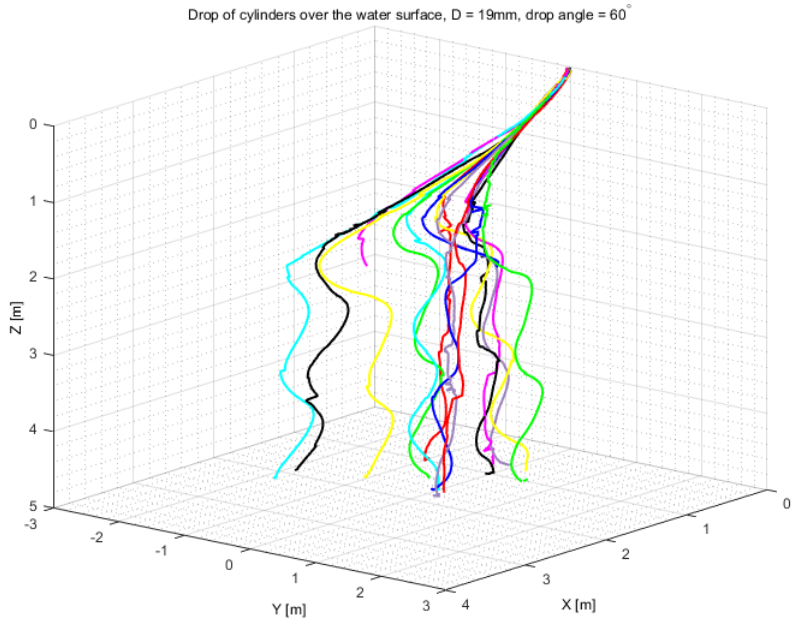

Figure 87: X-Y-Z view: Drop of 19mm diameter cylinders over the water surface at 60° initial angle. Each coloured line represents a drop.

A.6.5 75° initial drop angle

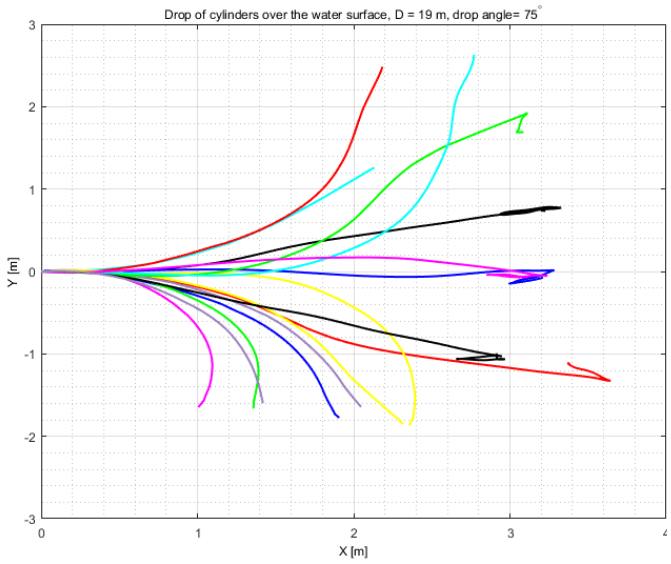

Figure 88: X-Y view: Drop of 19mm diameter cylinders over the water surface at 75° initial angle. Each coloured line represents a drop.

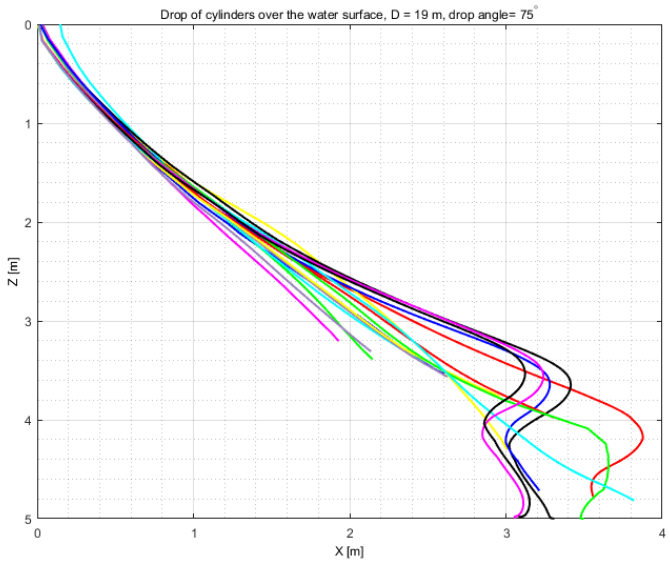

Figure 89: X-Z view: Drop of 19mm diameter cylinders over the water surface at 75° initial angle. The X-coordinates are radial coordinates from the XY plane and each coloured line represents a drop.

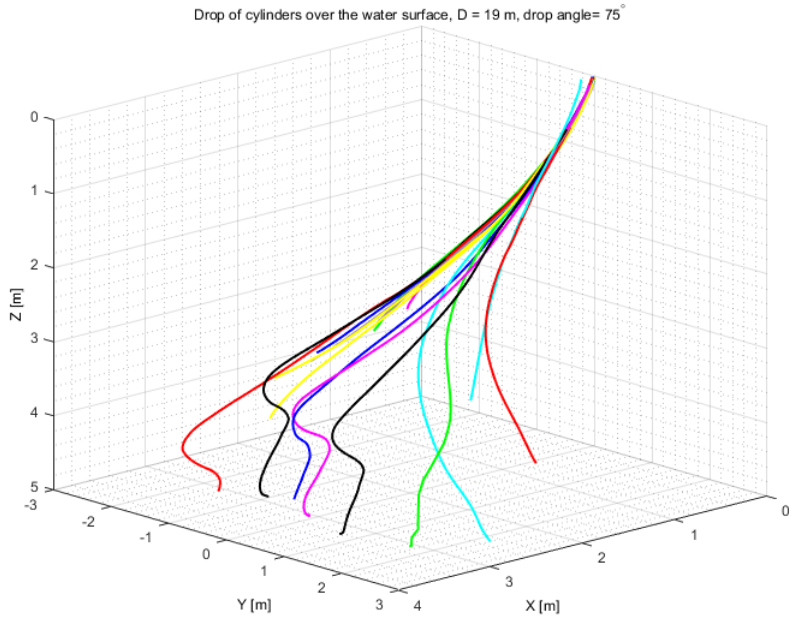

Figure 90: X-Y-Z view: Drop of 19mm diameter cylinders over the water surface at 75° initial angle. Each coloured line represents a drop.

A.7 Drop of open 10 mm cylinders under the water surface

A.7.1 15° initial drop angle

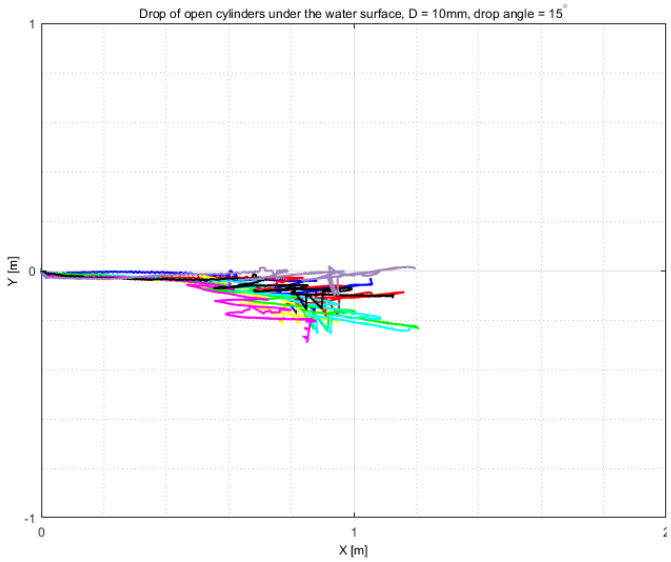

Figure 91: X-Y view: Drop of open 10mm diameter cylinders under the water surface at 15° initial drop angle. Each coloured line represents a drop.

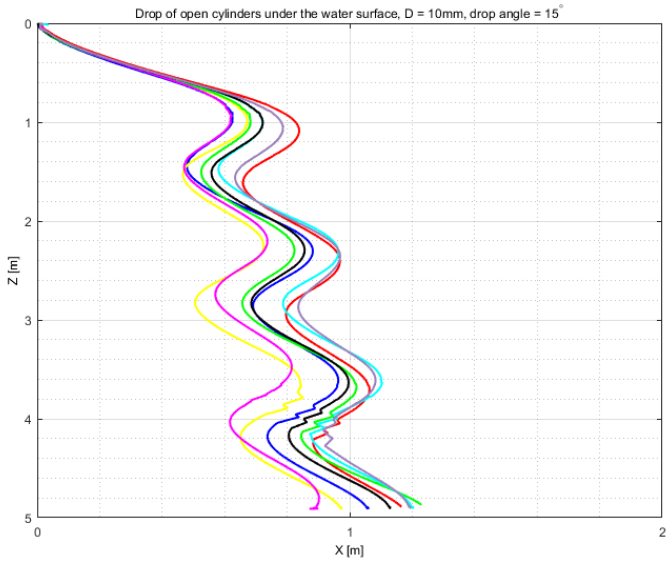

Figure 92: X-Z view: Drop of open 10mm diameter cylinders under the water surface at 15° initial drop angle. The X-coordinates are radial coordinates from the XY plane and each coloured line represents a drop.

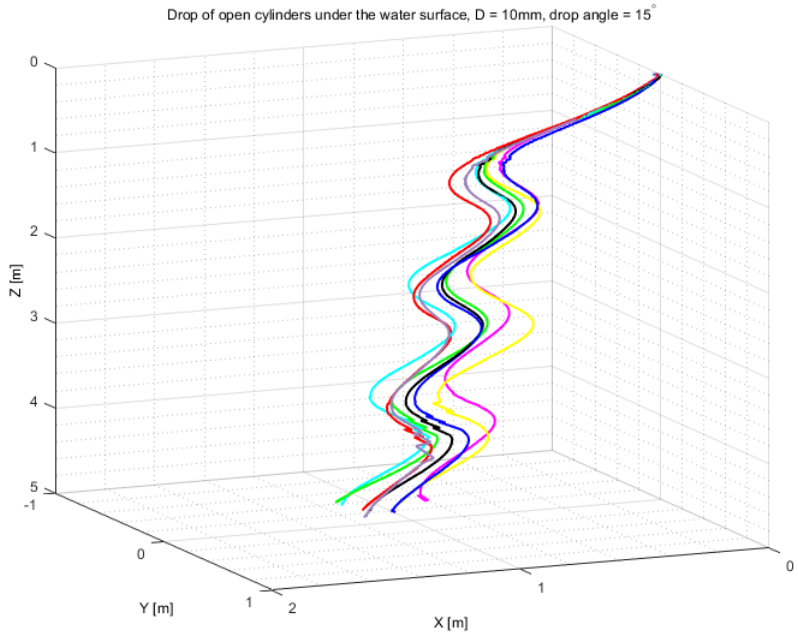

Figure 93: X-Y-Z view: Drop of open 10mm diameter cylinders under the water surface at 15° initial drop angle. Each coloured line represents a drop.

A.7.2 30° initial drop angle

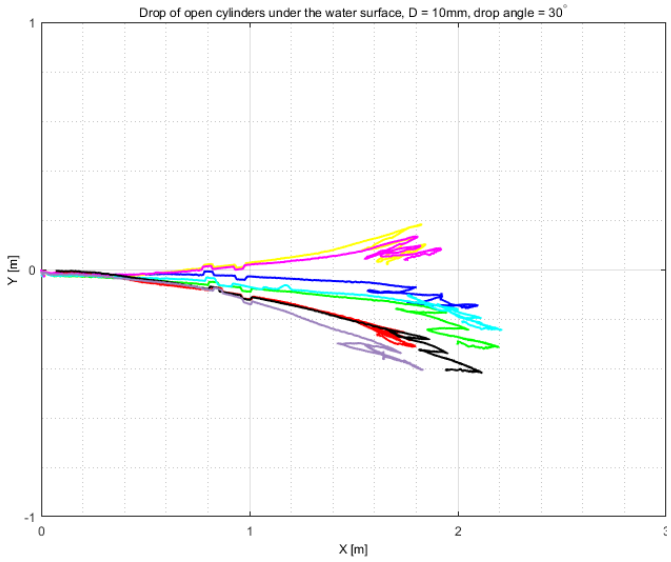

Figure 94: X-Y view: Drop of open 10mm diameter cylinders under the water surface at 30° initial drop angle. Each coloured line represents a drop.

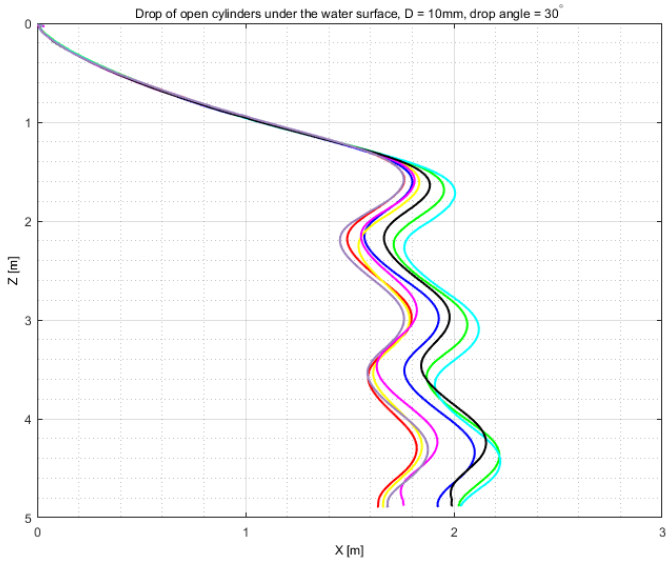

Figure 95: X-Z view: Drop of open 10mm diameter cylinders under the water surface at 30° initial drop angle. The X-coordinates are radial coordinates from the XY plane and each coloured line represents a drop.

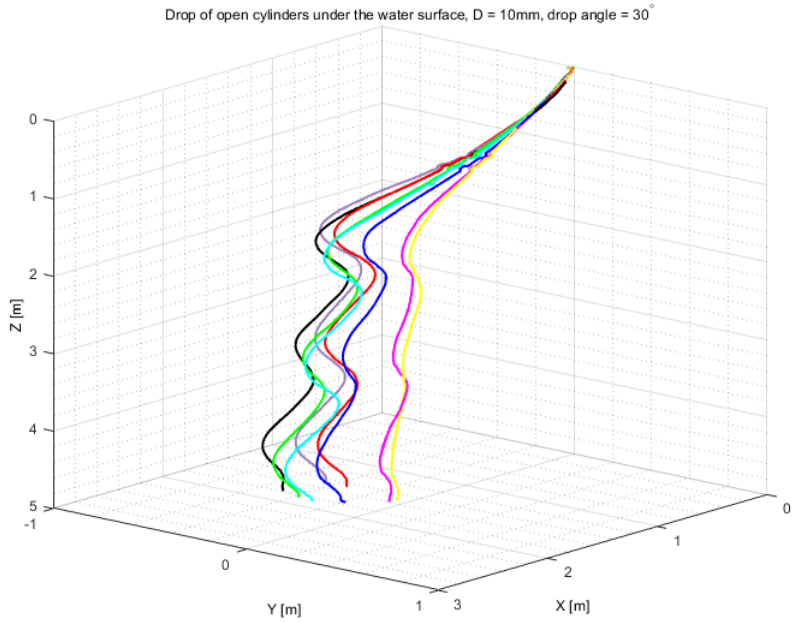

Figure 96: X-Y-Z view: Drop of open 10mm diameter cylinders under the water surface at 30° initial drop angle. Each coloured line represents a drop.

A.7.3 45° initial drop angle

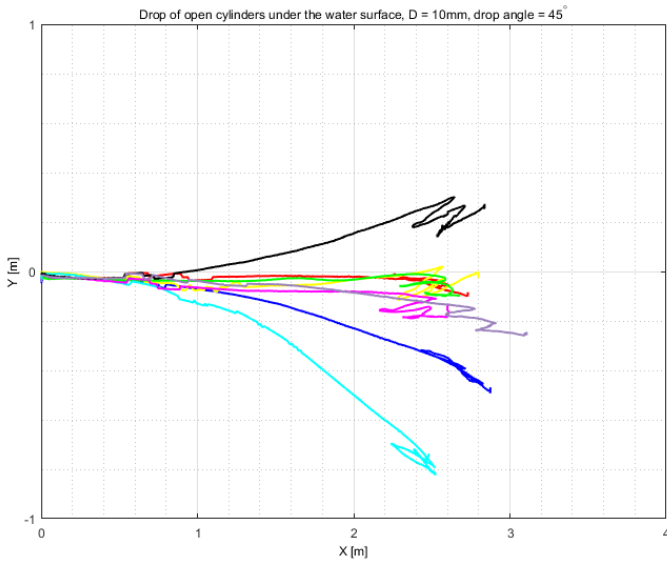

Figure 97: X-Y view: Drop of open 10mm diameter cylinders under the water surface at 45° initial drop angle. Each coloured line represents a drop.

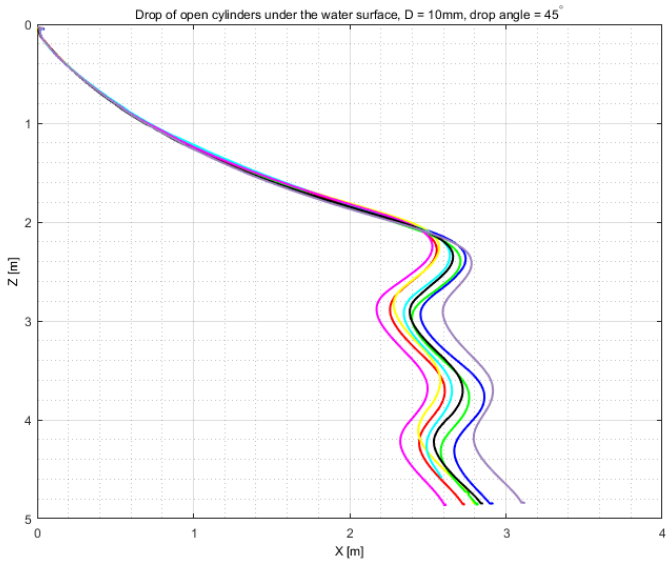

Figure 98: X-Z view: Drop of open 10mm diameter cylinders under the water surface at 45° initial drop angle. The X-coordinates are radial coordinates from the XY plane and each coloured line represents a drop.

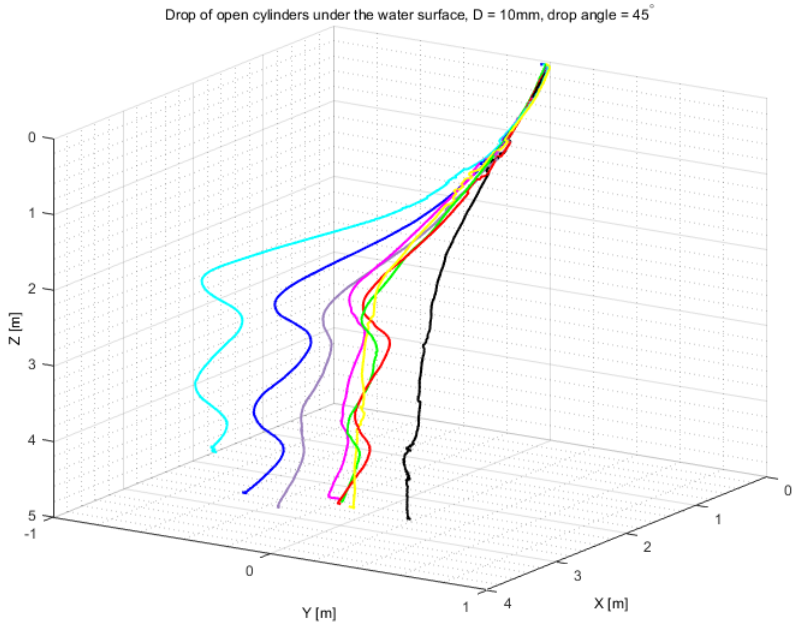

Figure 99: X-Y-Z view: Drop of open 10mm diameter cylinders under the water surface at 45° initial drop angle. Each coloured line represents a drop.

A.7.4 60° initial drop angle

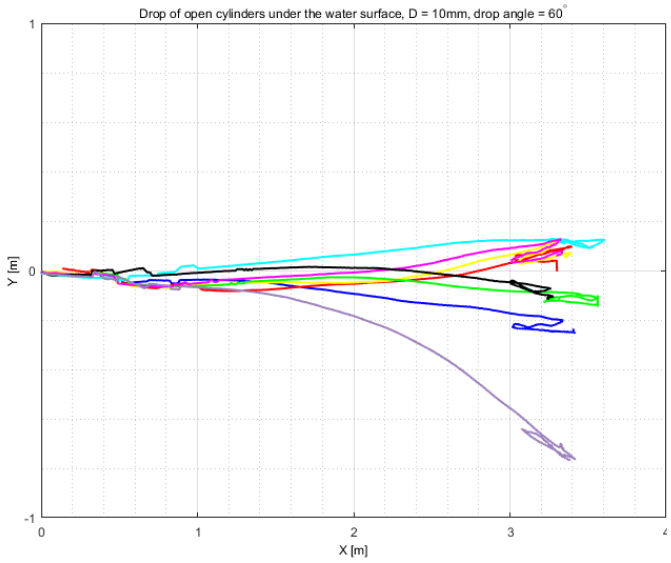

Figure 100: X-Y view: Drop of open 10mm diameter cylinders under the water surface at 60° initial drop angle. Each coloured line represents a drop.

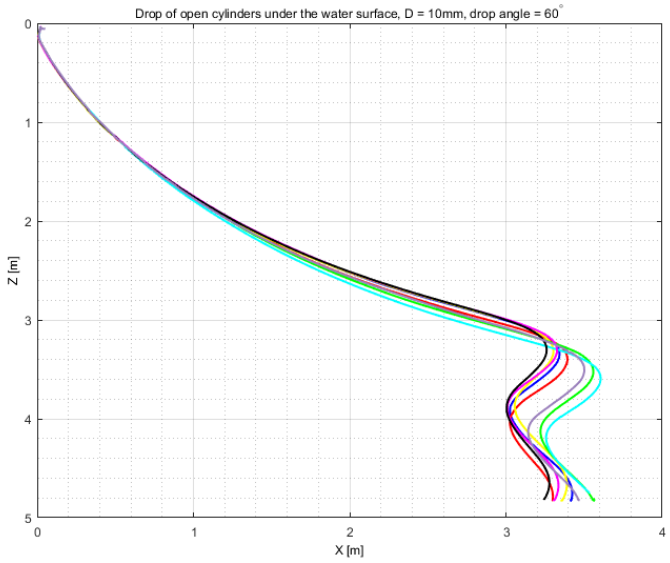

Figure 101: X-Z view: Drop of open 10mm diameter cylinders under the water surface at 60° initial drop angle. The X-coordinates are radial coordinates from the XY plane and each coloured line represents a drop.

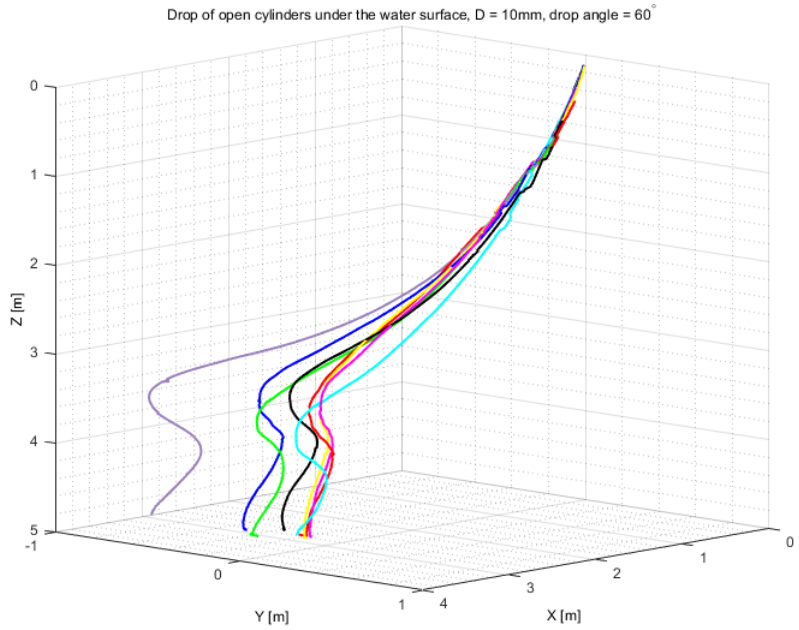

Figure 102: X-Y-Z view: Drop of open 10mm diameter cylinders under the water surface at 60° initial drop angle. Each coloured line represents a drop.

A.7.5 75° initial drop angle

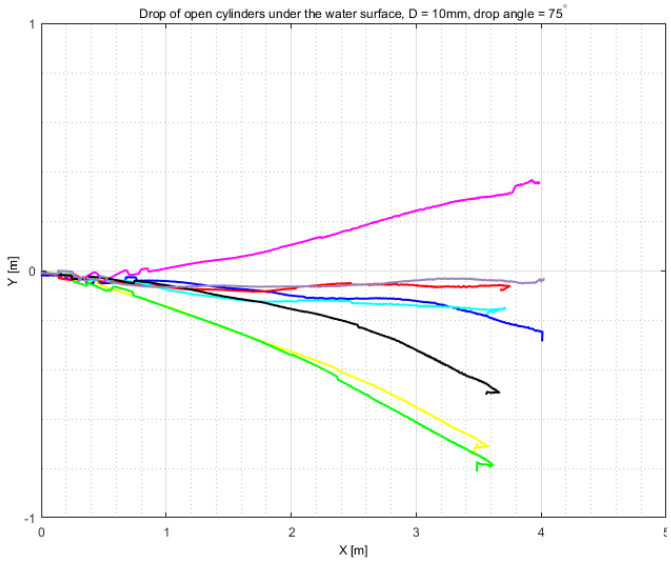

Figure 103: X-Y view: Drop of open 10mm diameter cylinders under the water surface at 75° initial drop angle. Each coloured line represents a drop.

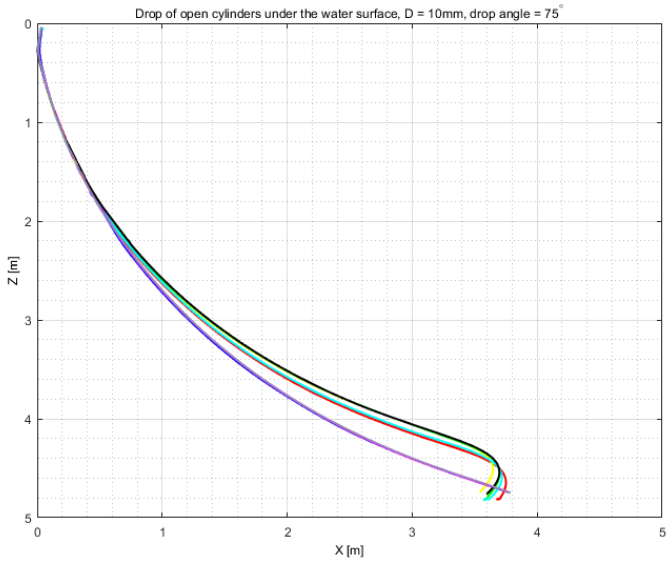

Figure 104: X-Z view: Drop of open 10mm diameter cylinders under the water surface at 75° initial drop angle. The X-coordinates are radial coordinates from the XY plane and each coloured line represents a drop.

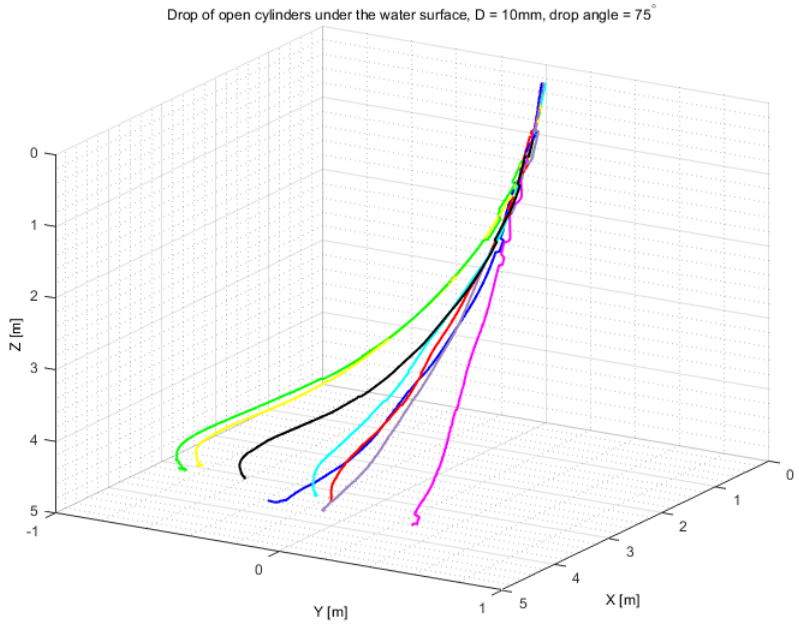

Figure 105: X-Y-Z view: Drop of open 10mm diameter cylinders under the water surface at 75° initial drop angle. Each coloured line represents a drop.

A.8 Drop of open 19 mm cylinders under the water surface

A.8.1 30° initial drop angle

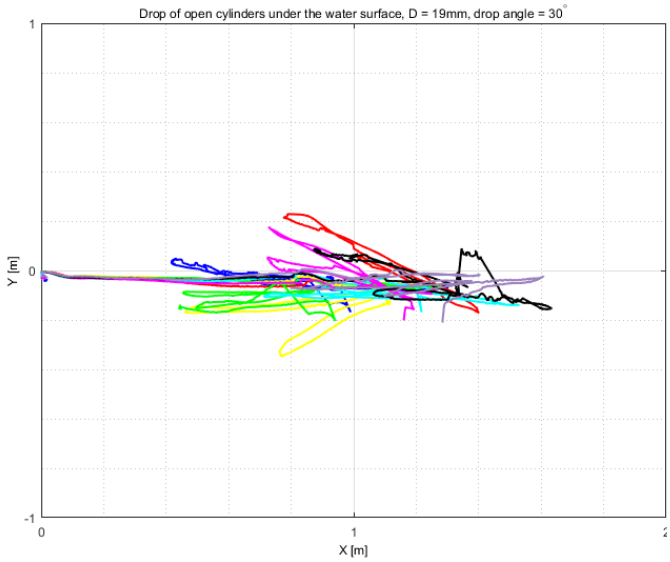

Figure 106: X-Y view: Drop of open 19 mm diameter cylinders under the water surface at 30° initial drop angle. Each coloured line represents a drop.

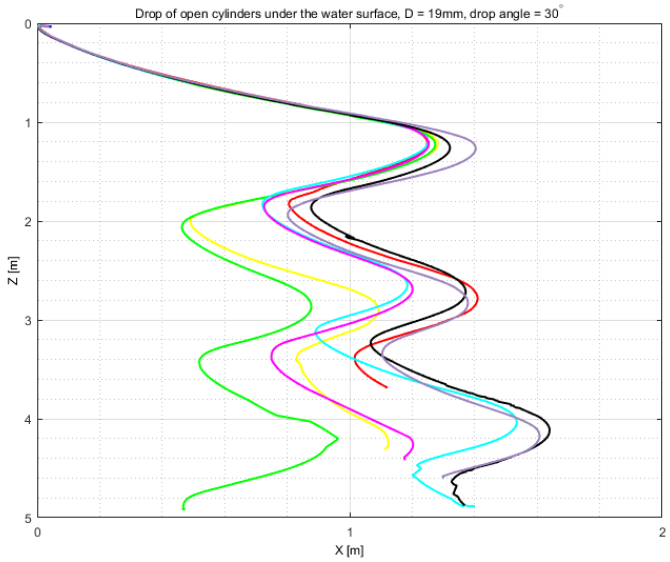

Figure 107: X-Z view: Drop of open 19 mm diameter cylinders under the water surface at 30° initial drop angle. The X-coordinates are radial coordinates from the XY plane and each coloured line represents a drop.

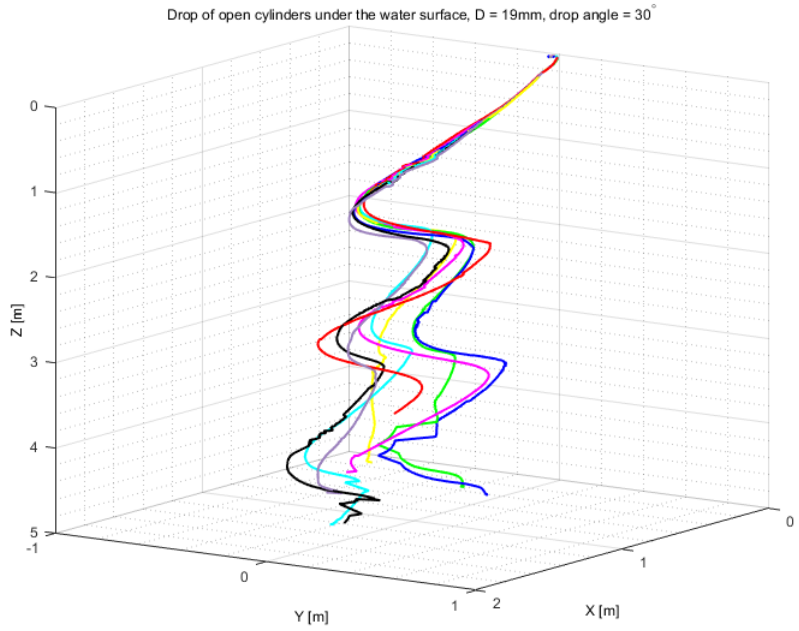

Figure 108: X-Y-Z view: Drop of open 19mm diameter cylinders under the water surface at 30° initial drop angle. Each coloured line represents a drop.

A.8.2 45° initial drop angle

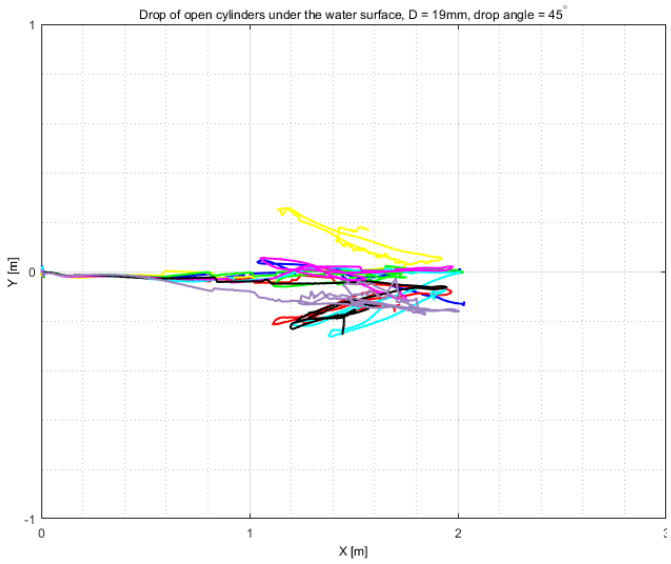

Figure 109: X-Y view: Drop of open 19 mm diameter cylinders under the water surface at 45° initial drop angle. Each coloured line represents a drop.

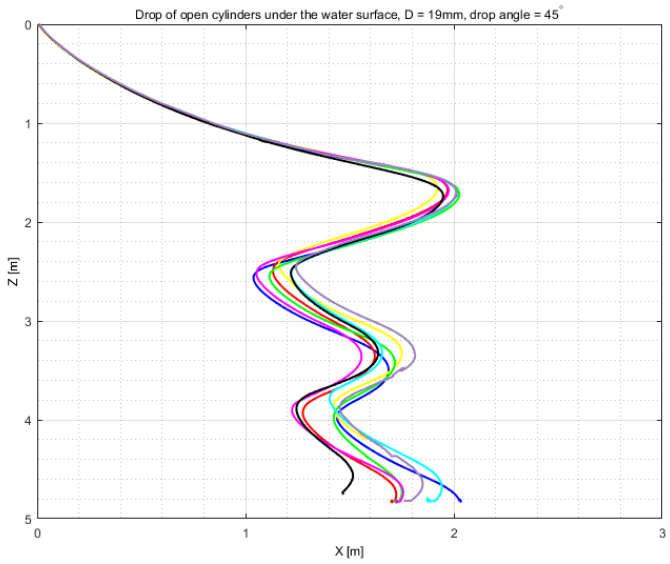

Figure 110: X-Z view: Drop of open 19 mm diameter cylinders under the water surface at 45° initial drop angle. The X-coordinates are radial coordinates from the XY plane and each coloured line represents a drop.

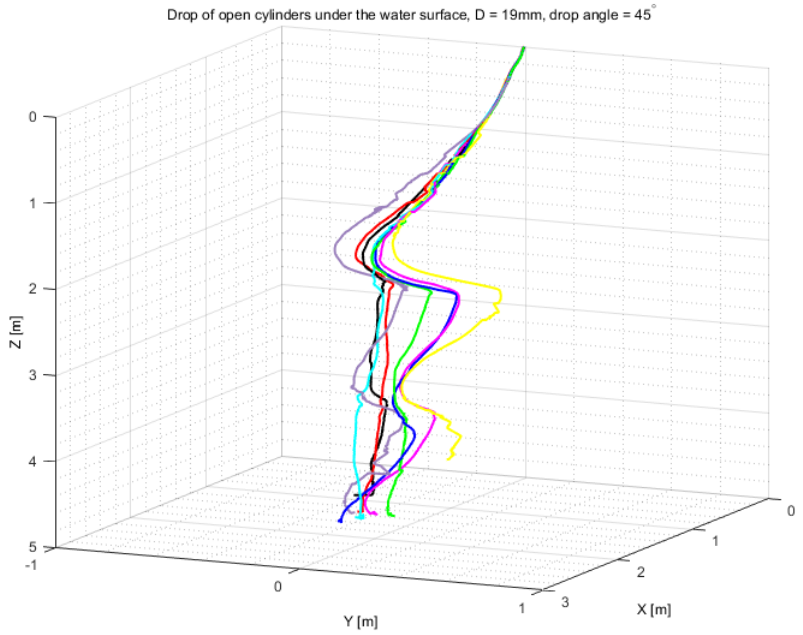

Figure 111: X-Y-Z view: Drop of open 19mm diameter cylinders under the water surface at 45° initial drop angle. Each coloured line represents a drop.

A.8.3 60° initial drop angle

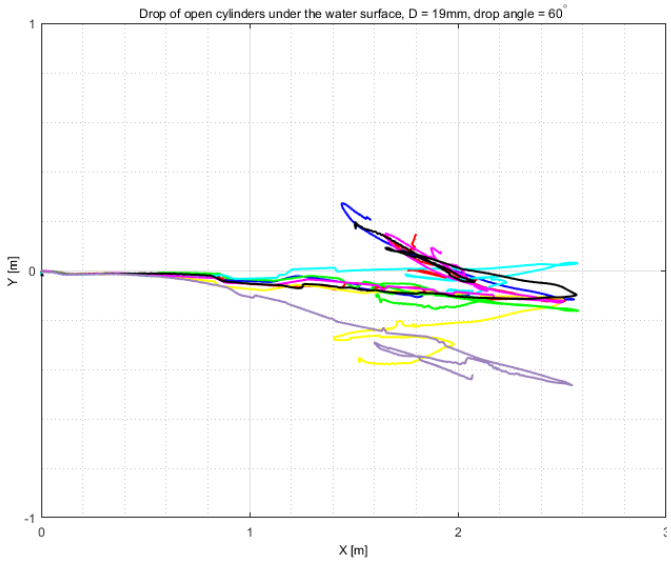

Figure 112: X-Y view: Drop of open 19 mm diameter cylinders under the water surface at 60° initial drop angle. Each coloured line represents a drop.

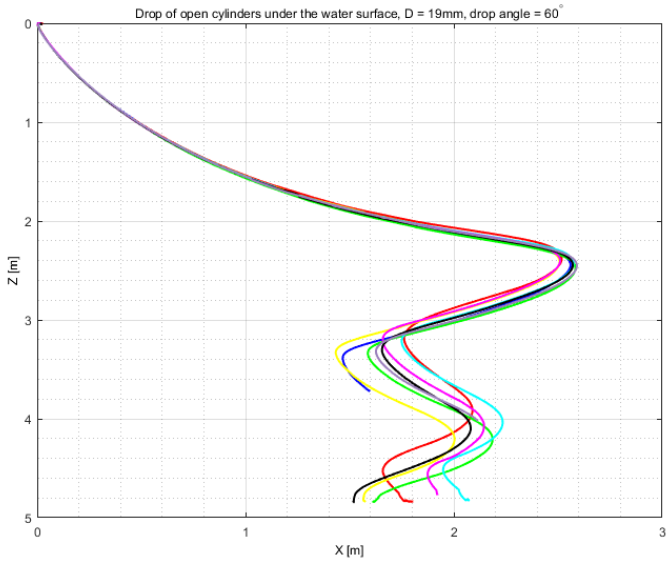

Figure 113: X-Z view: Drop of open 19 mm diameter cylinders under the water surface at 60° initial drop angle. The X-coordinates are radial coordinates from the XY plane and each coloured line represents a drop.

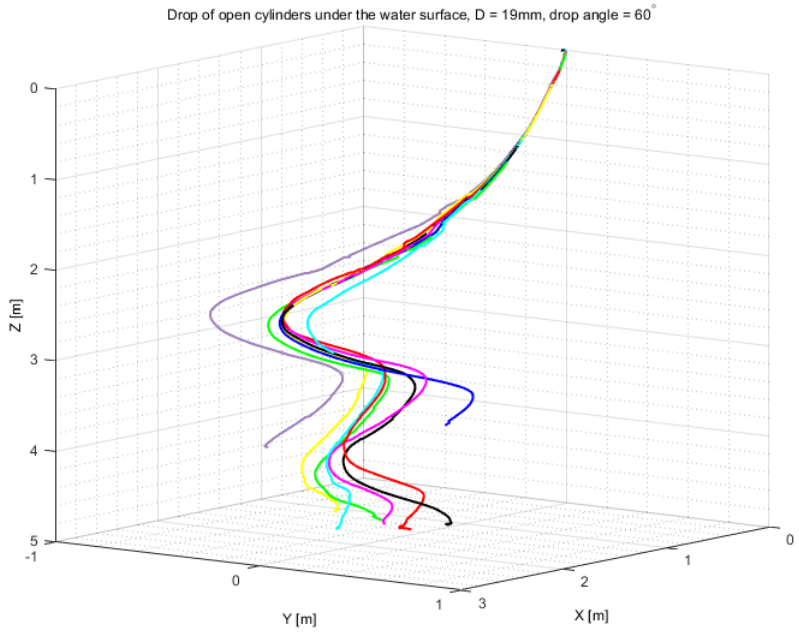

Figure 114: X-Y-Z view: Drop of open 19mm diameter cylinders under the water surface at 60° initial drop angle. Each coloured line represents a drop.

A.8.4 75° initial drop angle

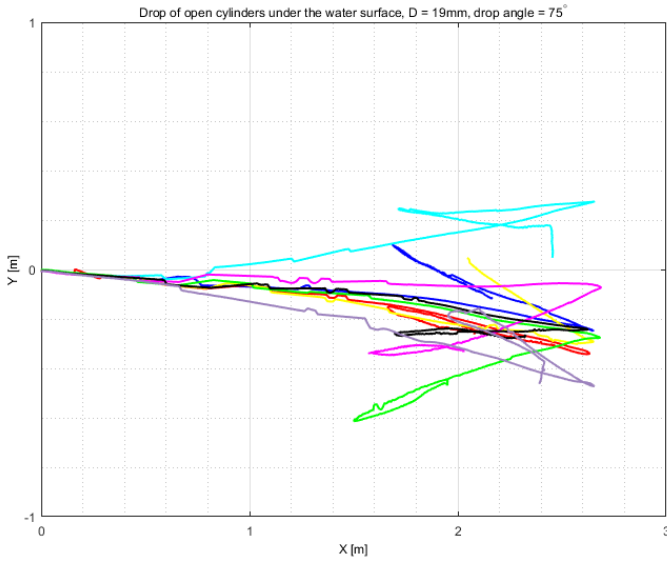

Figure 115: X-Y view: Drop of open 19 mm diameter cylinders under the water surface at 75° initial drop angle. Each coloured line represents a drop.

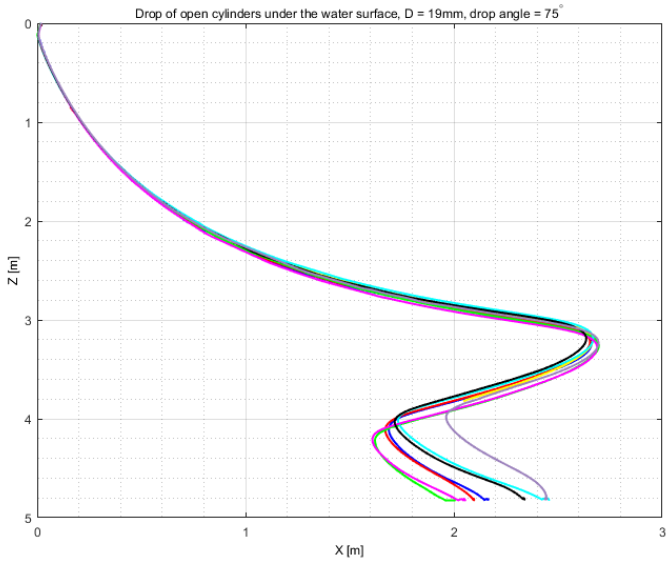

Figure 116: X-Z view: Drop of open 19 mm diameter cylinders under the water surface at 75° initial drop angle. The X-coordinates are radial coordinates from the XY plane and each coloured line represents a drop.

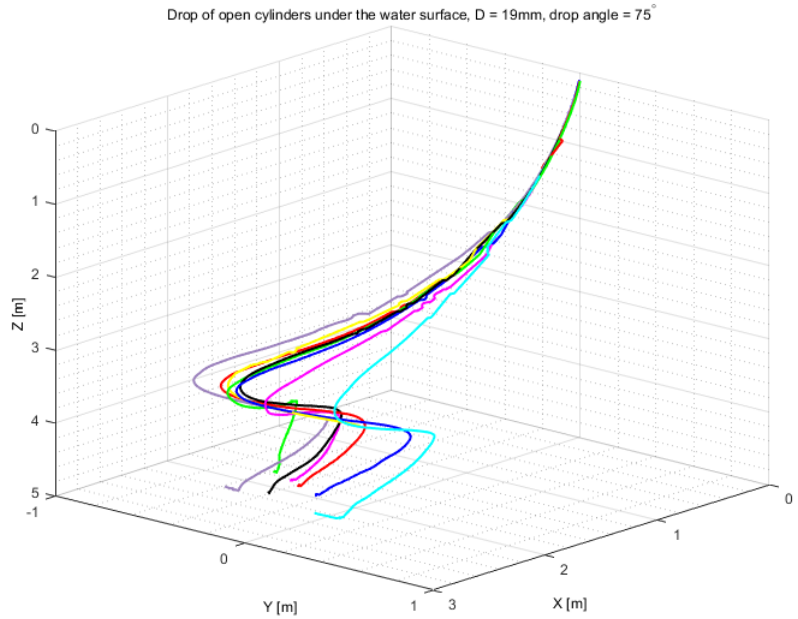

Figure 117: X-Y-Z view: Drop of open 19mm diameter cylinders under the water surface at 75° initial drop angle. Each coloured line represents a drop.

A.9 Drop of 10mm diameter cylinders under the water surface with COG displaced with 1.4cm (COG over COV)

A.9.1 15° initial drop angle

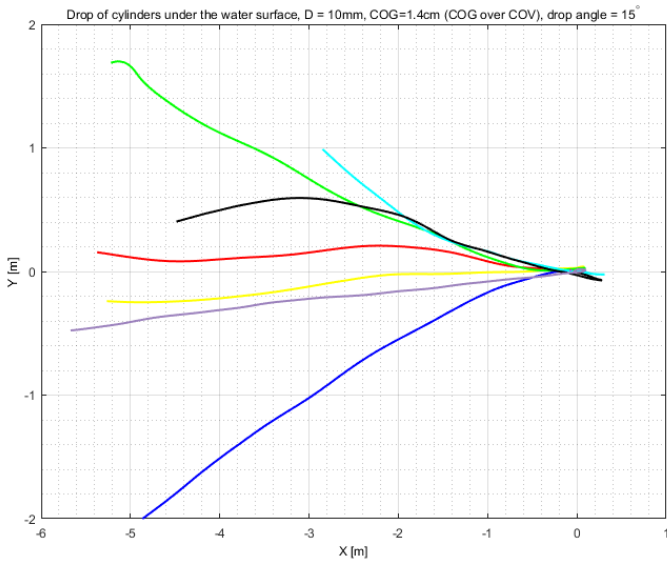

Figure 118: X-Y view: Drop of 10mm diameter cylinders under the water surface at 15° initial angle with COG displaced 1.4cm (Centre of Gravity (COG) over Centre of Volume (COV)). Each coloured line represents a drop. NB! The fore end of the cylinder has been tracked for this drop.

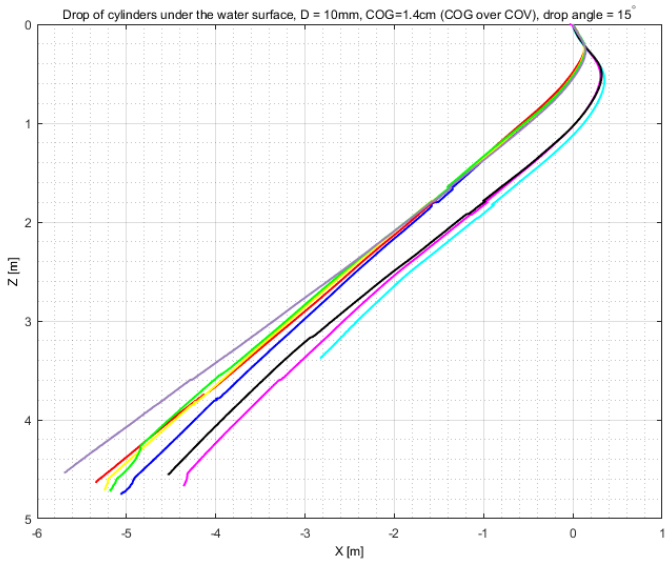

Figure 119: X-Z view: Drop of 10mm diameter cylinders under the water surface at 15° initial angle with COG displaced 1.4cm (Centre of Gravity (COG) over Centre of Volume (COV)). The X-coordinates are radial coordinates from the XY plane and each coloured line represents a drop. NB! The fore end of the cylinder has been tracked for this drop.

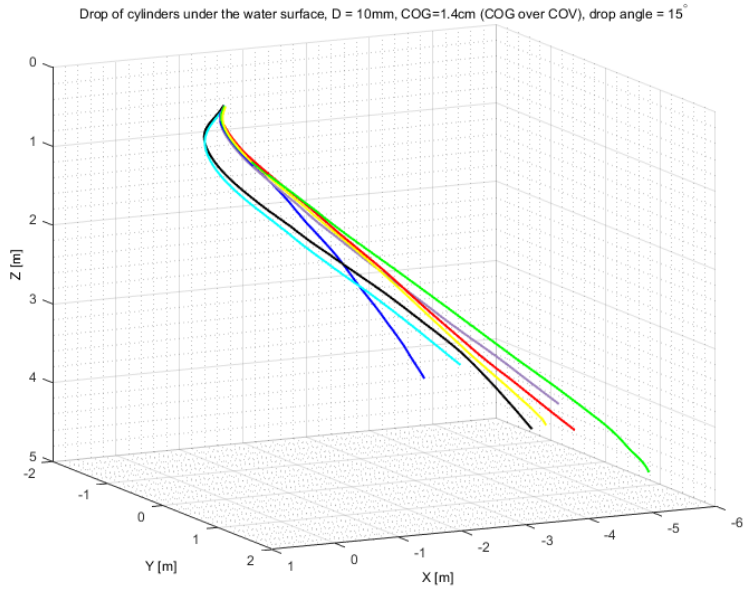

Figure 120: X-Y-Z view: Drop of 10mm diameter cylinders under the water surface at 15° initial angle with COG displaced 1.4cm (Centre of Gravity (COG) over Centre of Volume (COV)). Each coloured line represents a drop. NB! The fore end of the cylinder has been tracked for this drop.

A.9.2 30° initial drop angle

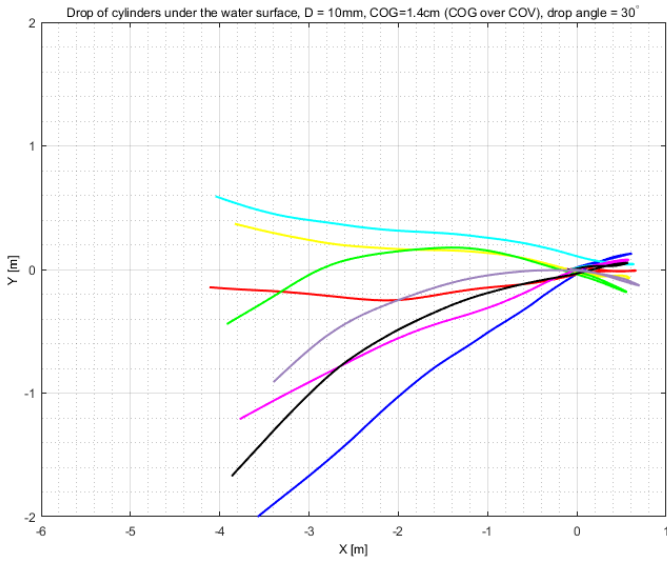

Figure 121: X-Y view: Drop of 10mm diameter cylinders under the water surface at 30° initial angle with COG displaced 1.4cm (Centre of Gravity (COG) over Centre of Volume (COV)). Each coloured line represents a drop. NB! The fore end of the cylinder has been tracked for this drop.

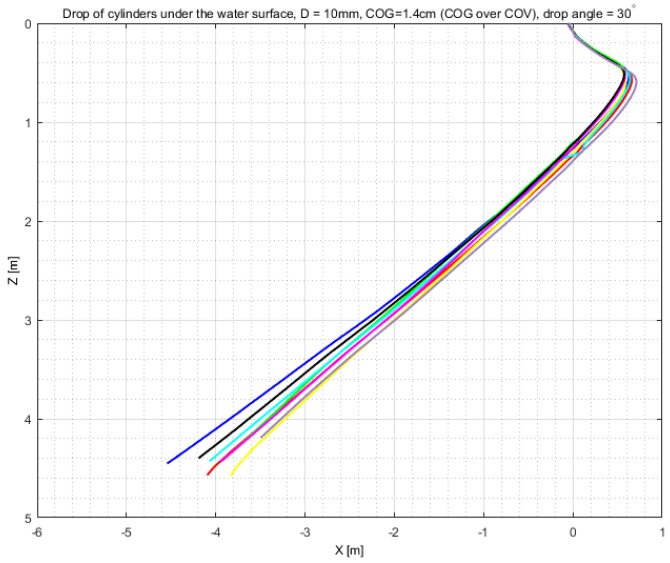

Figure 122: X-Z view: Drop of 10mm diameter cylinders under the water surface at 30° initial angle with COG displaced 1.4cm (Centre of Gravity (COG) over Centre of Volume (COV)). The X-coordinates are radial coordinates from the XY plane and each coloured line represents a drop. NB! The fore end of the cylinder has been tracked for this drop.

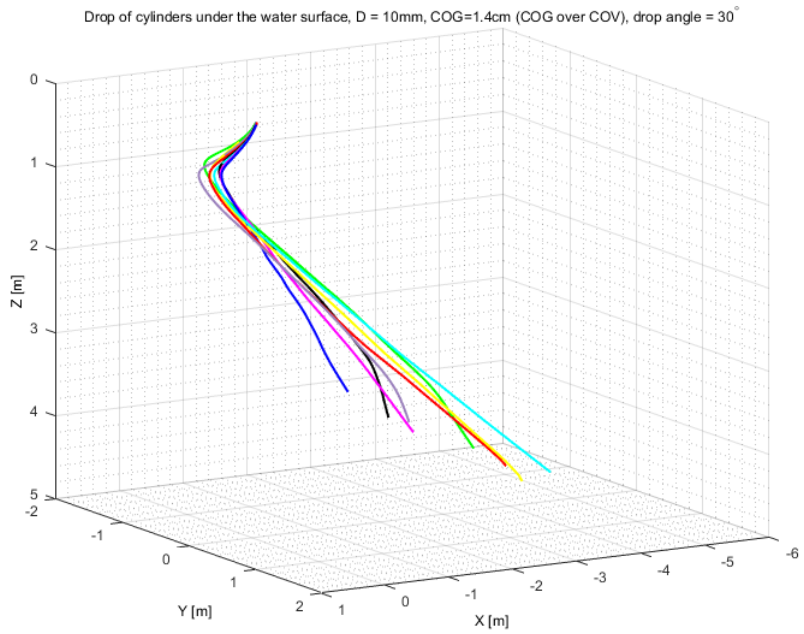

Figure 123: X-Y-Z view: Drop of 10mm diameter cylinders under the water surface at 30° initial angle with COG displaced 1.4cm (Centre of Gravity (COG) over Centre of Volume (COV)). Each coloured line represents a drop. NB! The fore end of the cylinder has been tracked for this drop.

A.9.3 45° initial drop angle

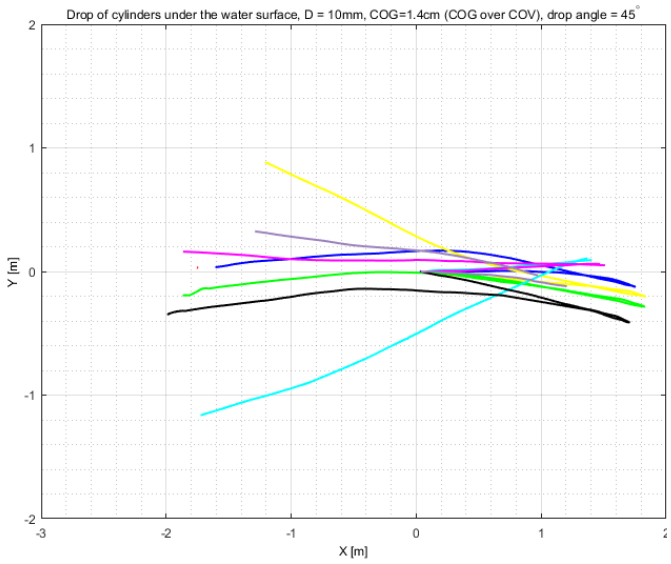

Figure 124: X-Y view: Drop of 10mm diameter cylinders under the water surface at 45° initial angle with COG displaced 1.4cm (Centre of Gravity (COG) over Centre of Volume (COV)). Each coloured line represents a drop. NB! The fore end of the cylinder has been tracked for this drop.

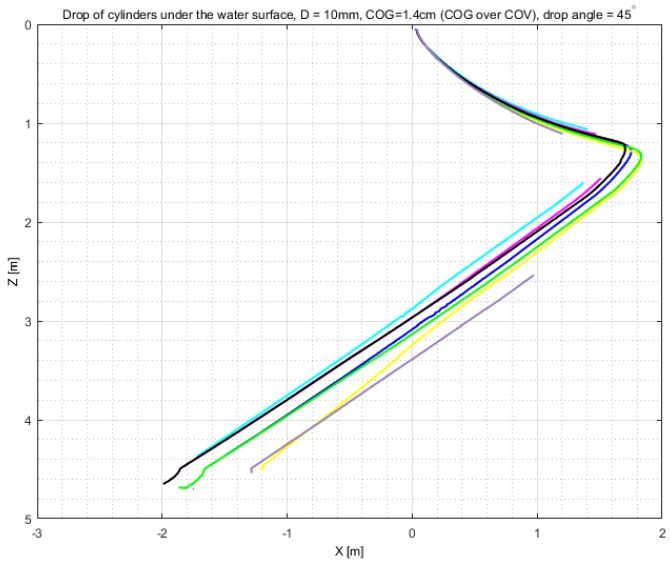

Figure 125: X-Z view: Drop of 10mm diameter cylinders under the water surface at 45° initial angle with COG displaced 1.4cm (Centre of Gravity (COG) over Centre of Volume (COV)). The X-coordinates are radial coordinates from the XY plane and each coloured line represents a drop. NB! The fore end of the cylinder has been tracked for this drop.

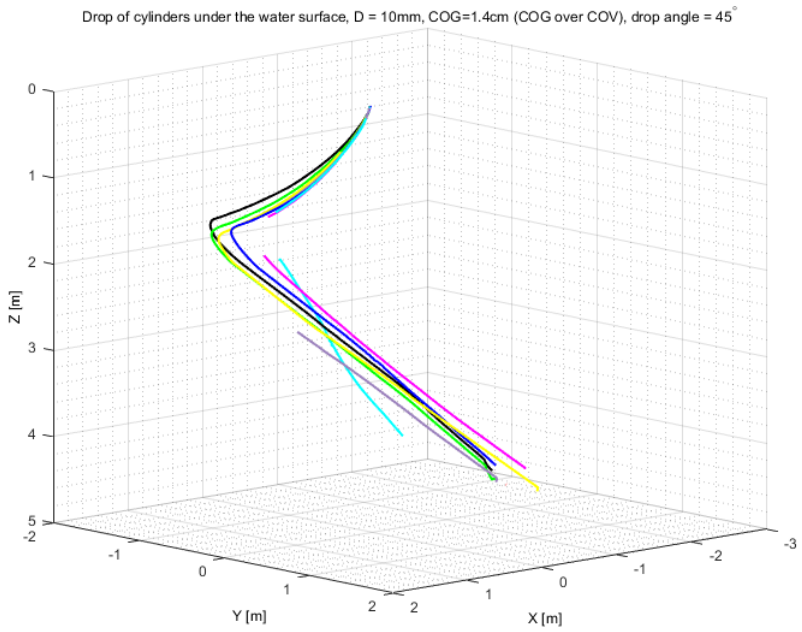

Figure 126: X-Y-Z view: Drop of 10mm diameter cylinders under the water surface at 45° initial angle with COG displaced 1.4cm (Centre of Gravity (COG) over Centre of Volume (COV)). Each coloured line represents a drop. NB! The fore end of the cylinder has been tracked for this drop.

A.9.4 60° initial drop angle

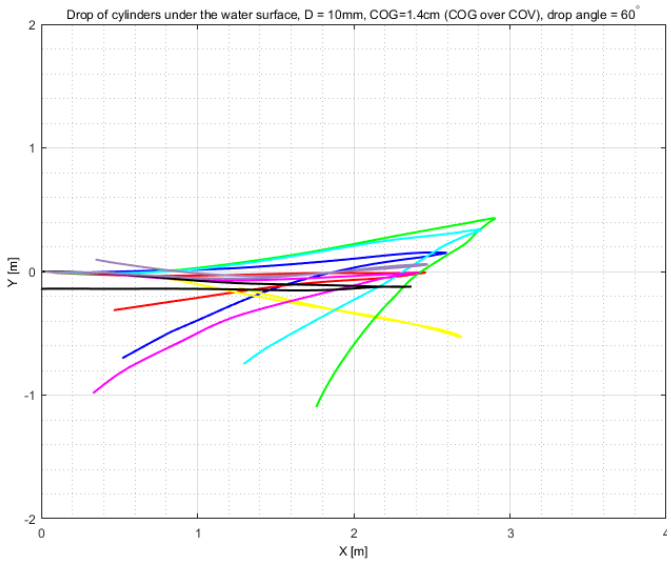

Figure 127: X-Y view: Drop of 10mm diameter cylinders under the water surface at 60° initial angle with COG displaced 1.4cm (Centre of Gravity (COG) over Centre of Volume (COV)). Each coloured line represents a drop.

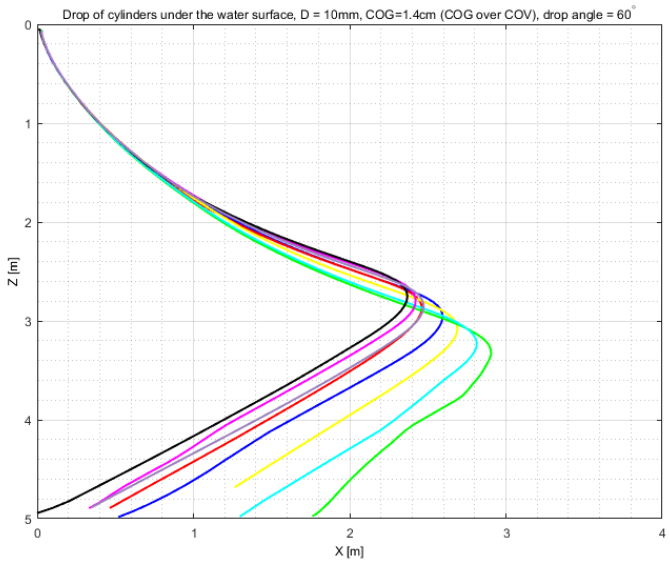

Figure 128: X-Z view: Drop of 10mm diameter cylinders under the water surface at 60° initial angle with COG displaced 1.4cm (Centre of Gravity (COG) over Centre of Volume (COV)). The X-coordinates are radial coordinates from the XY plane and each coloured line represents a drop.

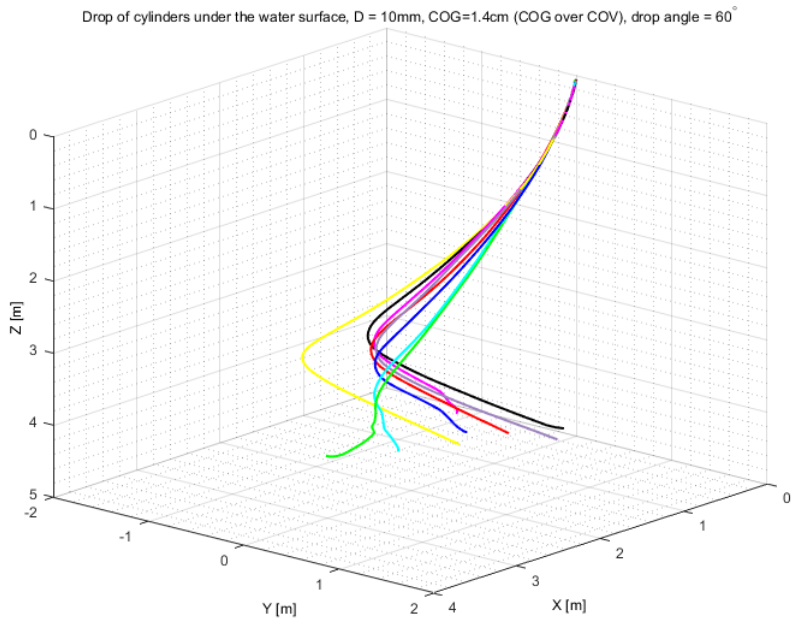

Figure 129: X-Y-Z view: Drop of 10mm diameter cylinders under the water surface at 60° initial angle with COG displaced 1.4cm (Centre of Gravity (COG) over Centre of Volume (COV)). Each coloured line represents a drop.

A.9.5 75° initial drop angle

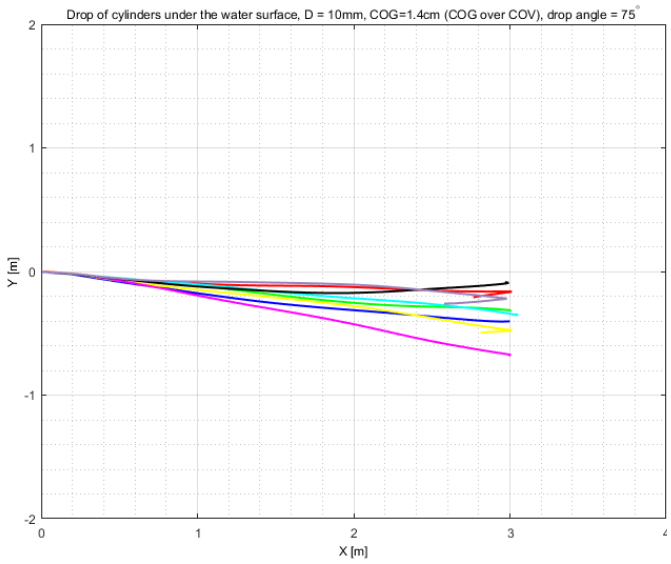

Figure 130: X-Y view: Drop of 10mm diameter cylinders under the water surface at 75° initial angle with COG displaced 1.4cm (Centre of Gravity (COG) over Centre of Volume (COV)). Each coloured line represents a drop.

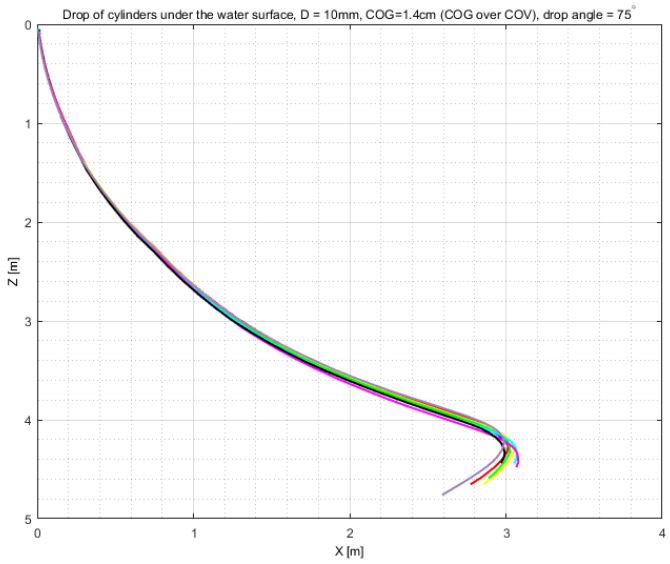

Figure 131: X-Z view: Drop of 10mm diameter cylinders under the water surface at 75° initial angle with COG displaced 1.4cm (Centre of Gravity (COG) over Centre of Volume (COV)). The X-coordinates are radial coordinates from the XY plane and each coloured line represents a drop.

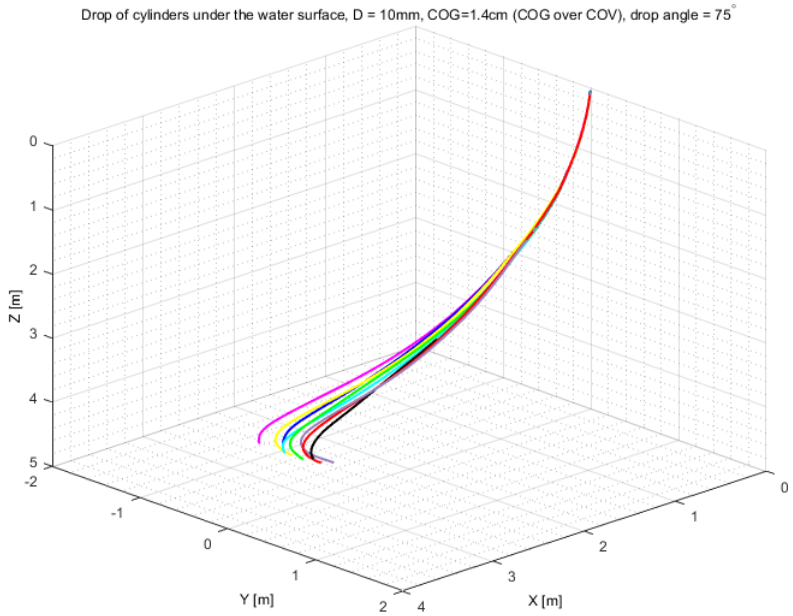

Figure 132: X-Y-Z view: Drop of 10mm diameter cylinders under the water surface at 75° initial angle with COG displaced 1.4cm (Centre of Gravity (COG) over Centre of Volume (COV)). Each coloured line represents a drop.

A.10 Drop of 10mm diameter cylinders under the water surface with COG placed with 1.4 cm (COG under COV)

A.10.1 15° initial drop angle

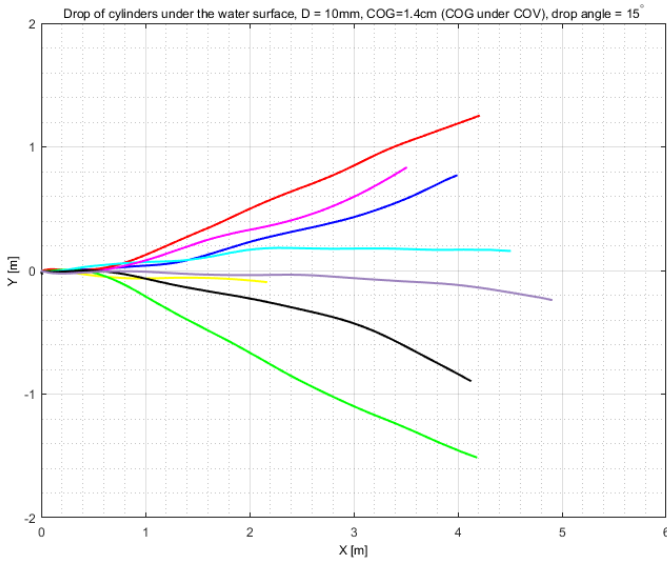

Figure 133: X-Y view: Drop of 10mm diameter cylinders under the water surface at 15° initial angle with COG displaced 1.4 cm (Centre of Gravity (COG) under Centre of Volume (COV)). Each coloured line represents a drop.

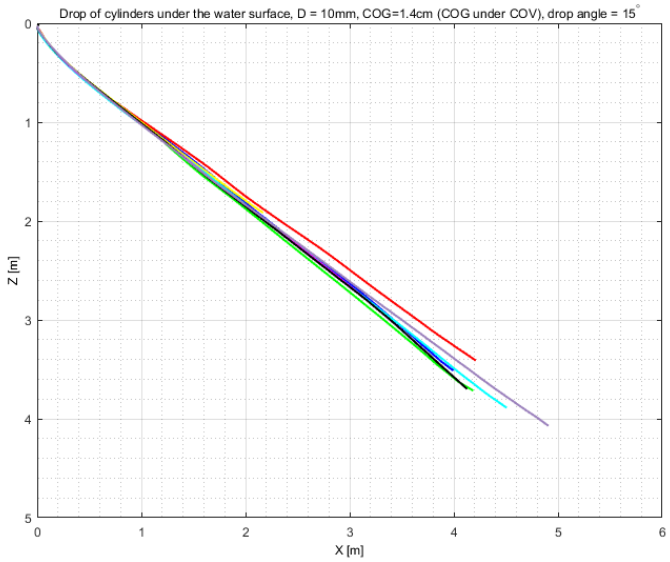

Figure 134: X-Z view: Drop of 10mm diameter cylinders under the water surface at 15° initial angle with COG displaced 1.4 cm (Centre of Gravity (COG) under Centre of Volume (COV)). The X-coordinates are radial coordinates from the XY plane and each coloured line represents a drop.

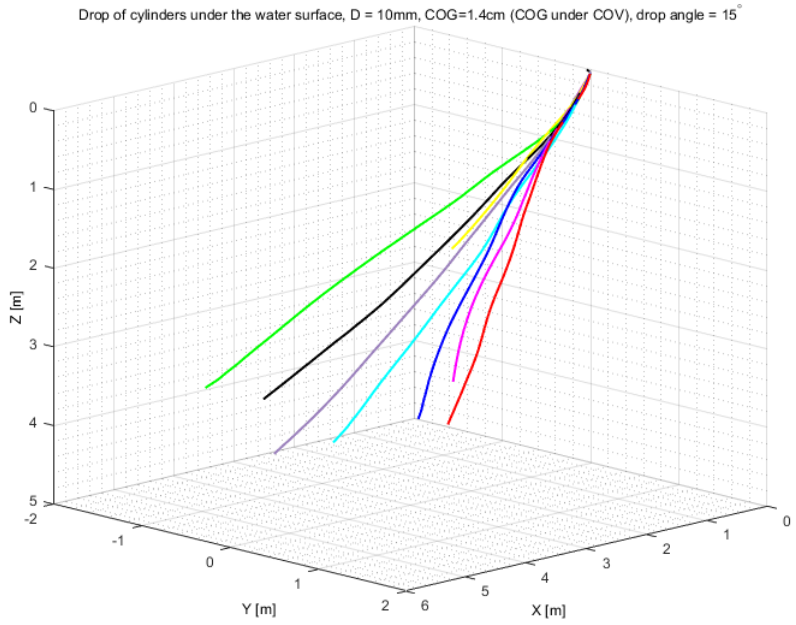

Figure 135: X-Y-Z view: Drop of 10mm diameter cylinders under the water surface at 15° initial angle with COG displaced 1.4 cm (Centre of Gravity (COG) under Centre of Volume (COV)). Each coloured line represents a drop.

A.10.2 30° initial drop angle

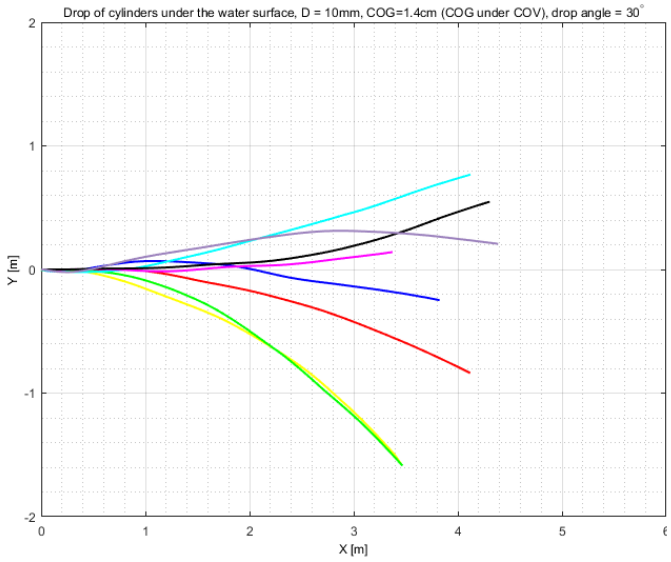

Figure 136: X-Y view: Drop of 10mm diameter cylinders under the water surface at 30° initial angle with COG displaced 1.4 cm (Centre of Gravity (COG) under Centre of Volume (COV)). Each coloured line represents a drop.

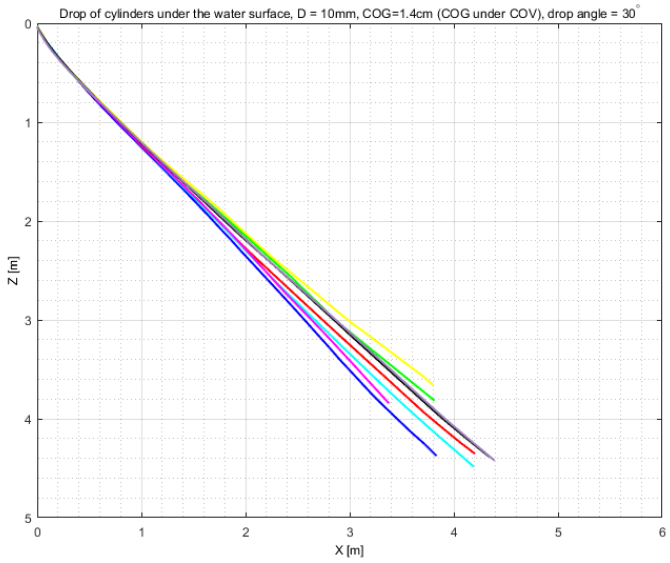

Figure 137: X-Z view: Drop of 10mm diameter cylinders under the water surface at 30° initial angle with COG displaced 1.4 cm (Centre of Gravity (COG) under Centre of Volume (COV)). The X-coordinates are radial coordinates from the XY plane and each coloured line represents a drop.

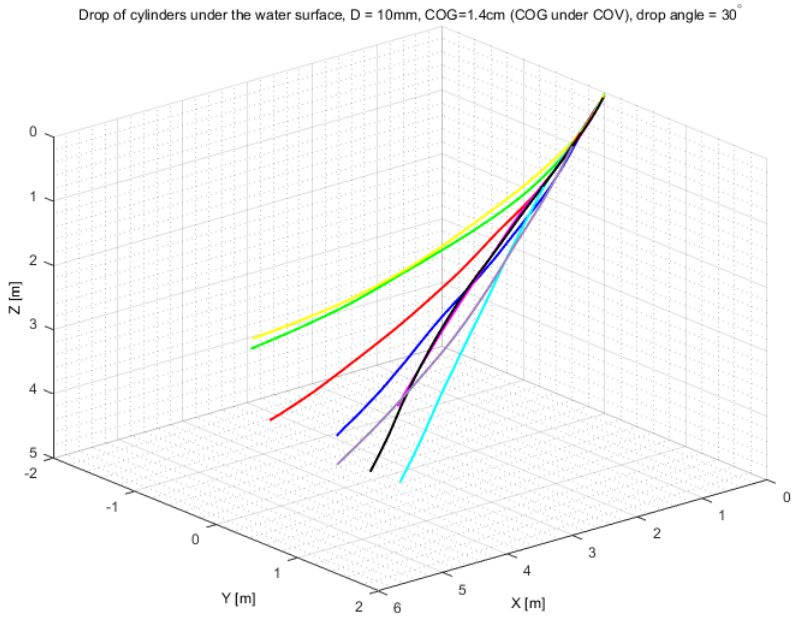

Figure 138: X-Y-Z view: Drop of 10mm diameter cylinders under the water surface at 30° initial angle with COG displaced 1.4 cm (Centre of Gravity (COG) under Centre of Volume (COV)). Each coloured line represents a drop.

A.10.3 45° initial drop angle

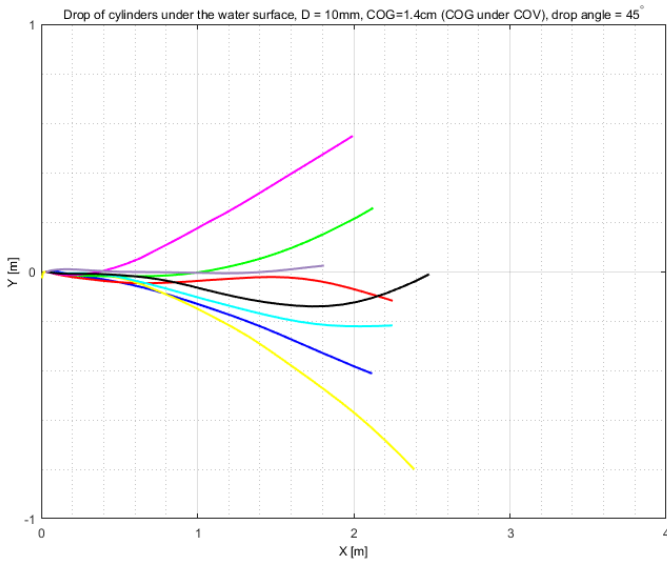

Figure 139: X-Y view: Drop of 10mm diameter cylinders under the water surface at 45° initial angle with COG displaced 1.4 cm (Centre of Gravity (COG) under Centre of Volume (COV)). Each coloured line represents a drop.

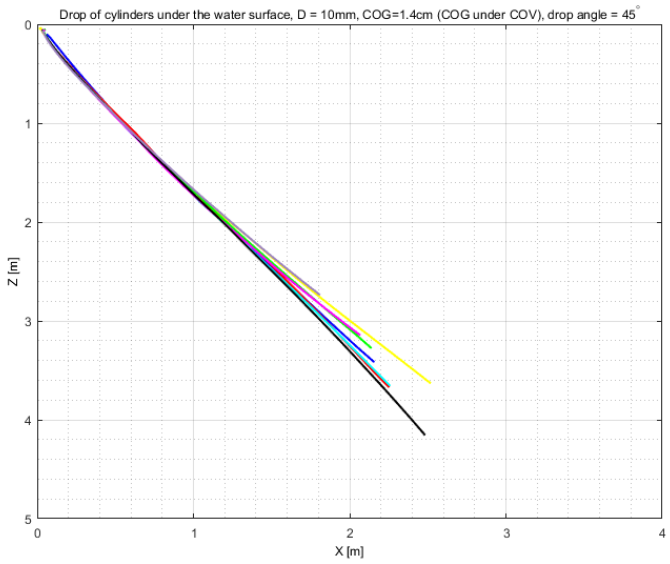

Figure 140: X-Z view: Drop of 10mm diameter cylinders under the water surface at 45° initial angle with COG displaced 1.4 cm (Centre of Gravity (COG) under Centre of Volume (COV)). The X-coordinates are radial coordinates from the XY plane and each coloured line represents a drop.

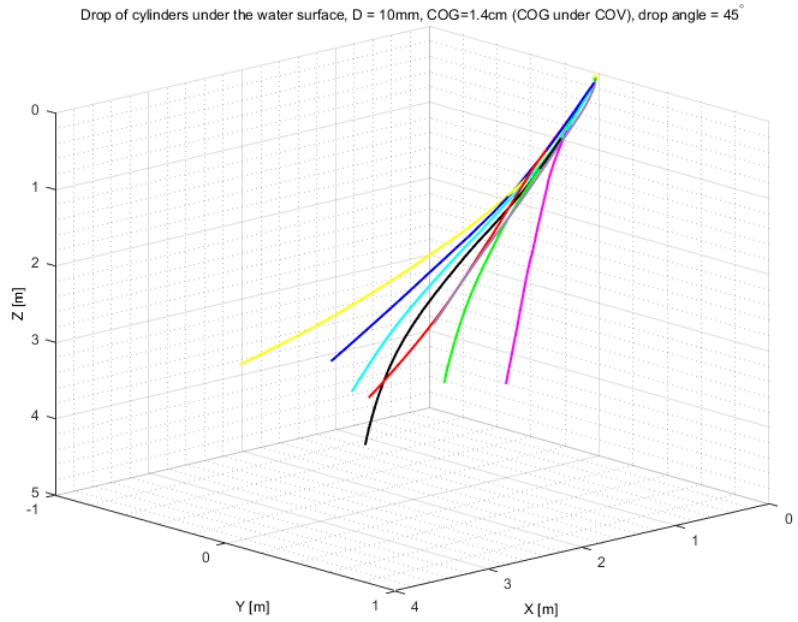

Figure 141: X-Y-Z view: Drop of 10mm diameter cylinders under the water surface at 45° initial angle with COG displaced 1.4 cm (Centre of Gravity (COG) under Centre of Volume (COV)). Each coloured line represents a drop.

A.10.4 60° initial drop angle

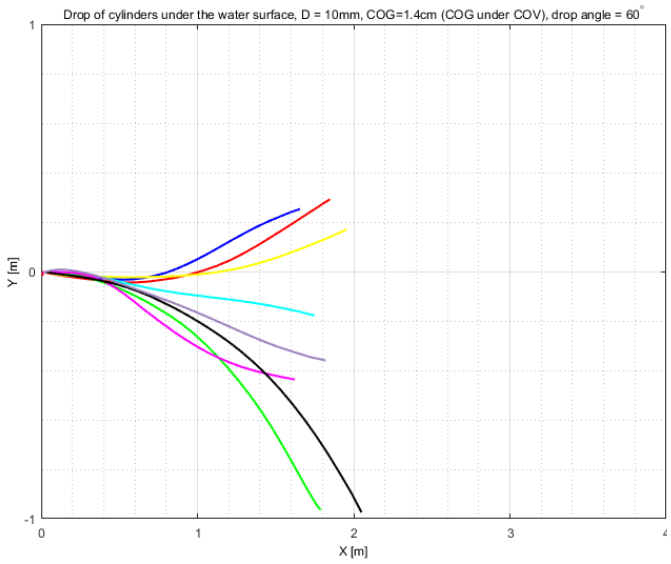

Figure 142: X-Y view: Drop of 10mm diameter cylinders under the water surface at 60° initial angle with COG displaced 1.4cm (Centre of Gravity (COG) under Centre of Volume (COV)). Each coloured line represents a drop.

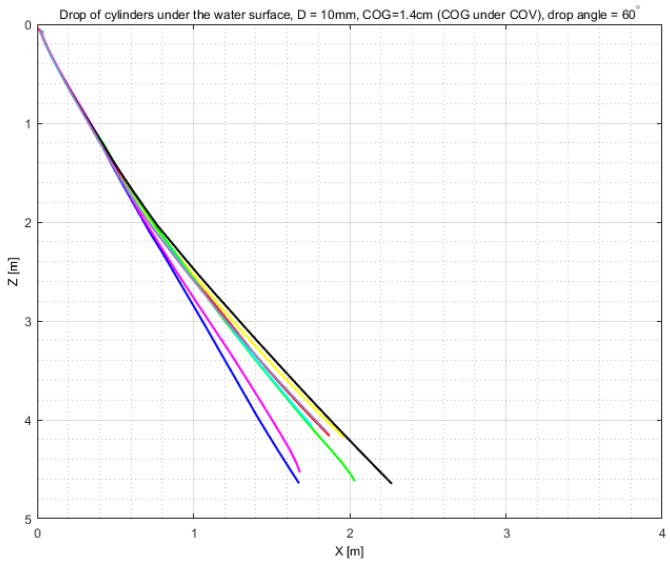

Figure 143: X-Z view: Drop of 10mm diameter cylinders under the water surface at 60° initial angle with COG displaced 1.4cm (Centre of Gravity (COG) under Centre of Volume (COV)). The X-coordinates are radial coordinates from the XY plane and each coloured line represents a drop.

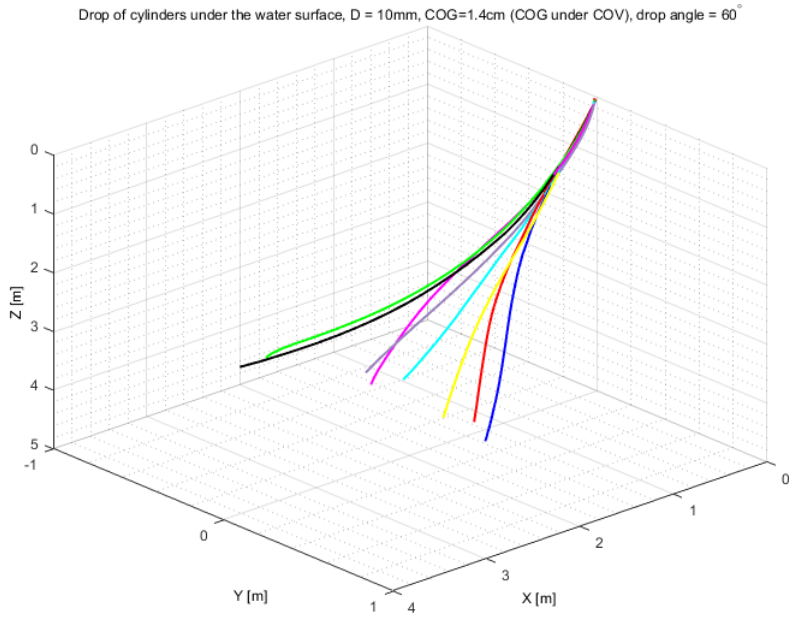

Figure 144: X-Y-Z view: Drop of 10mm diameter cylinders under the water surface at 60° initial angle with COG displaced 1.4cm (Centre of Gravity (COG) under Centre of Volume (COV)). Each coloured line represents a drop.

A.10.5 75° initial drop angle

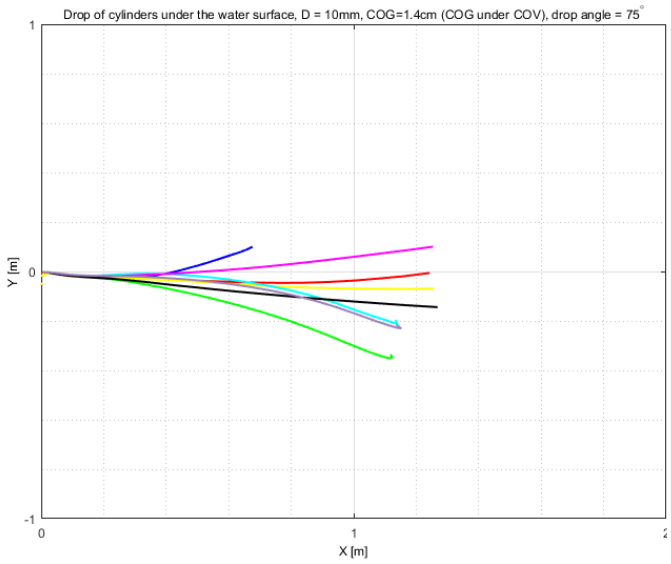

Figure 145: X-Y view: Drop of 10mm diameter cylinders under the water surface at 75° initial angle with COG displaced 1.4cm (Centre of Gravity (COG) under Centre of Volume (COV)). Each coloured line represents a drop.

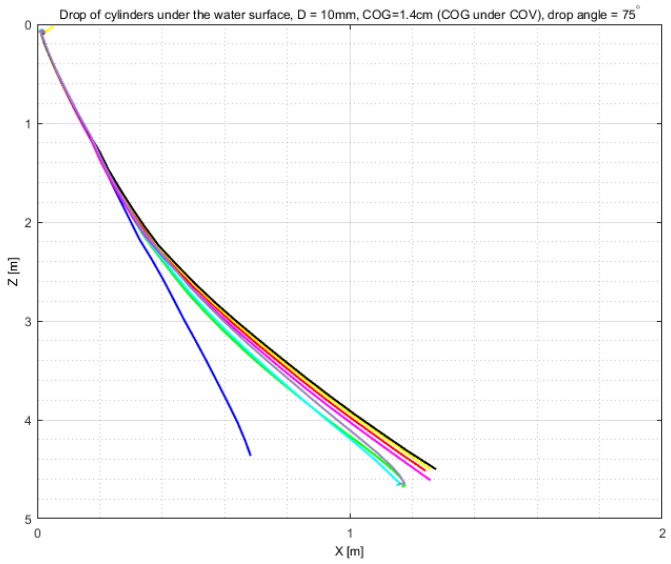

Figure 146: X-Z view: Drop of 10mm diameter cylinders under the water surface at 75° initial angle with COG displaced 1.4cm (Centre of Gravity (COG) under Centre of Volume (COV)). The X-coordinates are radial coordinates from the XY plane and each coloured line represents a drop.

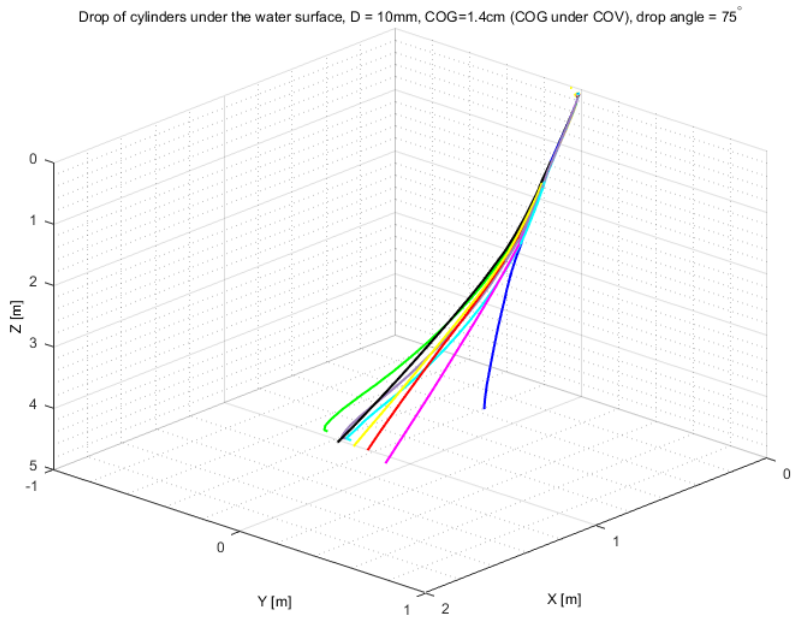

Figure 147: X-Y-Z view: Drop of 10mm diameter cylinders under the water surface at 75° initial angle with COG displaced 1.4cm (Centre of Gravity (COG) under Centre of Volume (COV)). Each coloured line represents a drop.

A.11 Drop of 10mm diameter cylinders under the water surface with COG placed with 3cm (COG over COV)

A.11.1 15° initial drop angle

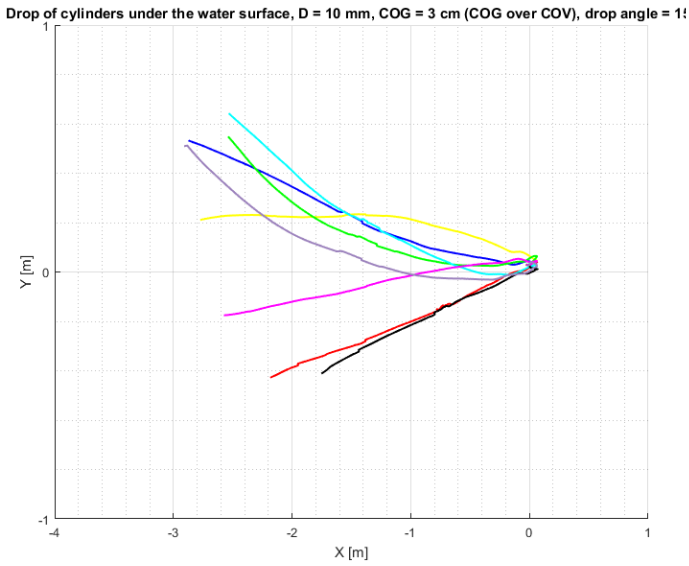

Figure 148: X-Y view: Drop of 10mm diameter cylinders under the water surface at 15° initial angle with COG displaced 3cm (Centre of Gravity (COG) over Centre of Volume (COV)). Each coloured line represents a drop.

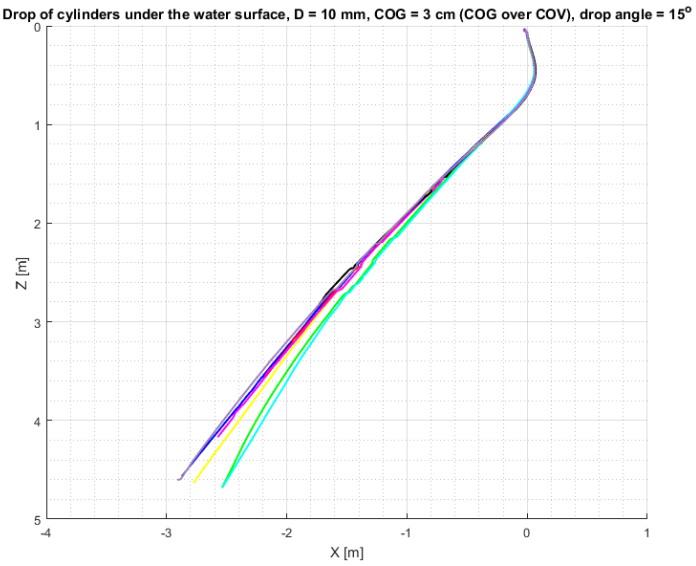

Figure 149: X-Z view: Drop of 10mm diameter cylinders under the water surface at 15° initial angle with COG displaced 3cm (Centre of Gravity (COG) over Centre of Volume (COV)). The X-coordinates are radial coordinates from the XY plane and each coloured line represents a drop.

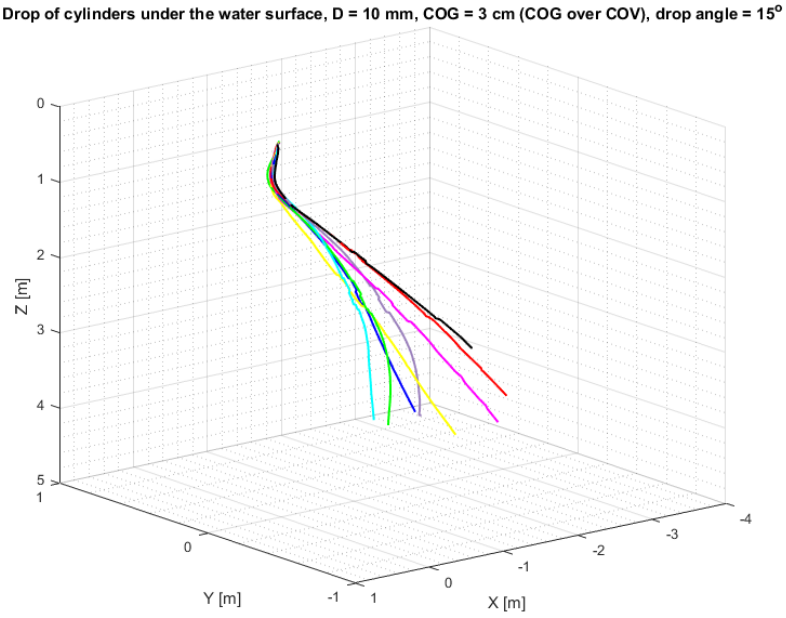

Figure 150: X-Y-Z view: Drop of 10mm diameter cylinders under the water surface at 15° initial angle with COG displaced 3cm (Centre of Gravity (COG) over Centre of Volume (COV)). Each coloured line represents a drop.

A.11.2 30° initial drop angle

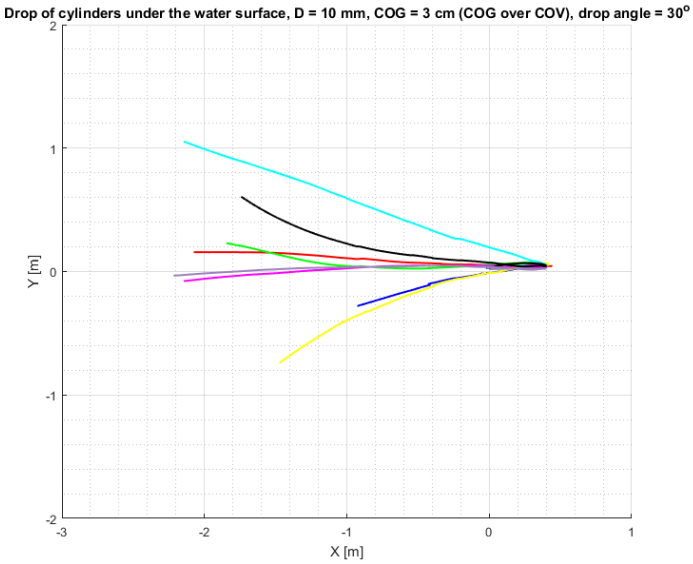

Figure 151: X-Y view: Drop of 10mm diameter cylinders under the water surface at 30° initial angle with COG displaced 3cm (Centre of Gravity (COG) over Centre of Volume (COV)). Each coloured line represents a drop.

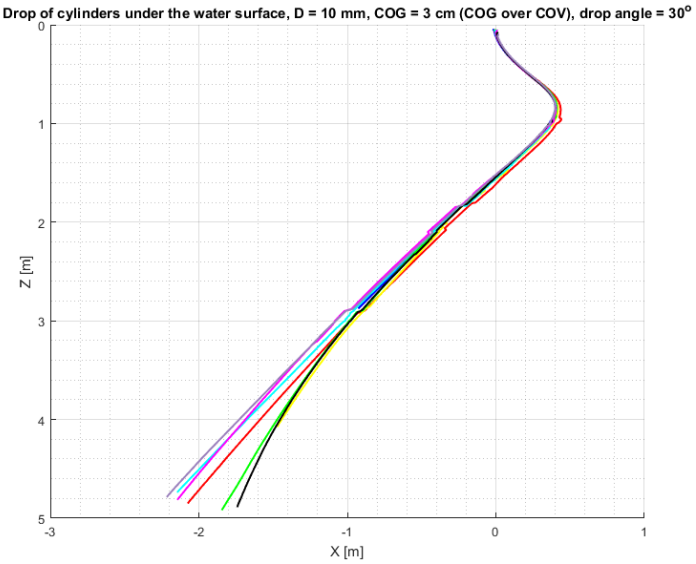

Figure 152: X-Z view: Drop of 10mm diameter cylinders under the water surface at 30° initial angle with COG displaced 3cm (Centre of Gravity (COG) over Centre of Volume (COV)). The X-coordinates are radial coordinates from the XY plane and each coloured line represents a drop.

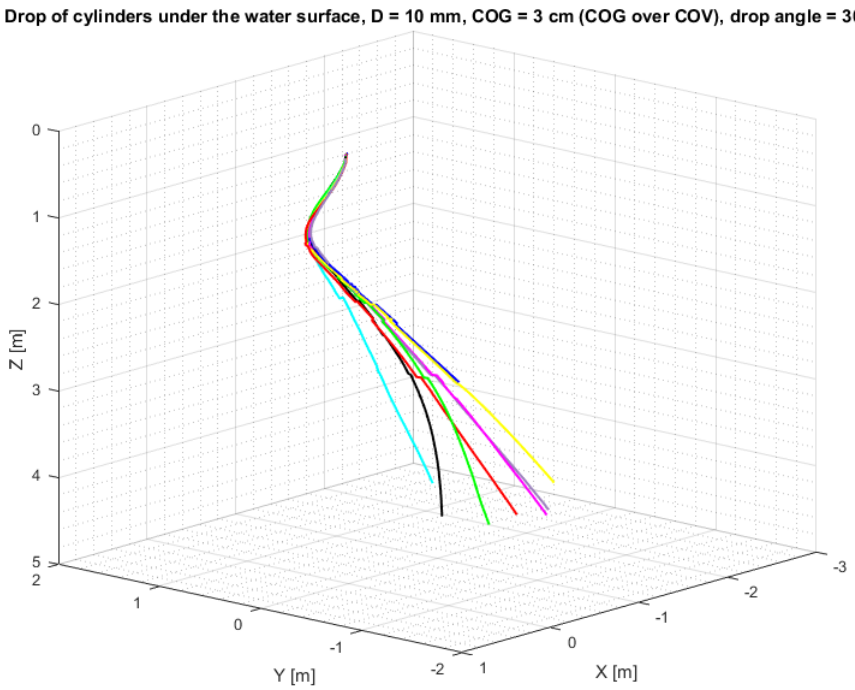

Figure 153: X-Y-Z view: Drop of 10mm diameter cylinders under the water surface at 30° initial angle with COG displaced 3cm (Centre of Gravity (COG) over Centre of Volume (COV)). Each coloured line represents a drop.

A.11.3 45° initial drop angle

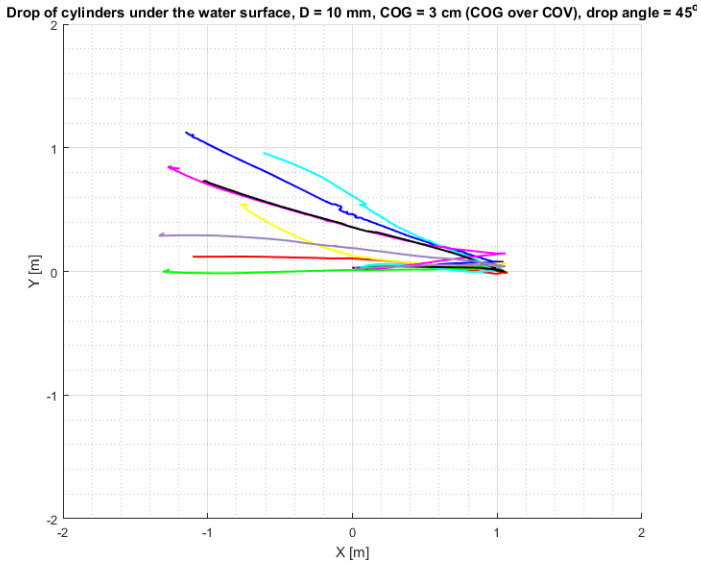

Figure 154: X-Y view: Drop of 10mm diameter cylinders under the water surface at 45° initial angle with COG displaced 3cm (Centre of Gravity (COG) over Centre of Volume (COV)). Each coloured line represents a drop.

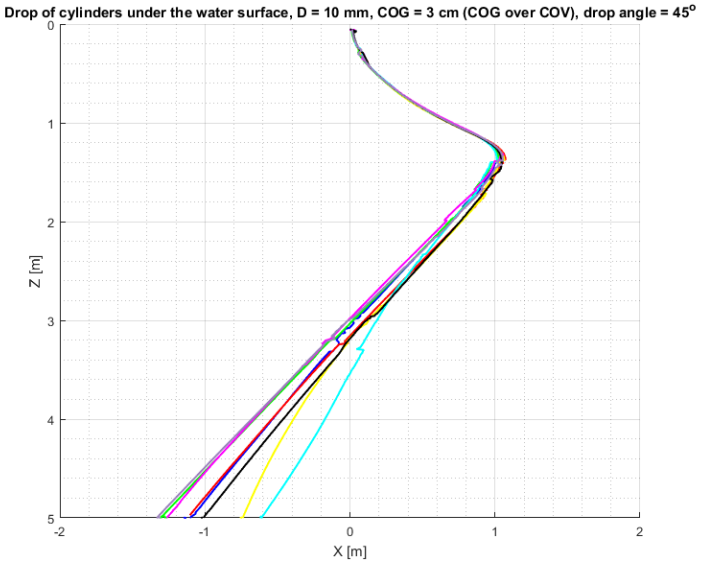

Figure 155: X-Z view: Drop of 10mm diameter cylinders under the water surface at 45° initial angle with COG displaced 3cm (Centre of Gravity (COG) over Centre of Volume (COV)). The X-coordinates are radial coordinates from the XY plane and each coloured line represents a drop.

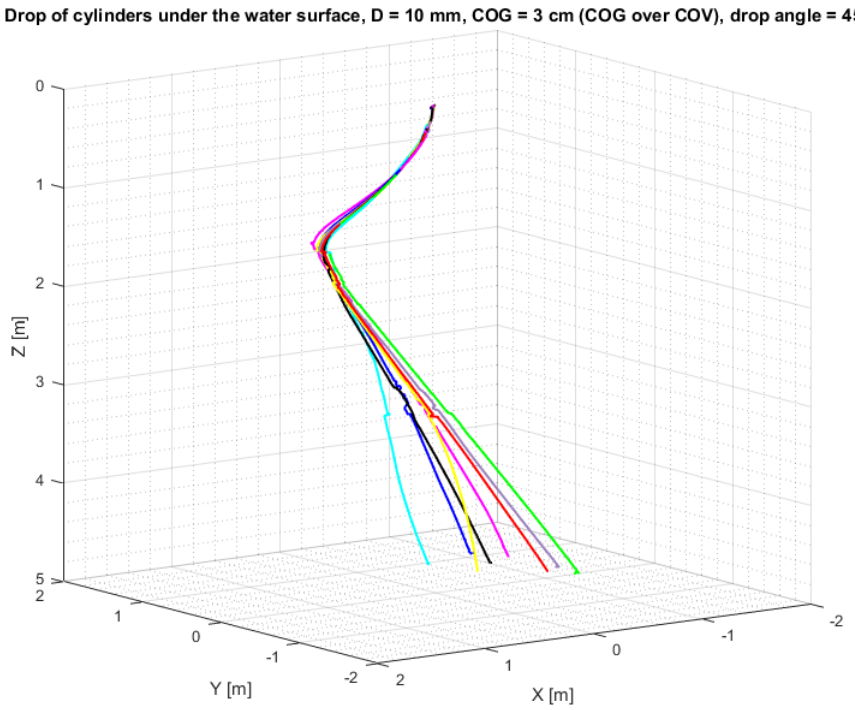

Figure 156: X-Y-Z view: Drop of 10mm diameter cylinders under the water surface at 45° initial angle with COG displaced 3cm (Centre of Gravity (COG) over Centre of Volume (COV)). Each coloured line represents a drop.

A.11.4 60° initial drop angle

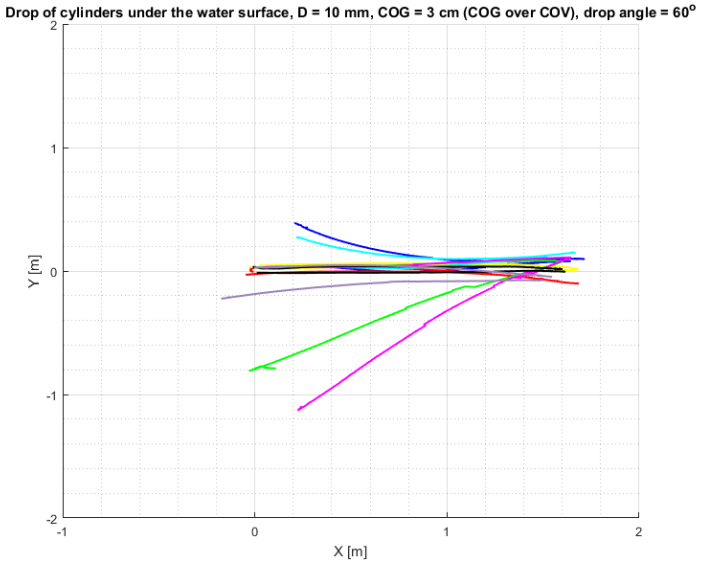

Figure 157: X-Y view: Drop of 10mm diameter cylinders under the water surface at 60° initial angle with COG displaced 3cm (Centre of Gravity (COG) over Centre of Volume (COV)). Each coloured line represents a drop.

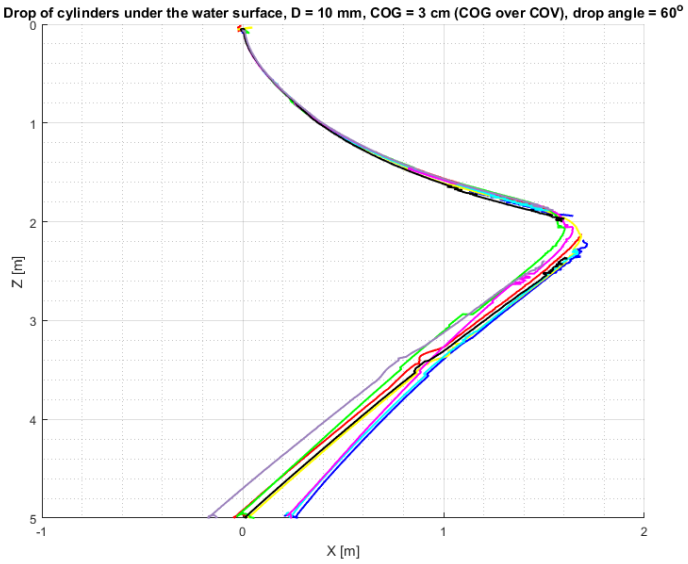

Figure 158: X-Z view: Drop of 10mm diameter cylinders under the water surface at 60° initial angle with COG displaced 3cm (Centre of Gravity (COG) over Centre of Volume (COV)). The X-coordinates are radial coordinates from the XY plane and each coloured line represents a drop.

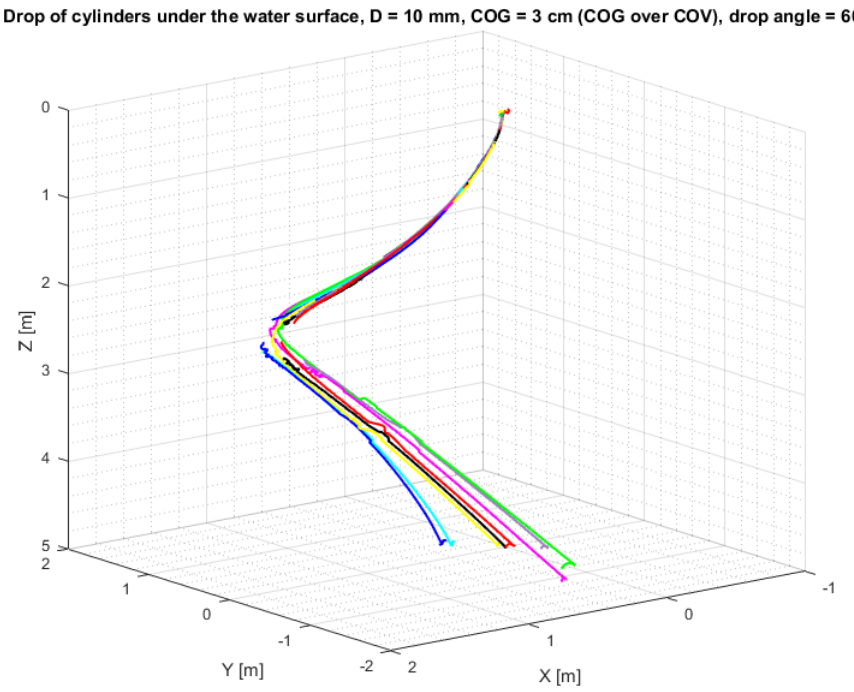

Figure 159: X-Y-Z view: Drop of 10mm diameter cylinders under the water surface at 60° initial angle with COG displaced 3cm (Centre of Gravity (COG) over Centre of Volume (COV)). Each coloured line represents a drop.

A.11.5 75° initial drop angle

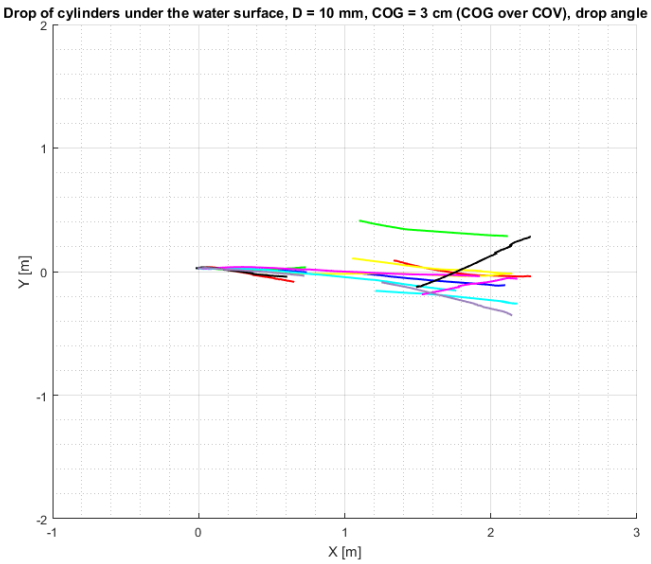

Figure 160: X-Y view: Drop of 10mm diameter cylinders under the water surface at 75° initial angle with COG displaced 3cm (Centre of Gravity (COG) over Centre of Volume (COV)). Each coloured line represents a drop.

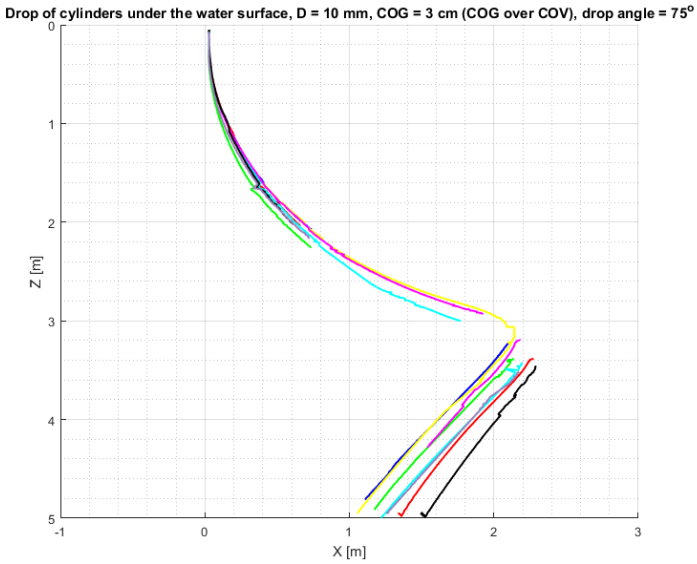

Figure 161: X-Z view: Drop of 10mm diameter cylinders under the water surface at 75° initial angle with COG displaced 3cm (Centre of Gravity (COG) over Centre of Volume (COV)). The X-coordinates are radial coordinates from the XY plane and each coloured line represents a drop.

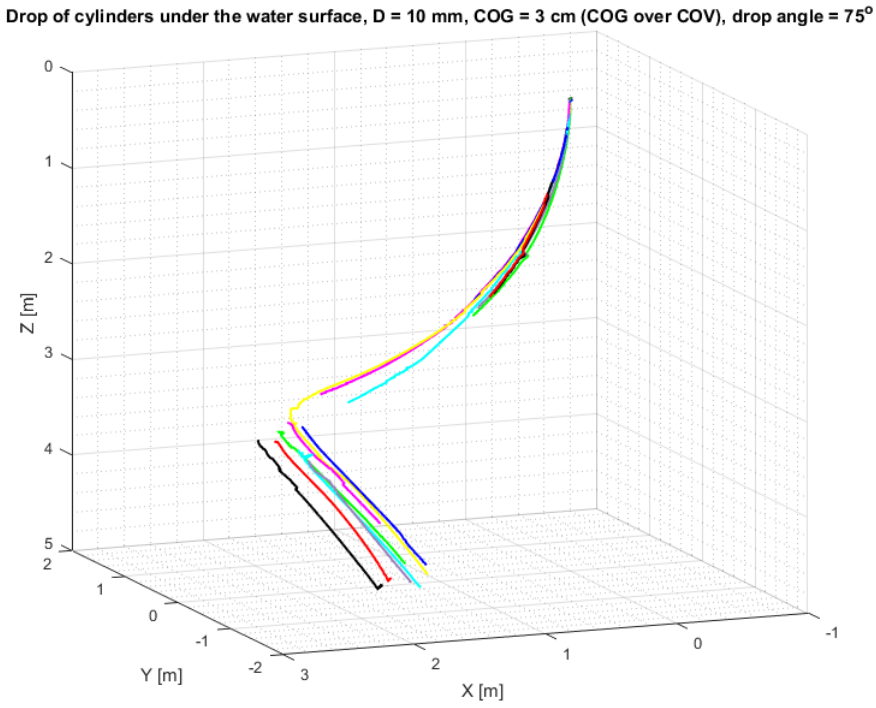

Figure 162: X-Y-Z view: Drop of 10mm diameter cylinders under the water surface at 75° initial angle with COG displaced 3cm (Centre of Gravity (COG) over Centre of Volume (COV)). Each coloured line represents a drop.

A.12 Drop of 10mm diameter cylinders under the water surface with COG placed with 3cm (COG under COV)

A.12.1 15° initial drop angle

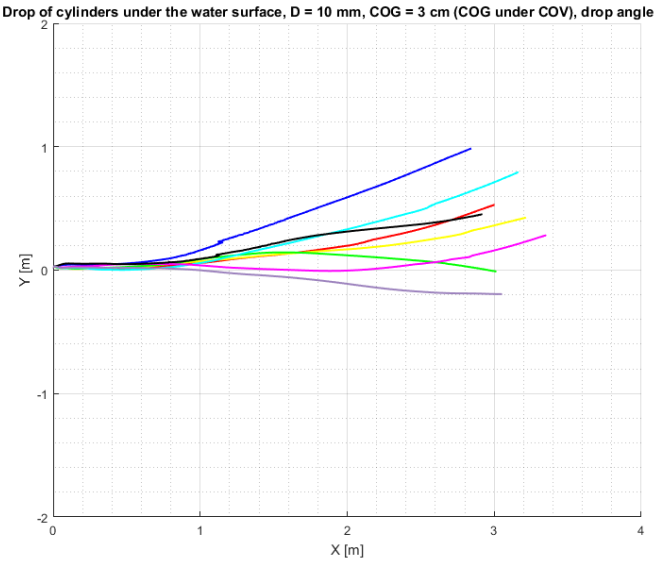

Figure 163: X-Y view: Drop of 10mm diameter cylinders under the water surface at 15° initial angle with COG displaced 3cm (Centre of Gravity (COG) under Centre of Volume (COV)). Each coloured line represents a drop.

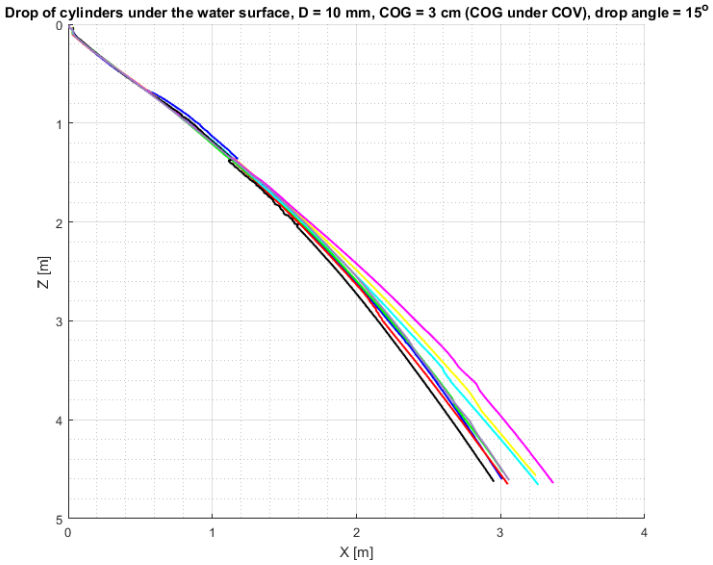

Figure 164: X-Z view: Drop of 10mm diameter cylinders under the water surface at 15° initial angle with COG displaced 3cm (Centre of Gravity (COG) under Centre of Volume (COV)). The X-coordinates are radial coordinates from the XY plane and each coloured line represents a drop.

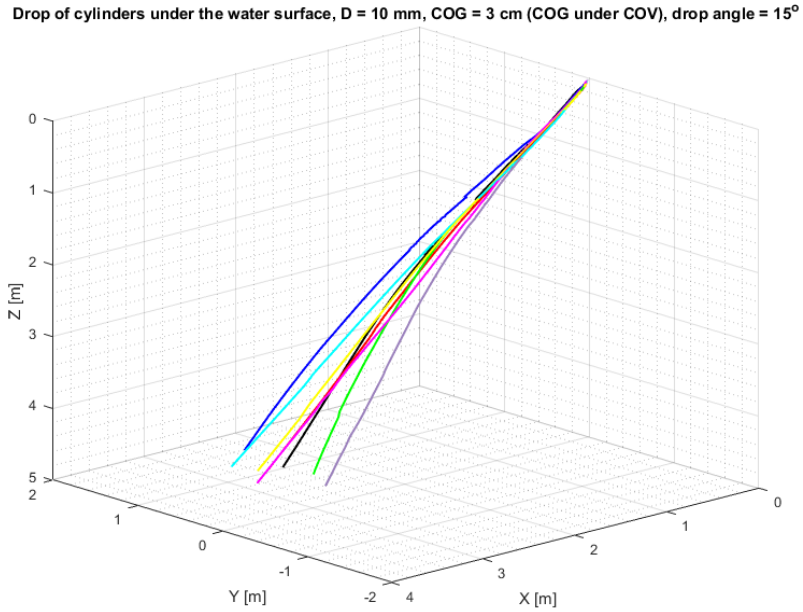

Figure 165: X-Y-Z view: Drop of 10mm diameter cylinders under the water surface at 15° initial angle with COG displaced 3cm (Centre of Gravity (COG) under Centre of Volume (COV)). Each coloured line represents a drop.

A.12.2 30° initial drop angle

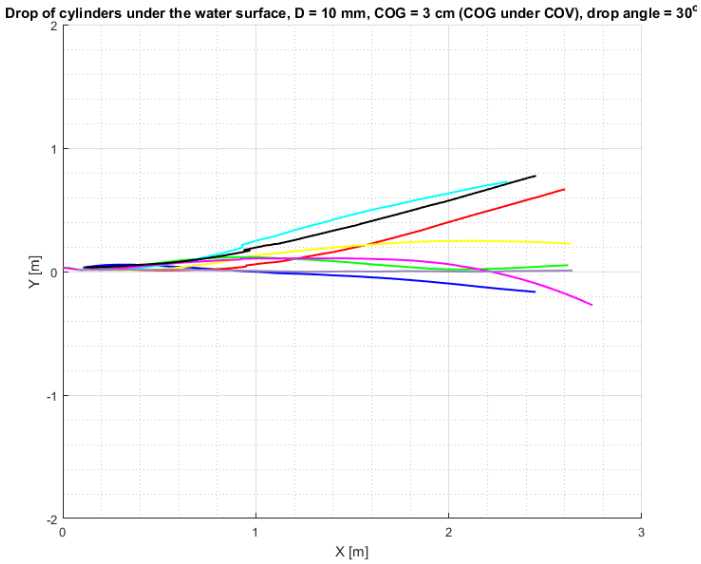

Figure 166: X-Y view: Drop of 10mm diameter cylinders under the water surface at 30° initial angle with COG displaced 3cm (Centre of Gravity (COG) under Centre of Volume (COV)). Each coloured line represents a drop.

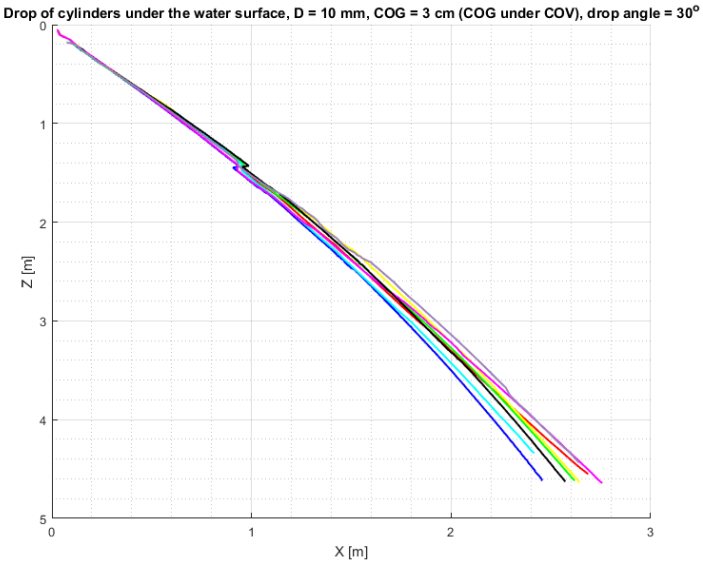

Figure 167: X-Z view: Drop of 10mm diameter cylinders under the water surface at 30° initial angle with COG displaced 3cm (Centre of Gravity (COG) under Centre of Volume (COV)). The X-coordinates are radial coordinates from the XY plane and each coloured line represents a drop.

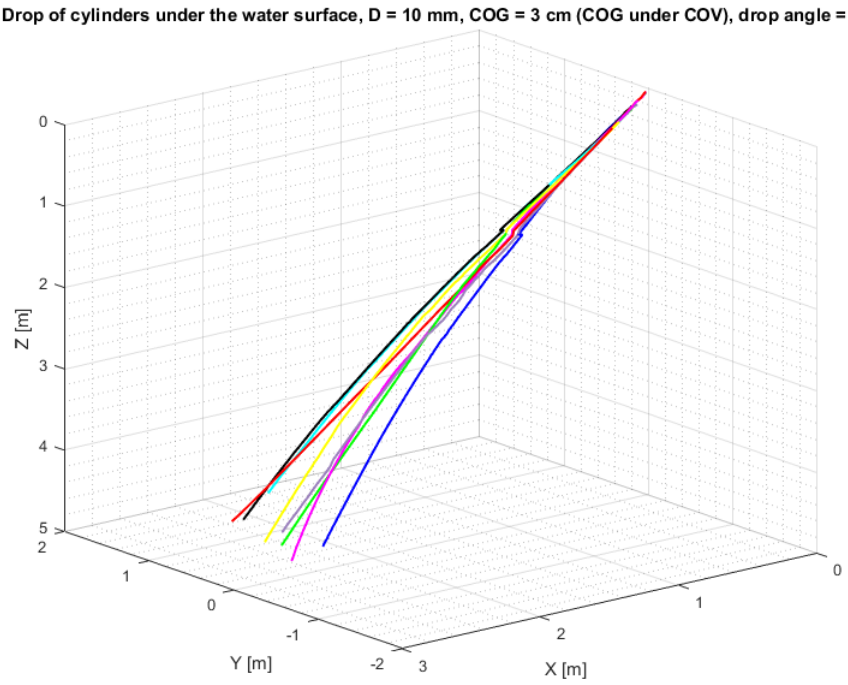

Figure 168: X-Y-Z view: Drop of 10mm diameter cylinders under the water surface at 30° initial angle with COG displaced 3cm (Centre of Gravity (COG) under Centre of Volume (COV)). Each coloured line represents a drop.

A.12.3 45° initial drop angle

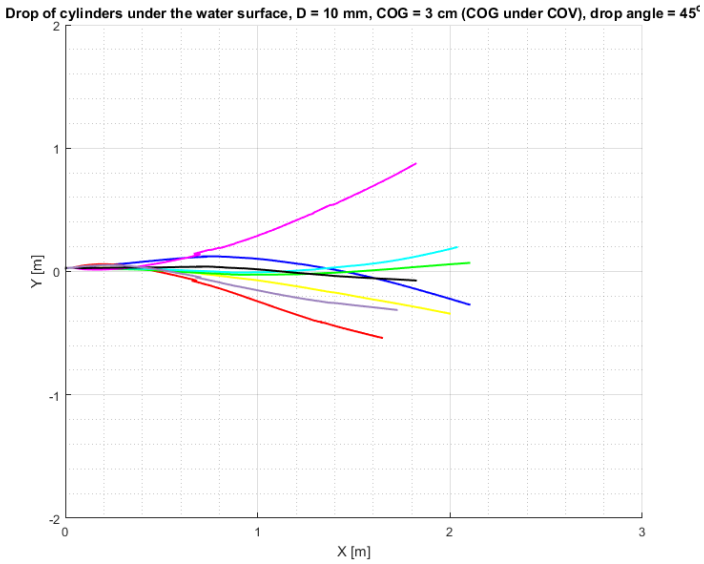

Figure 169: X-Y view: Drop of 10mm diameter cylinders under the water surface at 45° initial angle with COG displaced 3cm (Centre of Gravity (COG) under Centre of Volume (COV)). Each coloured line represents a drop.

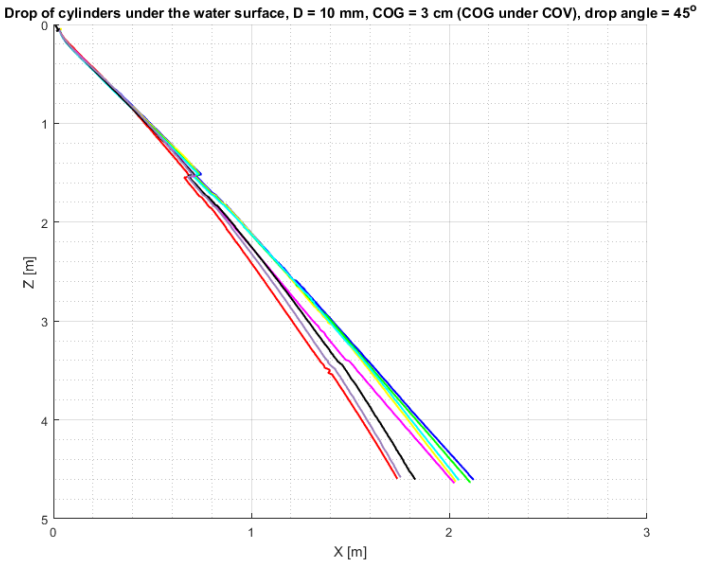

Figure 170: X-Z view: Drop of 10mm diameter cylinders under the water surface at 45° initial angle with COG displaced 3cm (Centre of Gravity (COG) under Centre of Volume (COV)). The X-coordinates are radial coordinates from the XY plane and each coloured line represents a drop.

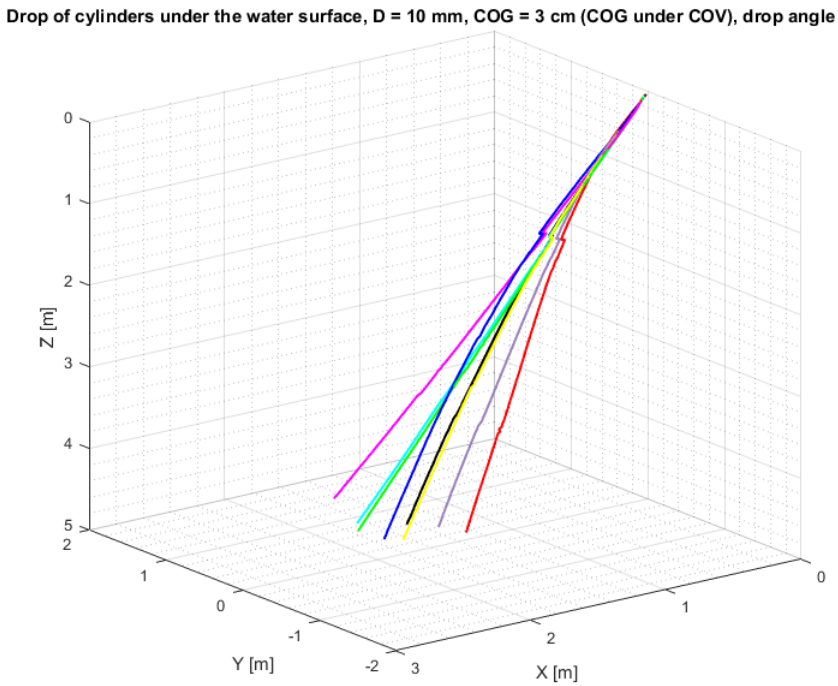

Figure 171: X-Y-Z view: Drop of 10mm diameter cylinders under the water surface at 45° initial angle with COG displaced 3cm (Centre of Gravity (COG) under Centre of Volume (COV)). Each coloured line represents a drop.

A.12.4 60° initial drop angle

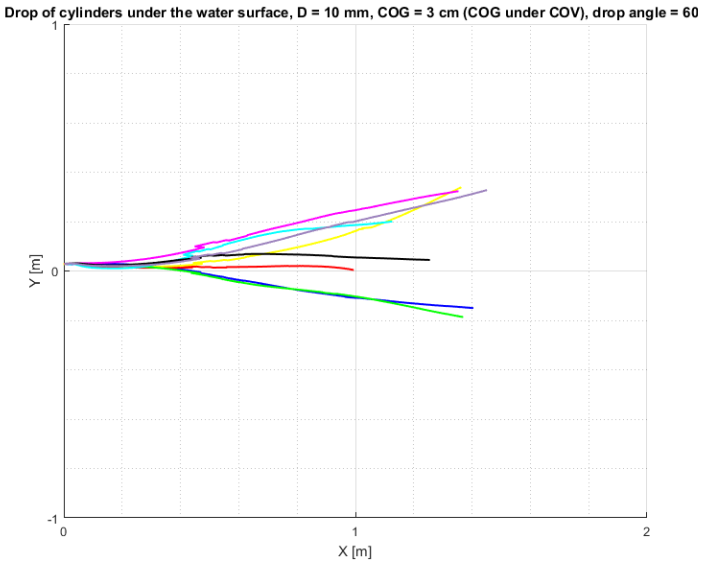

Figure 172: X-Y view: Drop of 10mm diameter cylinders under the water surface at 60° initial angle with COG displaced 3cm (Centre of Gravity (COG) under Centre of Volume (COV)). Each coloured line represents a drop.

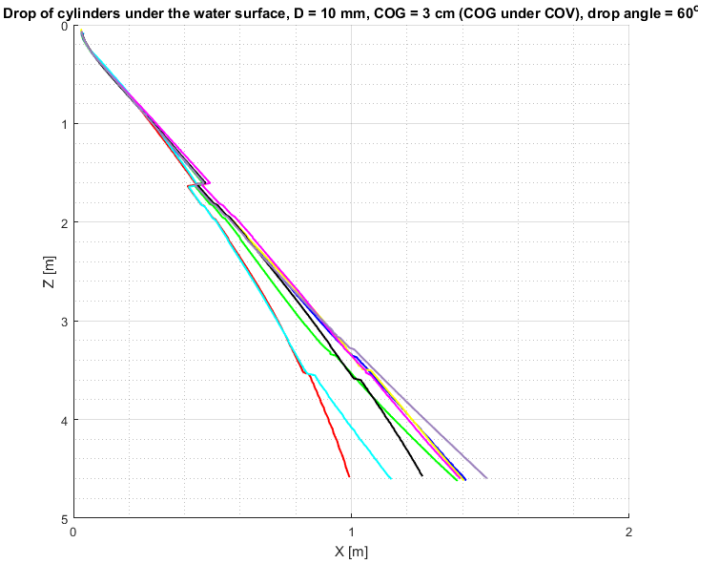

Figure 173: X-Z view: Drop of 10mm diameter cylinders under the water surface at 60° initial angle with COG displaced 3cm (Centre of Gravity (COG) under Centre of Volume (COV)). The X-coordinates are radial coordinates from the XY plane and each coloured line represents a drop.

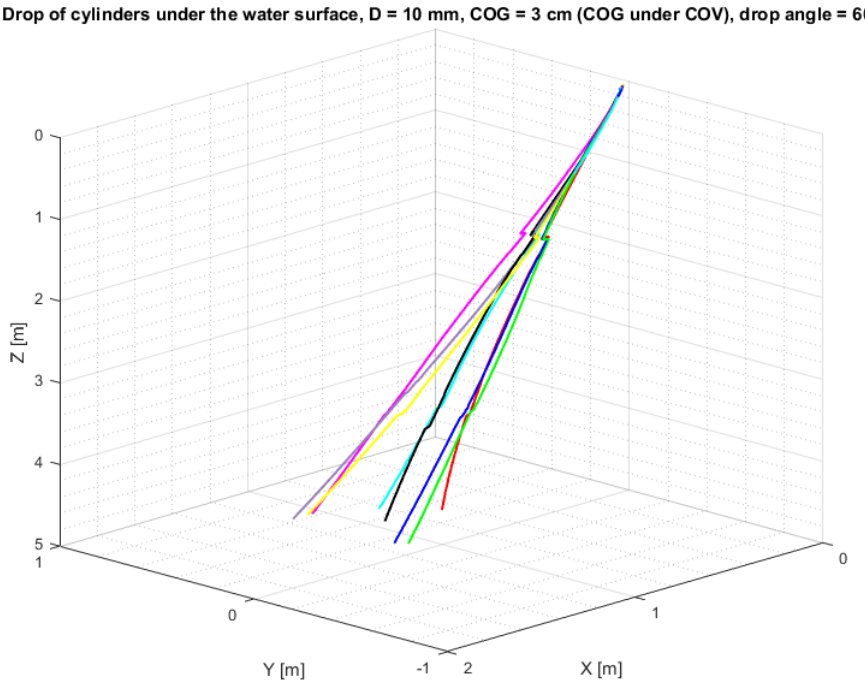

Figure 174: X-Y-Z view: Drop of 10mm diameter cylinders under the water surface at 60° initial angle with COG displaced 3cm (Centre of Gravity (COG) under Centre of Volume (COV)). Each coloured line represents a drop.

A.12.5 75° initial drop angle

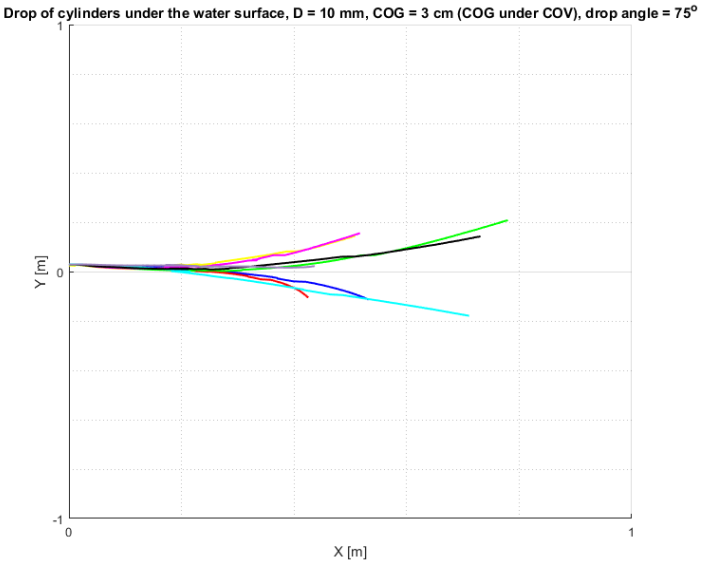

Figure 175: X-Y view: Drop of 10mm diameter cylinders under the water surface at 75° initial angle with COG displaced 3cm (Centre of Gravity (COG) under Centre of Volume (COV)). Each coloured line represents a drop.

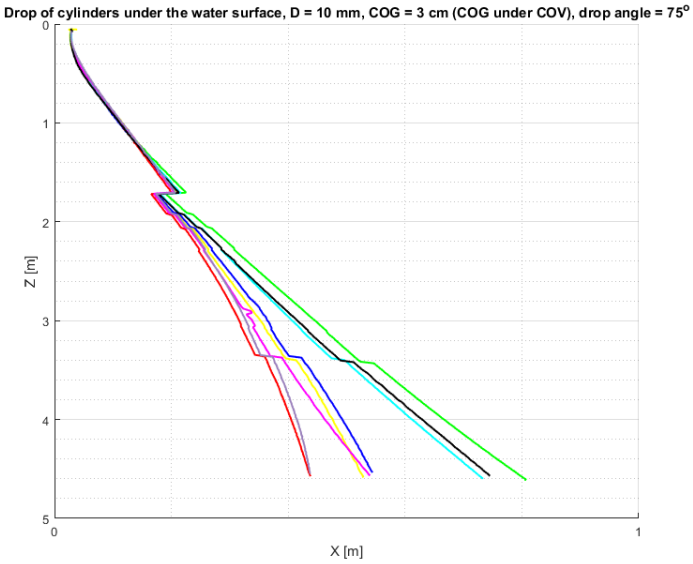

Figure 176: X-Z view: Drop of 10mm diameter cylinders under the water surface at 75° initial angle with COG displaced 3cm (Centre of Gravity (COG) under Centre of Volume (COV)). The X-coordinates are radial coordinates from the XY plane and each coloured line represents a drop.

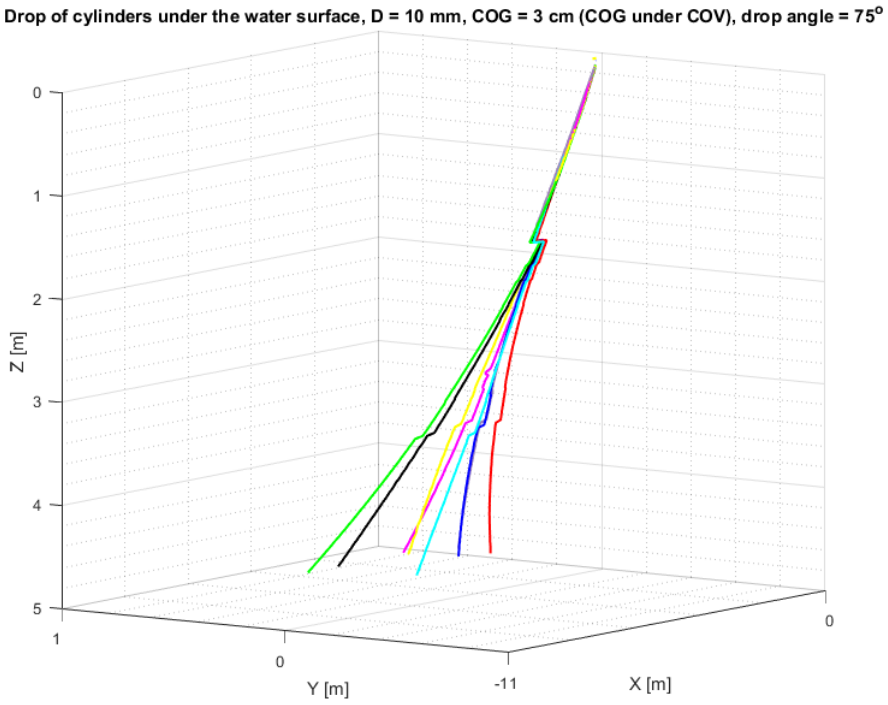

Figure 177: X-Y-Z view: Drop of 10mm diameter cylinders under the water surface at 75° initial angle with COG displaced 3cm (Centre of Gravity (COG) under Centre of Volume (COV)). Each coloured line represents a drop.

B Velocity plots

B.1 Velocity of 10 mm cylinder dropped from under the water surface

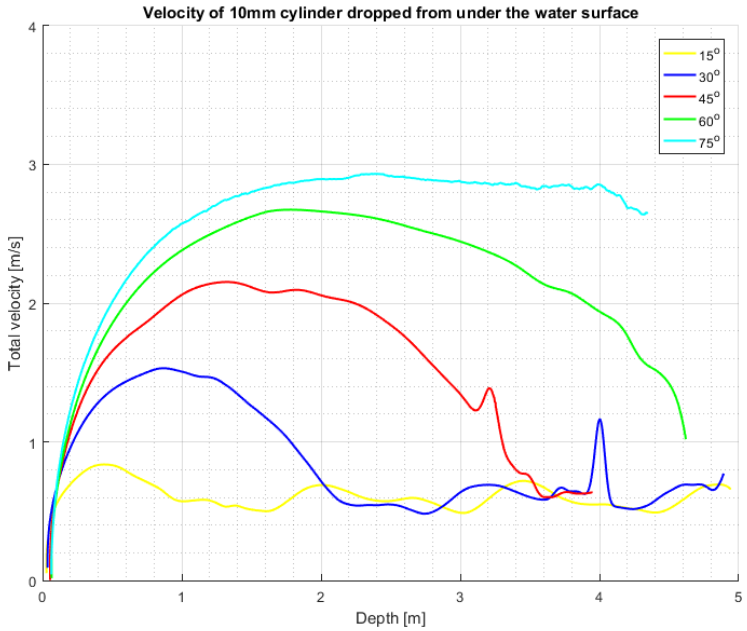

Figure 178: Total velocity compared to depth for closed 10 mm cylinders. The cylinders are dropped under the surface with initial drop angles of 15^o, 30^o, 45^o, 60^o and 75^o. Each plot line represent an example of the total velocity development.

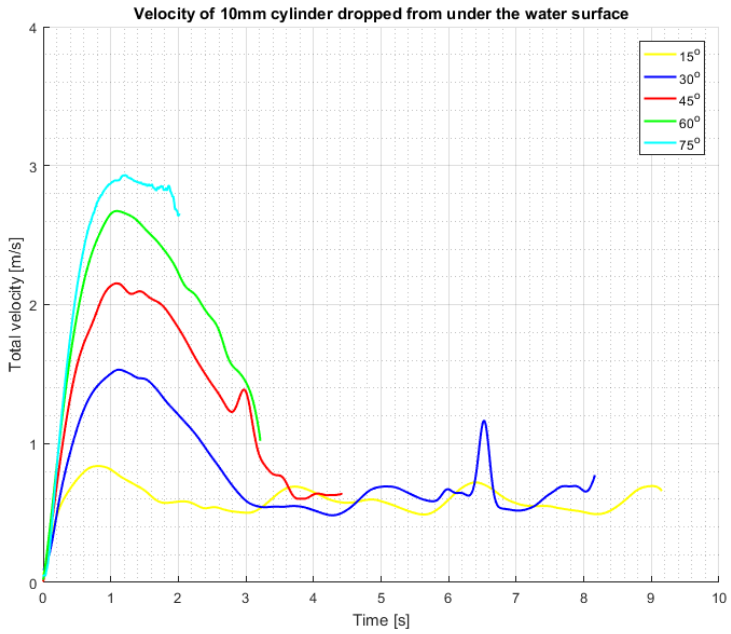

Figure 179: Total velocity compared to time for closed 10 mm cylinders. The cylinders are dropped under the surface with initial drop angles of 15^o, 30^o, 45^o, 60^o and 75^o. Each plot line represent an example of the total velocity development.

B.2 Velocity of 16 mm cylinder dropped from under the water surface

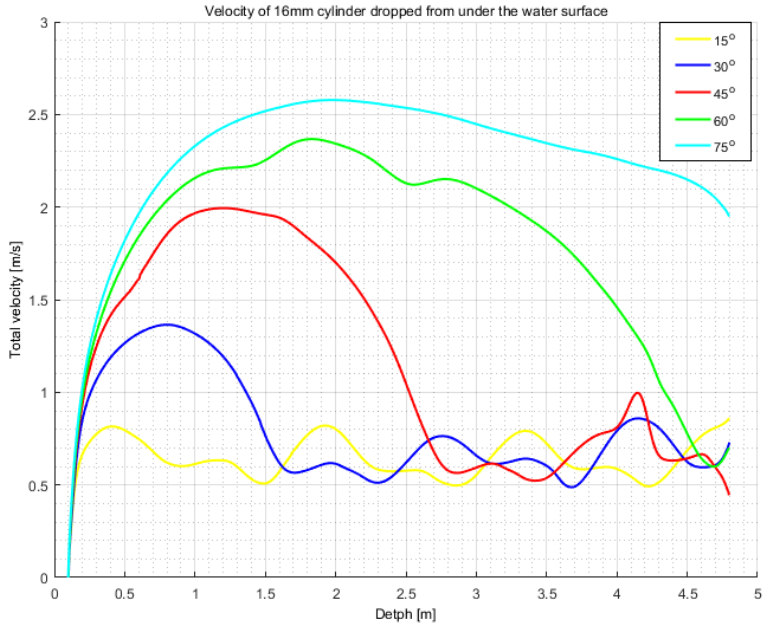

Figure 180: Total velocity compared to depth for closed 16 mm cylinders. The cylinders are dropped under the surface with initial drop angles of 15^o, 30^o, 45^o, 60^o and 75^o. Each plot line represent an example of the total velocity development.

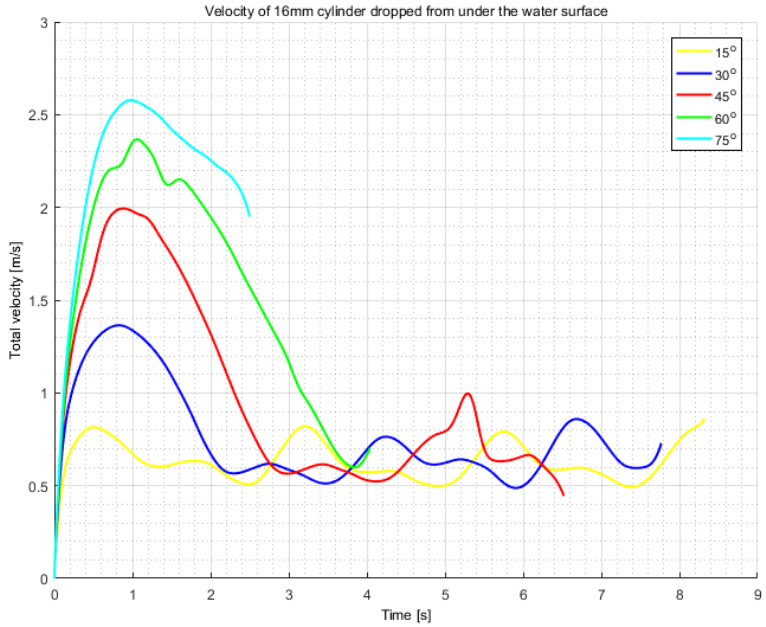

Figure 181: Total velocity compared to time for closed 16 mm cylinders. The cylinders are dropped under the surface with initial drop angles of 15^o, 30^o, 45^o, 60^o and 75^o. Each plot line represent an example of the total velocity development.

B.3 Velocity of 19 mm cylinder dropped from under the water surface

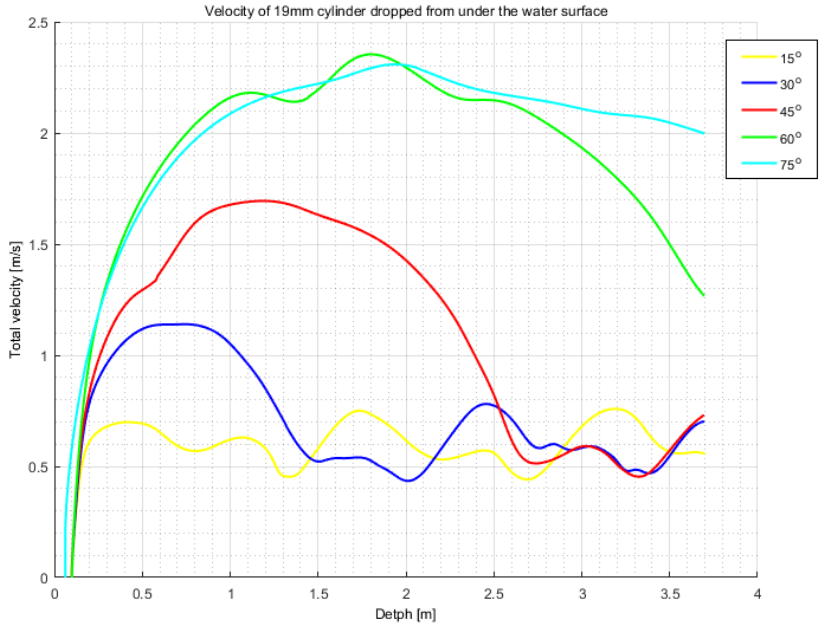

Figure 182: Total velocity compared to depth for closed 19 mm cylinders. The cylinders are dropped under the surface with initial drop angles of 15^o, 30^o, 45^o, 60^o and 75^o. Each plot line represent an example of the total velocity development.

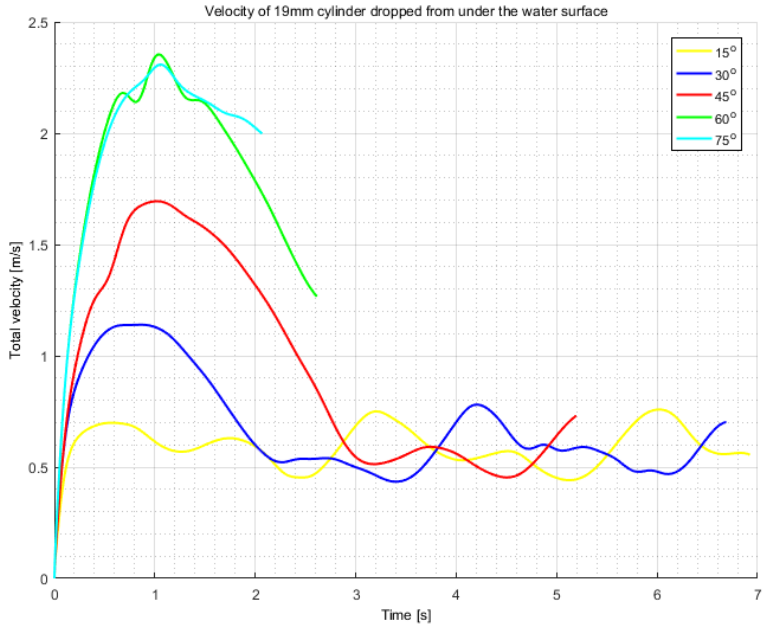

Figure 183: Total velocity compared to time for closed 19 mm cylinders. The cylinders are dropped under the surface with initial drop angles of 15^o, 30^o, 45^o, 60^o and 75^o. Each plot line represent an example of the total velocity development.

B.4 Velocity of 10 mm cylinder dropped from above the water surface

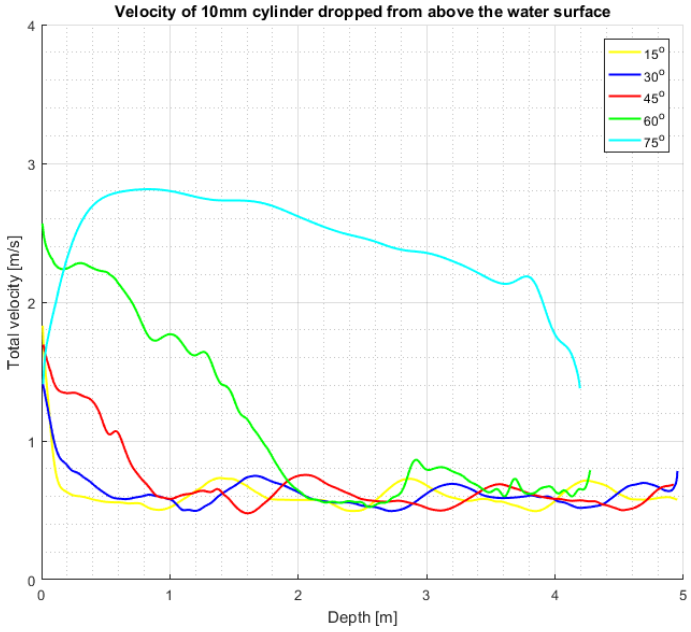

Figure 184: Total velocity compared to depth for closed 10 mm cylinders. The cylinders are dropped above the surface with initial drop angles of 15^o, 30^o, 45^o, 60^o and 75^o. Each plot line represent an example of the total velocity development.

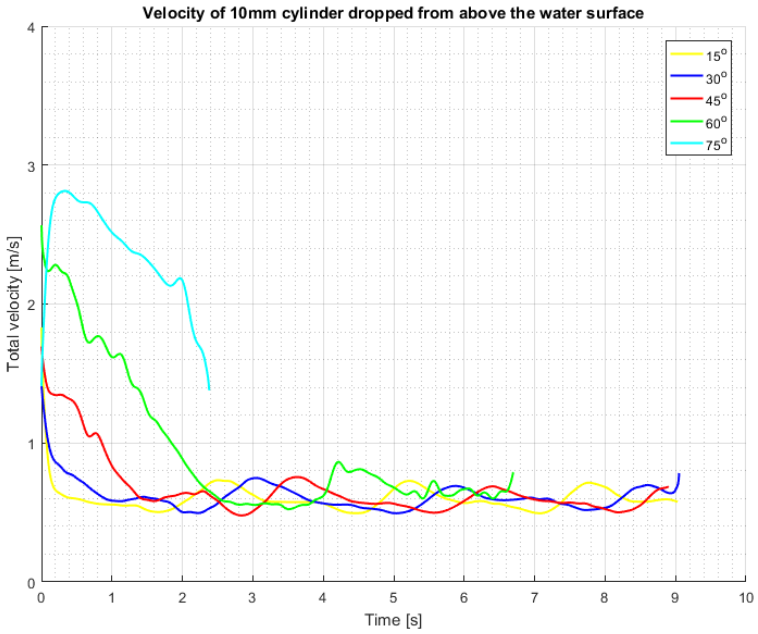

Figure 185: Total velocity compared to time for closed 10 mm cylinders. The cylinders are dropped above the surface with initial drop angles of 15^o, 30^o, 45^o, 60^o and 75^o. Each plot line represent an example of the total velocity development.

B.5 Velocity of 16 mm cylinder dropped from above the water surface

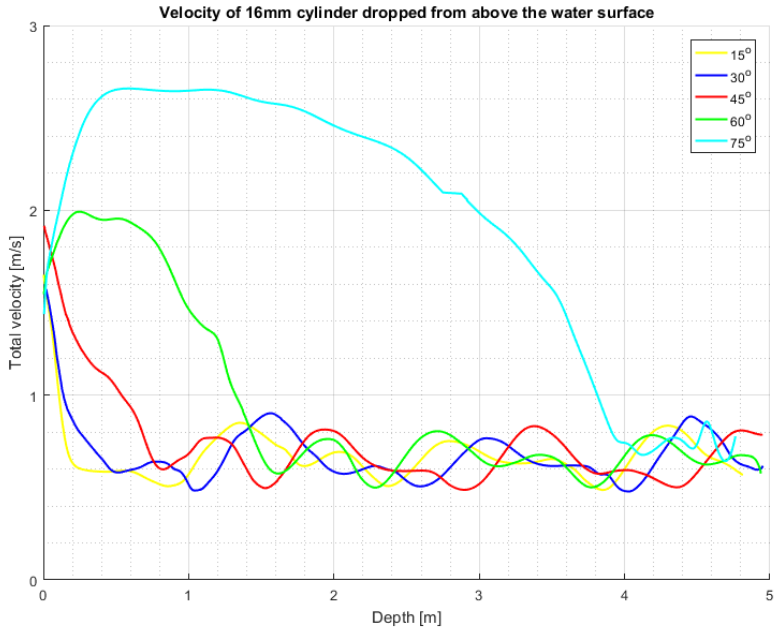

Figure 186: Total velocity compared to depth for closed 16 mm cylinders. The cylinders are dropped above the surface with initial drop angles of 15^o, 30^o, 45^o, 60^o and 75^o. Each plot line represent an example of the total velocity development.

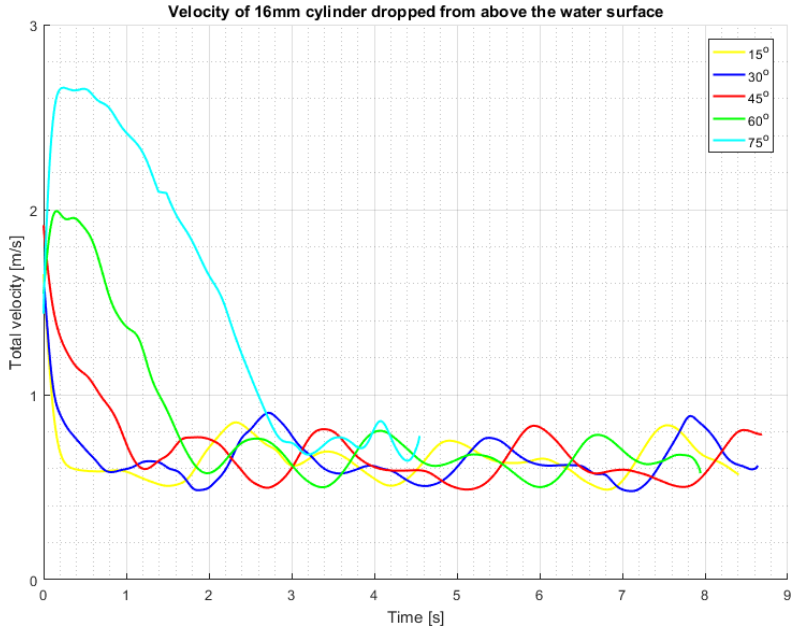

Figure 187: Total velocity compared to time for closed 16 mm cylinders. The cylinders are dropped above the surface with initial drop angles of 15^o, 30^o, 45^o, 60^o and 75^o. Each plot line represent an example of the total velocity development.

B.6 Velocity of 19 mm cylinder dropped from above the water surface

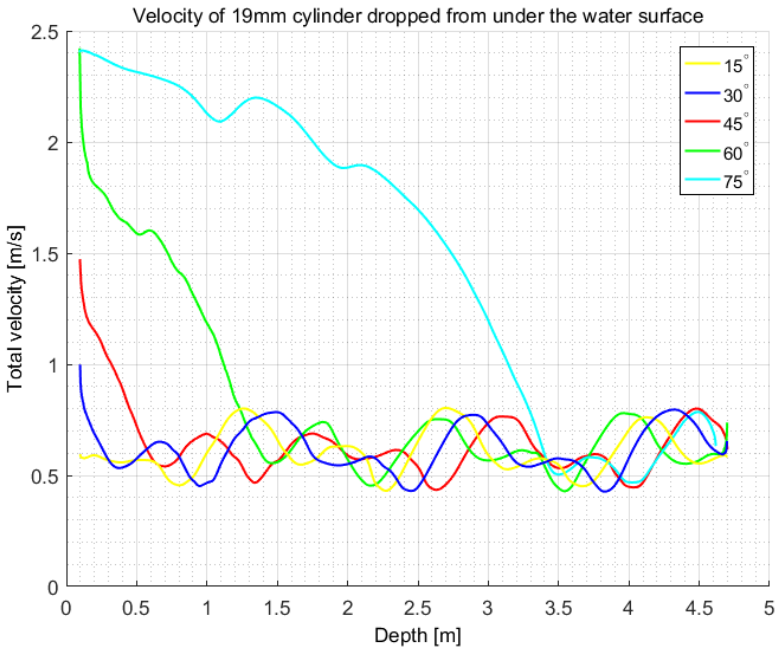

Figure 188: Total velocity compared to depth for closed 19 mm cylinders. The cylinders are dropped above the surface with initial drop angles of 15^o, 30^o, 45^o, 60^o and 75^o. Each plot line represent an example of the total velocity development.

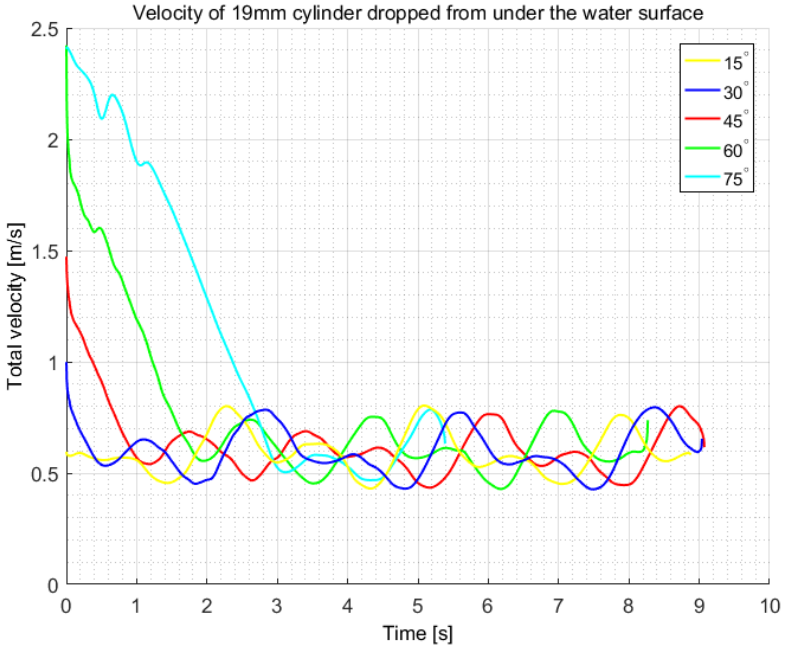

Figure 189: Total velocity compared to time for closed 19 mm cylinders. The cylinders are dropped above the surface with initial drop angles of 15^o, 30^o, 45^o, 60^o and 75^o. Each plot line represent an example of the total velocity development.

B.7 Velocity of open 10 mm cylinders dropped from under the water surface

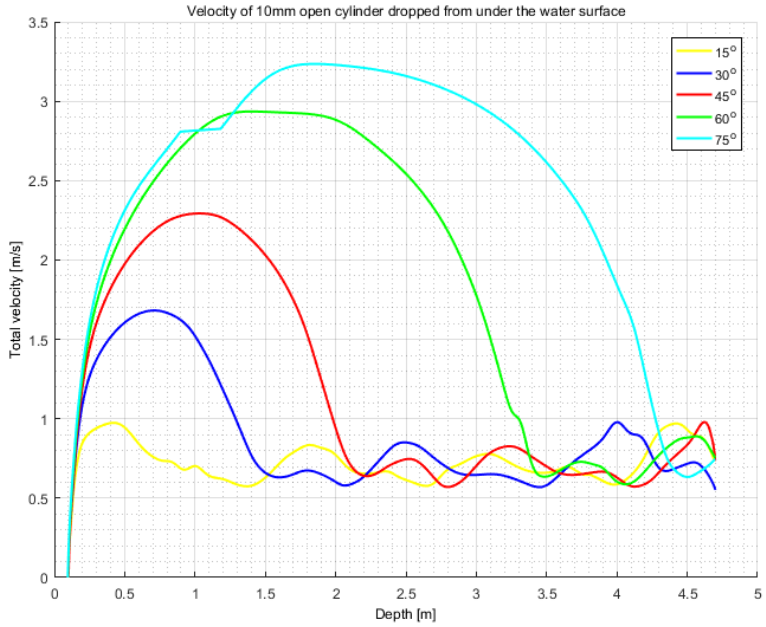

Figure 190: Total velocity compared to depth for open 10 mm cylinders. The cylinders are dropped under the surface with initial drop angles of 15^o, 30^o, 45^o, 60^o and 75^o. Each plot line represent an example of the total velocity development.

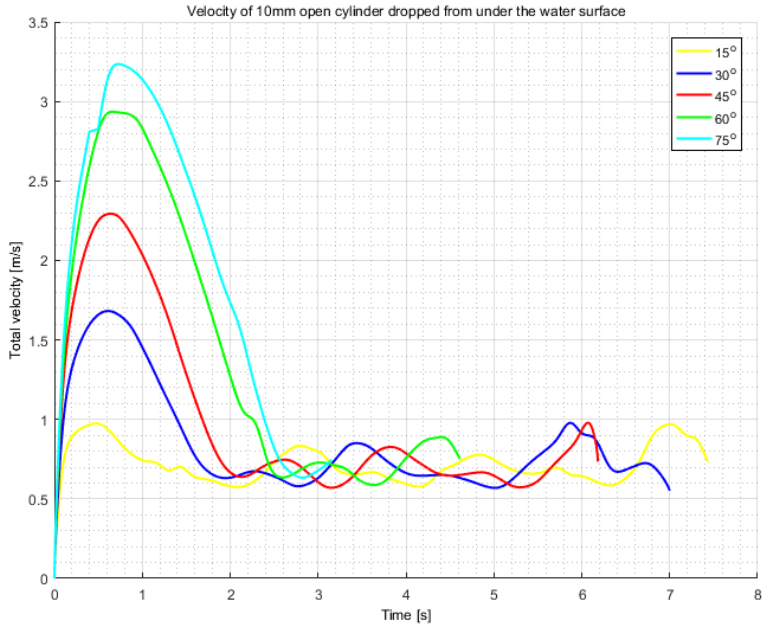

Figure 191: Total velocity compared to time for open 10 mm cylinders. The cylinders are dropped under the surface with initial drop angles of 15^o, 30^o, 45^o, 60^o and 75^o. Each plot line represent an example of the total velocity development.

B.8 Velocity of open 19 mm cylinders dropped from under the water surface

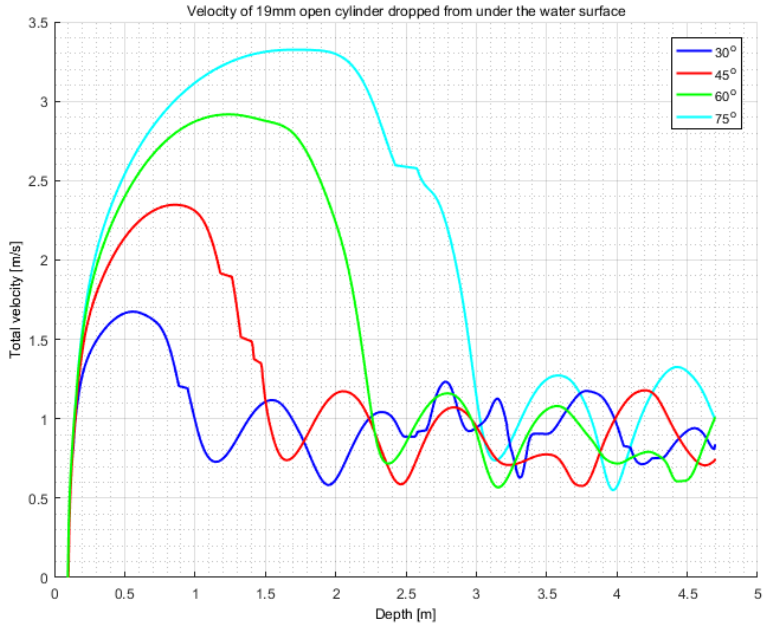

Figure 192: Total velocity compared to depth for open 19 mm cylinders. The cylinders are dropped under the surface with initial drop angles of 30^o, 45^o, 60^o and 75^o. Each plot line represent an example of the total velocity development.

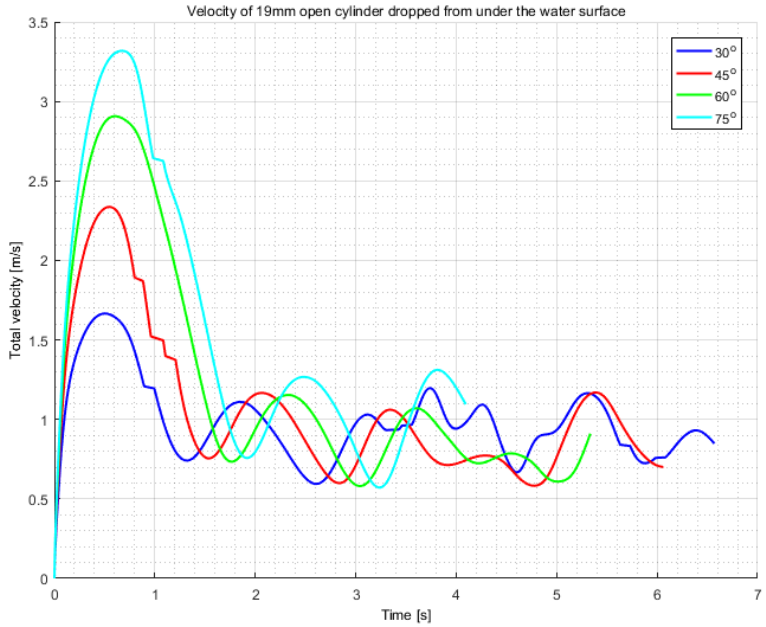

Figure 193: Total velocity compared to time for open 19 mm cylinders. The cylinders are dropped under the surface with initial drop angles of 30^o, 45^o, 60^o and 75^o. Each plot line represent an example of the total velocity development.

B.9 Velocity of 10 mm cylinder dropped from under the water surface with COG displaced 1.4 cm (COG above COV)

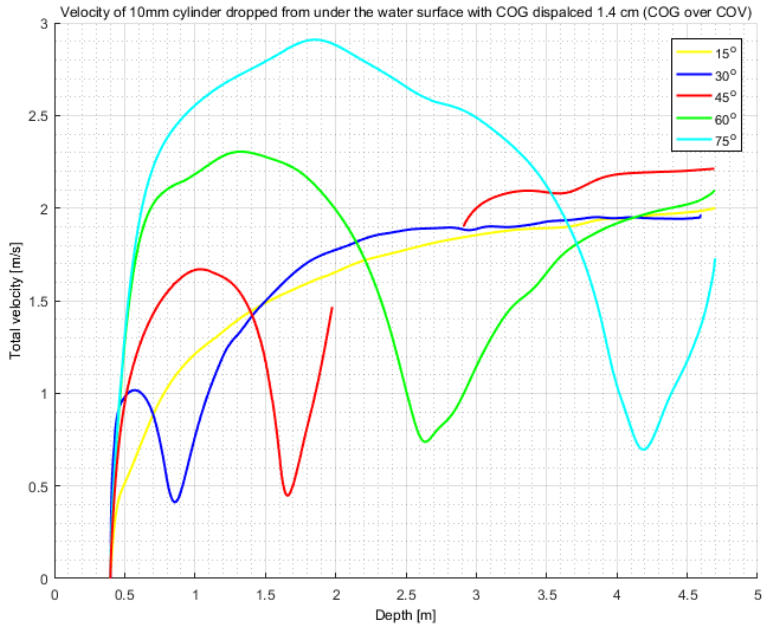

Figure 194: Total velocity compared to depth for cylinders with COG displaced 1.4 cm (Centre of Gravity (COG) over Centre of Volume (COV)). The cylinders are dropped under the surface with initial drop angles of 15^o, 30^o, 45^o, 60^o and 75^o. Each plot line represent an example of the total velocity development.

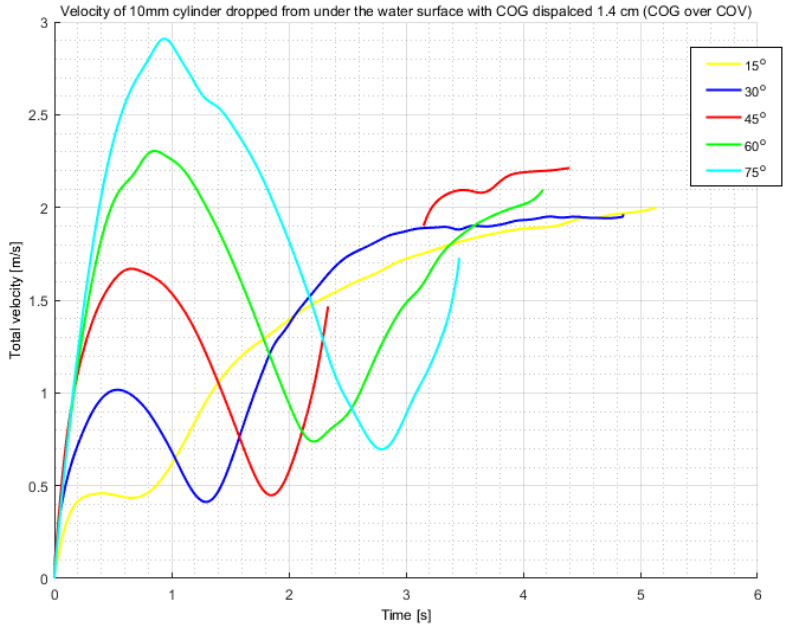

Figure 195: Total velocity compared to time for cylinders with COG 1.4 (Centre of Gravity (COG) over Centre of Volume (COV)). The cylinders are dropped under the surface with initial drop angles of 15^o, 30^o, 45^o, 60^o and 75^o. Each plot line represent an example of the total velocity development.

B.10 Velocity of 10 mm cylinder dropped from under the water surface with COG displaced 1.4 cm (COG under COV)

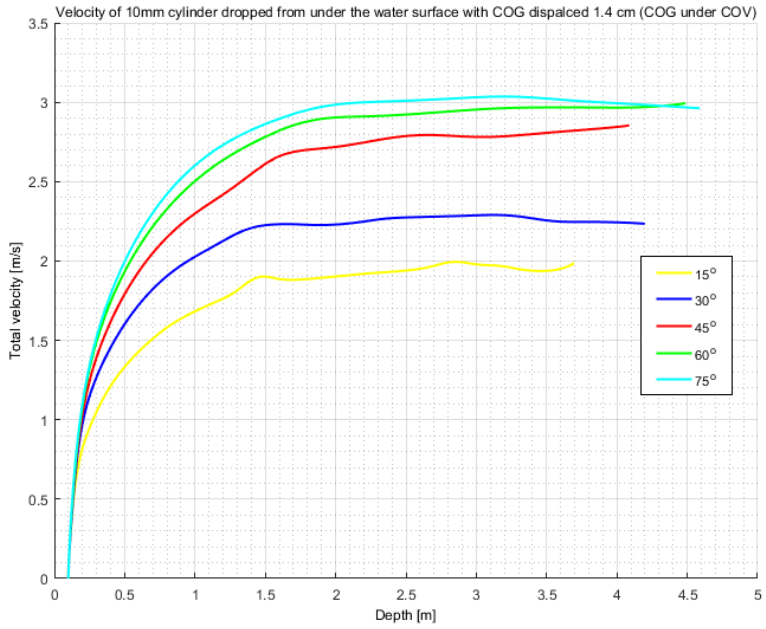

Figure 196: Total velocity compared to depth for cylinders with COG 1.4 cm (Centre of Gravity (COG) under Centre of Volume (COV)). The cylinders are dropped under the surface with initial drop angles of 15^o, 30^o, 45^o, 60^o and 75^o. Each plot line represent an example of the total velocity development.

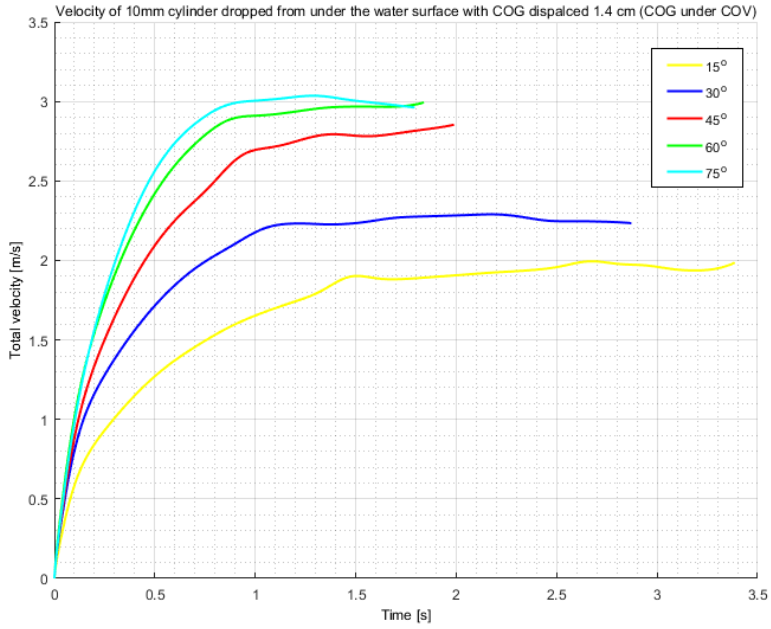

Figure 197: Total velocity compared to time for cylinders with COG 1.4 cm (Centre of Gravity (COG) under Centre of Volume (COV)). The cylinders are dropped under the surface with initial drop angles of 15^o, 30^o, 45^o, 60^o and 75^o. Each plot line represent an example of the total velocity development.

B.11 Velocity of 10 mm cylinder dropped from under the water surface with COG displaced with 3 cm (COG above COV)

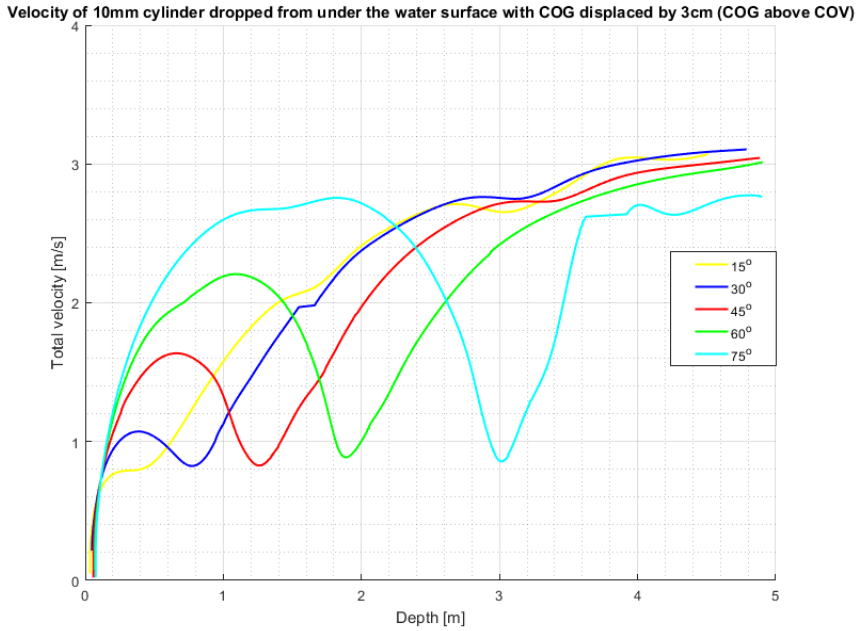

Figure 198: Total velocity compared to depth for cylinders with COG 3 cm (Centre of Gravity (COG) over Centre of Volume (COV)). The cylinders are dropped under the surface with initial drop angles of 15^o, 30^o, 45^o, 60^o and 75^o. Each plot line represent an example of the total velocity development.

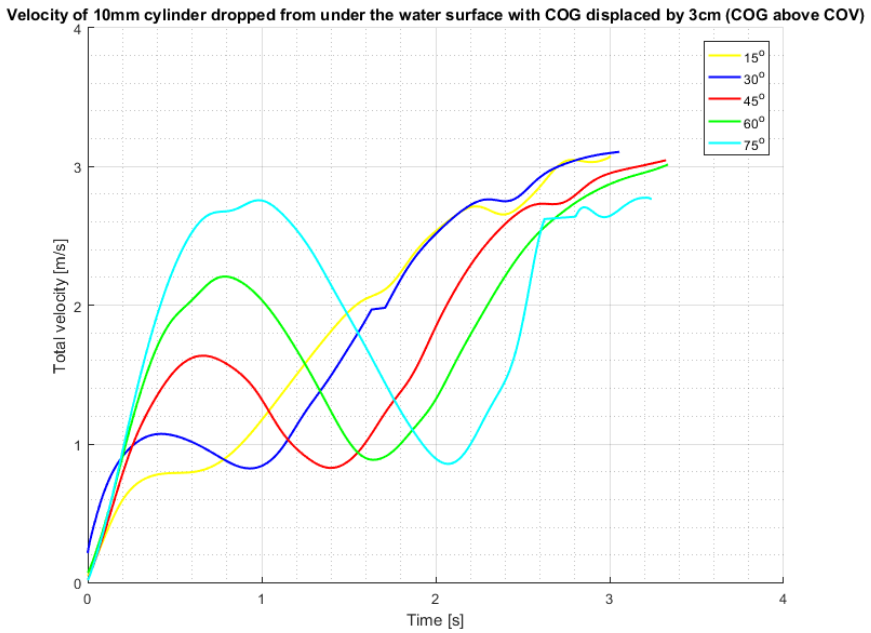

Figure 199: Total velocity compared to time for cylinders with COG 3 cm (Centre of Gravity (COG) over Centre of Volume (COV)). The cylinders are dropped under the surface with initial drop angles of 15^o, 30^o, 45^o, 60^o and 75^o. Each plot line represent an example of the total velocity development.

B.12 Velocity of 10 mm cylinder dropped from under the water surface with COG displaced with 3 cm (COG under COV)

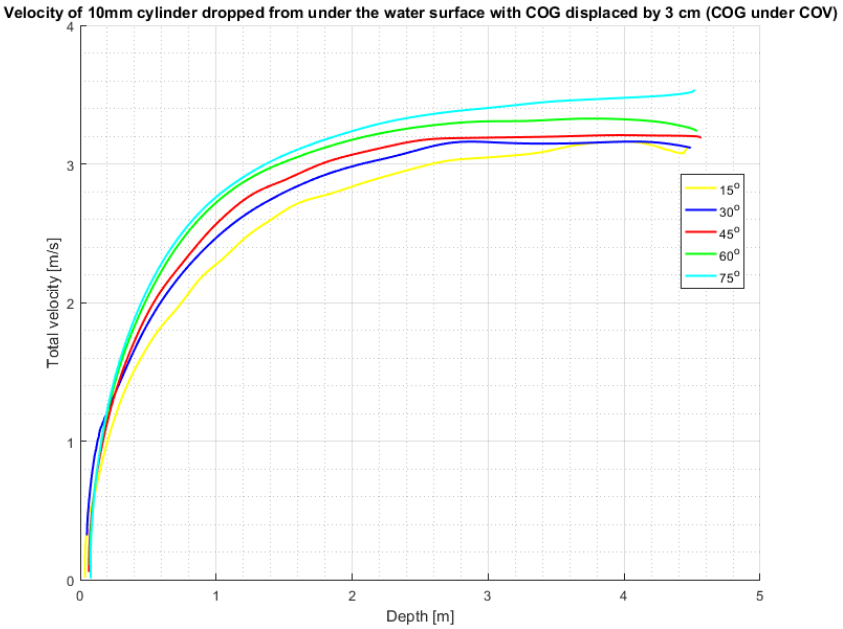

Figure 200: Total velocity compared to depth for cylinders with COG 3 cm (Centre of Gravity (COG) under Centre of Volume (COV)). The cylinders are dropped under the surface with initial drop angles of 15^o, 30^o, 45^o, 60^o and 75^o. Each plot line represent an example of the total velocity development.

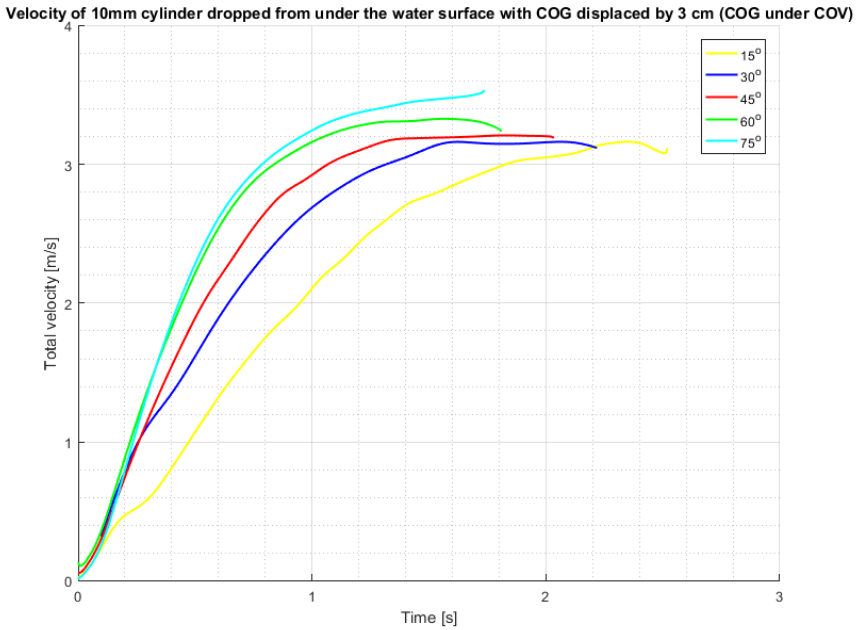

Figure 201: Total velocity compared to time for cylinders with COG 3 cm (Centre of Gravity (COG) under Centre of Volume (COV)). The cylinders are dropped under the surface with initial drop angles of 15^o, 30^o, 45^o, 60^o and 75^o. Each plot line represent an example of the total velocity development.

C Position tables

C.1 Position data for drop of 10, 16 and 19 mm diameter cylinders dropped from under the water surface

Table 1: Position data for closed 10 mm diameter cylinders with closed ends dropped from under the water surface. The table shows radial x-position, y-position and z-position with the corresponding standard deviations at the first and second turn, and at 3 and 4 m depth. Empty cells are due to the fact that the first and second turn does not occur for the drop angles in question.

10 mm cylinder dropped from under the water surface								
Drop angle	**First turn**				**Depth: 3m**			
	rad. x-pos. [m]	**st. dev. [m]**	**z-pos. [m]**	**st. dev. [m]**	**y-pos. [m]**	**st. dev. [m]**	**rad. x-pos. [m]**	**st. dev. [m]**
15°	0.73	0.08	1.13	0.06	-0.02	0.04	0.62	0.18
30°	2.37	0.35	2.20	0.27	-0.13	0.34	2.22	0.37
45°	3.79	0.53	3.63	0.56	-0.14	0.70	3.01	0.30
60°					0.04	0.18	1.71	0.13
75°					-0.01	0.08	0.88	0.09
	Second turn				**Depth: 4m**			
	rad. x-pos. [m]	**st. dev. [m]**	**z-pos. [m]**	**st. dev. [m]**	**y-pos. [m]**	**st. dev. [m]**	**rad. x-pos. [m]**	**st. dev. [m]**
15°	0.46	0.10	1.72	0.08	-0.01	0.05	0.89	0.19
30°	2.14	0.40	2.79	0.24	-0.10	0.36	2.32	0.56
45°	3.17	0.37	3.83	0.19	-0.04	0.81	3.67	0.51
60°					0.06	0.50	2.79	0.39
75°					0.02	0.18	1.49	0.18

Table 2: Position data for 16 mm diameter cylinders with closed ends dropped from under the water surface. The table shows radial x-position, y-position and z-position with the corresponding standard deviations at the first and second turn, and at 3 and 4 m depth.Empty cells are due to the fact that the first and second turn does not occur for the drop angles in question.

16 mm cylinder dropped from under the water surface								
Drop angle	**First turn**				**Depth: 3m**			
	rad. x-pos. [m]	**st. dev. [m]**	**z-pos. [m]**	**st. dev. [m]**	**y-pos. [m]**	**st. dev. [m]**	**rad. x-pos. [m]**	**st. dev. [m]**
15°	0.49	0.05	0.98	0.04	-0.03	0.05	0.41	0.13
30°	1.61	0.23	1.72	0.18	0.05	0.32	1.57	0.30
45°	2.89	0.11	2.93	0.10	-0.05	0.27	2.86	0.09
60°					-0.33	0.26	1.76	0.21
75°					0.05	0.08	0.93	0.03
	Second turn				**Depth: 4m**			
	rad. x-pos. [m]	**st. dev. [m]**	**z-pos. [m]**	**st. dev. [m]**	**y-pos. [m]**	**st. dev. [m]**	**rad. x-pos. [m]**	**st. dev. [m]**
15°	0.26	0.06	1.53	0.04	-0.05	0.04	0.79	0.17
30°	1.33	0.30	2.32	0.12	0.07	0.27	1.51	0.35
45°	2.56	0.10	3.56	0.14	-0.05	0.27	2.79	0.12
60°					-0.73	0.59	2.94	0.45
75°					0.16	0.26	1.68	0.04

Table 3: Position data for 19 mm diameter cylinders with closed ends dropped from under the water surface. The table shows radial x-position, y-position and z-position with the corresponding standard deviations at the first and second turn, and at 3 and 4 m depth. Empty cells are due to the fact that the first and second turn does not occur for the drop angles in question.

19 mm cylinder dropped from under the water surface								
Drop angle	**First turn**				**Depth: 3m**			
	rad. x-pos. [m]	**st. dev. [m]**	**z-pos. [m]**	**st. dev. [m]**	**y-pos. [m]**	**st. dev. [m]**	**rad. x-pos. [m]**	**st. dev. [m]**
15°	0.40	0.07	0.88	0.06	-0.02	0.08	0.22	0.12
30°	1.47	0.09	1.60	0.07	-0.08	0.15	1.40	0.12
45°	2.76	0.16	2.84	0.14	-0.18	0.42	2.68	0.23
60°					-0.47	0.43	1.63	0.33
75°					-0.05	0.15	0.99	0.07
	Second turn				**Depth: 4m**			
	rad. x-pos. [m]	**st. dev. [m]**	**z-pos. [m]**	**st. dev. [m]**	**y-pos. [m]**	**st. dev. [m]**	**rad. x-pos. [m]**	**st. dev. [m]**
15°	0.16	0.12	1.41	0.04	-0.02	0.06	0.35	0.18
30°	1.12	0.11	2.18	0.12	-0.10	0.14	1.35	0.19
45°	2.36	0.16	3.44	0.15	-0.21	0.29	2.58	0.13
60°					-0.73	1.08	2.48	0.67
75°					-0.11	0.46	1.81	0.17

C.2 Position data for drop of 10, 16 and 19 mm diameter cylinders dropped from over the water surface

Table 4: Position data for 10 mm diameter cylinders with closed ends dropped from over the water surface. The table shows radial x-position, y-position and z-position with the corresponding standard deviations at the first and second turn, and at 3 and 4 m depth. Empty cells are due to the fact that the first and second turn does not occur for the drop angle in question.

10 mm cylinder dropped from over the water surface								
Drop angle	**First turn**				**Depth: 3m**			
	rad. x-pos. [m]	**st. dev. [m]**	**z-pos. [m]**	**st. dev. [m]**	**y-pos. [m]**	**st. dev. [m]**	**rad. x-pos. [m]**	**st. dev. [m]**
15°	0.17	0.03	0.44	0.03	0.00	0.03	0.32	0.09
30°	0.50	0.07	0.63	0.07	0.00	0.08	0.51	0.17
45°	1.24	0.11	1.04	0.08	-0.01	0.08	1.14	0.26
60°	2.64	0.20	2.09	0.16	0.22	0.23	2.43	0.34
75°					-0.32	0.42	2.03	0.14
	Second turn				**Depth: 4m**			
	rad. x-pos. [m]	**st. dev. [m]**	**z-pos. [m]**	**st. dev. [m]**	**y-pos. [m]**	**st. dev. [m]**	**rad. x-pos. [m]**	**st. dev. [m]**
15°	0.03	0.04	0.98	0.04	-0.02	0.03	0.22	0.12
30°	0.23	0.18	1.25	0.06	0.01	0.10	0.70	0.25
45°	0.89	0.15	1.64	0.05	-0.04	0.15	1.47	0.28
60°	2.36	0.34	2.74	0.07	0.20	0.31	2.64	0.57
75°					-0.28	0.71	3.21	0.24

Table 5: Position data for 16 mm diameter cylinders with closed ends dropped from over the water surface. The table shows radial x-position, y-position and z-position with the corresponding standard deviations at the first and second turn, and at 3 and 4 m depth.

16 mm cylinder dropped from over the water surface								
Drop angle	**First turn**				**Depth: 3m**			
	rad. x-pos. [m]	**st. dev. [m]**	**z-pos. [m]**	**st. dev. [m]**	**y-pos. [m]**	**st. dev. [m]**	**rad. x-pos. [m]**	**st. dev. [m]**
15°	0.17	0.03	0.38	0.06	0.02	0.04	0.29	0.17
30°	0.44	0.05	0.57	0.05	0.01	0.05	0.32	0.22
45°	0.97	0.08	0.85	0.07	0.09	0.13	0.54	0.19
60°	2.03	0.16	1.64	0.11	-0.13	0.18	1.74	0.15
75°	3.65	0.57	4.13	0.31	0.24	0.55	2.23	0.24
	Second turn				**Depth: 4m**			
	rad. x-pos. [m]	**st. dev. [m]**	**z-pos. [m]**	**st. dev. [m]**	**y-pos. [m]**	**st. dev. [m]**	**rad. x-pos. [m]**	**st. dev. [m]**
15°	0.02	0.08	0.92	0.07	0.05	0.11	0.16	0.29
30°	0.16	0.13	1.16	0.07	0.04	0.05	0.34	0.26
45°	0.44	0.09	1.62	0.09	0.03	0.08	0.90	0.22
60°	1.70	0.57	2.35	0.19	-0.15	0.18	1.66	0.14
75°	3.46	0.20	4.55	0.26	0.39	1.16	3.40	0.49

Table 6: Position data for 19 mm diameter cylinders with closed ends dropped from over the water surface. The table shows radial x-position, y-position and z-position with the corresponding standard deviations at the first and second turn, and at 3 and 4 m depth.

19 mm cylinder dropped from over the water surface								
Drop angle	**First turn**				**Depth: 3m**			
	rad. x-pos. [m]	**st. dev. [m]**	**z-pos. [m]**	**st. dev. [m]**	**y-pos. [m]**	**st. dev. [m]**	**rad. x-pos. [m]**	**st. dev. [m]**
15°	0.15	0.01	0.42	0.01	0.00	0.03	0.22	0.13
30°	0.34	0.04	0.51	0.05	-0.06	0.08	0.14	0.19
45°	0.90	0.06	0.84	0.07	-0.14	0.29	0.48	0.09
60°	1.96	0.35	1.68	0.34	-0.32	0.71	1.58	0.44
75°					-0.37	0.90	2.22	0.27
	Second turn				**Depth: 4m**			
	rad. x-pos. [m]	**st. dev. [m]**	**z-pos. [m]**	**st. dev. [m]**	**y-pos. [m]**	**st. dev. [m]**	**rad. x-pos. [m]**	**st. dev. [m]**
15°	-0.06	0.03	1.04	0.20	-0.03	0.03	0.04	0.15
30°	-0.05	0.09	1.14	0.17	-0.08	0.13	0.05	0.20
45°	0.45	0.07	1.52	0.07	-0.12	0.16	0.64	0.17
60°	1.44	0.46	2.35	0.26	-0.36	0.72	1.54	0.54
75°	3.46	0.20	4.55	0.26	-0.43	1.50	2.83	0.47

C.3 Position data for drop of 10 and 19 mm diameter cylinders with open ends dropped from under the water surface

Table 7: Position data for 10 mm diameter cylinders with open ends dropped from under the water surface. The table shows radial x-position, y-position and z-position with the corresponding standard deviations at the first and second turn, and at 3 and 4 m depth. All empty cells are due to the fact that the cylinder does not have a second turn at 75°.

10 mm cylinder with open ends dropped from under the water surface								
Drop angle	**First turn**				**Depth: 3m**			
	rad. x-pos. [m]	**st. dev. [m]**	**z-pos. [m]**	**st. dev. [m]**	**y-pos. [m]**	**st. dev. [m]**	**rad. x-pos. [m]**	**st. dev. [m]**
15°	0.71	0.08	1.01	0.04	-0.10	0.04	0.72	0.10
30°	1.85	0.09	1.63	0.05	-0.17	0.19	1.90	0.13
45°	2.63	0.10	2.31	0.06	-0.18	0.25	2.35	0.14
60°	3.41	0.13	3.41	0.11	-0.06	0.18	2.89	0.13
75°	3.70	0.04	4.57	0.05	-0.10	0.08	1.30	0.07
	Second turn				**Depth: 4m**			
	rad. x-pos. [m]	**st. dev. [m]**	**z-pos. [m]**	**st. dev. [m]**	**y-pos. [m]**	**st. dev. [m]**	**rad. x-pos. [m]**	**st. dev. [m]**
15°	0.55	0.07	1.51	0.06	-0.15	0.08	0.85	0.13
30°	1.59	0.11	2.21	0.04	-0.19	0.18	1.91	0.14
45°	2.33	0.14	2.90	0.03	-0.22	0.28	2.57	0.17
60°	3.09	0.10	4.01	0.13	-0.10	0.25	3.12	0.12
75°					-0.20	0.24	2.62	0.26

Table 8: Position data for 19 mm diameter cylinders with open ends dropped from under the water surface. The table shows radial x-position, y-position and z-position with the corresponding standard deviations at the first and second turn, and at 3 and 4 m depth. No measurement exist of for drop angle 15°, hence the empty cells.

19 mm cylinder with open ends dropped from under the water surface								
Drop angle	**First turn**				**Depth: 3m**			
	rad. x-pos. [m]	**st. dev. [m]**	**z-pos. [m]**	**st. dev. [m]**	**y-pos. [m]**	**st. dev. [m]**	**rad. x-pos. [m]**	**st. dev. [m]**
15°								
30°	1.29	0.05	1.23	0.02	-0.07	0.04	1.08	0.19
45°	1.98	0.04	1.70	0.03	-0.06	0.10	1.44	0.10
60°	2.55	0.03	2.43	0.03	-0.09	0.14	1.95	0.08
75°	2.67	0.02	3.23	0.03	-0.18	0.19	2.37	0.08
	Second turn				**Depth: 4m**			
	rad. x-pos. [m]	**st. dev. [m]**	**z-pos. [m]**	**st. dev. [m]**	**y-pos. [m]**	**st. dev. [m]**	**rad. x-pos. [m]**	**st. dev. [m]**
15°								
30°	0.68	0.16	1.93	0.10	-0.06	0.09	1.20	0.37
45°	1.15	0.08	2.51	0.05	-0.07	0.14	1.38	0.10
60°	1.62	0.12	3.29	0.07	-0.10	0.19	2.09	0.10
75°	1.71	0.12	4.10	0.09	-0.14	0.24	1.79	0.09

C.4 Position data for drop of 10 mm diameter cylinders with centre of gravity displaced 1.4 cm.

Table 9: Position data for 10 mm diameter cylinders with closed ends and the centre of gravity displaced 1.4 cm. The cylinders is dropped with the initial position of the centre of gravity (COG) over the cylinder volume centre (COV). The table shows radial x-position, y-position and z-position with the corresponding standard deviations at the first and second turn, and at 3 and 4 m depth. The empty cells are due to the fact that a second turn does not occur.

10 mm cylinder with COG displaced 1.4 cm dropped from under the water surface (COG over COV)								
Drop angle	**First turn**				**Depth: 3m**			
	rad. x-pos. [m]	**st. dev. [m]**	**z-pos. [m]**	**st. dev. [m]**	**y-pos. [m]**	**st. dev. [m]**	**rad. x-pos. [m]**	**st. dev. [m]**
15°	0.21	0.10	0.36	0.15	0.04	0.66	-3.01	0.33
30°	0.65	0.05	0.57	0.03	-0.25	0.46	-2.10	0.11
45°	1.74	0.09	1.29	0.08	0.02	0.26	0.09	0.21
60°	2.62	0.21	2.97	0.21	0.03	0.28	2.53	0.17
75°	3.04	0.03	4.31	0.05	-0.16	0.05	1.26	0.02
	Second turn				**Depth: 4m**			
	rad. x-pos. [m]	**st. dev. [m]**	**z-pos. [m]**	**st. dev. [m]**	**y-pos. [m]**	**st. dev. [m]**	**rad. x-pos. [m]**	**st. dev. [m]**
15°					-0.27	0.94	-4.35	0.41
30°					-0.57	0.80	-3.43	0.20
45°					0.01	0.54	-1.04	0.24
60°					-0.13	0.14	1.72	0.46
75°					-0.31	0.15	2.73	0.06

Table 10: Position data for 10 mm diameter cylinders with closed ends and the centre of gravity displaced 1.4 cm. The cylinders is dropped with the initial position of the centre of gravity (COG) under the cylinder volume centre (COG). The table shows radial x-position, y-position and z-position with the corresponding standard deviations at the first and second turn, and at 3 and 4 m depth. The empty cells are due to the lack of turns.

10 mm cylinder with COG displaced 1.4 cm dropped from under the water surface (COG under COV)								
Drop angle	**First turn**				**Depth: 3m**			
	rad. x-pos. [m]	**st. dev. [m]**	**z-pos. [m]**	**st. dev. [m]**	**y-pos. [m]**	**st. dev. [m]**	**rad. x-pos. [m]**	**st. dev. [m]**
15°					0.22	0.81	3.55	0.16
30°					-0.18	0.54	2.77	0.14
45°					-0.07	0.32	1.89	0.06
60°					-0.15	0.17	1.19	0.08
75°					-0.05	0.03	0.60	0.03
	Second turn				**Depth: 4m**			
	rad. x-pos. [m]	**st. dev. [m]**	**z-pos. [m]**	**st. dev. [m]**	**y-pos. [m]**	**st. dev. [m]**	**rad. x-pos. [m]**	**st. dev. [m]**
15°					0.20	1.28	4.65	0.22
30°					-0.43	1.08	3.79	0.27
45°					-0.16	0.57	2.59	0.17
60°					-0.22	0.38	1.70	0.16
75°					-0.09	0.09	0.98	0.04

C.5 Position data for drop of 10 mm diameter cylinders with centre of gravity displaced 3 cm.

Table 11: Position data for 10 mm diameter cylinders with closed ends and the centre of gravity displaced 3 cm. The cylinders is dropped with the initial position of the centre of gravity over the cylinder volume centre. The table shows radial x-position, y-position and z-position with the corresponding standard deviations at the first and second turn, and at 3 and 4 m depth. The empty cells are due to the fact that no second turn occur.

10 mm cylinder with COG displaced 3 cm dropped from under the water surface (COG over COV)								
Drop angle	**First turn**				**Depth: 3m**			
	rad. x-pos. [m]	**st. dev. [m]**	**z-pos. [m]**	**st. dev. [m]**	**y-pos. [m]**	**st. dev. [m]**	**rad. x-pos. [m]**	**st. dev. [m]**
15°	0.07	0.01	0.45	0.01	0.03	0.28	-1.81	0.09
30°	0.41	0.01	0.84	0.01	-0.04	0.47	-1.10	0.15
45°	1.04	0.02	1.35	0.02	0.25	0.17	0.13	0.30
60°	1.66	0.03	2.15	0.05	-0.03	0.11	1.18	0.07
75°	2.14	0.00	3.17	0.07	0.25	0.87	1.96	0.44
	Second turn				**Depth: 4m**			
	rad. x-pos. [m]	**st. dev. [m]**	**z-pos. [m]**	**st. dev. [m]**	**y-pos. [m]**	**st. dev. [m]**	**rad. x-pos. [m]**	**st. dev. [m]**
15°					0.07	0.45	-2.49	0.19
30°					0.04	0.50	-1.66	0.14
45°					0.41	0.29	-0.71	0.15
60°					-0.12	0.30	0.65	0.15
75°					-0.03	0.19	1.80	0.14

Table 12: Position data for 10 mm diameter cylinders with closed ends and the centre of gravity displaced 3 cm. The cylinders is dropped with the initial position of the centre of gravity under the cylinder volume centre. The table shows radial x-position, y-position and z-position with the corresponding standard deviations at the first and second turn, and at 3 and 4 m depth. The empty cells are due to the lack of turns in the trajectory of the cylinders.

10 mm cylinder with COG displaced 3 cm dropped from under the water surface (COG under COV)								
Drop angle	**First turn**				**Depth: 3m**			
	rad. x-pos. [m]	**st. dev. [m]**	**z-pos. [m]**	**st. dev. [m]**	**y-pos. [m]**	**st. dev. [m]**	**rad. x-pos. [m]**	**st. dev. [m]**
15°					0.23	0.24	2.26	0.09
30°					0.20	0.23	1.85	0.05
45°					-0.03	0.23	1.33	0.08
60°					0.07	0.11	0.84	0.07
75°					0.01	0.04	0.37	0.05
	Second turn				**Depth: 4m**			
	rad. x-pos. [m]	**st. dev. [m]**	**z-pos. [m]**	**st. dev. [m]**	**y-pos. [m]**	**st. dev. [m]**	**rad. x-pos. [m]**	**st. dev. [m]**
15°					0.33	0.33	2.81	0.12
30°					0.24	0.34	2.34	0.07
45°					-0.05	0.36	1.73	0.12
60°					0.10	0.17	1.14	0.12
75°					0.02	0.10	0.52	0.10

D Velocity tables

D.1 Velocity tables for drop of 10, 16 and 19 mm diameter cylinders dropped from under the water surface

Table 13: The average maximal velocity and standard deviation for 10, 16 and 19 mm cylinders with closed ends, dropped from under the water surface.

Cylinders dropped from under the water surface						
Drop angle	**10 mm**		**16 mm**		**19 mm**	
	Average max. vel. [m/s]	std. dev. [m/s]	Average max. vel. [m/s]	std. dev. [m/s]	Average max. vel. [m/s]	std. dev. [m/s]
15°	0.85	0.02	0.85	0.03	0.79	0.02
30°	1.53	0.09	1.33	0.09	1.17	0.03
45°	2.17	0.09	1.92	0.07	1.70	0.03
60°	2.68	0.07	2.43	0.10	2.43	0.10
75°	2.96	0.05	2.60	0.02	2.33	0.03

D.2 Velocity tables for drop of 10, 16 and 19 mm diameter cylinders dropped from over the water surface

Table 14: The average maximal velocity and standard deviation for 10, 16 and 19 mm cylinders with closed ends, dropped from over the water surface.

Cylinders dropped from over the water surface						
Drop angle	**10 mm**		**16 mm**		**19 mm**	
	Average max. vel. [m/s]	std. dev. [m/s]	Average max. vel. [m/s]	std. dev. [m/s]	Average max. vel. [m/s]	std. dev. [m/s]
15°	1.91	0.50	1.56	0.19	0.78	0.03
30°	1.51	0.15	1.74	0.35	0.81	0.04
45°	1.76	0.30	1.66	0.20	1.22	0.04
60°	2.13	0.19	2.09	0.20	1.79	0.07
75°	2.88	0.14	2.65	0.09	2.39	0.05

D.3 Velocity tables for drop of 10 and 19 mm diameter cylinders with open ends dropped from under the water surface

Table 15: The average maximal velocity and standard deviation for 10 and 19 mm cylinders with open ends, dropped from under the water surface.

Cylinders with open ends dropped from under the water surface				
Drop angle	**10 mm**		**19 mm**	
	Average max. vel. [m/s]	std. dev. [m/s]	Average max. vel. [m/s]	std. dev. [m/s]
15°	1.05	0.05		
30°	1.68	0.05	1.66	0.03
45°	2.35	0.07	2.32	0.04
60°	2.87	0.06	2.89	0.02
75°	3.29	0.05	3.30	0.02

D.4 Velocity tables for drop of 10 mm diameter cylinders with centre of gravity displaced 1.4 cm

Table 16: The average maximal velocity and standard deviation for 10 mm cylinders with closed ends and the centre of gravity displaced 1.4 cm, dropped from under the water surface. The cylinders is dropped with the initial position of the centre of gravity (COG) over and under the cylinder volume centre (COV).

Cylinders with COG displaced 1.4 cm dropped from under the water surface				
Drop angle	**COG over COV**		**COG under COV**	
	Average max. vel. [m/s]	std. dev. [m/s]	Average max. vel. [m/s]	std. dev. [m/s]
15°	1.88	0.20	2.03	0.10
30°	1.94	0.11	2.33	0.15
45°	2.11	0.05	2.75	0.13
60°	2.39	0.04	2.98	0.04
75°	2.88	0.03	3.08	0.05

D.5 Velocity tables for drop of 10 mm diameter cylinders with centre of gravity displaced 3 cm

Table 17: The average maximal velocity and standard deviation for 10 mm cylinders with closed ends and the centre of gravity (COG) displaced 3 cm, dropped from under the water surface. The cylinders is dropped with the initial position of COG over and under the cylinder volume centre (COV).

Cylinders with COG displaced 3 cm dropped from under the water surface				
Drop angle	**COG over COV**		**COG under COV**	
	Average max. vel. [m/s]	std. dev. [m/s]	Average max. vel. [m/s]	std. dev. [m/s]
15°	2.94	0.18	3.20	0.09
30°	3.04	0.12	3.22	0.05
45°	3.03	0.07	3.27	0.11
60°	3.06	0.13	3.33	0.10
75°	2.82	0.09	3.47	0.09